Universidad de Huelva

Departamento de Ingeniería Electrónica, de Sistemas Informáticos y Automática

Precision farming based technologies for olive grove management optimization

Memoria para optar al grado de doctor presentada por:

Miguel Noguera Manzano

Fecha de lectura: 3 de diciembre de 2024

Bajo la dirección de los doctores:

José Manuel Andújar Márquez

Borja Millán Prior

Huelva, 2024

Universidad de Huelva

Programa de Doctorado de Ciencia y Tecnología Industrial y Ambiental

Línea de investigación: Ingeniería Eléctrica, Electrónica, de Control y Robótica

Centro de Investigación en Tecnología, Energía y Sostenibilidad (CITES)

Universidad de Huelva

PRECISION FARMING BASED TECHNOLOGIES FOR OLIVE GROVE MANAGEMENT OPTIMIZATION

Tesis doctoral con mención de doctor internacional presentada por:

Miguel Noguera Manzano

Bajo la dirección de los doctores:

José Manuel Andújar Márquez

Borja Millán Prior

Huelva, 2024

Dr. José Manuel Andújar Márquez, Catedrático de Universidad de la Escuela Técnica Superior de Ingeniería de la Universidad de Huelva,

Dr. Borja Millán Prior, Profesor Contratado Doctor de la Escuela Politécnica de Ingeniería de la Universidad de Oviedo,

CERTIFICAN:

Que D. Miguel Noguera Manzano, Graduado en Biología por la Universidad de Granada, ha realizado bajo nuestra dirección y dentro del programa de doctorado de Ciencia y Tecnología Industrial y ambiental (CyTIA), y en la línea de investigación de Ingeniería Eléctrica, Electrónica, de Control y Robótica, el trabajo correspondiente a su Tesis Doctoral titulada:

Tecnologías basadas en la agricultura de precisión para la optimización de la gestión del olivar.

Revisado el presente trabajo, estimamos que puede ser presentado al Tribunal que ha de juzgarlo.

Y para que así conste a efectos de lo establecido por el Real Decreto 99/2011 y por la normativa Reguladora del título de Doctor de la Universidad de Huelva, autorizamos la presentación de este trabajo en la Universidad de Huelva.

Huelva, a 02 de julio de 2024

Director: Dr. José Manuel Andújar Márquez

Director: Dr. Borja Millán Prior

Doctorando: D. Miguel Noguera Manzano

Agradecimientos

En primer lugar, quiero mostrar mis agradecimientos a mis directores de Tesis, Dr. José Manuel Andújar y Dr. Borja Millán. José Manuel, gracias por apostar por mí, tu confianza y exigencia han hecho posible la consecución de todos los éxitos que ameritan esta Tesis. Borja tu apoyo intelectual ha ampliado mis horizontes y ha sido un pilar fundamental para el desarrollo profesional que he alcanzado en estos años que hemos compartido juntos, por ello siempre te estaré agradecido.

Asimismo, quiero agradecer a mis compañeros de laboratorio: Ponce, Diego, Gamero, Rocio, Daniel, Roca, Cirilo y David, así como otros tantos miembros del TEP-192. En ellos he encontrado compañeros de trabajo muy capaces además de buenos amigos, lo cual es fundamental para superar los retos que hemos afrontado juntos. Gracias por todos los buenos momentos.

Me gustaria agradecer especialmente a Arturo Aquino. Has sido lo más parecido a un director sin serlo. Sirviéndome de ejemplo me has ayudado a relativizar desafíos de los que creía no ser capaz. Debido a esto hoy me siento más orgulloso de la persona que soy.

Quiero mostrar mis agradecimientos a los colegas del Instituto Nacional de Investigación Agraria y Veterinaria (INIAV) de Portugal. En especial a Antonio Cordeiro y José Silvestre. El tiempo que he compartido con ustedes ha tenido un gran impacto en mi a nivel profesional. Su guía ha sido, sin duda, esencial para alcanzar los hitos que han conformado esta Tesis.

A mi familia, y especialmente a mis padres. Gracias por aportarme el amor y la exigencia que me han llevado a ser el hombre que hoy soy. Gracias por transmitirme que no hay reto que no pueda afrontar, aun cuando yo mismo no lo veía asequible. Vuestro orgullo es mi motor, y creo firmemente que mis éxitos os pertenecen tanto como a mí mismo.

Quiero agradecer a Marta. Eres mi compañera de vida. Contigo, los buenos momentos son mejores y los malos parecen no serlo tanto. Gracias por estar siempre a mi lado y por quererme con mis virtudes y defectos.

Gracias a todos los amigos que me hacéis disfrutar de la vida, y me dais buenos consejos cuando los necesito.

Table of contents

Abstract

Precision oliviculture aims to enhance the quality and productivity of olive orchards while reducing environmental impact through optimized resource utilization. The implementation of these strategies requires the development of methodologies to characterize the state of olive trees with high spatial and temporal resolution.

This thesis aims to develop accessible methodologies for assessing the water and nutritional needs olive crops, as well as the olive fruit quality.

The first milestone of this thesis has been the development of a thermal camera based on a low-cost infrared sensor to assess the water status of olive trees. The canopy temperature and the crop water stress index (CWSI) were compared with two standardized water status indicators (predawn leaf water potential and stomatal conductance), obtaining promising results ($R^2 \geq 0.80$). A significant aspect of this work is the proposed method for obtaining the thresholds needed to calculate the CWSI. This approach simplifies the automation of the process, as the reference limits are extracted from the temperature histogram, avoiding the need to measure artificial surfaces or meteorological variables.

The second milestone involved developing a methodology to assess the nutritional status of olive trees based on analysing and modelling spectral images captured by an unmanned aerial vehicle. A crucial step of this methodology is the proposed image processing technique. It utilizes a digital surface model to filter out background information, improving the quality of spectral data by reducing the impact of background noise. The 5 reflectance data extracted from the images were used to train various modelling tools (partial least squares regression, artificial neural network (ANN), support vector regression, and gaussian process regression) using reference values of NPK leaf content. The ANN models achieved the best results (LNC: $R^2 = 0.63$; LPC: $R^2 = 0.89$; LKC: $R^2 = 0.93$).

The third milestone focused on developing a low-cost multispectral device capable of characterising key quality parameters of intact olives. A prototype based on a commercial sensor was initially built and evaluated in a controlled laboratory experiment. The 18 reflectance values acquired by the sensor were used as input for ANN models, with three key olive quality indicators serving as reference data: moisture (M), titratable acidity (TA), and oil content per fresh weight (OCFW). The results obtained from the ANN models were promising (H: $R^2 = 0.78$; TA: $R^2 = 0.86$; OCFW: $R^2 = 0.62$).

Encouraged by the laboratory results, a portable device based on the same sensor was developed. Its potential was evaluated in a field experiment, taking spectral measurements on-site. The results of this work were encouraging as the estimates of the oil content per dry matter (OCDM) ($R^2 = 0.86$), OCFW ($R^2 = 0.86$), and M ($R^2 = 0.89$) were better than those obtained under laboratory conditions, although the estimation of TA ($R^2 = 0.21$) was worse. Alternatively, the potential of the device to characterize quality

indicators of red grapes in field conditions was evaluated, obtaining good results (Solid soluble content: $R^2 = 0.70$; TA: $R^2 = 0.67$). This suggests the potential of the device beyond olive trees.

The results obtained in the research conducted in this Thesis indicate the potential of the developed solutions to support decision-making in the context of precision oliviculture. The low cost and ease of use of the proposed solutions make them accessible for all kind of olive growers.

Keywords: Olive, precision farming, sensors, spectroscopy, artificial neural networks.

Resumen

La olivicultura de precisión busca mejorar la calidad y productividad de los olivares, reduciendo su impacto ambiental a través de la optimización del uso de recursos. La implementación de estrategias basadas en olivicultura de precisión requiere el desarrollo de metodologías para caracterizar el estado de los olivos con una alta resolución espacial y temporal.

El objetivo de esta Tesis es desarrollar metodologías accesibles para la estimación del estado hídrico y nutricional del olivar, así como la calidad del fruto.

En primer hito de esta Tesis ha sido el desarrollo de una cámara térmica basada en un sensor infrarrojo de bajo coste para evaluar el estado hídrico de los olivos. La temperatura del dosel y el índice de estrés hídrico del cultivo (CWSI) se compararon con dos indicadores de estado hídrico estandarizados (potencial hídrico foliar antes del amanecer y conductancia estomática), obteniendo resultados prometedores ($R^2 \geq 0.80$). Un aspecto relevante de este trabajo es el método propuesto para obtener los umbrales necesarios para calcular el CWSI. Este enfoque simplifica la automatización del proceso, ya que los límites de referencia se extraen del histograma de temperaturas, evitando la necesidad de medir superficies artificiales o variables meteorológicas.

El segundo hito consistió en el desarrollo de una metodología para evaluar el estado nutricional de los olivos basada en el análisis y modelización de imágenes espectrales tomadas desde un vehículo aéreo no tripulado. Una parte esencial de esta metodología fue el procesamiento de imágenes, que permite la identificación de los píxeles del dosel, descartando información de fondo mediante el uso de un modelo digital de superficie. Esto mejora la calidad de los datos espectrales, disminuyendo el perjuicio ocasionado por la presencia de distractores. Los 5 datos de reflectancia extraídos de las imágenes se usaron para entrenar varias herramientas de modelización (regresión por mínimos cuadrados parciales, redes neuronales artificiales (ANN), regresión de soporte vectorial, y procesos de regresión gaussiana) utilizando valores de referencia del contenido foliar de NPK. Las modelos ANN arrojaron los mejores resultados (LNC: R2 = 0.63; LPC: R2 = 0.89; LKC: R2 = 0.93).

El tercer hito consistió en el desarrollo de un dispositivo multiespectral de bajo coste con capacidad de caracterizar parámetros de calidad de aceitunas intactas. Inicialmente se desarrolló un prototipo basado en un sensor comercial, y este se evaluó en un experimento realizado en condiciones de laboratorio. Los 18 valores de reflectancia adquiridos por el sensor se usaron para alimentar modelos ANN usando como referencia 3 indicadores de calidad de aceituna (humedad: M; acidez titulable: TA; y contenido de aceite en materia fresca: OCFW). Las respuestas de los modelos ANN fueron prometedoras (M: R2 = 0.78; TA: R2 = 0.86; OCFW: R2 = 0.62).

Estos resultados impulsaron el desarrollo de un dispositivo portátil, basado en el mismo sensor. El potencial de este se evaluó en un experimento de campo, tomando las medidas espectrales sobre el terreno. Los resultados de este trabajo fueron alentadores ya que las

estimaciones del contenido de aceite por materia seca (OCDM) (R2 = 0.86), OCFW (R2 = 0.86) y M (R2 = 0.89) superaron a las obtenidas en condiciones de laboratorio, aunque que la estimación de TA (R2 = 0.21) fue peor. Alternativamente, se evaluó el potencial del dispositivo para caracterizar indicadores de calidad de uvas en condiciones de campo, obteniendo buenos resultados (Solidos solubles totales: R2 = 0.70; TA: R2 = 0.67). Esto sugiere el potencial del dispositivo en cultivos diferentes del olivo.

Los resultados obtenidos en la investigación realizada en esta Tesis indican el potencial de las soluciones desarrolladas para apoyar la toma de decisiones en el contexto de la olivicultura de precisión. El bajo coste y la facilidad de uso de las soluciones propuestas las hacen accesibles para todo tipo de olivicultores.

Palabras clave: Olivo, agricultura de precisión, sensores, espectroscopia, redes neuronales artificiales.

List of abbreviations

Acousto-Optical Tunable Filter	AOTF
Air temperature	T_{air}
All-terrain vehicle	ATV
Analog-to-digital converter	ADC
Ante meridiem	AM
Artificial neural network	ANN
Canopy temperature	T_{canopy}
Coefficient of determination	R^2
Coefficient of variation of the RMSE	CVRMSE
Crop evapotranspiration	ETc
Crop water stress index	CWSI
Data standard deviation	σ
Digital surface model	DSM
Downwelling light sensor	DLS
Electrical conductivity	CEa
Electrically erasable programmable read-only memory	EEPROM
Error probability	EP
European Regional Development Fund	ERDF
Field of view	FOV
Fully irrigated	FI
Gaussian process regression	GPR
Ground sample distance	GSD
Inductively coupled plasma optical emission spectrometry	ICP-OES
Infrared	IR
Integrated circuit	IC
Inter-integrated circuit protocol	I^2C
International Standarization Organization	ISO
Leaf nitrogen content	LNC
leaf phosphorus content	LPC
leaf potassium content	LKC
Leaf transpiration rate	Em
Leaf water potential	Ψ_l
Leave-one-out cross-validation	LOOCV
Light Detection and Ranging	LiDAR
Lithium-ion Polymer	LiPo
Mid-infrared	MIR
Moisture	M
Moisture stress index	MSI
Multilayer perceptron algorithms with backpropagation	MLP-BP
Near-infrared	NIR
Noise equivalent temperature differenc	NETD
Non-water stress baseline	NWSB
Normalized difference vegetation index	NDVI
Nuclear magnetic resonance	NMR

Oil content per dry matter	OCDM
Oil content per fresh weight	OCFW
Partial least squares regression	PLSR
Photosynthetically active radiation	PAR
Polylactic acid	PLA
Post meridiem	PM
Predawn leaf water potential	Ψ_{PD}
Printed Circuit Board	PCB
Proportional to absolute temperature	PTAT
Random access memory	RAM
Ratio of performance to deviation	RPD
Red-Green-Blue	RGB
Regulated deficit irrigated	RDC
Remotely piloted aircraft systems	RPAS
Root mean square error	RMSE
Root mean square error of prediction	RMSEP
Secure digital	SD
Serial peripheral interface	SPI
Shortwave infrared	SWIR
Soil-adjusted vegetation index	SAVI
Soluble solid content	SSC
Stem water potential	Ψ_{st}
Stomatal conductance	g_s
Super high density	SHD
Support vector regression	SVR
Temperature of a fully transpiring leaf	T_{wet}
Temperature of a non-transpiring leaf	T_{dry}
Thin film transistor- liquid crystal display	TFT-LCD
Three-dimensional	3D
Time-Of-Flight	TOF
Titratable acidity	TA
Two-dimensional	2D
Unmanned aerial vehicle	UAV
Unmanned ground vehicles	UGV
Vapor pressure deficit	VPD
Vegetation indices	VI
Visible	VIS
Wet artificial reference surface	WARS

1. Introduction

1.1. Importance of the olive grove

The connection between the olive crop (*Olea europaea* L.) and the countries of the Mediterranean basin is rooted in cultural and environmental reasons. In these regions, the olive tree is one of the oldest and most traditionally cultivated plant species. It is believed that the first variety of olive tree cultivated by humans appeared in the Middle East around 5500 years ago [1]. While the exact location of its original development is still debated, it appears clear that the expansion of olive cultivation came from the domestication of wild varieties of olive trees that, millennia ago, grew spontaneously in Mediterranean woodlands [2]. The earliest written sources document that olive oil was an integral part of everyday life in antiquity. It was not only used in food but also had applications in medicine, cosmetics, and for liturgical purposes [3]. However, despite being tied to Mediterranean cultures since ancient times, its expansion in the form of single crop cultivation is relatively recent, mainly dating from the last three centuries and especially in the late nineteenth century. During this period, agriculture expanded significantly due to new market opportunities, leading to increased internal and external demand. Large-scale specialized olive growing was a part of this development. Specifically, the relative improvements in the potential profitability of the crop promoted its expansion until it reached the importance seen today [4]. A key factor in this expansion is the strong adaptation of olive crops to grow under drought stress, making them suitable for enhancing the value of arid and semi-arid Mediterranean crop areas.

At present, the olive crop is crucial for the agricultural sector of many countries in the Mediterranean basin. Olive oil is the primary by-product of the oliviculture sector, increasingly regarded by consumers as a vital ingredient for a healthy diet due to its richness in valuable nutrients and bioactives with medicinal and therapeutic benefits. [5]. Worldwide, the total area dedicated to olive tree cultivation is approximately 11.5 million hectares, distributed across about 40 countries. The top olive producers are Spain, Italy, Greece, and Portugal, while other Mediterranean countries such as Tunisia, Morocco, Algeria, Egypt, and Turkey also make significant contributions to olive production. In the 2020/2021 harvest campaign, European Union olive oil production reached 2051 thousand tonnes of final product, accounting for 68.1% of worldwide production. Considering the harvesting campaigns from 2016/2017 to 2019/2020, the European Union produced 65% of the world's olive oil, consumed 50%, and accounted for 67% of the exports [6]. When it comes to the economic value of this sector, in recent years, the European Union's olive oil production has reached a total value of five billion euros, with Spain and Italy alone generating 80% of that value. These data highlights the significance of the olive sector as a crucial driver of socio-economic development in the countries of the Mediterranean basin.

The olive sector must confront numerous challenges in response to the current scenario. Indeed, enhancing the yield of horticultural commodities to meet increasing demand

while managing acceptable production costs and adopting environmentally sustainable farming practices is a pervasive issue in modern agriculture [7].

1.2. Evolution of olive cultivation systems

Traditionally, olive cultivation systems have featured low planting densities, with trees arranged in squares and distances between them measuring 5–7 meters by 6–8 meters (Figure 1). In these conditions, the planting density ranges from 100 to 300 trees per hectare, allowing ample soil area for each tree and enabling the development of large three-dimensional (3D) forms. The canopies of these trees can reach heights and diameters exceeding 5 m, with volumes exceeding 130 m^3. In such conditions, the total canopy volume can easily reach 15,000 to 30,000 m^3 per hectare, depending on the number of trees planted [8]. The olive tree is characterized by an extensive root system and the high capacity of its trunk and large branches to accumulate water and nutrient reserves. These features enable the tree to withstand environmental stresses, including high light intensity, elevated temperatures (the large canopy provides protection from sunburn), and prolonged periods of drought. These adaptations allow traditional olive groves to achieve satisfactory yields under rain-fed conditions, reducing dependence on agricultural inputs [9]. However, the main drawbacks of traditional olive orchards are associated with their distinct alternating bearing pattern, which is influenced by the age of the trees. Older trees are often susceptible to wood decay, which can impede the flow of nutrients through the phloem from the roots to the shoots. Consequently, this reduces the vigour needed to promote the annual renewal of vegetation, even during high-yielding years [10]. This phenomenon is frequently exacerbated by the lack of water for irrigation and the extended time intervals between pruning events, typically carried out every 4–5 years due to economic considerations. Additionally, mechanizing management operations (harvesting, pruning, etc.) in these circumstances is unsustainable, constituting the primary factor contributing to the economic inefficiency of these systems.

Figure 1. Image of traditional olive orchard.

To overcome these limitations, new cultivation systems were explored, showing a clear trend towards increasing plant density. Thus, the concept of intensive olive groves has emerged, characterized by planting densities of 300–1000 trees/ha. These cultivation systems also follow a square or rectangle plantation pattern, with distances of 5–6 m between rows and 2–3 m on the row. The potential minimal distances between trees within the row depend on factors such as the availability of water, the vigour of the cultivar, and the length of the growing season. The training form of the trees is also a decisive factor that must be selected based on the growing conditions. The most popular options include the globe, the vase, the monocone, and the polyconic vase [8]. As plant density increases, the size of the trees decreases, resulting in a lower productive potential per tree compared to traditional olive groves. However, the greater number of trees per unit area significantly increases productivity in terms of cultivated surface. Additionally, the smaller size of the trees makes mechanized harvesting operations easier, as the shakers used to remove the fruits require less energy and are easier to operate. However, the larger plant density of intensive cultivation systems increases the canopy surface, raising the evaporative demand. This fact makes it necessary to irrigate the field, especially during the summer drought period. This crop configuration allows for the partial mechanization of pruning through topping and, less commonly, hedging operations, performed using disk saws mounted on mobile bars and operated by a tractor. However, these 'non-selective' pruning operations often require manual finishing by expert operators to balance the canopy's structure. These features make intensive olive cultivation more profitable than traditional olive orchards [11].

Although the intensive olive system has demonstrated to be more profitable than traditional ones, there are several issues susceptible to improvement. From a social and economic perspective, the goal of reducing reliance on manual labour is becoming progressively more critical. This is not only due to the associated high costs but also because of the challenge of finding specialized labour, which is further exacerbated by the gradual depopulation of rural areas. In olive cultivation, the income levels attainable with the traditional and intensive groves are frequently modest due to the extensive reliance on manual labour. Thus, the sustainability of this vital production sector hinges on the feasibility of fully automating the harvesting process and, to some extent, pruning operations. Indeed, these are the only management practices that continue to heavily depend on manual labour today, posing a threat to the economic viability of the entire production process.

To address these shortcomings, new cultivation systems, like the super high density (SHD) planting system, have been proposed in recent decades. This is the latest generation of plantings, characterized by extremely high density (> 1500 trees/ha). The most remarkable feature of these cultivation systems is the arrangement and structure of the trees. They are arranged in rectangular layouts, with spacings of 1-1.5 x 3-3.5 m, trained to form continuous hedgerows, creating a two-dimensional (2D) tree shape, in contrast to the traditional 3D forms (Figure 2). This crop configuration prioritizes maximizing the productivity of the land unit or the population of trees within the

orchard system over the high fruit yields obtained by individual trees. One of the main advantages of SHD plantings is the ability to conduct olive pruning and harvesting using fully mechanized continuous systems, significantly reducing the time required for these management practices. Furthermore, it involves minimizing the reliance on manpower, which is essential for cost savings. This becomes even more crucial in a context marked by the challenge of finding specialized labour due to the gradual depopulation of rural areas. Other significant advantages of SHD plantings include early and abundant fruiting, beginning as early as 3–4 years from planting with initial yields of 3-4 t/ha. These yields can exceed 10 t/ha in subsequent years. The superior agronomic performance of hedgerow olive orchards compared to traditional ones is attributed to the higher proportion of one- to two-year-old shoots and branches in dwarfed trees. These young structures bear reproductive organs, unlike the old wood fraction that is more common in vigorous, larger trees [12].

Figure 2. Image of a super high density (SHD) olive orchard.

As stated above, SHD orchards involve several advantages that enhance their profitability. Nevertheless, the elevated density of trees per area increases the evaporative demand of the entire crop, necessitating exhaustive fertirrigation programs. SHD orchards are nowadays supported by standard cultivation protocols that facilitate their management [13]. However, they treat the field as homogeneous surfaces, disregarding spatial variability. Thus, frequently, an unsuitable use of agronomic resources occurs. This usually results in excessive use, causing economic loss and environmental damage. There are multiple standard crop parameters that are important for supporting decisions regarding crop management. Nevertheless, the shortcomings of traditional methods to monitor these parameters limit their use, resulting in the mentioned deficiencies regarding olive crop management. Indeed, there is considerable potential for enhancing the management paradigm in olive cultivation. By addressing the limitations of traditional methods and embracing innovative technologies and approaches, olive growers can optimize resource use, improve crop productivity, and enhance sustainability.

1.3. Traditional resources to suport olive management

The choice of a cultivation system will influence the vegetative and productive behavior of the olive tree and will require suitable management based on the agro-climatic conditions. As depicted in the section above, the evolution of the olive cultivation system has resulted in crops with higher plant densities, which, due to their better profitability, are likely to become the predominant olive cultivation system in the future. These cultivation systems encompass a higher crop evapotranspiration rate, increasing the demand for agronomic inputs and making field management more complex. These facts reveal the need to improve traditional agronomic practice. Although these include others concerns such as, phytosanitary management, soil management, pruning, etc., in this work, we are going to focus on fertilization, irrigation, and fruit quality control for being the main topics of this Thesis.

1.3.1. Fertilization. Nutritional status assessment

Fertilization has an impact on the vegetative and productive performance of the olive crop as well as the entire agroecosystem. Maintaining foliar nutrient concentrations within certain thresholds is beneficial for productivity and quality (size, oil content, etc.)[14,15]. The traditional method used for assessing the nutrient status of olive trees is foliar chemical analysis. These methods involve collecting leaf samples and transporting them to a laboratory, usually an external service contracted by the grower. The experimental protocol for chemical analysis relies on a tedious process that requires complex equipment, so it must be conducted by expert personnel. In these conditions, evaluating the nutritional status of the crop entails a high cost for the grower. Furthermore, there is a time delay between sample collection and access to the information, which reduces the reliability of the results. These limitations restrict the number of sample points that growers can consider, and the number of sampling campaigns that can be conducted during the season, leading to poor spatio-temporal resolution in monitoring. The deficiencies of traditional resources to assess the variability in nutritional needs within the crop have led to the current fertilization paradigm, typically characterized by single circuits that allow homogeneous applications of fertilizers without considering the actual needs of the crop and the real availability [16]. In fact, excessive doses of fertilizers are often applied, leading to an increase in vegetative growth at the expense of productivity. The olive crop is especially sensitive to this condition, which results in a most remarkable alternations in production. This also increases the need for crop management actions, resulting in higher costs. Moreover, the excessive use of fertilizers can lead to a detriment of oil quality, characterized by a decrease in polyphenol content [17,18]. On the other hand, excessive fertilizer usage exacerbates environmental problems, leading to phenomena such as the eutrophication of water reserves [19].

1.3.2. Irrigation. Water status assessment

Irrigation is a decisive factor concerning the quality and quantity of olives fruits. Excessive irrigation doses can lead to a reduction of the phenolic component of fruits. On the other hand, deficient irrigation doses cause a decrease in productivity. An adequate irrigation program, however, results in increased production and a reduction in production alternation [20]. Unfortunately, it is difficult to reach the right balance. The olive tree presents strong resistance and tolerance to water stress, due to its multiple physiological adaptations [9]. In traditional systems, olives have an average water requirement of 1500-2500 m^3/ha, allowing them to thrive in rain-fed conditions. The evolution of olive cultivation systems, marked by increasing plant density, has resulted in crops with higher evapotranspiration rates. In these circumstances, irrigation is needed to maintain acceptable production levels since rainfall is not enough to supply that demand. It is important to remark that olives benefit from deficit irrigation strategies, the correct application of which requires precise information on the dynamics of crop water stress [21]. However, irrigation schedules are typically designed based on estimations of crop evapotranspiration. Furthermore, they are applied uniformly over large field areas without considering the factors of crop heterogeneity that affect water use efficiency. For this reason, many zones of the field receive inadequate irrigation doses. Moreover, the depletion of water resources persists due to ongoing overuse. All these factors make it evident that there is a necessity to develop techniques and agronomic choices able to maximize crop water efficiency. This goal can be pursued through various approaches, including adjusting the volume of water supplied, adopting distinct approaches for different phenological stages, modifying irrigation distribution methods (such as micro-irrigation or sprinklers), and implementing efficient agronomic practises (pruning and fertilization). In this regard, precision irrigation can yield outstanding outcomes by pinpointing variations in water stress across the field. Nonetheless, to attain this objective, it is crucial to precisely measure the water status of crops, enabling the establishment of a predetermined stress level. The standard parameters to assess water stress in olive trees are stem water potential (Ψ_{st}), leaf water potential (Ψ_l), leaf transpiration rate (Em), and stomatal conductance (g_s). However, these parameters are impractical for agronomic applications and remain restricted to research purposes [22]. This fact is due to their labour demanding, time-consuming nature, and necessity of expert and trained personnel.

1.3.3. Quality. Fruit ripeness assessment

The concept of quality in fruit products is broad and complex. It encompasses many attributes with varying significance based on the interests and expectations of different stakeholders in the chain, from producers to consumers. In the case of the olive, two main products are obtained from olive fruits: olive oil (the juice of the fruit) and table olives, each of which has its own criteria for assessing quality. However, this Thesis is only centred in olives destinated to oil production. From an agronomic perspective, the ripeness level at harvest holds significant importance for growers as it directly influences

the market value of their produce. Olive mills use objective chemical parameters to assess the received olive harvest, which determine the fee obtained by the respective grower. So, the decision regarding the optimal harvest time must hinge upon achieving the ideal balance between oil quantity and quality. Within the harvesting period, growers analyse these ripening indicators to decide whether to advance or delay the date of harvesting within the harvest period. The process of oil accumulation and its chemical transformation throughout the ripening of olives is influenced by a multitude of agronomic factors, including the cultivar, soil characteristics, environmental conditions, nutritional status, water availability, and the incidence of pathologies [23]. Since these factors exhibit variation across the crop area, maturation can take place at varying rates across different sections of a field, resulting in a heterogeneous ripening status. Agronomic practices can help mitigate this heterogeneity and promote more uniform ripening. Furthermore, the capacity to mechanically harvest olives in a short time increases the viability of determining the time of harvest using olive quality as criterium. For these reasons, an efficient method for assessing ripening status is essential for proper olive crop management.

The chemical indicators most used for classifying olives into different commercial qualities are fat content, moisture, and acidity. Traditionally, the assessment of these parameters has been carried out through conventional laboratory techniques using established analytical methods. A common approach for determining acidity in olive fruits involves the titration of olive oil [24]. Fat content can be established through methods like Soxhlet extraction [25] or advanced techniques such as nuclear magnetic resonance (NMR) [26]. Moisture content is typically determined by employing a drying oven and Karl Fischer titration [27]. These traditional chemical methods have adverse environmental consequences due to their extensive solvent usage. Additionally, they demand skilled personnel and specialized laboratory equipment, incurring significant expenses. Furthermore, they are destructive, labour-intensive due to the need for sample collection, and time-consuming, with results often taking several days to become available. This delay can impede timely harvest decisions. All these limitations result in poor spatio-temporal resolution in monitoring. Thus, most growers accomplish homogeneous harvesting supported by subjective criteria such as intuition and visual interpretation. Precise control of the quality of olive fruits would enable optimal crop surface management. Firstly, it would allow for site-specific treatments to address heterogeneity during growth and early ripening phases. Furthermore, growers could devise harvest strategies aimed at diversifying production.

1.4. Precision Oliviculture

The drawbacks of traditional techniques for supporting olive management underline the need to explore alternative approaches and technologies. In this regard, precision farming is highlighted as a potential solution.

Olive cultivation has shown a significant response to improved crop management practices. This is evident in the substantial increase, dating back to the 1980s, in the establishment of research groups dedicated to understanding the biology of the olive

species and its interactions with the environment. These research efforts have contributed to the improvement of crop management practices and the development of innovative cropping systems aimed at establishing more sustainable olive orchards [8,9,15]. As a result, knowledge about olive biology and cultivation has considerably expanded. Research into root system distribution, nutrient absorption, and nutrient balance has enabled the adjustment of inputs to meet the specific nutritional requirements of trees, thereby diminishing the environmental consequences associated with fertilization [17,28,29]. Investigations into the dynamics of transpiration and the assessment of olive tree water status have paved the way for implementing precise deficit irrigation strategies, resulting in a substantial enhancement of water use efficiency [20,30–32]. On the other hand, research into olive fruit maturation and how abiotic stresses affect it has improved crop management techniques for maximizing production and quality [33,34]. All these, along with scientific breakthroughs in other agronomical areas, have increased the efficiency of olive cultivation through more precise crop management strategies. This has given rise to the concept of precision oliviculture, which is understood as the application of the precision farming paradigm to the olive sector.

Precision farming is a management approach designed to assess spatial and temporal variations within an agroecosystem and apply location-specific treatments through the utilization of diverse technologies and methodologies [35]. The variability within a crop is influenced by spatial and temporal variations in factors such as soil quality, partial incidence of plant diseases, exposure to solar radiation and water sources, climate conditions, etc. Thus, unlike the traditional paradigm of agronomic management, which relies on a homogeneous use of resources, precision farming aims to allocate them to plants according to their specific needs in a segmented manner. The main advantages of this practice encompass optimised input usage, reduced environmental impact, enhanced crop yields, and improved product quality. All of these contribute to an increase in crop profitability.

The first milestone to develop precision oliviculture strategies relies on the development of sensors capable of gathering information of interest to support decision-making in the context of olive cultivation. The literature often categorizes sensing techniques into two categories based on the distance between the sensor and the measured object, namely remote sensing, and proximal sensing. The main feature of proximal sensing is the high accuracy of the data compared to remote sensing. However, the larger distance to the object when using remote sensing techniques entails continuous measurements in space, in contrast to proximal sensing, which provides point data that must be spatialized to refer to the entire crop. For these reasons, to effectively define precision farming strategies, it is essential to have a thorough understanding of the variables to be investigated and the appropriate acquisition platform on which they will be deployed. Indeed, the same sensor can yield significantly distinct information when employed on remote sensing or proximal sensing platforms. Thus, a variety of sensors can be used to monitor the numerous variables that exert an impact the plant growth environment.

From a broad perspective, the agronomic variables to monitor for correctly applying precision farming can be divided in variables affecting soil, environment, and crop [36].

Nowadays, some sensors have been standardized for commercial use. Regarding soil, sensors that measure soil water content are common, with those based on electromagnetic methods being among the most widely used (time domain reflectometry [37], time domain transmission [38], capacitance [39], and impedance sensors [40]). Further, conductance and optical techniques can provide insights into soil pH and ionic composition [41]. Another example is the use of electromagnetic induction sensors, which measure the electrical conductivity of the soil. This helps characterize the type of soil and delineate the field into homogeneous zones [42]. Regarding environment, there is a wide range of sensors that characterize different environmental variables of the field. These includes sensors for wind speed and direction (anemometers), sensors for air temperature and humidity (thermistor sensors, thin film resistance sensors, capacitive sensors and hygrometer sensors), sensors for rainfalls (pluviometers), sensors for crop evapotranspiration (lysimeters), optical sensors for measuring CO_2 levels, sensors for sun radiation (pyranometers), and sensors for barometric pressure (piezoelectric barometric pressure, capacitive barometric pressure, resistive barometric pressure, microelectromechanical systems, and microelectromechanical systems) among others [41,43]. Regarding crop status variability, which is the topic addressed in this Thesis, optical sensors are the most used in the context of olive cultivation [44]. These sensors can capture the electromagnetic energy of a focused object (biological tissue). The extent of the electromagnetic spectrum and the different dynamics of interaction between electromagnetic radiation and object arouse a variety of optical sensing techniques [45]. Thus, there are optical sensors based in reflectance measurements (RGB [46], multispectral [47], hyperspectral [48] , Raman [49], visible, near-infrared (VIS-NIR) 'point' spectroscopy [50]), optical sensors based in fluorescence measurements [51], optical sensors based on Light Detection and Ranging (LiDAR) [52], thermal infrared (IR) sensors (thermography) [53], etc.

The electromagnetic energy reflected or emitted by vegetal tissues (leaves, fruits, etc.) is influenced by their chemical composition and structure. Thus, an olive tree in optimal conditions has a specific spectral signature, which can be precisely characterized by means of a set of spectral responses at discrete bands. Accordingly, negative effects suffered by the crop will have an impact on its spectral signature. In the same way, olive fruits undergo physicochemical modifications due to ripening or external disturbances, which may modify their spectral signature. These changes can be evaluated by analysing the three processes of absorption, reflection, and transmission in the spectrum. Therefore, reflectance spectroscopy is based on measuring the reflectance of electromagnetic radiation at different wavelengths in the range from 350 to approximately 2500 nm. This range includes the frequency bands most commonly used in precision farming, such as: visible (VIS), near-infrared (NIR), and shortwave infrared (SWIR). The spectral sensors may be cameras with the ability to capture images (raster information) in various spectral bands or point sensor that give just one measure of a

focused area. Regarding spectral cameras, their utilization varies based on the spatial, spectral, and temporal resolutions they provide. The spatial resolution is defined as the size of the area represented in a single pixel, which depends on the field of view of the sensor and the focus distance. Spectral resolution is determined by the range of the electromagnetic spectrum covered, the number of spectral bands acquired, and the width of those spectral bands. Temporal resolution is linked to the hosting platform of the sensor rather than the sensor itself, and it denotes the time interval between successive acquisitions of the same object. Remote sensors can be classified based on their mode of operation, type of acquisition, and the number of covered bands, including multispectral and hyperspectral. On the other hand, fluorescence sensors measure the emission of visible light that occurs when certain compounds, such as pigments (chlorophyll, carotenoids, anthocyanins, etc.) absorb light at a specific wavelength and then emit light at a different wavelength. Both reflectance and fluorescence sensors can be categorized as active or passive, depending on whether they use an artificial light source or measurement is based on ambient light. Anyway, the acquired spectral variables are processed through mathematical techniques to establish a quantitative or qualitative relationship with the agronomical parameter of interest. Once the calibration model is developed and validated, it can then be used to characterize new samples.

LiDAR sensors use the Time-Of-Flight (TOF) principle to determine the distances of objects based on the time interval between laser pulse emission and return, upon backscattering from an object. In an agronomical context, LiDAR can be used to acquire a point cloud of returns, providing a 3D digital representation of the vegetation environment, where each point is characterized by an XYZ coordinate. This highly specific 3D point cloud has the potential to develop methodologies for directly retrieving canopy structural attributes. Similar approaches have been proposed but based on ultrasonic sensors [54]. In this case, the emitted signal, whose return time is used to calculate the distance to the target, is an ultrasonic wave instead of a laser beam.

Thermal IR sensors are commonly used in thermography, a technique that involves measuring the infrared radiation emitted by objects to determine their temperature. Emissivity is a material property that describes how efficiently a surface emits thermal radiation compared to an ideal black body at the same temperature. A value of 1 indicates perfect emissivity (ideal black body), while lower values indicate less efficient emission. Thus, knowing the emissivity value of vegetation makes it possible to determine its temperature based on the infrared radiation emitted by it, which has been shown to be related to the water status of crops.

Each source offers unique information, highlighting the importance of understanding their specific capabilities. This Thesis is focused on optical sensors due to their high potential for precision farming applications and the availability of low-cost solutions. In the following sections, we will discuss the state of the art in the use of optical sensors for assessing nutritional status, water status, and fruit quality in the context of olive cultivation.

1.4.1 Nutritional status assesstment of olive trees

In precision agriculture, sensors capable of detecting electromagnetic energy reflected or emitted by plants are used to identify nutritional deficiencies. This is because leaf reflectance is influenced by various factors, including the presence or absence of specific molecules and environmental conditions in certain regions of the electromagnetic spectrum. For example, in VIS wavelengths, leaf reflectance is influenced by photosynthetic pigments like chlorophyll a, chlorophyll b, and carotenoids, while in the NIR, it's affected by leaf structure, the presence of water, and substances like lignin, cellulose, starch, proteins, and nitrogen. Given that modifications in photosynthetic activity are related to plant health and, therefore, to nutritional status, the spectral response of the canopy within these specific spectral regions can serve as a valuable tool for predicting these parameters [55]. The first attempts to model the nutritional status of olives using spectral data were based on parametric regression methods, with the most popular being vegetation indices (VI). These are numerical metrics or mathematical formulas calculated from few bands that correlate with qualitative parameters of vegetation such as the health, and vigour of plants [56]. There are numerous VI with different agronomic significance; nevertheless, the most popular in olive cultivation are the normalized difference vegetation index (NDVI) [57] and the soil-adjusted vegetation index (SAVI)[58]. The NDVI is a normalization between the red and near infrared bands. Due to the normalization process involved in its calculation, NDVI values fall within a range of 0 to 1, having a sensitive response to canopy growth or vigour. On the other hand, the SAVI was designed to improve the sensitivity of NDVI to soil background. For this purpose, SAVI introduces a correction factor, ranging from 0 to 1, based on the degree of vegetation coverage. When this value is close to 0, SAVI is equal to NDVI. The main drawback of these kinds of VIs is their unspecific character, as they are influenced by several abiotic and biotic sources of stress, beyond nutritional stress [59,60]. Thus, these VIs offer a qualitative estimation of plant vigour, which can correlate with a variety of stress factors. So, despite bringing useful information, their use in an agronomic context requires expert interpretation.

Traditionally, the definition of VIs was logically inferred from the knowledge of the relationship between the spectral bands used and the agronomic significance of the respective index [59]. Afterwards, the advent of linear nonparametric regression methods such as partial least squares regression (PLSR), along with pre-process methods for spectral data (smoothing, standard normal variate, first and second derivative, etc.), improved the precision and information obtained from VIs [61]. PLRS techniques allow to extrapolation of spectral information of the crop from the entire reflectance spectrum (350–2500 nm). For this purpose, PLSR reduces the high collinearity found in high spectral resolution spectra by compressing the data into non-correlated principal components [62]. This mathematical approach enables the extraction of information from a broader spectrum and the development of quantitative models for biophysical parameters of vegetation, in contrast to the qualitative estimation provided by VIs. In this regard, PLRS models fed with hyperspectral data have been used to predict the leaf

nitrogen content (LNC) of olive trees [61,63]. Further, PLRS models have been evaluated with combined approaches based on the use of NIR spectroscopy and portable energy dispersive X-Ray fluorescence for the estimation of the leaf content of additional nutritional elements of olive trees [51].

The advances in data sciences have generated nonlinear nonparametric regression methods (machine learning), which have demonstrated high potential for modelling spectral data [64]. In this regard, some researchers have evaluated the potential of new machine learning methods for modelling the nutritional status of plants using spectral data, although in crops different from olive [65–68].

1.4.2 Water status assesstment of olive trees

Precision irrigation in olive orchards has contrasting benefits on crop development and production [69]. The spatially variable application of water supposes a more sustainable crop management offering environmental and economic adventages (cost reduction, improved equilibrium between production and vegetation, and enhanced quality of the final product) [20]. However, proper utilization of precision irrigation strategies requires suitable methods to characterize the water status of the crop. For that purpose, numerous aproaches have been proposed.

Indirect estimations of water status are done either from soil water content or meteorological measurements. Soil water measurements are simple to conduct and comprehend. A diverse array of methods and instruments are available for both direct and indirect measurement of soil moisture content, including neutron probes and a wide range of capacitance or electromagnetic sensors such as time-domain reflectometry, capacitative probes, resistance probes, etc. Most of these instruments exploit the distinction in dielectric constants between water and other soil components. Therefore, their output signals can be directly correlated with moisture content. In contrast, resistance and voltaic probes are more reliant on the conductive properties of soil solutions [70]. The main drawback of this kind of devices is that they are proximal sensors with a limited spatial resolution, so the substantial spatiotemporal variability, typically present in cultivated soils, constrains their effectiveness for irrigation scheduling. On the other hand, methods based on meteorological measurements have been the most widely used in traditional olive management. In this sense, the crop coefficient approach is the most acknowledged [71]. In addition to meteorological data, this method requires accurate coefficients related to the specific crop and the fraction of soil covered by the canopy. Published values of both coefficients are available, but their empirical nature limits their use in orchards with varying characteristics or locations. This issue has been addressed by several authors, who have proposed different variations of the original index [72,73]. The crop coefficient method and its adaptations are indeed valuable for scheduling irrigation in olive orchards. Nonetheless, the empirical nature of the method and its inability to offer real-time assessment of crop water requirements, which entails the recording of meteorological variables over specific

time periods before calculating potential evapotranspiration, curtail its suitability for precision irrigation.

The limitations of methods for assessing water needs from soil and meteorological measurements have spurred the development of approaches that rely on plant-based measurements. The advantage of plant-based methods lies in their ability to encompass the plant's response to the water conditions in both the soil and the surrounding atmosphere. Also, certain plant-based methods enable continuous and automated data recording and can be readily integrated with data transmission systems, leading to a high temporal resolution. This applies to methods reliant on measurements of sap flow, trunk diameter fluctuations, and leaf turgor pressure. However, these approaches rely on proximal sensors that can measure a single individual, so achieving a truly representative spatial resolution would require a large number of sensors, resulting in unprofitable costs.

The most promising methods to monitor the water status of olive trees are those based on optical techniques, such as thermography and/or spectral imaging [74]. Termal and spectral images can be captured both at the plant level (ground-based imagery) and from above the crop (airborne imagery). The fact that these approaches are based on proximal/remote sensors provides a higher spatial resolution compared to those based on direct measurements on plants. Indirect evaluations of the water status of olive trees through spectral imaging are viable because water content can significantly impact the spectral signatures of the crop [75]. The electromagnetics regions that are more influenced by water status are the visible (VIS), near infrared (NIR), and shortwave infrared (SWIR) domains. Research studies have reported good estimations of olive leaf water potential by means of VIs based on the canopy reflectance of these spectral regions. The VIs more suitable in this sense were the moisture stress index (MSI) and the normalized difference water index (NDWI), which combine SWIR and NIR wavelengths, finding poorer performances with the VI based just on the VIS domain [76]. While the use of VIs appears promising for managing crop water stress, it is worth noting that high correlations are not consistently observed. This is because water stress is a condition that can lead to changes in leaf structure and its spectral response, but these alterations may not always manifest in the short term. Furthermore, water stress is intertwined with various other stress factors, including nutrition and the management of the olive grove itself. These complexities can affect the reliability of VIs as the sole indicator of water stress.

On the other hand, thermography-based aproaches rely on the isohydric behaviour of olive trees. The isohydric behaviour is a feature of plant species adapted to drought conditions. It consist of the regulation of the degree of stomatal opening as a function of the water availability. The relationship between leaf temperature and stomatal regulation is well-known [77–79]. The leaf transpiration involves water loss throught the stomata, which changes from liquid to gas due to the evaporation process. Briefly, solar radiation increases the energy levels of the water molecules near the stomata, raising their kinetic energy until it surpasses the cohesion exerted by the surface tension of the

water, causing it to change to gas and flow into the atmosphere. As molecules with higher energy escape and those that remain have lower average kinetic energy, the temperature of the leaves decreases. As mentioned above, the isohydric behavior allows olive trees to regulate transpiration rates to prevent water loss. Therefore, the temperature of the leaves of a tree with sufficient water availability should be close to the air temperature, while in the case of stressed trees, it should be higher. However, leaf temperature itself is unsuitable as a water strees indicator, as it is highly susceptible to environmental conditions. For these reasons, it is preferred to use normalized indices [60,80], among which the most widely used is the crop water strees index (CWSI). This index was proposed by Jackson et al. (1981) [81] and Idso et al. (1981) [82] and can take values within the range of 0 to 1, signifying varying degrees of crop stress and well-irrigated conditions, respectively. The correlation between CWSI and numerous water strees parameters such as stem water potential, leaf water potential, leaf transpiration rate, and stomatal conductance, has been widely demostrated [32,83,84]. Nevertheless, its calculation seem to be under slight discusion. The calculation of the CWSI relies on two thresholds: the non-water-stressed baseline (T_{wet}), which represents a fully transpiring crop, and the maximum stressed baseline (T_{dry}), which corresponds to a non-transpiring crop. The accurate determination of these thresholds is crucial to ensure the precision of CWSI as an indicator of water stress. Numerous aproaches have been proposed to calculate both baselines. In this sense, T_{wet} can be determined through several methods, such as: (1) the non-water stress baseline (NWSB) using a linear regression function between canopy temperature (T_{canopy}), air temperature (T_{air}), and vapor pressure deficit (VPD) [81]; (2) the wet artificial reference surface (WARS), which mimics crops in abundant water status and is considered as the temperature of a fully transpiring crop [85]; and (3) a statistical method based on histogram analysis of canopy temperature [86,87]. On the other hand, several approaches have also been proposed for the estimation of T_{dry}, such as: (1) a mathematical estimation based on meteorological variables related to isothermal radiation [79,88]; (2) a dry reference leaf coated with vaseline to avoid transpiration [79]; (3) an empirical method based on adding a fixed threshold of 5-7 °C to the air temperature [83,86]; and (4) a statistical method based on histogram analysis of canopy temperature [86,87]. All these aproaches have been proved with good results in several crops. However, there is no consensus on which method is the most suitable.

1.4.3 Fruit quality assesstment

Assessing fruit ripeness through proximal and/or remote sensing is indeed an area of growing interest in agriculture. Spectral imaging techniques are among the most promising technologies for assessing fruit quality in a non-destructive manner [89–91]. Numerous studies have demonstrated the suitability of spectral sensing for the characterization of fruit ripeness in several crops [92]. Concerning olive sector, spectroscopy, including both visible and near-infrared (VIS-NIR) spectroscopy and other related techniques, has been widely used in the olive oil production process for various purposes [93]. This non-destructive technology enables the determination of

several important properties at different stages of the process. Some of the applications of spectroscopy in olive oil production include:

- Olive paste quality: Spectroscopy is used to assess the quality of the olive paste obtained during the crushing or pressing of olives. It can help identify issues such as paste homogeneity, moisture content, and oil content [94,95]. These techniques show accuracy comparable to those provided by standard chemical methods, with the advantages of involving less intensive sample handling, fewer reagents and solvents, and being faster.
- Monitoring oil extraction: During the olive oil extraction process, spectroscopy can be employed to monitor various parameters, including oil content in the paste, oil quality (acidity, peroxide value, etc.), and the presence of impurities [96].
- Oil quality analysis: Spectroscopy can determine the chemical composition and quality of the final olive oil product. This includes assessing parameters such as acidity, peroxide value, and fatty acid composition [97–99].
- Authentication and adulteration detection: Spectroscopy can be used to detect adulteration or verify the authenticity of olive oil products by analysing their spectral profiles. This is especially important in ensuring the quality and authenticity of extra virgin olive oil [100].
- Process Optimization: Spectroscopy can aid in optimizing the olive oil production process by providing real-time data on key parameters, enabling producers to make adjustments as needed [101,102].

These applications demonstrate the versatility and utility of spectroscopy in the olive oil production industry, helping ensure the quality and authenticity of olive oil products. However, this Thesis is centred in the agronomic application of remote sensing to assess the maturity of olive fruit, which is crucial for making more informed decision regarding crop management, as well as determining the optimal time for harvesting. In this regard, it is especially interesting the estimation of quality parameters directly from intact olive fruits. The use of spectral sensing to characterize intact olive fruits is a relatively mature topic. The first approaches intended to estimate quality parameters of intact olive fruits were accomplished in laboratory conditions. In this sense, portable NIR systems have been evaluated to assess oil and moisture content of intact olive fruits as a decision support tool in olive breeding programs [103,104]. Other works have explored the potential of NIR Acousto-Optical Tunable Filter (NIR-AOTF) technology for determining the oil content and phenolic compounds of olive fruits of different varieties at various stages of development [105,106]. Additionally, NIR diode array systems integrated onto a conveyor belt have been evaluated for assessing moisture, acidity, and oil content in intact olive fruits [107]. Afterwards, the same authors conducted a comparison between the mentioned methodology and an offline system based on a grating monochromator, obtaining similar accuracy between the online and offline approaches [108]. Previous research had studied the suitability of the NIR spectrum to predict moisture and oil content in fresh olives with promising results [109]. Indeed,

laboratory NIR scanners are currently commercially available for determining basic chemical parameters of intact olives [110]. The strong correlation between the NIR spectral range and the quality indicators of olive fruits is attributed to the reflectance response of chemical groups linked to these parameters. These chemical groups in the NIR spectral range include water (1460 and 1920 nm, associated with hydroxyl groups) and fat content (1145 nm, 1160 nm, 1175 nm, 1185 nm, 1210 nm, 1245 nm, 1260 nm, and 1275 nm, linked to aliphatic esters, alkyl groups, and alkenes).

The potential of other spectral regions such as VIS and mid-infrared (MIR) to assess quality parameters of intact olive fruits has also been demonstrated. In this sense, the combined use of NIR and MIR spectral bands to predict water and oil content of olive fruits has demonstrated advantages compared to using the NIR and MIR bands separately [111]. Other studies have reported on the potential of portable VIS/NIR spectrometers for predicting oil content and other quality parameters such as moisture, and free acidity of intact olives [112–114]. The predictive ability of the VIS spectral domain for ripening indicators of olives is attributed to the correlation between the evolution of these parameters and the colour changes experienced by the fruits. These colour changes result from alterations in the composition of pigments in the olives as they ripen. During the ripening process, olive fruit accumulates anthocyanins as its oil content increases. Simultaneously, as ripening advances, photosynthetic activity diminishes, and the concentration of both chlorophylls and carotenoids progressively decreases. Finally, at the end of the maturation process, the fruit takes on a violet or purple hue due to the accumulation of anthocyanins (Figure 3) [115].

Figure 3. Colour changes in olive fruits from early to advanced maturation stages.

The adaptation of these methodologies to in-field operations would offer numerous advantages, including simultaneous multiple measurements and real-time decision-making. However, the impact of environmental variables (temperature, moisture, pressure, ambient light, etc.) on NIR measurements, which are easily controlled under laboratory conditions, poses a challenge for applying such methodologies in the field. Consequently, approaches utilizing spectral sensing to assess the ripening status of olives under field conditions are scarce. Despite this challenge, several authors have addressed these issues. In this sense, comparative studies using portable NIR-AOTF spectrophotometers for assessing quality parameters of intact olive fruits, both in field and laboratory conditions, have concluded that although slightly better results are

obtained under laboratory conditions, the results obtained in the field are also accurate enough to decide the optimal harvest date [116,117].

1.5. Challenges and future perspective of Precision Oliviculture

Precision oliviculture, with its focus on leveraging technology for optimized and sustainable olive cultivation, faces several challenges and holds exciting prospects. The precision farming management of olive cultivation has various areas for improvement, such as the development of sensors with higher capabilities, the implementation of better mathematical modelling methods, the automation of data collection, and cost reduction.

The continuous advancement in the electronics industry makes sensors with better capabilities available to the agricultural sector. Specifically, in the field of spectral vision, devices with increased spatial and temporal resolutions are emerging. For example, the latest generation hyperspectral systems can acquire multiple narrow spectral bands across a wide range, covering from the visible domain to the deep infrared. Thus, it is foreseeable that advancements in the engineering industry will offer devices capable of capturing variations in the spectral signature of vegetation related to changes in parameters of interest for agronomic management with greater precision. Furthermore, resources for data modelling have expanded with new data-driven approaches, such as machine learning. Machine learning regression algorithms have the potential to generate adaptive, robust relationships, and once trained, they can be applied very quickly. Typically, machine learning methods can handle the strong nonlinearity of the functional dependence between the biophysical parameter and the observed reflected radiance. The combination of technical advances in sensor technology with improvements in mathematical modelling methods opens the door to confirming previous work and continuing to enhance these methodologies for achieving operational applications.

Another area for improvement in precision oliviculture is the automation of data acquisition. Increasing the temporal resolution of the measurements enhances the representativeness of the monitoring methodologies. For this purpose, it is necessary to separate the data collection process from human intervention. Otherwise, the associated costs due to the required workforce would make it economically unfeasible to carry out monitoring with sufficient spatio-temporal resolution. Recently, an increasing number of researchers have integrated imaging technology with various monitoring platforms, applying these integrated approaches to orchard management, moving beyond empirical baseline monitoring [118]. Depending on the scale of the surface to be monitored and the type of data to be collected, there are different types of data acquisition strategies. These approaches encompass handheld devices manually operated, wireless sensor networks, unmanned ground vehicles (UGV), unmanned aerial vehicles (UAV), aerial sensing (including drones and planes), and spectral satellite sensing. Traditionally, human observers visually inspect and monitor crops, soil conditions, and other agricultural parameters. This method is labour-intensive and may lack scalability for large areas, but it also implies a subjective component related to human perception. Handheld devices, such as spectrometers or portable sensors, are

used for on-site measurements. This allows for more specific and targeted data collection compared to manual observation, but it also lacks scalability. Networks of sensors strategically placed across an agricultural area collect real-time data, offering continuous monitoring. However, the spatial resolution is limited by the cost of each node and the size of the surface area to be monitored. UGVs equipped with sensors traverse agricultural fields, collecting data. This method improves efficiency and reduces the need for manual labour. UAVs equipped with various sensors (such as cameras, multispectral, or hyperspectral sensors) fly over agricultural fields to capture high-resolution imagery. They provide detailed and timely information about crops. However, the implementation of data acquisition based on unmanned platforms (UGV and UAV) poses engineering challenges. Larger aircraft, including planes, may be equipped with advanced sensors for broader coverage of agricultural regions. These platforms can cover extensive areas efficiently but may require specialized equipment, and the flight missions involve hight costs. Satellites equipped with spectral sensors capture data over large agricultural areas. However, it also has limitations for certain aspects of orchard management characterization, primarily due to the lack of spatial resolution. Each monitoring platform has its own advantages and limitations, and the choice depends on factors such as the scale of the operation, the desired level of detail, and the frequency of data collection. Advances in technology continue to enhance the capabilities of these monitoring platforms in precision agriculture. Thus, future research efforts should be aimed at standardizing data collection protocols based on autonomous platforms to assess parameters of interest for crop management.

Improving the affordability and user-friendliness of precision agriculture methodologies is also an area for improvement. Most current precision farming methodologies are based on expensive equipment, which requires expert knowledge for its use. These facts restrict the applicability of these methods in smallholder farming settings, which constitute a significant portion of the productive sector in many countries. Thus, the adoption of precision oliviculture practices may require significant investments in technology and training for farmers. Overcoming financial barriers and providing accessible training programs will be essential for widespread adoption and success. Enabling the widespread use of precision oliviculture techniques would have a twofold benefit for the olive sector. On the one hand, comprehensive control of crop development would allow for the implementation of actions to mitigate the natural variability of the crop. This includes different maturation rates, partial incidence of plant pathogens, or unequal efficiency in the use of hydrological or nutritional resources, among other factors. On the other hand, the widespread and continuous use of these technologies would yield a vast amount of information, enabling the inference of valuable knowledge about how biotic and abiotic factors affect the crop. Thus, the olive crop management paradigm would have a broad scope for improvement. All these factors would result in more profitable crops and would provide the agri-food industry with better resources to generate products with higher added value. However, all of this involves developing user-friendly innovative solutions, affordable for all kinds of growers.

This goal is becoming increasingly feasible thanks to improvements in the electronics industry. Enhancements in hardware technology have resulted in sensors with higher performance at lower prices. Additionally, innovative software designs bring algorithms that improve the capacity to model biophysical parameters of vegetation using information acquired by these sensors. These factors have motivated a trend toward the development of affordable sensors for agronomic use [50,119,120]. In this sense, custom build devices based on low-cost NIR sensors have been tested to measure chlorophyll content in rice leaves as an indicator of nitrogen needs [121]. The potential of commercially available, low-cost, portable NIR sensors for estimating quality parameters of kiwifruit, apples, feijoas, and avocados have been compared with more expensive spectrometers obtaining promising results [122]. Furthermore, methodologies have been proposed for plant stress detection and field mapping based on a low-cost, handheld multispectral device utilizing NDVI assessment. This approach is based on a device that incorporates an integrated multispectral light source, including four wavelengths (850, 630, 535, and 465 nm). This setup allows for the simultaneous illumination and reception of leaf reflectance measurements. The reflectance measurements are wirelessly transmitted to Android-operated devices for processing and data storage. The performance of this system was compared in laboratory conditions against a hyperspectral device and a handheld commercial multispectral sensor, and in field conditions against the multispectral sensor [123]. Other studies have demonstrated the suitability of custom-built multispectral devices, based on low-cost optical sensors (AS7265x, ams-OSRAM AG, Premstätten, Austria), for assessing the percentage of grass cover and vine vigour in field conditions [124]. The same optical sensor has been used to develop a photosynthetically active radiation (PAR) sensor, which was evaluated indoors and outdoors, yielding results that surpassed those obtained by commercially available lab-grade PAR sensors [125]. The same optical sensor has also been employed in developing a spectroscopic system intended to monitor nitrogen changes in nutrient solutions for micro indoor smart hydroponics systems [126]. These works serve as evidence of the potential of low-cost systems for agronomic applications.

1.6. Motivation of the Thesis

Given the context described above, this Thesis, presented as a collection of high impact published articles, encompasses research conducted over the past four years. Its objective is to contribute to the state of the art of precision agriculture techniques within the olive sector. As detailed, significant scientific efforts have been made in recent decades to enhance the economic and environmental sustainability of the olive sector. This has manifested in the development of new cultivation systems and management approaches. However, even in the present day, certain innovations still raise uncertainty about their profitability and appear insufficient to address the challenges faced by the olive industry. Hence, there exists an opportunity to enhance the olive sector through the adoption of precision agriculture techniques. Therefore, this Thesis addresses various issues related to olive cultivation. In broad terms, the themes addressed in this Thesis encompass technologies supporting irrigation, fertilization, and fruit quality assessment within the context of olive cultivation. One of the primary challenges in

standardizing precision agriculture techniques at a commercial scale is ensuring their economic viability. Many of the methodologies proposed at the research level rely on expensive equipment that is out of reach for the majority of olive growers. Furthermore, these equipments also require an expert knowledge for their use, which distances them from the general user. For these reasons, this Thesis aims to leverage advances in the electronics industry and new data-driven approaches to develop methods that support olive management, with a special focus on making them affordable in terms of both economy and ease of use.

1.7. Scientific contributions of the Thesis

This Thesis is presented as a compilation of publications. In this format, four articles published in high-impact indexed journals, along with an additional work currently in peer review process, are put forward as the focal point of the dissertation. These works represent the milestones achieved throughout the conducted research, aligning with the initially established lines of argument. Below, the works are listed, offering details about their publication, and providing a concise overview, including their significant novel contributions to the state of the art. In Section 4, a comprehensive overview of the mentioned works can be found. Additionally, a utility model granted in the context of the research conducted during the realization of this Thesis has been included.

Article 1. A new low-cost device based on thermal infrared sensors for olive tree canopy temperature measurement and water status monitoring.

Authors: Miguel Noguera, Borja Millán, Juan José Pérez-Paredes, Juan Manuel Ponce, Arturo Aquino, and José Manuel Andújar.

Journal: Remote Sensing (ISSN: 2072-4292).

Editorial: MDPI.

Reference: Remote Sens. 2020, 12(4), 723.

DOI: 10.3390/rs12040723

Year: 2020

Quality index (Journal Citation Reports®, 2020): 27/200 (Q1) in the category "Geosciences, Multidisciplinary", 10/32 (Q2) in the category "Remote Sensing", 8/29 (Q2) in the category "Imaging Science & Photographic Technology", and 76/274 (Q2) in the category "Environmental Sciences". Impact Factor of 4.848.

This work comprises the development and evaluation of a low-cost thermal infrared sensor for assessing water status of olive trees based on its canopy temperature. The relationship between leaf temperature and water status in species with isohydric behaviour is a relatively mature topic. However, most research aimed at assessing the water status of olive trees using thermal sensors has been conducted with expensive equipment that is unaffordable for most olive growers. With this background in mind, the goal of this research was to develop a tool for supporting decisions regarding water

use management that is affordable for all kinds of olive growers. In the first instance, the performance of the developed device was compared with that of a commercial thermal camera. Once the accuracy of the low-cost IR thermal camera was demonstrated, a field evaluation was conducted. For that purpose, an experimental setup was implemented to induce different levels of water stress in a commercial SHD olive orchard. The canopy temperature measured with the proposed device and the Crop Water Stress Index (CWSI) calculated from it, were compared with two widely accepted water status indicators (predawn leaf water potential and stomatal conductance). The obtained results were promising, reaching coefficients of determination (R^2) over 0.79. Furthermore an adaptive method, inspired by the one proposed by Park et al. [87], was suggested for obtaining the thresholds required to calculate the CWSI. This approach simplifies the automation of water status monitoring, as the reference baselines needed to calculate CWSI are extracted directly from thermal images, avoiding the need for the measurement of artificial surfaces or meteorological variables. The outcomes provided by the developed device support its suitability for fast, low-cost, and reliable estimation of olive grove water status, even eliminating the need for supervised acquisition of reference temperatures. The newly developed device can be used for water management, reducing water usage, and for overall improvements to olive orchard management.

Article 2. Nutritional status assessment of olive crops by means of the analysis and modelling of multispectral images taken with UAVs.

Authors: Miguel Noguera, Arturo Aquino, Juan Manuel Ponce, António Cordeiro, José Silvestre, Rocío Calderón, Maria da Encarnação Marcelo, Pedro Jordão, and José Manuel Andújar.

Journal: Biosystems Engineering (ISSN: 15375110).

Editorial: Elsevier.

Reference: Biosystems Engineering. 2021, 211, 1-18.

DOI: 10.1016/j.biosystemseng.2021.08.035

Year: 2021

Quality index (Journal Citation Reports®, 2021): 8/59 (Q1) in the category “Agriculture, Multidisciplinary”, and 4/14 (Q2) in the category “Agricultural Engineering”. Impact Factor of 5.002.

The main novelty of this work is that it provides evidence that monitoring olive tree leaf Phosphorus content (LPC) and leaf Potassium content (LKC) using spectral data acquired under field conditions may be viable. To the best of our knowledge, most attempts in the development of non-destructive methods for plant nutrient status assessment using spectral data have focused on modelling foliar nitrogen content (LNC). In fact, the majority of the few studies that focused on LPC and LKC estimation have been conducted under laboratory conditions at the leaf scale [67,127–129]. In this sense,

the proposed image processing methodology is an essential part of the approach, as it is crucial for the accurate acquisition of spectral information from a zenithally perspective using a UAV. This is because this image processing allows the isolation of canopy pixels, discarding background information by using a digital surface model (DSM). In this manner, the proposed approach can accurately segment olive canopies, being robust against the presence of shadows, weeds, or other common distractors. The five reflectance data extracted from the processed images were used as input to train several retrieval techniques (partial least squares regression, artificial neural network (ANN), support vector regression, and Gaussian process regression) using ground truth values of NPK leaf content as a reference. The ANN models yielded the best results among the evaluated retrieval techniques (LNC (R^2 = 0.63), LPC (R^2 = 0.89), LKC (R^2 = 0.93)). The obtained results indicate the potential of the proposed methodology to support fertilization decisions in the context of olive management. Moreover, it should be stressed that, contrary to other solutions, the one presented in this paper could be potentially affordable for small-scale growers, as it does not make use of expensive sensors like LiDAR or hyperspectral devices, nor heavy unmanned aerial vehicles.

Article 3. Methodology for olive fruit quality assessment by means of a low-cost multispectral device.

Authors: Miguel Noguera, Borja Millan, Arturo Aquino, and José Manuel Andújar.

Journal: Agronomy (ISSN: 2073-4395).

Editorial: MDPI.

Reference: Agronomy. 2022, 12(5), 979.

DOI: 10.3390/agronomy12050979

Year: 2022

Quality index (Journal Citation Reports®, 2022): 16/88 (Q1) in the category “Agronomy”, and 60/239 (Q2) in the category “Plant Science”. Impact Factor of 3.700.

Olive fruit ripening characterization is a critical factor for olive growers. The traditional chemical methods imply numerous limitations (requirement for expert personnel, tedious procedures, high cost, etc.). These limitations result in a poor spatial-temporal resolution in monitoring and compel growers to adopt homogeneous harvesting based on subjective criteria such as intuition and visual decisions. In the last decades, spectroscopy-based approaches have been proposed as an alternative to chemical methods. However, these approaches rely on the use of hyperspectral devices, whose complexity and high cost limits their applicability for smallholder farming settings. In response to this context, the present work was aimed at conducting an initial evaluation of the capabilities of a low-cost multispectral sensor for assessing quality parameters of intact olive fruits. To that end, a prototype based on this component was developed and evaluated in an experiment carried out under controlled laboratory conditions. A set of 507 olive samples were analysed with the proposed device. After data pre-processing,

artificial neural network (ANN) models were trained using the 18 reflectance signals acquired by the sensor as input and three olive quality indicators (moisture, acidity, and fat content) as targets. The responses of the ANN models were promising, reaching coefficient-of-determination values of 0.78, 0.86, and 0.62 for fruit moisture, acidity, and fat content, respectively. The performance demonstrated by the proposed system was promising, indicating its potential for assessing the quality status of intact olive fruits. The low-cost and ease of use of the proposed system pave the way for the implementation of an olive fruit quality appraisal system affordable for all olive growers. Thus, this work represents the first step toward the development of a handheld device specifically designed for in-field applications.

Article 4. Olive fruit ripening assessment under field conditions based on a low-cost multispectral device and ANN models.

Authors: Miguel Noguera, Borja Millan, Arturo Aquino, and José Manuel Andujar.

This article, yet to be published, extends the study carried out in the previous work aiming to transfer the results obtained in laboratory conditions to an in-field scenery. The promising results obtained with the initial prototype encouraged the development of a second device adapted for use under field conditions. Thus, a handheld device was designed based on the same multispectral sensor. The remaining components of the device had to be adapted to give it a compact form and make it capable of operating in-field conditions without the need for the support of other devices. Once developed, a field experiment was conducted to evaluate the potential of the device. During two consecutive campaigns, the ripening process of an olive experimental field was monitored in parallel with the proposed device and traditional methods. Thus, a dataset of ground truth values of various ripening indicators (oil content per dry matter (OCDM), oil content per fresh weight (OCFW), moisture (M), and titratable acidity (TA)) and the spectral signature of the respective samples was acquired. Afterwards, these parameters were used as targets to develop ANN models fed with the 18 reflectance values of the samples, after being corrected. The results of this work had some disparities respect the obtained in the previous research. Concretely, the estimation of OCDM (R^2 = 0.86), OCFW (R^2 = 0.86), and M (R^2 = 0.89) were better than those obtained in laboratory conditions for OCFW (R^2 = 0.62), and M (R^2 = 0.86), while the estimation of TA in this work (R^2 = 0.21) was worse than that obtained previously (R^2 = 0.86). Even considering that fact, the obtained results were also promising, indicating the potential of the developed device to assess quality parameters of olive fruits in-field conditions. Thus, the present work paves the way for the implementation of an affordable useful tool for supporting management decisions related to olive maturation, such as determining the optimal moment for harvest.

Article 5. New, low-cost, hand-held multispectral device for in-field fruit-ripening assessment.

Authors: Miguel Noguera, Borja Millan, and José Manuel Andújar.

Journal: Agriculture (ISSN: 2077-0472).

Editorial: MDPI.

Reference: Agriculture. 2023, 13 (1), 4.

DOI: 10.3390/agriculture13010004.

Year: 2023.

Quality index (Journal Citation Reports®, 2022): 17/88 (Q1) in the category "Agronomy". Impact Factor of 3.600.

This work is part of complementary research aimed at evaluating the potential of the proposed device for assessing quality indicators of red grapes. For that purpose, a field experiment in a commercial vineyard was carried out. The developed device was used to acquire the spectral signature of eighty red-grape samples in a date close to the optimum time for harvesting according to the winery's manager. Subsequently, the grape samples were analysed using standard chemical methods to generate ground-truth values of ripening status indicators (soluble solid content (SSC) and titratable acidity (TA)). The eighteen pre-process reflectance measurements were used as input for training artificial neural network models to estimate the two target parameters (SSC and TA). The obtained results were promising (R^2 = 0.70 for SSC; and R^2 = 0.67 for TA), indicating the potential of the developed device to provide valuable information related to crops other than olive trees.

Industrial and intellectual property. Sistema para la monitorización del estado fisiológico de cultivos y del desarrollo del fruto.

Authors: José Manuel Andújar Marquez, Juan Manuel Ponce Real, Arturo Aquino, Martín, Borja Millán Prior, Diego Tejada Guzmán, Miguel Noguera Manzano, Juan Manuel Enrique Gómez, and Antonio Javier Barragán Piña.

Type of grant: Utility model.

Entity holding the rights: Universidad de Huelva.

Request number: U202231923.

Country of registration: Spain.

Grant date: 24/04/2023

The outcomes obtained as consequence of the realization of this Thesis were materialized in the grant of a utility model. The invention comprises a network of multispectral sensors for continuous monitoring of the crop's water and nutritional status and the

ripening status of fruits. The present invention consists of two types of nodes, one for foliar monitoring and the other for monitoring fruit ripening, distributed in a variable number depending on the crop's extension. Both nodes have multispectral sensors that allow determining the absorption spectrum in the case of the canopy and the reflectance spectrum in the case of fruits. From this information, the physiological state of the crop and the ripening status are estimated through computer tools. The data collected by the entire sensor network are wirelessly transmitted to the cloud and collected and integrated by a server.

2. Objectives and methodology

2.1. Objectives

This Thesis addresses the potential of spectral sensing technologies to provide solutions to the olive sector within the scope of precision Agriculture, placing special emphasis on the development of economically affordable and user-friendly technologies. In a broad context, the main goal of the conducted research is to develop various methodologies based on spectral sensing to assess agronomic parameters of interest. These methodologies aim to support olive management, optimizing the use of agricultural inputs, and enhancing the efficiency of the olive sector in economic and environmental terms. To that end, several issues related to olive grove management were addressed in the research carried out. Broadly, the themes dealt with in this Thesis can be separated into technologies for the support of irrigation, fertilization, and fruit quality assessment in the context of olive cultivation. The specific objectives stablished for the development of this Thesis are presented below:

- **Objective 1. Development and evaluation of a low-cost device based on a thermal infrared sensor to assess water status of olive trees.**

  The isohydric behaviour of olive trees cause that water availability has an impact on the temperature of its canopy. Based on this fact, it was proposed a low-cost thermal infrared device as a tool for identify trees under water stress conditions in a commercial super hight density olive orchard.

- **Objective 2. Development of a methodology to assess the nutritional status of olive trees based on the analysis and modelling of multispectral images taken with an UAV.**

  The interaction between electromagnetic energy and the olive tree canopy is influenced by its nutritional status. Based on this principle, a methodology was proposed to assess the foliar content of N, P, and K using algorithms fed with spectral data extracted from multispectral images acquired with an UAV.

- **Objective 3.1. Evaluation of the capabilities of a low-cost multispectral sensor for assessing quality parameters of intact olive fruits under laboratory conditions.**

  The electromagnetic energy reflected by olive fruits varies throughout the ripening process. On this basis, a methodology was proposed to characterize quality parameters of intact olive fruits using algorithms fed with spectral data acquired with a low-cost multispectral device. This research represented a preliminary stage aimed at exploring the capabilities of a commercial multispectral sensor to assess the quality status of intact olive fruits. Therefore,

the experiments were carried out under controlled laboratory conditions. Satisfactory results from this initial evaluation would encourage subsequent research aimed at adapting the sensor to operate in field conditions.

- **Objective 3.2. Development and evaluation of a low-cost multispectral device for assessing quality parameters of intact olive fruits under field conditions.**

  Considering the positive results obtained in the experiments conducted under laboratory conditions, it was proposed to design a handheld device. This device was based on the same multispectral development board but was specifically adapted to operate in field conditions. The proposed device was used to acquire the spectral signature of olive fruits directly in the field. These data were used to develop algorithms aimed at estimating quality parameters of olive fruits.
  Additionally, the developed device was evaluated to assess quality indicators of grapes in a field experiment.

2.2. Methodology

The methodologies employed during the research, aimed at achieving the aforementioned objectives, are outlined below. A brief description of the specific procedures and techniques used throughout the experimentation is provided. The reader is encouraged to refer to the corresponding published documents, compiled in section 4, for a more in-depth study.

2.2.1. Methodology for Objective 1. Development and evaluation of a low-cost device based on a thermal infrared sensor to assess water status of olive trees.

The initial stage of the research was the development of the prototype. Before its evaluation in an agronomic context, the performance of the device was compared to a commercial thermal camera in a controlled scenario, obtaining satisfactory results.

After verifying the correct performance of the device, the next stage was to evaluate its suitability to measure olive canopy temperature and to assess water status from it. For this, a field experiment in a commercial olive orchard was conducted. A SHD olive orchard of the Arbequina variety was used as experimental area. An experimental setup was implemented to induce varying levels of water stress on olive trees. Two groups of five rows of trees were established, and each group was subjected to an alternative irrigation treatment: one group received normal irrigation covering 100% of crop evapotranspiration, while the other group received a deficit treatment covering only 50%. After several months of exposure to the different treatments, the water status of the olive trees was assessed using two widely accepted methods: predawn leaf water potential and stomatal conductance. Four sample point were established in both groups. Leaf water potential measurements were acquired once just before dawn. Stomatal conductance measurements were taken early in the morning (10 AM) and during midday (3 PM). Simultaneously with the stomatal conductance measurements, four thermal images of the sunlit canopy and four of the shaded canopies at each sample

point were taken. The mean temperature of the set of pixels acquired by the camera was considered representative of the canopy temperature. Based on the canopy temperature data, the crop water stress index (CWSI) was calculated using an approach based on the method proposed by Park et. [87]. This approach involved calculating the temperature thresholds required to compute CWSI from the temperature distribution histogram of the entire set of thermal images.

Finally, the canopy temperature measured with the proposed device and the calculated CWSI were compared with the corresponding measurements of stomatal conductance in both sampling events and the predawn leaf potential.

2.2.2. Methodology for Objective 2. Development of a methodology to assess the nutritional status of olive trees based on the analysis and modelling of multispectral images taken with an UAV.

The sensor employed in this research was a commercial multispectral camera specially designed for agronomic applications. Concretely, a MicaSense RedEdge-M™ (MicaSense, Inc., Seattle, WA, USA). The objective of this research was to develop mathematical models that, based on spectral data acquired with the sensor, could estimate the foliar content of N, P, and K in olive trees. This required the prior establishment of an experimental framework in which the target parameters exhibit high variability, so that situations of nutrient deficiency and excess are represented. For this purpose, the fertigation system of two commercial SHD olive orchards (*Olea Europaea*, cv. Arbequina and Arbosana) were manipulated to establish three treatments: a normal fertigation based on the company's scheme, and two modalities with regulated deficit: medium stress, with 61% of normal fertigation, and moderate stress, with 50% of normal fertigation. These treatments were applied for a sufficient duration to impact the nutritional status of the trees. Within the areas subjected to each treatment, 12 sampling points were selected and geolocated.

The experimental fields were flown over with the UAV, capturing spectral images of the entire area. On the same day as the flight, all sample points were examined to obtain ground truth values of the levels of foliar N, P, and K through standard chemical methods. The multispectral camera equipped on the UAV cover five spectral bands (blue, green, red, red-edge, and near-infrared). Thus, after flying over the experimental field, five sets of spectral images were collected. An image processing method was defined to integrate all the spectral images gathered during the flight into orthomosaics. This allowed for the automatic extraction of information from discrete points, discarding noisy data. The final step involved evaluating various statistical tools for generating estimation models. After reviewing the state of the art, a non-parametric linear method, namely Partial Least Squares Regression (PLSR), and three non-linear non-parametric methods driven by machine learning, namely Artificial Neural Network (ANN), Support Vector Regression (SVM), and Gaussian Process Regression (GPR), were selected. These models were fed with the reflectance values obtained from the processed orthomosaics and were trained using the foliar content of N, P, and K as the target variables. The

experimental field was considered as a whole, without differentiating between olive varieties, with the aim of increasing the volume and range of the dataset. The models were externally tested using 25% of the dataset. The performance of the models was measured considering the coefficient of determination (R^2) and the root mean square error (RMSE) between the foliar content of different nutrients (determined by chemical analysis) and the respective model's response.

2.2.3. Methodology for Objective 3.1. Evaluation of the capabilities of a low-cost multispectral sensor for assessing quality parameters of intact olive fruits under laboratory conditions.

The initial stage of this research focused on developing the prototype. To assess the device's potential, an experiment was conducted in collaboration with a professional olive mill. During the harvest season of 2020–2021, 507 olive samples, provided by olive growers for evaluation, were initially analysed using the mill's resources and then with the proposed device. The reference data for the target parameters (moisture, acidity, and oil content per fresh weight) were determined using an industrial-standard NIR analyser. Immediately after being analysed with the NIR analyser, the olive samples were placed in a circular container with a diameter of 14 cm, depth of 5 cm, and capacity of 500 g. Subsequently, the olive samples were positioned inside the acquisition chamber of the spectral system, under the light source and the multispectral sensor, at an equal distance from both (15 cm). Four spectral captures were taken for each olive sample. Between captures, the olive samples were rotated 90 degrees, and the average reflectance of the four spectra was considered as representative data for each sample. As the spectral sensor is punctual, no image processing was applied beyond normalizing the reflectance based on captures of a reference board.

The corrected reflectance of the 18 spectral bands captured by the sensor were used as input variables to train three ANN models using the oil content per fresh weight, moisture, and acidity of the olive samples as target variables. The model validation was performed externally using 10% of the dataset. The performance of the quality estimation models was measured using the coefficient of determination (R^2) and the root mean square error of prediction (RMSEP) between the reference parameters and the output of the respective model.

2.2.4. Methodology for Objective 3.2. Development and evaluation of a low-cost multispectral device for assessing quality parameters of intact olive fruits under field conditions.

In view of the results obtained in the previous phase of this research, a new prototype was developed with the objective of creating a tool that is reliable and easy to operate under field conditions by non-specialized personnel. Prior to the in-field evaluation of the device, a specific experiment was conducted to validate its capabilities in avoiding the interference of environmental radiation. This experiment involved exposing the device to various levels of environmental radiation. To assess the statistical significance

of the environmental radiation levels on the performance of the proposed device, a one-way analysis of variance (ANOVA) with a significance level (α) of 0.05 was conducted.

A field experiment was conducted to assess the capability of the proposed device for quantitatively evaluating quality indicators of intact olive fruits. The study site was a commercial olive orchard (*Olea Europaea*, cv. Picual). Periodic sample collections were carried out during two consecutive ripening campaigns. The first sample collection took place after the post-summer fruit growth (October) and was repeated weekly until harvest (December), resulting in a total of 146 samples. Each sample consisted of approximately 200 g of olives collected from the same branch of a randomly selected tree. The spectral signature of the samples was acquired immediately after being picked. The measuring container was filled with approximately 50 g of olives. Subsequently, the device dome was fitted with the container, and three consecutive spectral captures were taken. This process was repeated four times per sample, resulting in 12 spectral measurements per sample (3 captures/container x 4 containers). Afterward, the samples were packaged, labelled, and refrigerated for transportation to the laboratory. The reference data for the target parameters (oil content per dry matter (OCDM), oil content per fresh weight (OCFW), moisture (M), and titratable acidity (TA)) were determined using chemical standard methods by an external laboratory.

The initial step in data pre-processing involved averaging the 12 spectral signatures from each olive sample. Consequently, each sample was represented by 18 reflectance data. These data were normalized using the spectral signature of a calibrated reflectance surface as a reference. Additionally, the pre-processed spectra were smoothed for noise removal by applying the Savitzky–Golay method [130]. After considering various parameter settings, the width of the selection window was adjusted to five points, and a second-order polynomial was employed to fit the data. No derivatives of the data were calculated, as only a simple smoothing was intended. Finally, the pre-processed reflectance values of the 18 spectral bands acquired by the sensor were used as input variables to train 4 ANN models using OCDM, OCFW, M, and TA, respectively, as target variables. The validation of the model was made externally with the 15% of the dataset. The performance of the estimation models was evaluated through the coefficient of determination (R^2), the root–mean–square error of prediction (RMSE), the coefficient of variation of the RMSE (CVRMSE) and the ratio of performance to deviation (RPD) between the reference values of ripening indicators determined by standard methods and those estimated by ANN models. Furthermore, paired t-tests for dependent samples were also conducted to verify the results from the R^2, RMSE, CVRMSE, and RPD analyses.

Additionally, the developed device was evaluated to assess quality indicators of grapes in a field experiment. The study site was a commercial vineyard (*Vitis vinifera* L., cv. Syrah). In this case, the sample collection was conducted on a single date, near to the optimum harvest time according to the winery's manager. To capture a broad range of ripening stages, a total of 80 grape samples were randomly collected, covering the entire vineyard. A grape cluster was considered a sample unit, and each cluster was harvested

using pruning shears. The spectral signature of each cluster was acquired immediately after harvest. The measurement methodology involved positioning the dome of the device against the upper part of the grape cluster and capturing the spectral signature. Two captures were acquired per sample, and the average reflectance of the two spectra was considered as representative data for each sample. After processing, each sample was packaged, labelled, and refrigerated in a portable cooler during its transport to the laboratory. In this study, soluble solid content (SSC) and titratable acidity (TA) were used as target variables, as they are routinely considered by the wine industry to determine the ripening status of grapes [131].

The mean reflectance signature of each grape sample was calibrated by normalization, using the spectral signature of a known reflectance surface as a reference. The normalized reflectance of the 18 spectral bands captured by the sensor was used as input variables to train two ANN models to estimate the SSC and TA, respectively. Leave-one-out cross-validation (LOOCV) was employed as the validation method, chosen for its suitability given the volume of the dataset (n = 80). Additionally, the model validation was performed externally using 25% of the dataset. The training was repeated for two consecutive times, resulting in a test set of 40 samples. The performance of the estimation models was measured using the coefficient of determination (R^2), the root–mean–square error of prediction (RMSE), and the coefficient of variation of the RMSE (CVRMSE) between the actual values of the ripening indicators determined by chemical methods and those estimated by the ANN models. Additionally, paired samples (t-tests) for dependent samples were also conducted to confirm the results from the R^2, RMSE, and CVRMSE analyses.

3. Materials

The following subsections describe technical aspects of the various investigations conducted in this Thesis, such as the experimental setups, the agronomical parameters used as reference, the equipment used during the execution of the experiments, the data processing methods, and the estimation models employed. In section 4, the corresponding documents can be consulted for more comprehensive information on these aspects.

3.1. Case estudies

As stated above, the research from which this Thesis derived addressed three different lines of investigation. The three research lines coincide in that their theme is the modelling of agronomic parameters using data acquired with sensors. This type of research requires a preliminary phase aimed at creating an experimental framework in which the target agronomic parameter is represented across a wide range of values. So that all possible situations that may occur in a real-world context are represented. In this sense, the representativeness of the dataset from which to develop an estimation model is crucial to ensure its quality and, especially, its generalization capability.

The objectives outlined in this Thesis required the establishment of 5 experimental frameworks. Regarding the part of the research focused on achieving the goals pursued in objective 1, it was conducted in a commercial SHD olive orchard (*Olea europaea* L. cv. Arbequina) located in Elvas, Portugal (38°49'33.6"N, 7°07'53.76"W), and managed by ElaiaTM (SovenaTM Group, Alges, Portugal). The tree spacing of this field is 1.35 m x 3.75 m (inter and intra-row, respectively), resulting in 2116 trees/ha. This field is equipped with a drip irrigation system that allows for precise adjustment of the irrigation doses applied. This irrigation system was implemented through two irrigation treatments, each aimed at supplying water requirements and inducing stress, respectively. Thus, two experimental plots were established: fully irrigated (FI) plots and regulated deficit irrigated (RDC) plots. Five consecutive tree rows were selected for each plot, consisting of one experimental row (central row) and four guard rows. Four trees from the experimental row were chosen as sample points, resulting in a total of 8 sample points. The irrigation scheduling consisted of daily drip irrigation for the FI plants, calculated to cover 100% of crop evapotranspiration. In contrast, the RDC plants were subjected to alternating periods of drought and irrigation, each lasting one week. Consequently, under this irrigation schedule, FI plants received approximately 480 m^3/ha per month between May and September, whereas RDC plants received only 240 m^3/ha per month.

The research focused on achieving objective 2 of this Thesis was carried out on the previously described crop, along with a second one of the Arbosana variety (*Olea europaea* L. cv. Arbosana). Both crops are located in proximity (38°50'6.9" N, 7°07'25.9" W) and share the same cultural conditions; the only difference lies in the variety of olive being cultivated. The drip irrigation system of these crops allows for the application of

fertilizers diluted in the irrigation solutions. In the commercial context, the fertilizers doses applicated are adjusted based on the chemical analysis of leaves and the phenological phase of the vegetative cycle. The experimental framework in this case consisted of three fertigation treatments: one control based on maintaining the fertigation doses normally applied in the company scheme (NF), and two modalities of regulated deficit—medium stress (RDF_1), with 61% of normal fertigation, and moderate stress (RDF_2), with 50% of normal fertigation. In each olive variety, three rows were selected per treatment (with a minimum of 50 olive trees per row). On both sides of the sampled rows, two guard rows were established, receiving the same fertigation treatments. Within the sampled rows, four olive trees were chosen as sample points, resulting in a total of 12 sample points per treatment. Finally, two samples were discarded due to sampling errors, resulting in a final volume of 70 samples (35 of cv. Arbequina and 35 of cv. Arbosana).

Concerning the segment of the research dedicated to achieving the goals outlined in objective 3, the experimental framework established for objective 3.1 must be differentiated from that established for objective 3.2. The objective 3.1 consisted of a preliminary evaluation of the selected multispectral sensor to characterize quality indicators of intact olive fruits under laboratory conditions. This part of the research was conducted in collaboration with a commercial olive mill (Nuestra Señora de la Oliva, S.C.A., Gibraleón, Spain). Part of the typical activities of these types of companies is the quality assessment of olive samples provided by olive growers for appraisal. Thus, over the course of an entire harvest campaign, they receive samples with a wide range of ripening states. Taken advantage of this fact, during the 2020-2021 harvest season, the olive samples received by the olive mill were analysed with the mill's resources and subsequently with the proposed device. A total of 507 olive samples of four varieties were analysed (*Olea europaea* L., cv. Picual (54.2%), cv. Arbequina (28.6%), cv. Arbosana (7.7%), and cv. Verdial (9.5%)).

The objective 3.2 was to evaluate a device based on the same multispectral sensor to characterize quality indicators of intact olive fruits under field conditions. The quality indicators used as targets in this research vary during the maturation process. So, instead of an intervention in the crop management aimed at modulating the target parameters, in this case, periodic sample collections were performed, covering the entire ripening process. Thus, the first sample collection was conducted after the post-summer fruit growth (October) and was repeated weekly until harvest (December). These experiments were conducted over two consecutive campaigns, resulting in a final volume of 146 samples. The study site was a commercial olive orchard (*Olea Europaea*, cv. Picual), provided by Nuestra Señora de la Oliva, S.C.A., and located in the province of Huelva, Spain (37°20'28.96" N, 7°01'54.98" W). This olive orchard has a plant spacing pattern of 7x7 m, which corresponds to a traditional cultivation system. A plot of one hectare was delimited for sampling. This delimitation was intended to minimize sources of variability affecting maturation, making the principal factor of variability the evolution of the fruits along the campaign.

Alternatively, the developed device was evaluated to assess quality indicators of grapes in a field experiment. The study site was a commercial vineyard (*Vitis vinifera* L., cv. Syrah) located in the *Condado de Huelva* (Bodegas Contreras Ruiz S.L., Rociana del Condado, Spain). The experimental field covered an area of approximately 1000 m^2. The soil in the study area exhibits a heterogeneous structure and composition, with sandy loam areas alternating with clay-loam zones. This irregular pattern in the structure and composition of the soil is reflected in the physiology of the plants. Consequently, there are plants with different ripening rates, resulting in high variability according to the quality parameters considered in this research. This variability enabled the attainment of a broad range of quality indicators in a single sample campaign. Therefore, the field experiment was conducted in a single day, proximate to the optimum harvest time as advised by the winery's manager. To capture the maximum variability in terms of grape ripening stages, the entire vineyard was covered by randomly collecting a total of 80 samples.

3.2. Agronomical parameters to model

The modelling of agronomical parameters using data acquired with sensors requires a reference dataset of the target parameter obtained by standard methods. Below, the reference parameters used in the different parts of the research conducted to address the objectives of this Thesis are listed.

Objective 1 was related to the water status assessment of olive trees, so an indicator of this physiological condition was required. In this case, predawn leaf water potential (Ψ_{PD}) and stomatal conductance (g_s) were selected as water status indicators due to their widespread use in research. The Ψ_{PD} was measured using a Scholander-type pressure chamber (SF-Pres-20, Solfranc Tecnologías, Vila-Seca, Spain)(Figure 4a). On the other hand, the g_s was measured using a leaf porometer (SC-1, Decagon Devices, NE Hopkins Ct. Pullman, USA) (Figure 4b). The maximum daily g_s in olive trees can be observed around 10 AM. As the day progresses, there is an increase in vapor pressure deficit, to which the olive trees respond by closing their stomata, thus limiting their ability to dissipate canopy temperature. To evaluate if this effect had an impact on the correlation between g_s and canopy temperature, measurements of g_s were acquired both early in the morning (10 AM) and during midday (15 PM).

Figure 4. Images of reference parameters measurement process; a) Ψ_{PD} with the pressure chamber, b) g_s with the leaf porometer.

Objective 2 was related to the nutritional status assessment of olive trees. In this part of the research, leaf nitrogen, phosphorus, and potassium content (LNC; LPC; LKC) were defined as target parameters, as they are widely accepted indicators of the nutritional status of olive orchards. These three macronutrients are primarily considered for planning fertigation programs in agronomic contexts and are obtained by means of chemical methods from foliar samples. On the flight day, approximately 100 ± 20 g of leaves were collected from each sampled point, taken from the middle of the last spring terminal shoots. The samples were placed in plastic bags and refrigerated for transport to the laboratory. For this research, the foliar analyses were outsourced to an external laboratory. LNC was determined by the Kjeldahl method [132]. On the other hand, LPC, and LKC were determined by inductively coupled plasma optical emission spectrometry (ICP-OES)[133].

Objective 3 was related to the quality status assessment of olive fruits. In this part of the research, oil content per fresh weight, moisture, and titratable acidity were used as quality indicators, as they are widely employed by growers to determine the optimum time for harvest in agronomic contexts. In the first stage of this part of the research (Objective 3.1) these parameters were assessed using an industrial-standard near-infrared analyser (OliveScan 2, Foss, Hilleroed, Denmark), since this was the procedure commonly employed by the olive mill. In the second stage of this part of the research (Objective 3.2) the characterization of these parameters was outsource to an external laboratory and carried out through chemical methods. Fat or oil content was determined in its two variants: oil content per dry matter (OCDM) and oil content per fresh weight (OCFW). Reference analysis of OCFW was undergone by using the Soxhlet methodology (UNE 55030:1961)[25]. The determination of moisture was carried out through the drying method in an oven at 105 °C (ISO662:2016)[27]. OCDM was calculated based on

OCFW and moisture. And titratable acidity was determined by means of titration (UNE-EN ISO 660:2020)[24].

On the other hand, in the complementary research aimed at assessing quality indicators of grapes, soluble solid content and titratable acidity were used as target parameters, given that they are routinely considered by the wine industry to determine the ripening status of grapes. The soluble solid content was determined using a temperature-compensating digital refractometer (HI96801, Hanna instruments, Eibar, Spain). The titratable acidity was characterized using an automatic titralyser (LDS1155500, Laboratoires Dujardin-Salleron, Dujardin-Salleron, France).

3.3. Spectral sensing equipment

All the spectral equipment used in this Thesis, except for the equipment used to accomplish objective 2, are custom-built devices developed for ease of use and affordability.

To accomplish the objective 1 of this Thesis a thermal infrared device was developed (Figure 5). This device was developed on a low-cost platform (Arduino MEGA 2560, Arduino LLC, Monza, Italy). Additionally, it was equipped with a screen that allows for monitoring the proper functioning of the device during field use, an SD card for data storage, an activation button, an interconnection board, and a battery. All of these components were housed in a case created through 3D printing. The integrated IR sensor was embedded in the integrated circuit (IC)(MLX90620, Melexis, Premstaettem, Belgium). It operates in a temperature range suitable for agricultural applications (-40°C to +85°C), with a resolution of 16x4 pixels and a 40° field of view, making it suitable for manual image capture. The mentioned IR sensor provides a temperature value for each pixel and was configured to determine the average temperature of all pixels. Thus, with each image, the measured temperature value for each pixel, as well as the overall average temperature of the image, was stored.

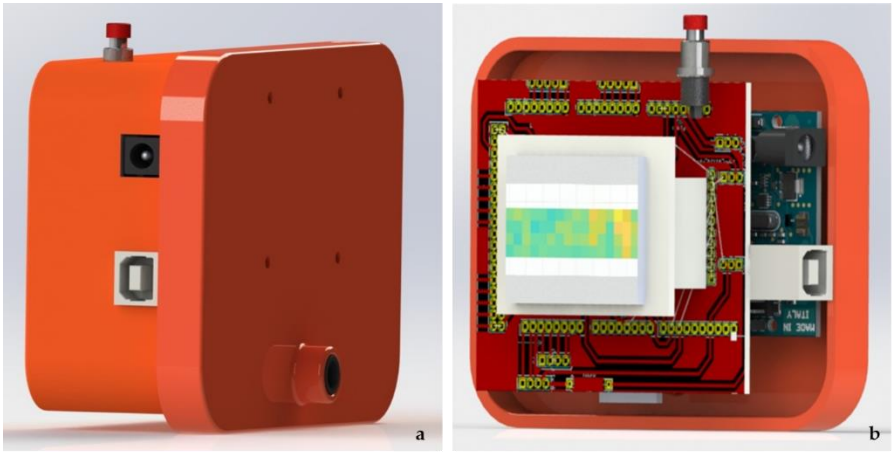

Figure 5. 3D representation of the developed thermal IR device. a) Device casing. b) Partial cut showing its elements.

In this work, additionally, a commercially available infrared camera (Testo 875-1i, Testo SE & Co, Titisee-Neustadt-Baden-Württemberg, Germany) was used as a reference to

evaluate the accuracy of the developed device in a laboratory test carried out prior to its in-field evaluation.

The device used to accomplish objective 2 was a commercial multispectral camera specially designed for agronomic applications (MicaSense RedEdge-M, MicaSense, Inc., Seattle, USA)(Figure 6).

Figure 6. Images of the used multispectral camera. a) MicaSense RedEdge-M™ and its downwelling light sensor (DLS). b) MicaSense RedEdge-M™ and its DLS equipped on the RPAS during flight.

This camera includes five CMOS sensors, each with modified sensitivity thanks to band-pass filters, making them individually sensitive to narrow bands within the visible spectrum (VIS) (blue, green, red, red-edge), and near-infrared (NIR). Figure 7 illustrates its spectral sensitivity. All the sensors are 1280 x 960 pixels in size, resulting in a ground sample distance (GSD) of around 8 cm per pixel when capturing at an elevation of 120 m. The camera was equipped with a GPS device for image georeferencing and a 5-band downwelling light sensor (DLS). The DLS along with the use of a reflectance panel, enable radiometric calibration. All these sensors were mounted on an unmanned aerial vehicle (DJI™ Matrice 100, SZ DJI Technology Co., Ltd., Shenzhen, China)).

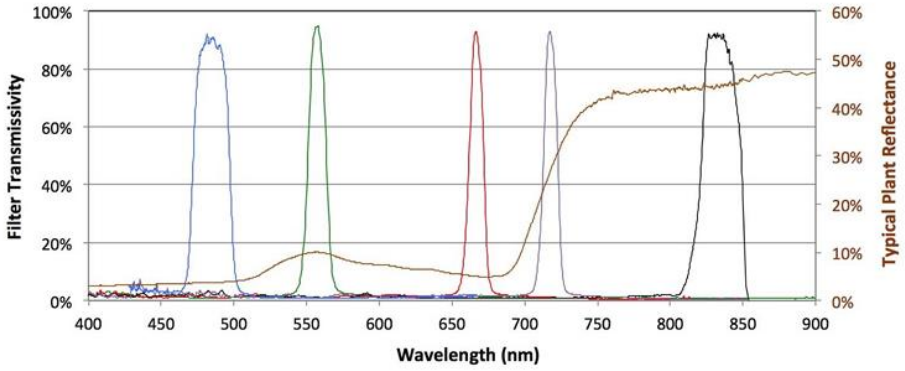

Figure 7. MicaSense RedEdge-M™ spectral response. Picture taken from MicaSense RedEdge-MTM Multispectral Camera User Manual, © 2017 MicaSense, Inc.

Objective 3.1 consisted of an initial evaluation of the capabilities of a low-cost multispectral development board (AS7265x, ams-OSRAM AG, Premstätten, Austria) to characterize quality indicators of intact olive fruits. This board is composed of three main chips: AS72651, AS72652, and AS72653. These chips are sensible to six different bands

(by including six optical filters each) in the range between 410 nm and 940 nm, with a full width at half maximum (FWHM) of 20 nm (Figure 8). Thus, the AS7265x development board results in a low-cost, 18-channel multispectral sensor. This sensor is punctual, so it acquires just one reflectance measure of the focused area.

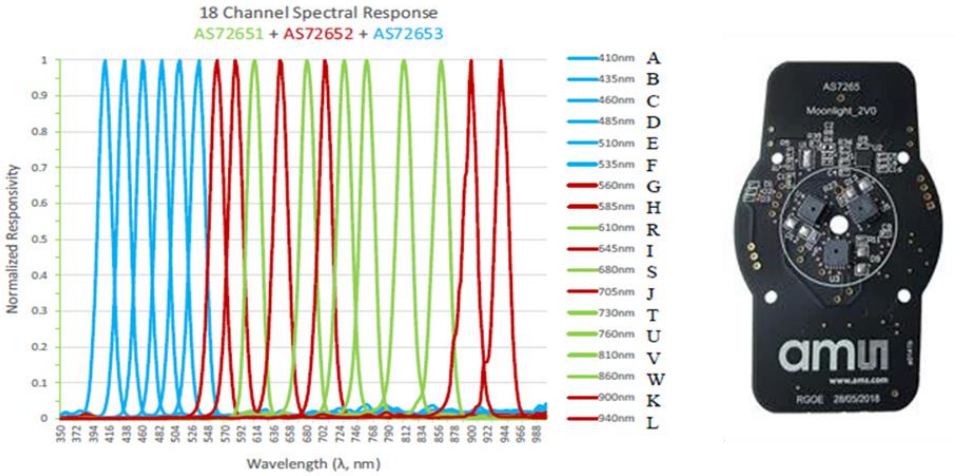

Figure 8. Image of the AS7265x development board (right), and the combined spectral response of its 3 main chips (left). Pictures taken from the AS7265x datasheet, © 2018 ams OSRAM group.

Given that it was an initial evaluation, a simple prototype was developed, mainly based on three components: the AS7265x development board, a halogen light source, and a controller board (Arduino MKR zero, Arduino LLC, Monza, Italy). The halogen lamps emit a broadband spectrum, allowing for accurate reflectance measurements. The spectral sensor and the controller board were housed in a 3D-printed enclosure (sensor box), which was equipped with a thin round layer of PTFE placed in front of the sensor. This layer served as a diffuser and helped standardize the spectral signal. Apart from the previously described elements, a bracket based on a photographic tripod allowed for the setup of the sensor box and the light source with a 90° angle between them and a fixed distance to the samples (Figure 9). This setup aimed at ensuring that the radiation emitted by the light source was reflected by the sample and captured by the sensor correctly. The whole system was kept enclosed within an opaque acquisition chamber during measurements to prevent interference from ambient light. Spectral data capture was managed by a computer through custom-developed software interfaced with the Arduino board. The software awaits user input to capture a sample spectrum. When capturing is triggered, the Arduino board sends the command to the sensor and gathers data. Then, the acquired data are sent to a computer and stored in an SD card for further analysis.

Figure 9. Image of the initial multispectral prototype during measurement.

To achieve objective 3.2, a handheld device specially designed for in-field applications was developed (Figure 10). To reduce costs and simplify maintenance, commercial components were selected. However, some printed circuit boards were developed to simplify the assembly. The main component of the proposed device was the AS7265x development board. The device was also equipped with an array of three IR-broadband LED emitters (OSLON P1616 SFH 4737, OSRAM GmbH, Munich, Germany). This component was developed specifically for spectroscopy applications, providing a wide emission spectrum in the VNIR with the advantage of requiring less power and generating less heat dissipation than a halogen lamp. The control of the device is carried out by a controller board, specifically an Arduino MKR Zero. It was chosen for its small form factor, low power consumption, affordability, and the availability of an SD card slot. This controller board was implemented with a custom software developed using the Arduino IDE. Briefly, when the device is powered on, it generates a new file to store measurements and remains in an idle state, awaiting activation by the user. In this state, pressing the pushbutton triggers the controller board to coordinate a light emission by the LED emitter (with a current selectable by software) and capture by the sensor. The acquired data and relevant information, such as file names, are stored on an SD card for later analysis. All the device components were housed in an enclosure, designed using Freecad 0.16 and manufactured with a 3D printer using polylactic acid 3D printer filament. The enclosure consisted of 4 different parts: handle, dome, main enclosure, and lid (Figure 4a). The handle houses an end-stop switch, which serves as the trigger. The switch is installed inside the handle, and the wires to connect to the interconnection board are conducted inside the handle to the main enclosure. The dome holds the light source and was designed to ensure that the sample is placed at a 45° angle with the light source and the sensor. It also integrates a light-diffusion film (OptSaver L-9960, Kimoto LDT, Opfikon, Switzerland). It was placed in front of the sensor to homogenize the radiation received by the sensor. The main enclosure comprised a box-type structure.

The AMS AS7265x development board, Arduino MKR Zero, and interconnection board were stacked inside and secured in place with the assistance of two 3D-printed separators. The lid seals the sensor for in-field operation and features an OLED display to assist and guide the user during measurement. Specifically, it utilizes a 1.3-inch panel with a resolution of 128 by 64 pixels. The entire system was powered by a 2s LiPo (Lithium-ion Polymer) battery connected to the device controller board. This is the only component that was housed outside the enclosure, to easy its replacement and avoid temperature interferences. Additionally, a container was designed to fit with the device's dome (Figure 10b). This container was designed to hold the olive samples during the measurement, thus preventing interference from environmental radiation.

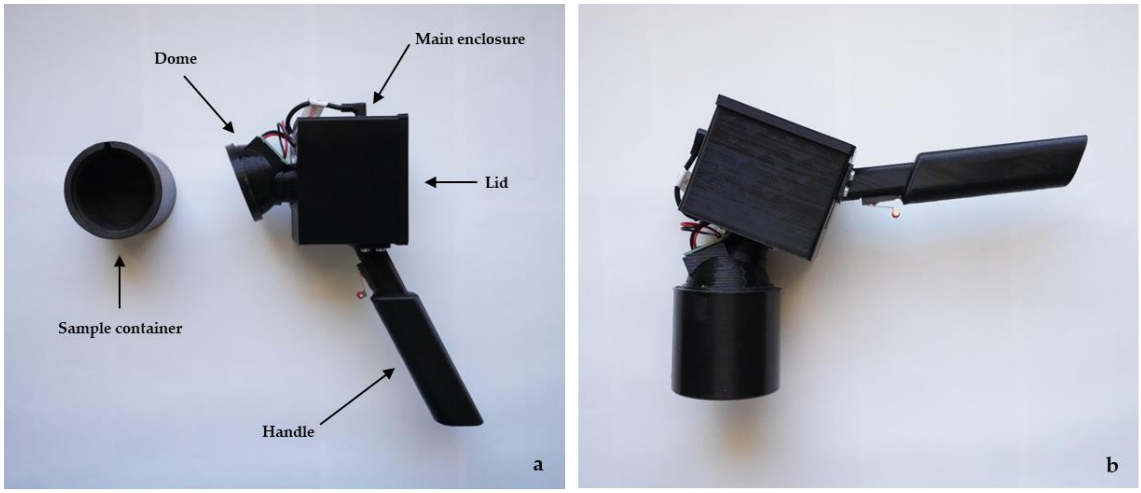

Figure 10. Images of the developed handle multispectral system. a) Image of the handheld multispectral system indicating the four different parts of its enclosure. b) Image of the measuring container fitted with the device´s dome during measurement.

3.4. Data procesing methods

The raw data acquired with sensors usually need to undergo a subsequent processing phase, which should be tailored to the nature of the data acquired by the sensor and the logistics of data acquisition.

The research conducted to achieve objective 1 of this Thesis was centred on a thermal IR sensor. This sensor is a temperature sensor array (16 × 4 pixels) that measures the thermal radiation of a target and estimates its temperature in a non-contact manner. However, the raw temperature data obtained by the IR sensor must be corrected to obtain canopy temperature values. This process is carried out automatically by the sensor and consists of three steps: (1) the raw temperature data are operated in conjunction with the stored calibration values to standardize the sensor response and obtain the temperature corresponding to each pixel; (2) a PTAT sensor (included in the integrated circuit) adjust the IR temperature values based on the ambient temperature; (3) and finally, an emissivity correction is performed, as the initial measurement by the sensor assumes the object to be a perfect black-body emitter. On the other hand, the canopy temperature measured with the proposed IR sensor was used to calculate the CWSI. In this work, an

approach based on the method proposed by Park et. [87] was employed to determine the threshold necessary to calculate CWSI (T_{wet} and T_{dry}). This approach involved employing an adaptive approximation based on the TIR histograms derived from the images. It is assumed that T_{wet} and T_{dry} can be extracted from the coldest and the hottest part of the temperature distribution histogram of the thermal images, respectively (n = 64 pixels/imagen × 32 imagens/ measurement cycle = 2048 temperature values). The collected measurements feature normal density distributions; however, there were some data represented at a reasonably low frequency that were considered outliers (i.e., non-representative canopy temperature), so they were discarded.

The research related to objective 2 was centred on a multispectral camera mounted on a RPAS. The measurements acquired by this device correspond to the reflected radiation from the focused area in discrete spectral bands. However, the incident radiation varies even within a sampling event, making measurements incomparable across different scenarios. To address this, the incident radiation was characterized during the flights using a 5-band DLS that covers the same bands acquired by the sensor. Additionally, before each flight, a known reflectance panel was measured. The characterization of incident radiation allowed for the radiometric calibration of the reflectance signal acquired by the camera. This calibration consisted of normalization based on the known incident radiation. Furthermore, in this work, spectral images were acquired with an UAV from a zenithal perspective. Under these conditions, the raw images included background information mainly related to the soil, shadows, and weeds, along with information from the olive canopy, which was the true focus of this work. Therefore, the background information was considered noise, and if not removed, it could negatively impact the effectiveness of the estimation models developed using this information. To address this issue, an image processing method was developed aimed at isolating the canopy pixels while discarding the background information. The first step of this methodology consisted of building image mosaics by overlapping the individual images taken during a flight mission. These images were previously radiometrically corrected using information registered by the camera's DLS sensor and the images captured of a reference board. In parallel, a 3D point cloud associated with the orthomosaics was generated as well, in which an elevation value is assigned to each pixel. Then, a greyscale image representing a digital surface model (DSM) of the orthomosaics was generated from the 3D point cloud. This image was used to generate a mask isolating the tree canopy from the background of the image. This mask was applied to each of the spectral image mosaics, resulting in filtered images containing only canopy-related information. To assign a value to each sampling point, an area of 15 x 15 pixels was standardized, considering it representative of a single individual. Finally, considering the georeferencing data, the mean of the values contained in all the pixels within that area was determined for each sampling point. Thus, obtaining 5 reflectance values for each sample point.

The research conducted to achieve objective 3 was based on proximal and point sensors. This means that measurements were taken in close proximity to the target, and the data

provided by the sensors corresponded to a single pixel when compared to cameras. Furthermore, these devices include an artificial light source that illuminates the object during measurement, and its spectral emission was quite stable compared to ambient light. For these reasons, the need for data processing in these works was lesser. In these cases, data processing consisted of normalizing the reflectance data based on captures of a known reflectance surface. This normalization aimed to prevent eventual contaminations of ambient radiation, especially concerning measurements taken in-field conditions. Moreover, in all the works, each sample was captured repeatedly, with the representative data of each sample being the result of averaging the different measurements.

3.5. Estimation models

In the research conducted to achieve the objective 1 of this Thesis, the canopy temperature measured with the developed IR thermal device and the calculated Crop Water Stress Index (CWSI) were considered direct indicators of the water status of the olive trees. For this reason, a development of quantitative estimation models was not undertaken. The consistency of the canopy temperature and the CWSI as water status indicators was evaluated based on a linear regression between the explanatory variables (canopy temperature measured by the sensor and CWSI calculated from it) and the response variables (predawn leaf water potential and stomatal conductance). Four linear regression models were developed to assess the correlation between each explanatory variable and the response variables separately. This method was chosen due to the presumed direct correlation between the explanatory and response variables, which was confirmed by the goodness of fit of the linear regression model.

In the research related to accomplishing objective 2, a different type of sensor was employed. It was a multispectral camera, so after applying the proposed image processing method, five explanatory variables were available for each target parameter. The initial hypothesis in this case was that complex relationships between the explanatory variables would be required to estimate the target parameters (foliar content of N, P, and K). The increasing number of explanatory variables, typical of spectral sensors, requires reliable and efficient retrieval techniques that enable the interpretation of spectral observations and their translation into biophysical variables. For this reason, four non-parametric methods were evaluated to develop estimation models of the N, P, and K leaf content using the five reflectance data as inputs. Nonparametric methods directly define regression functions based on information from the given spectral data and associated variables; they are data-driven methods. In contrast to parametric regression methods, nonparametric methods do not explicitly define spectral band relationships. Instead, they optimize the regression algorithm through an inherent learning phase based on training data. After reviewing the state of the art, one linear nonparametric regression method (partial least squares regression (PLSR)) and three nonlinear nonparametric methods (artificial neural network (ANN), support vector regression (SVR), and Gaussian process regression (GPR)), also referred to as machine learning regression algorithms, were evaluated as retrieval techniques. The main

difference between linear and nonlinear methods is their ability to apply nonlinear transformations, providing a methodological advantage when the relationship between the explanatory variables and the response variables is nonlinear.

The results of this research suggested a superior performance of the ANN models compared to the other tested methods. Therefore, in the research aimed at accomplishing objective 3, which also focused on spectral data modelling, ANN models were selected as the retrieval technique. Given that the ANN has been the most employed modelling method in this Thesis, a more detailed description of this method is provided below.

3.5.1. Artificial neural network models

An ANN is a non-linear, non-parametric method (machine learning method). This approach consists of a structure of neurons linked together and arranged in layers (Figure 11). The neurons of different layers are interconnected, and each connection has a specific weight. Each neuron essentially performs a linear regression followed by a non-linear function. Briefly, the ANN architecture works to minimize the mean–square deviation through the error-correction learning rule. Thus, the error is minimized by adjusting the weight of each layer of neurons during the training process [62]. These characteristics allow for an extraordinary connection between complex spectral information and key parameters without any constraint on the sample distribution. This makes ANN approaches appropriate for defining complex non-linear relationships that normally exist between spectral signatures of vegetation and biophysical parameters. Previously experimental studies have demonstrated the potential of ANNs for assessing biophysical parameters of vegetation by means of spectral data [134–141].

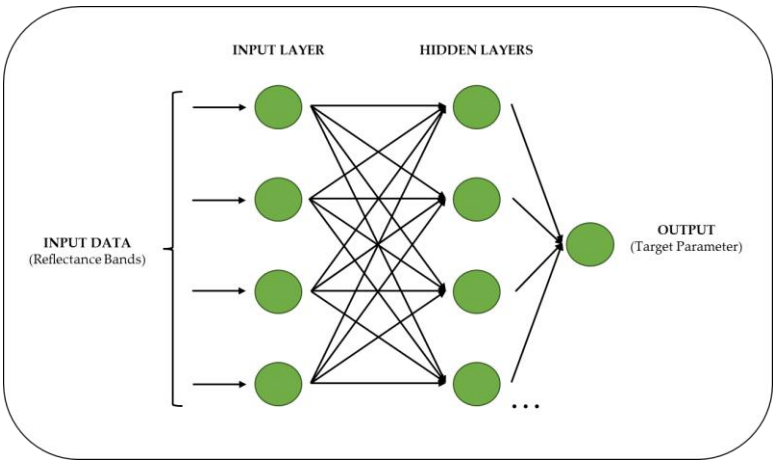

Figure 11. Schematic illustrations of the generic architecture of multilayer perceptron algorithm.

Specifically, the type of ANN models used in this Thesis were multilayer perceptron algorithms with backpropagation (MLP-BP). MLP-BP consists of two steps: (1) feedforward the values, and (2) calculate the error and propagate it back to the earlier layers. To be precise, forward propagation is part of the backpropagation algorithm but comes before backpropagating. In this Thesis the architectures of the ANNs employed and the training process were adapted to each application to maximize performance

based on the data provided by the sensors used, the target parameter, and the features of the dataset in each case. For this reason, train, and model parameters such as the subdivision of the dataset for training and external validation, the number of hidden layers, the number of neurons in the hidden layers, the number of inputs, the activation functions of the hidden layers, and the output layer functions, as well as the training algorithms, can vary between works. For more detailed information on each case, the reader is encouraged to refer to the respective documents (section 4).

3.6. Equipment for data processing and estimation model development

The implementation of the image analysis and estimation models proposed in this Thesis required different software and development environments. In the next section, the most relevant ones are listed along with the topic addressed when used:

3.6.1. Data preprocessing, estimation models development, and automated procedures for training, validation, and testing.

- MATLAB (The MathWorks Inc., Natick, Massachusetts, USA), releases 2019b, 2020a, and 2022b.
- MATLAB Image Processing Toolbox, release 2018a.
- MATLAB Deep Learning Toolbox, release 2018a.
- Orange: Data Mining Toolbox in Python (University of Ljubljana, Ljubljana and Portorož, Slovenia), release 3 [142].
- Microsoft Excel (Microsoft Corp., Redmond, Washington, USA) release 2211.

3.6.2. UAV flight planning and execution.

- DJI™ Flight Planner software (AeroScientific- Spatial Scientific Pty. Ltd., Adelaide, Australia).
- Litchi (VC Technology Ltd.©, London, UK).

3.6.3. Photogrammetry.

- Pix4D™ Mapper software (Pix4D S.A., Prilly, Switzerland).

4. Results

In the following section, the four articles published in high-impact journals that comprise this Thesis are compiled, organised according to the topics addressed. Furthermore, an additional work yet to be published (article 4) is included.

4.1. Water status assessment

4.1.1. Article 1

A New Low-Cost Device Based on Thermal Infrared Sensors for Olive Tree Canopy Temperature Measurement and Water Status Monitoring

Miguel Noguera, Borja Millán, Juan José Pérez-Paredes, Juan Manuel Ponce, Arturo Aquino, and José Manuel Andújar.

Published in:

Journal: Remote Sensing (ISSN: 2072-4292).

Editorial: MDPI.

Reference: Remote Sens. 2020, 12(4), 723.

DOI: 10.3390/rs12040723

Year: 2020

Quality index (Journal Citation Reports®, 2020): 27/200 (Q1) in the category "Geosciences, Multidisciplinary", 10/32 (Q2) in the category "Remote Sensing", 8/29 (Q2) in the category "Imaging Science & Photographic Technology", and 76/274 (Q2) in the category "Environmental Sciences". Impact Factor of 4.848.

remote sensing

MDPI

Article

A New Low-Cost Device Based on Thermal Infrared Sensors for Olive Tree Canopy Temperature Measurement and Water Status Monitoring

Miguel Noguera [1], Borja Millán [1,*], Juan José Pérez-Paredes [2], Juan Manuel Ponce [1], Arturo Aquino [1] and José Manuel Andújar [1]

[1] University of Huelva, Department of Electronic Engineering, Computer Systems and Automation, La Rábida, Palos de la Frontera, 21819 Huelva, Spain; miguel.noguera@diesia.uhu.es (M.N.); jmponce.real@diesia.uhu.es (J.M.P.); arturo.aquino@diesia.uhu.es (A.A.); andujar@diesia.uhu.es (J.M.A.)

[2] Chapingo Autonomous University, Post-graduate program in Agricultural Engineering and Integral Water Use, Chapingo, 56227, Mexico; al18129294@chapingo.mx

* Correspondence: borja.millan@diesia.uhu.es; Tel.: +34 959-217-64

Received: 16 December 2019; Accepted: 21 February 2020; Published: 22 February 2020

Abstract: In recent years, many olive orchards, which are a major crop in the Mediterranean basin, have been converted into intensive or super high-density hedgerow systems. This configuration is more efficient in terms of yield per hectare, but at the same time the water requirements are higher than in traditional grove arrangements. Moreover, irrigation regulations have a high environmental (through water use optimization) impact and influence on crop quality and yield. The mapping of (spatio-temporal) variability with conventional water stress assessment methods is impractical due to time and labor constraints, which often involve staff training. To address this problem, this work presents the development of a new low-cost device based on a thermal infrared (IR) sensor for the measurement of olive tree canopy temperature and monitoring of water status. The performance of the developed device was compared to a commercial thermal camera. Furthermore, the proposed device was evaluated in a commercially managed olive orchard, where two different irrigation treatments were established: a full irrigation treatment (FI) and a regulated deficit irrigation (RDC), aimed at covering 100% and 50% of crop evapotranspiration (ETc), respectively. Predawn leaf water potential (Ψ_{PD}) and stomatal conductance (g_s), two widely accepted indicators for crop water status, were regressed to the measured canopy temperature. The results were promising, reaching a coefficient of determination $R^2 \geq 0.80$. On the other hand, the crop water stress index (CWSI) was also calculated, resulting in a coefficient of determination $R^2 \geq 0.79$. The outcomes provided by the developed device support its suitability for fast, low-cost, and reliable estimation of an olive orchard's water status, even suppressing the need for supervised acquisition of reference temperatures. The newly developed device can be used for water management, reducing water usage, and for overall improvements to olive orchard management.

Keywords: thermal infrared; remote sensor; water stress; irrigation; canopy temperature; stomatal conductance; predawn leaf water potential; olive

1. Introduction

Water management has become a key factor in sustainable agriculture, especially in regions such as the Mediterranean, where water scarcity problems are rising [1]. Traditional olive orchard cultivation is the most widespread method [2]. This approach is based on having rain-fed trees at a density of 100–300 trees ha^{-1}, where irrigation is controlled through cultural practices, such as pruning, which reduces water requirements [3]. In recent years, many traditional orchards have been converted

into intensive and super high-density (SHD) hedgerow systems, with higher yields per ha and reduced managing costs due to augmented mechanization and automatization. Most of these new orchards are under irrigation scheduling, requiring 5000 m^3 ha^{-1} to replace maximum crop evapotranspiration in semi-arid regions, such as the south of Spain and Portugal [4].

Current irrigation practices depend on uniform applications of water over large fields, with varying degrees of heterogeneity (water retention capacity). Due to this heterogeneity, much of the field receives more water than needed [5]. Plant monitoring to assess the water status is required in order to optimize water usage, but it also has a direct impact on olive production and quality [6,7]. Mapping the spatio-temporal variability with conventional water stress assessment methods, such as a pressure chamber [8], is impractical due to the demanding work, required time and cost, and need for expert and trained personnel [9]. In addition, the reliability of the information provided by a pressure chamber decreases when the species display isohydric behaviour, characterized by strong stomatal regulation, reducing the sensitivity of leaf water potential measurements under conditions of low soil water content and high evaporative demand [6].

The relationship between leaf temperature and stomatal regulation was established many years ago [10–15]; when leaf transpiration occurs, water is lost through stomata, reducing leaf temperature. On the other hand, stomatal closure will result in leaf temperature rise, as no heat dissipation through evaporation occurs. Thereby, the temperature of transpiring leaves should be close to air temperature, while in the case of the stressed ones it should be higher [16]. This is the theoretical assumption that enables the estimation of water stress through canopy temperature.

The variability in environmental conditions, plant morphology, and meteorological factors could affect leaf temperature, and thus its precision in leaf transpiration and stomatal conductance (g_s) indicators [17]. Many indexes have been developed to normalize leaf temperature by taking previous reference measurements (reducing the disturbance of the environmental factor over canopy temperature) [18,19], with the crop water stress index (CWSI) [15] being one of the most widely used for a variety of crops [17,19,20]. The calculation of the CWSI relies on two thresholds: the non-water-stressed baseline (T_{wet}), which represents a fully transpiring crop, and the maximum stressed baseline (T_{dry}), which corresponds to a non-transpiring crop [17]. The proposed method for CWSI calculation avoids the need for reference temperatures, since the adaptative thresholds (T_{dry} and T_{wet}) are estimated from the temperature distribution histogram of the complete set of thermal images. This approach reduces the requirement for specialized equipment, the cost, and the time to perform each measurement. Moreover, this paves the way for the automation of water status monitoring. However, this advantage has a limitation—a wide range of water stress levels must exist in the field, resulting in representative canopy temperature values for stressed and non-stressed plants. Nevertheless, this assumption is deeply linked to the specific needs of precision agriculture itself, where homogeneous treatments (for example, same irrigation regime) result in heterogeneous responses linked to the non-uniformity of the field characteristics (soil properties, plot morphology, and microclimate, among others), and even to the different responses of plants.

Traditional temperature measurement techniques (using thermometers or thermocouples attached to the leaves) are impractical for large-scale experiments or industrial applications [21]. Remote infrared (IR) sensors, which could be used for canopy temperature assessment, have pushed the development of a wide range of applications, such as irrigation scheduling [14], its use as an indicator of plant physiology and ecophysiology [22], or plant phenotyping [23]. In this fashion, thermal cameras are used as manually operated portable devices [24], controlled trough mobile phones [25] or installed in all-terrain vehicles (ATVs) [9], aircrafts [26], satellites [27], or recently on remotely piloted aircraft systems (RPAS), usually called drones [28]. Satellite and aircraft-installed sensors can measure canopy temperatures remotely, but these applications do not typically have the spatial or temporal resolution necessary for irrigation decisions [29]. The reduced resolution provided by the microbolometer sensors, combined with the distance to the target, increase the problem of the "mixed-pixel value", where canopy and soil are present in a given pixel, considerably reducing the quality of the data [5,30]. Another

limitation is related to the atmospheric conditions, which may also affect image quality, and hence the derived measurements [31]. In addition, although zenithal images (the only ones available) are suitable for continuous crops, they are not appropriate for woody perennial vegetation with discontinuous canopies [5]. Moreover, they are too expensive and impractical for small-scale farms [28].

Some drawbacks of traditional thermal imaging techniques include the camera cost and resolution, and the time and labor needed to implement the techniques [32]. Sensor resolution must be high enough when used for remote acquisition or the precision of water stress assessment will be reduced. IR array sensors, used for proximal acquisition, can overcome these limitations, greatly reducing the cost and doubling the accuracy in temperature measurements from 1 °C to 0.5 °C, as reported by Martínez et al. [32]. The use of CWSI also enables the automation of the data acquisition as reference measurements are not needed, allowing for the installation of the sensor in vehicles or autonomous robots, which eases the mapping of the orchard. Moreover, cost saving will allow the sensors to be installed on a permanent basis, continuously monitoring the water needs in different locations of the orchard, covering its spatial variability. For this approach, the number of sensors would be determinant for a reliable estimation of the water needs of the crop. This would depend on the heterogeneity of the field characteristics, thereby it would be used with as many nodes as irrigation areas in the field, understanding an irrigation area as a zone with homogeneous water needs. According to this fact, the installation of such a sensor network would require a previous study of the field site. Moreover, it is important to highlight that the reduced cost will allow the increase of the number of nodes, which would have an advantage in ameliorating the spatial heterogeneity problem. On the other hand, as it will require specific manual measurements, this approach is intended for small farmers who cannot afford costly equipment, as described by Jason Shaw et al. [33]. In such cases, a small number of sample points can be representative of orchard status because of the reduced field dimensions or homogeneous conditions.

The goal of this research is to assess the suitability of a new low-cost device based on thermal infrared sensors integrated in a device. The developed tool includes a screen, a microcontroller and its associated software, and a battery for in-field plant water status assessment. To this end, a portable prototype device has been developed and validated through an experimental case study (real-case scenario). The prototype is based on a low-cost development platform which uses an Arduino MEGA™ development board (Arduino LLC, Turin, Italy), an IR temperature sensor array, and common electronic components. The portable prototype includes a secure digital (SD) card and a screen for in-field data storage and supervision. All these features are included in the proposed device at a cost of 145 euros. This cost corresponds to the version used in this research for specific measurements, but it could be reduced if the purpose is to install it permanently, since some components (screen, trigger button) would be expendable.

In the first instance, the performance of the developed device was compared with a commercial thermal camera. Once the accuracy of the low-cost IR thermal camera was demonstrated, a field evaluation was carried out, which included the validation of the acquired canopy temperature and the calculated CWSI against two widely accepted water stress indicators, namely g_s and Ψ_{PD}. This enabled the demonstration of the capacity of the developed device for estimating plant water status from measured canopy temperature.

2. Materials and Methods

2.1. Sensor Performance Evaluation

A laboratory test was performed to evaluate the low-cost IR sensor device. The accuracy of the measured temperature was compared to the data obtained with a Testo™ 875-1i infrared camera. The Testo IR camera has a resolution of 160 by 120, it is factory-calibrated following the standard ISO (International Standarization Organization) 9001:2008, and its thermal sensibility is under 50 mK at 30 °C.

For the experiment, a controlled temperature chamber and a uniform flat surface (a stack of white paper) were used. White paper was selected because it is easily obtainable and it provides a uniform surface with high emissivity, and it is commonly used as an emissivity reference for thermographic inspection [34]. The uniformity of the target ensures the accuracy of the test, even when the sensor does not capture the same target's area due to differential FOVs. The chamber was used to fix the temperature of the target, along with the sensor temperature. Two different temperatures were used, namely 20 °C (ambient temperature in the laboratory) and 30 °C (fixed temperature inside the chamber). The measurements corresponding to warmed targets were performed inside the chamber to reduce the target heat dissipation. Thirty minutes of exposure was used to ensure that both the target and the sensors met the desired temperature. Moreover, an additional five minutes was added to stabilize the sensors measurements after the power was switched on. The combination of two temperatures for both the target and the sensors generated 4 different combinations for each sensor:

- Sensor at ambient temperature (20 °C) measuring target at ambient temperature (20 °C).
- Sensor at ambient temperature (20 °C) measuring target at 30 °C.
- Sensor at 30 °C measuring target at ambient temperature (20 °C).
- Sensor at 30 °C measuring target at 30 °C.

Four images for each of the combinations were taken with the commercial camera (resulting in 76,800 pixels) and 8 images with the low-cost developed device (512 pixels). Mean and standard deviation were computed to evaluate both the estimated temperature and the pixel dispersion when measuring a uniform temperature target.

2.2. Experimental Case Study Design

The experimental case study to evaluate the sensor capabilities to estimate plant water status was carried out on 11th September, 2019, in a commercial olive orchard (*Olea europaea* L. cv. "Arbequina") located in Elvas, Portugal (38°49'33.6"N, 7°07'53.76"W), (Figure 1), at an elevation of around 180 m above sea level and administrated by Elaia™ (Sovena™ Group, Alges, Portugal). The experimental site is a SHD with tree spacing of 1.35 m × 3.75 m (inter and intra-row, respectively), resulting in 2116 trees/ha. The fertilization consists of a fertigation system with periodical adjustment of the nutrient content based on the chemical analysis of leaves. The weed in the experimental site was mechanically controlled. The orchard's soil has a heterogeneous composition, loan and sandy-loan areas are preponderant, but there are some clay-loan zones in the north of the crop. This irregular pattern relative to the composition of the soil has a correlation with the values of electrical conductivity (CEa). A variable amount of low and medium CEa values are observed, except for specific areas where the highest CEa values are shown. Finally, the pH determined in the soil was between 7 and 8.

The climate of the study area according to the Köppen–Geiger classification [35] is Csa (hot-summer mediterranean climate), with average annual rainfall of approximately 600 mm, concentrated from October to May and mostly distributed outside a 4-month summer drought period. During this drought period, irrigation is needed for acceptable production levels, since rainfall is not enough to cover plant water needs due to the plant density. In order to solve this, the orchard has been equipped with a drip irrigation system that supplies water during this period—from the endocarp sclerification (May) to the harvest time (September).

The mentioned irrigation system was modulated to have two distinct areas (two different treatments): full irrigated (FI) plots and regulated deficit irrigated (RDC) plots (50% of the FI dosage). The irrigation scheduling consisted of a daily drip irrigation for the FI plants, calculated to cover 100% of crop evapotranspiration. On the other hand, the RDC plants were exceptionally exposed to alternating drought and irrigated periods of one week. As a result of this irrigation schedule, FI plants received approximately 480 m^3/ha per month between May and September, while RDC plants received just 240 m^3/ha per month. Five tree rows, oriented from north to south with a homogeneous irrigation

scheduling, were selected for each plot: one experimental row (central row) and four guard rows. Four trees in the experimental row were chosen as representative for each treatment (Figure 1).

Figure 1. Location of the experimental case study in Elvas (Portugal). Deficit irrigated plot is enclosed in yellow lines and full irrigated plot in blue lines. Red dots correspond to the selected trees from each plot.

The day of the experiment (11th September) was a sunny day with winds that were not strong enough to be considered as a source of error for thermal measurements (8–12 Km/h). This date is situated at the end of the summer drought period typical of this climate zone, so there was no rain event close to this period.

Irrigation status was assessed using Ψ_{PD} the day of the experiment. Additionally, g_s measurements were acquired simultaneously with the image capture. According to the literature [6], the maximum daily g_s in olive trees can be observed around 10 AM. After this, a progressive increase in the vapor pressure deficit until afternoon occurs, and the plants respond by closing stomata, such that decreasing g_s counterbalances the deficit in vapor pressure. This fact limits the ability of plants to regulate their canopy temperature. In order to evaluate this effect, measurements were acquired early in the morning (10 AM) and during midday (15 PM). The canopy temperature was measured in both FI and RDC plants with the developed low-cost device based on thermal infrared sensors. The images were taken from a lateral perspective, avoiding the effects of the soil pixels. The horizontal field of view of the camera is 60°, so the images were taken from a distance of one meter, capturing a representative image of one single tree. Four thermal images of the sunlit canopy and four of the shaded canopies of each selected tree were taken (n = 8 images/tree x 4 tree/plot x 2 plots = 64 observations). The environmental temperature during the day of the experiment reached 26 °C at 10 AM and 34 °C at 15 PM. A whole measurement cycle lasted around 45 minutes, during which the weather conditions were stable (the distance between both treatment plots was just 100 metres).

2.3. Physiological Measurement

Olive trees, as drought-adapted species, show an isohydric behaviour characterized by strong stomatal regulation [6]. Due to this circumstance, the reliability of the pressure chamber measurements to estimate water status decreases during the day [6]. On the other hand, during the night, the stomata of the leaves are locked (the evaporative demand is minimal), so the leaf water potential is not influenced by transpiration, giving more reliable information of the water available in the soil [6]. Because of this, the leaf water potential was measured before dawn.

The Ψ_{PD} (MPa) is the required pressure for water mobilization through the plant (measured before dawn), which mainly depends on the balance between the water that is lost by transpiration and the water that is gained by absorption [8]. This variable was measured on two healthy leaves per tree (n = 2 leaves/tree × 4 tree/plot × 2 plots = 16 observations) with a Scholander-type pressure chamber (Solfranc Tecnologías^{TM}). The evening before the experiment, the leaves were covered with aluminium foil to avoid condensation on the leaf surface and enclosed in polyethylene bags to totally stop transpiration, according to the procedure of Gucci et al. [36]. Measurements within the pressure chamber were made with the leaves still enclosed in the plastic bag at 06 AM (before sunrise).

The g_s (mol m^{-2} s^{-1}) is the degree of stomatal opening, which is related to the water vapor exiting through the stomata of a leaf. Water stress induces stomatal closure, which in turn limits leaf transpiration, and hence the evaporative cooling process. This results in higher leaf and canopy temperature values [14,22]. The g_s was measured on four mature sunlit leaves per tree (n = 4 leaves/tree × 4 tree/plot × 2 plots = 32 observations), on the same trees used for the predawn leaf water potential measurements, using a model SC-1 leaf porometer (Decagon Devices^{TM}). Measurements of stomatal conductance were taken early in the morning (10 AM) and during midday (15 PM), simultaneously to thermal image acquisition.

2.4. Crop Water Stress Index Calculation

The crop water stress index (CWSI) was developed as a normalized index to quantify stress and reduce the disturbance of the environmental parameters affecting the relationship between water stress and canopy temperature [11,15]. It has been widely used as a water status indicator [19,20]. It provides the crop stress level based on canopy–air temperature differences. The CWSI algorithm applied in the study was introduced by Jones et al. [37], which can be represented as follows:

$$CWSI = \frac{T_{canopy} - T_{wet}}{T_{dry} - T_{wet}} \quad (1)$$

where T_{canopy} is canopy temperature from the thermal images; T_{wet} is the temperature of a fully transpiring leaf, or lower reference; and T_{dry} is the temperature of a non-transpiring leaf, also considered the upper reference. Therefore, as the CWSI index (Equation (1)) is the result of normalized canopy temperature based on high and low reference temperatures, the effects of environmental conditions are minimized, and the water status is the main factor determining the index value.

2.5. Adaptative Temperature Thresholds

With the aim of simplifying the in-field CWSI assessment, adaptive thresholds of T_{wet} and T_{dry} based on the method proposed by Park et al. [38] were estimated. The process involved using an adaptive approximation based on the TIR histograms derived from the images. It is assumed that T_{wet} and T_{dry} can be taken from the coldest and the hottest part of the temperature distribution histogram of the thermal images, respectively (n = 64 pixels/imagen × 32 imagens/ measurement cycle = 2048 temperature values). The collected measurements feature normal density distributions, however there were some data represented at a reasonably low frequency that were considered outliers (i.e., non-representative canopy temperature). To avoid the influence of the outliers, T_{dry} (Equation (2)) and T_{wet} (Equation (3)) were calculated according the following expressions:

$$T_{dry} = T_{canopy} + 2\sigma \quad (2)$$

$$T_{wet} = T_{canopy} - 2\sigma \quad (3)$$

where σ is the standard deviation. With this approach, we discarded 2.2% of the data situated at the upper and lower thresholds of the normal distribution of temperature. These data were considered

outliers, which could represent, for example, surfaces of the tree without transpiration capacity (branches or stems) [39].

2.6. Statistical Analyses

Analysis of variance (ANOVA) was used to compare the average values measured between treatments relative to plant-based variables and canopy temperatures. Error probability (EP) values below 0.01 were considered significant. The relationships between canopy temperature and CWSI index regarding the physiological measurements were evaluated through linear regression analyses. In all cases, the coefficient of determination R^2 was used to assess the quality of the statistical model.

3. Developed Device for Measuring Canopy Temperature and Water Status Monitoring

A new low-cost device based on a thermal infrared sensor for olive tree canopy temperature measurement and water status monitoring was developed. A block diagram of its architecture can be seen in Figure 2, with its physical implementation shown in Figure 3. The controller of the whole device is a low-cost development platform, specifically an Arduino™ MEGA 2560.

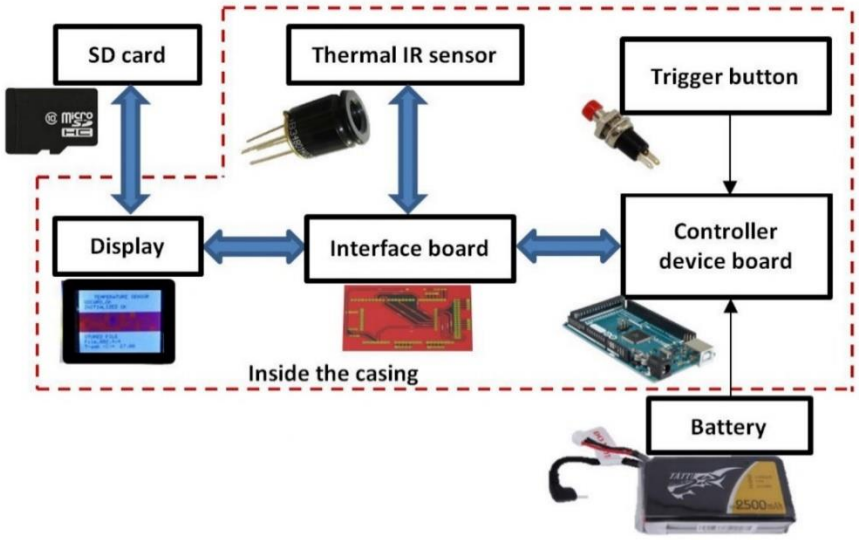

Figure 2. Block diagram of the developed low-cost device based on a thermal infrared sensor.

The blocks of the developed device depicted in Figure 2 are described below.

3.1. Thermal Infrared Sensor

The chosen low-cost thermal IR sensor is embedded in the integrated circuit (IC) MLX90620 (Melexis™). In addition to its low cost, the choice is based on the fact that it is a fully calibrated IR temperature sensor array (16 × 4 pixels) capable of remote non-contact temperature measurements, with 16-bit precision and noise equivalent temperature difference (NETD) under 0.5 K; its operating temperature is very suitable for operating in agriculture, specifically from −40 °C to +85°C. The sensor is encapsulated in a 4-lead TO-39 (metal can package) containing two chips: the thermal IR sensor with its associated signal conditioning hardware and an electrically erasable programmable read-only memory (EEPROM) chip used for calibration data storage. The sensor is available in two different field of view (FOV) configurations: 60° and 40°; the latter was selected, since it provides optimum temperature measurements of the central canopy zone at 1 m, resulting in an approximated measurement area of 75 cm (horizontal) by 10 cm (vertical) and a pixel size of 4.7 by 1.25 cm.

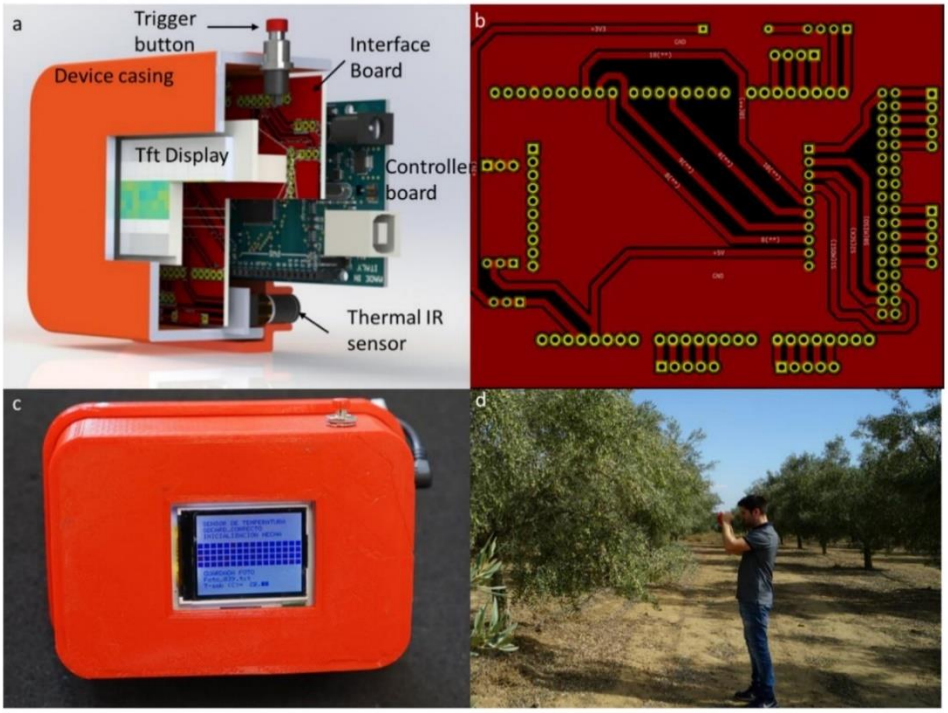

Figure 3. Developed device. (**a**) Partial cut showing all its elements. (**b**) PCB (Printed Circuit Board) layout of the interface board that connects the elements of the system. (**c**) Device casing showing the display during operation. (**d**) Field device operation for canopy temperature measurement.

The MLX90620 is an infrared sensor composed 64 thermopile units (16 by 4 array). Thermopiles are composed of several thermocouples in series. A thermocouple is a device that generates voltage when its dissimilar metals (thermocouples) are exposed to differential temperatures. The output voltage is directly proportional to the temperature differential from their junction point (related to the IR radiation of the object the sensor is pointed to) and the voltage measurement point, not to the absolute temperature. Thermocouples can be connected in series (forming thermopiles), increasing the magnitude of the voltage output, and thus reducing the error associated with measuring the small voltages they produce (in the millivolts range). The MLX90620 integrates its own circuit to amplify (a low-noise, chopper-stabilized amplifier) the sensor signal, which is then converted to digital by a fast-integrated 16-bit ADC that is also embedded in the chip. As previously described, a thermocouple's output is proportional to the temperature differential of the junction and the voltage measurement points, in this case the device package temperature that is measured by an additional sensor (also included in the chip package), a PTAT. To block wavelengths that are not relevant to the measurements, the sensor incorporates a long-wave filter in front of it.

The outputs of both IR and PTAT sensors are stored in an internal RAM and are accessible through a I^2C (Philips^{TM}) inter-integrated circuit communication protocol bus. The controller and the MLX90620 are connected using the I^2C bus through the interface board (described in the next section). The I^2C protocol uses a two-wire bus for bidirectional communication. Each I^2C integrated circuit has a unique identifying number (ID) and the master (in this case the device controller) communicates with each of them using its address.

3.2. Interface Board

The interface board that connects all the elements was designed using KiCad 5.1.4 as a single-sided circuit board (Figure 3b).

The system is powered by a 2s LiPo (Lithium-ion Polymer) battery connected to the device controller board (Arduino^{TM} MEGA 2560). To supply the device components, different voltage levels were implemented: the SD card reader and the display were powered with 5 V from the regulator of the device controller board; regarding MLX90620 IC, it requires 2.6 V for operation, so a diode was connected in the interface board to drop the voltage level down from the 3.3 volts available at the power rail of the device controller.

3.3. Display

In order to help and guide the user during the measurement, the developed device includes an Arduino display, specifically a 1.8 inch TFT-LCD (thin film transistor-liquid crystal display) with a resolution of 128 by 160 pixels, as well as a micro-SD slot (see Figures 2 and 3c). Both elements are ruled by the device controller through the interface board, using a bus based on the serial peripheral interface (SPI).

During operation, the display shows procedures, tasks, and data, as well as device status. In addition, the display shows a matrix (16 by 4) representing each of the IR temperature measurements. In order to provide very intuitive information, each pixel acquires its own RGB colour value, depending on the value of its temperature. The matrix is updated each second, coinciding with the update of the sensor measurements. The measurements and interest data, such as file names, were stored in a SD card.

The availability of an integrated display avoids the use of a computer in the field or some other external device to verify the status of the device and its proper operation, also delivering real-time data.

3.4. Device Casing

The device casing was designed using Freecad 0.16 and manufactured with a 3D printer using biodegradable polylactic acid (PLA) 3D printer filament. Two different parts were designed (front and back) to provide a perfect enclosure. A section of the device and its casing can be seen in Figure 3a, as well as its back in Figure 3c. All device elements are housed inside the developed casing, except the battery, which is installed outside to avoid temperature interferences with the IR sensor that could affect the precision of the measurement, as well as to simplify its field replacement.

3.5. Device Controller Board

The device controller board (Arduino^{TM} MEGA 2560) includes a microcontroller, which based on the written and uploaded program, performs the programmed functions. The program was developed, compiled, and uploaded to the device controller board using the Arduino^{TM} development environment version 1.8.9. The flow chart of Figure 4 shows the basic functionalities of the program.

The process to perform an IR temperature measurement requires successive steps, as depicted in the flowchart in Figure 4. These will be described below:

1. *Initialization.* During this process, all the elements of the device are initialized:
   - *Communication parameter configuration*: The baud rates and port assignation for the communication between the different components of the developed device are set up.
   - *SD card initialization*: The SD slot is checked for card presence, after which the files present are examined to determine the next image file name.
   - *Sensor calibration data read*: The registers containing the calibration information (determined during fabrication), including the offset and slope calibration value for every pixel, are read during this phase. The data is stored in the RAM of the device controller board for faster correction calculation.
   - *Display initialization*: The display is initialized, showing the status of the system and the errors during the process (if present).

2. *Temperature registers read:* The raw data of the temperature measured by the IR sensor is stored in the MLX90620 RAM. The value corresponding to every pixel and the temperature of the chip (through PTAT) are read by the device controller using the I^2C bus.
3. *Temperature correction:* The raw temperature data must be corrected to obtain canopy temperature values. This process is performed in three different steps:

   - *Sensibility per pixel correction:* The raw temperature data is operated in conjunction with the stored calibration values to standardize the sensor response and to obtain $T_{O(i,j)}$, the temperature corresponding to each pixel with the following equation:

$$T_{O(i,j)} = \sqrt[4]{\frac{V_{IR(i,j)\_COMPENSATED}}{\alpha_{(i,j)}} + (T_a + 273.15)^4} - 273.15 \quad (4)$$

     where $\alpha(i,j)$ corresponds to the individual pixel sensitivity coefficient calculated (as described in the MLX90620 datasheet) from data stored in EEPROM, Ta is the ambient temperature correction, calculated with Equation (5), and $V_{IR(i,j)\_COMPENSATED}$ is the parasitic free IR compensated signal, obtained with Equation (6).
   - *Ambient temperature correction:* The temperature of the sensor (ambient temperature) affects the measurements. To correct this, MLX90620 includes a PTAT sensor to adjust the IR temperature values. The equation that calculates the ambient temperature is described below:

$$Ta = \frac{-K_{T1} + \sqrt{K_{T1}^2 - 4K_{T2}(V_{TH}(25) - PTAT\_data)}}{2K_{T2}} + 25 \quad (5)$$

     where K_{T1}, K_{T2}, and V_{TH} are constants (fixed during the in-factory calibration) stored in the MLX90620 EEPROM (are defined by the manufacturer), and PTAT_data refers to the value measured by the in-chip temperature sensor.
   - *Emissivity correction:* The device measures the thermal radiation of a target and estimates its temperature as corresponding to a black body. The emissivity corrects the measurement considering that the object under study is not a perfect black-body emitter. The emissivity was set to 0.98, as this value has been reported to induce errors of less than 1 °C when measuring the canopy of different horticultural crops [40].

$$V_{IR(i,j)\_COMPENSATED} = \frac{V_{IR(i,j)\_TGC\_COMP}}{\varepsilon} \quad (6)$$

     where ε is the emissivity and $V_{IR(i,j)\_TGC\_COMP}$ corresponds to the pixel thermal value after the pixel sensibility and offset compensation process, as described in MLX90620 datasheet.
4. *Display update:* After all the corrections have taken place, the display is updated with the measured temperature. The temperatures are shown as a coloured matrix, with colour values reflecting the temperature associated with the corresponding pixel.
5. *File writing* (in the event of the trigger button is pressed): When the trigger button is pressed, the temperature measurement (already corrected) is stored in a file and saved on the micro SD card for further processing. The name of the file is automatically generated.

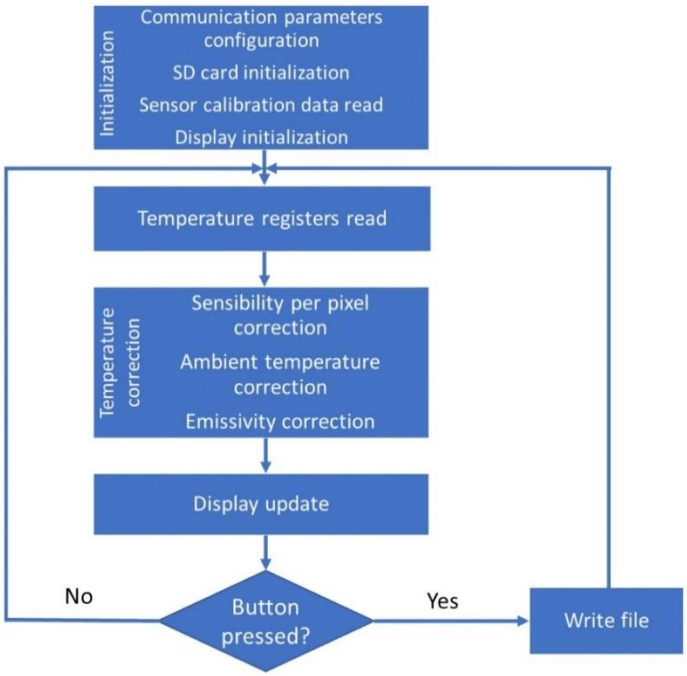

Figure 4. Measurements flow chart of the program of the developed low-cost device based on thermal infrared sensor.

3.6. Device Components and Cost

The labor required to manufacture, assemble, and test each element of the developed device, as well as housing them in the casing, is about 3 h for circuit board fabrication, 10 h for 3D printing of the device casing, and 2 h for final assembly and testing. Costs of the circuit and sensor components are shown in Table 1, with a cost of materials under 150 € for the whole device. As a comparison, the Testo^{TM} 875-1i used for the sensor performance evaluation has an acquisition cost of around 3500 €.

Table 1. List of the developed device components.

Description	Part Number	Manufacturer	Cost (€)
IR sensor	MLX90620	Melexis^{TM}	40
Arduino MEGA 2560	A000067	Arduino^{TM}	35
Arduino display and micro SD card reader	A000096	Arduino^{TM}	35
LiPo Battery 7.4v (2s)	TA-2500-2S1P	Tattu^{TM}	25
Other components (Interface board, button, PLA for device casing, etc.)	-	-	10
Total			145

4. Results

4.1. Sensor Performance Evaluation

The results of the evaluation of the two sensors under the two different operation conditions are represented in Table 2.

Table 2. Results of the performance of the measurement of a uniform temperature target. Both the sensors and the targets were tested at two temperatures, 20 °C and 30 °C.

Sensor	Sensor Temperature (°C)	Target Temperature (°C)	Average Measured Temperature (°C)	Measured Temperature Standard Deviation (°C)
Testo™ 875-1i	20	20	18.94	0.14
	20	30	30.50	0.62
	30	20	17.27	0.75
	30	30	33.73	1.78
Low-cost IR sensor device	20	20	22.78	0.77
	20	30	30.62	0.67
	30	20	22.33	0.77
	30	30	31.78	1.09

The precision of the measurements decreases as the sensor temperature increases, affecting both the commercial camera and the low-cost developed sensor. The performance of both sensors is similar in terms of both average temperature drift and dispersion of the values across the image.

4.2. Plant-Based Variables Reference Values

As described in Section 2, two different treatments were established in a commercial olive orchard: FI and RDC. In order to check the differences in water status, two physiological variables related to water stress were assessed for each treatment: g_s and Ψ_{PD}. Differences in these parameters between treatments would confirm the quality of the experimental case study design. The Ψ_{PD} was measured by a Scholander-type pressure chamber and the g_s by a leaf porometer.

Measured Ψ_{PD} responded to the water stress from the different irrigation treatments, oscillating between 0.32 and 3.73 MPa, with the lowest values corresponding to the FI treatment (Table 3). On the other hand, g_s was highest in the morning and declined continuously towards the afternoon in both irrigation treatments. However, statistical differences between irrigated treatments (related to the rate of decrease) could be found during the morning and afternoon, with reductions in g_s between RDC and FI plants of around 48% at 10 AM and 57% at 15 PM. The measured water stress indicator confirmed the differences in the physiological state of the plants subjected to different irrigation treatments.

Table 3. Measured reference values on September 11, 2019 for the experimental plot. Data collected at 10 AM and 15 PM. Note: FI, full irrigated treatment; RDC, deficit irrigation treatment; 1–4 represent selected trees from each part of the plot. Average values of the g_s followed by different letters are different at EP ≤ 0.01. Average values of the Ψ_{PD} followed by different letters are different at EP ≤ 0.01.

Treatments	Tree	g_s at 10:00 AM (mol m^{-2} s^{-1})	g_s at 15:00 PM (mol m^{-2} s^{-1})	Ψ_{PD} (MPa)
FI	**1**	561.13	441.83	0.49
	2	598.77	455.17	0.39
	3	656.47	475.60	0.51
	4	625.43	337.37	0.32
Average		610.45 a	427.49 c	0.43 a
RDC	**1**	363.40	166.97	3.73
	2	292.30	217.97	3.73
	3	327.33	160.33	3.43
	4	298.47	189.83	3.09
Average		320.38 b	183.78 d	3.49 b

4.3. Canopy Temperature

Once the physiological variability between treatments (FI and RDC) was confirmed, the experiment continued to try to verify that this physiological variability was related to differences in canopy

temperature. Therefore, simultaneously to the g_s data collection by the leaf porometer, the canopy temperature was measured using the developed device. The canopy temperature averaged per treatment showed that RDC trees presented higher crown temperatures than FI trees (Table 4). Additionally, as expected, larger disparities were found in the sunlit side of the canopy at 15 PM, with differences of up to 3.24 °C.

Table 4. Canopy temperature measured by the developed device on September 11, 2019 for the experimental plot. Data collected at 10 AM and 15 PM. Note: T_{canopy} sunlit (°C), canopy temperature of the sunlit face; T_{canopy} shaded (°C), canopy temperature of the shaded face; FI, full irrigated treatment; RDC, deficit irrigation treatment; 1–4 represent selected trees from each part of the plot. Average values followed by different letters are different at EP ≤ 0.01.

Treatments	Tree	T_{canopy} Sunlit (°C)		T_{canopy} Shaded (°C)	
		10:00 AM	15:00 PM	10:00 AM	15:00 PM
FI	1	30.69	34.93	27.02	33.10
	2	30.43	34.07	25.64	32.32
	3	30.79	36.15	26.23	32.01
	4	29.91	35.41	26.58	33.11
Average		30.45 a	35.14 c	26.37 e	32.63 g
RDC	1	32.58	38.62	27.48	33.23
	2	33.15	38.81	28.04	33.59
	3	32.55	38.04	28.35	33.60
	4	32.85	38.07	29.01	33.71
Average		32.78 b	38.38 d	28.22 f	33.53 h

On the other hand, T_{canopy} measured on the shaded side of the canopy also showed a significant response to varying irrigation levels (Table 4). However, these differences were smaller than those shown by the sunlit side. The larger disparities of this side were found at 10AM, with differences up to 1.85 °C.

4.4. Relationship Between Canopy Temperature and Plant-Based Variable Reference Values

The relationship between T_{canopy} (measured in the sunlit face of the canopy, Table 4) and the two plant-based variables (Ψ_{PD} and g_s, Table 3) is shown in Figure 5. Here, Ψ_{PD} exhibited a strong coefficient of determination (R^2) to canopy temperature: 0.96 at 10 AM and 0.90 at 15 PM. On the other hand, g_s showed a solid correlation to canopy temperature at 15 PM ($R^2 = 0.80$), with the best results obtained with the data collected at 10 AM ($R^2 = 0.94$). It must be noted that in the case of Ψ_{PD}, it was assessed before dawn (a unique measurement for the entire day), while the g_s was measured simultaneously to canopy temperature. The correlation of g_s with the measured temperature in the shaded face of the canopy was weaker: $R^2 = 0.81$ at 10 AM and $R^2 = 0.71$ at 15 PM. The Ψ_{PD} showed lower correlations: $R^2 = 0.71$ at 10 AM and $R^2 = 0.62$ at 15 PM. In view of these results, the measured temperature from the sunlit face of the canopy was selected for CWSI determination.

CWSI values derived from canopy temperatures (measured in the sunlit side) for each irrigation treatment against Ψ_{PD} and g_s are plotted in Figure 6. Significant linear regression coefficients can be obtained from all the relationships. The fit of the relationships between Ψ_{PD} and g_s with CWSI were similar, with coefficients of determination close to 0.90. The relationship between g_s and CWSI was slightly lower, especially at 15 PM, with a coefficient of determination of 0.80. However, a strong correlation was found at 10 AM with $R^2 = 0.94$. On the other hand, the Ψ_{PD} was the physiological variable that exhibited the tightest linear relationship with CWSI, with a coefficient of determination (R^2) of 0.96 at 10 AM and 0.90 at 15 PM. During the first afternoon hours (15 PM), lower correlations were obtained between g_s and both canopy temperature and CWSI index.

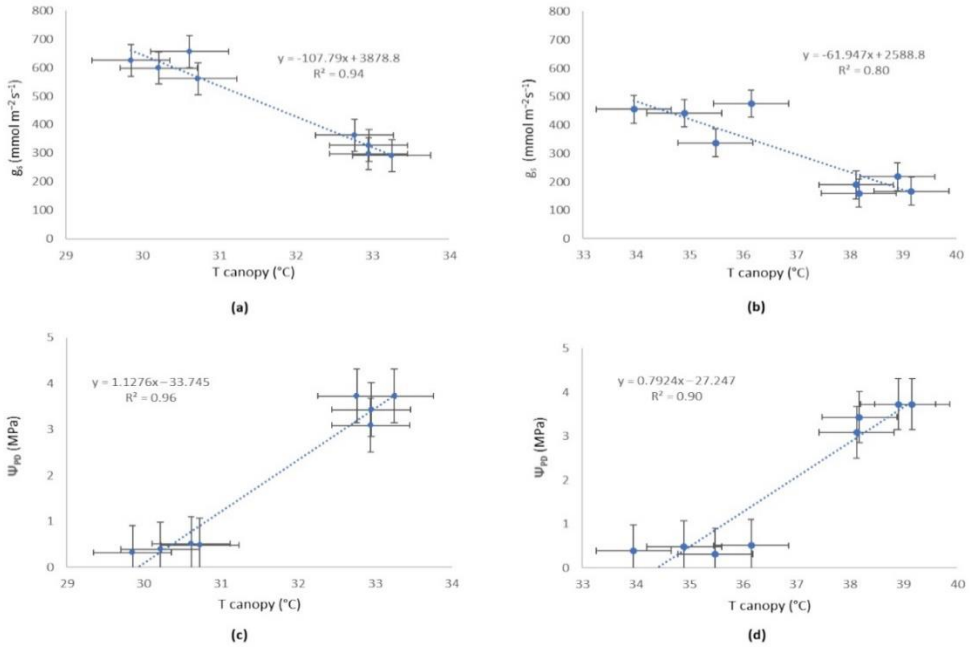

Figure 5. Sunlit face of the canopy: (**a**) relationships between stomatal conductance (g_s) and canopy temperature at 10 AM; (**b**) relationships between stomatal conductance (g_s) and canopy temperature at 15 PM; (**c**) relationships between predawn leaf water potential (Ψ_{PD}) and canopy temperature at 10 AM; (**d**) relationships between predawn leaf water potential (Ψ_{PD}) and canopy temperature at 15 PM. The bars represent standard error.

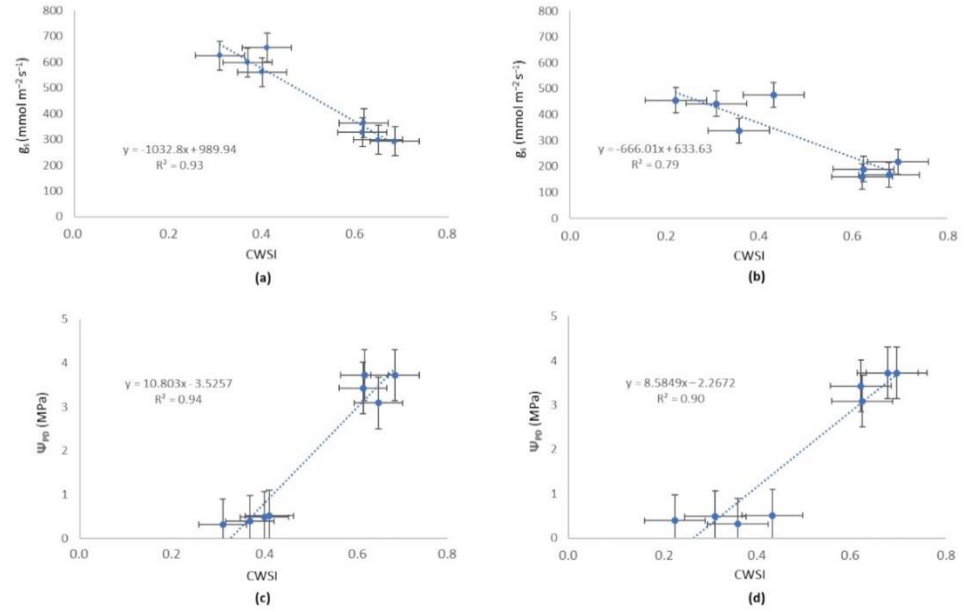

Figure 6. (**a**) Relationships between stomatal conductance (g_s) and CWSI at 10 AM. (**b**) Relationships between stomatal conductance (g_s) and CWSI at 15 PM. (**c**) Relationships between predawn leaf water potential (Ψ_{PD}) and CWSI at 10 AM. (**d**) Relationships between predawn leaf water potential (Ψ_{PD}) and CWSI at 15 PM. The bars represent standard error.

A dispersion in the values represented by the standard error bars can be observed in Figures 5 and 6. This was caused by the variance in the 4 images x 64 pixel/image = 256 values captured per sampling point (olive tree), corresponding to a standard deviation of 2.16 for the ones obtained at 10 AM and 2.51 for 15 PM. This variability could be associated with differences in leaf health, orientation, or age, among other possibilities. As shown in the correlations between thermal acquired data and physiological status, the area of the tree (and its corresponding mean) that was measured using the developed device is representative of plant water stress estimation.

5. Discussion

The first step towards the validation of the proposed low-cost IR sensor device was to compare its precision with a commercially available thermal camera. The relationship between canopy temperature and water status has been widely studied, even with low cost devices [25]. In this study, the accuracy of the sensor was evaluated against a commercially available thermal camera, resulting in comparable precision (in both measured temperature drift and pixel value dispersion) under different operational temperatures. A decrease in measurement precision was observed when the sensor operated at higher temperature (even when a correction is performed). Nevertheless, the commercial camera exhibited a similar effect; future works must be conducted to evaluate the influence of this effect for plant water status assessment.

The laboratory results showed than an error up to 2° C depending on operation conditions must be expected. To determine when this bias affects the utility of the sensor, an in-field experiment in an olive orchard was performed to evaluate the sensor capability of identifying different plant water statuses. The clear response of Ψ_{PD} to the different irrigation treatments showed the different physiological states of the plants. On the other hand, g_s showed a decreasing trend throughout the day in all measured plants, which could be due to the isohydric behaviour of the olive [6], but the rate of decrease was significantly higher in RDC plants. Comparable results were reported by Moriana et al. [41], who concluded that the capacity of stomata to regulate transpiration is lost when soil water is severely depleted. In addition, Torres-Ruiz et al. [42] found a total absence of leaf water potential (Ψ) regulation by stomatal closure when this variable was as low as 4.8 MPa. Both gs and Ψ_{PD} are two reliable indicators of water stress, which are widely accepted by the scientific community [22,43,44], so the differences between both treatments (represented in Table 2) confirm a clear response to varying irrigation levels.

On the other hand, T_{canopy} also showed a response to different irrigation treatments. As expected, the trees exposed to a water deficit showed the higher crown temperature and larger disparities were found in the sunlit face of the canopy at 15PM. This effect is caused by stomata closure in stressed trees, resulting in an increase in canopy temperature. This effect was partially inhibited in FI plants due to their delayed stomata closure, which resulted in a better transpiration capacity [44]. The canopy temperatures measured on the shaded side of the orchard also showed significant differences between treatments (Table 3). Nevertheless, the differences between the average values of the treatments were smaller when compared to the sunlit side. This fact was due to the lower exposure to sunlight of the shaded face, resulting in less heating of the leaves, and thus reduced differences between treatments, even when differences exist in terms of stomatal conductance (g_s) [11].

Once the variability in water status of the plants was ensured (as demonstrated by the reference measurement values showed in Table 3), the next step was to investigate whether this different water status had a relation with the low-cost IR sensor device measurements. For this, both CWSI and T_{canopy} were regressed against each water stress indicator (g_s and Ψ_{PD}). The correlation of g_s with the measured temperature in the shaded face of the canopy was weaker. For this reason, to establish the CWSI, the measured temperature in the sunlit face of the canopy (since it showed greater sensitivity [11]) was selected. Both CWSI and T_{canopy} showed a lower correlation with g_s at 15PM than at 10AM. This fact was also noticed by Ben-Gal et al. [45] and was attributed to the variation in environmental conditions during data collection and the isohydric behaviour of olive orchards [45]. The combination

of both facts attenuates the relation between measured g_s and obtained irrigation status indicators (T_{canopy} and CWSI). Isohydric behaviour is characterized by a cycle of g_s fluctuating during the day, independently of the water status of the tree. This means that the differences in g_s were attenuated by the decrease in the g_s of FI plants due to their isohydric behaviour. If the variations in the environmental conditions (incoming short-wave radiation, air temperature, relative humidity, wind speed, vapor pressure deficit) at 15 PM compared with 10 AM are added, a lesser degree of correlation between g_s and the temperature reached by the canopy was expected. On the other hand, Sepulcre-Cantó et al. [31] found that temperature obtained from airborne thermal imagery earlier in the morning was less affected by background effects than that measured at noon. Nevertheless, in the experimental case study, the thermal images were acquired from a lateral view, avoiding the soil temperature interference.

The crop water stress index (CWSI) was developed as a normalized index to quantify stress and overcome the effects of other environmental parameters affecting the relationship between stress and plant temperature [11,15], so differences were expected in the accuracy of the estimation of water stress by this parameter compared with using T_{canopy} alone. In this experimental case study, no relevant differences were found in the precision of CWSI in comparison with T_{canopy}. This fact was due to the measurements being collected in a short period of time, during which the environmental conditions did not show large variations. It is likely that lower correlations with canopy temperature would be shown by analysing multi-day datasets, since by using the CWSI, the influence of environmental conditions is removed [31]. This suggests that the canopy temperature may be a reliable indicator if the goal is simply comparing between the water status of plants within a given plot at a given time. Nevertheless, if a comparison over time to regulate irrigation is required, the use of the CWSI index will probably be preferable to the canopy temperature. Unfortunately, the data collected for this study cannot assess this hypothesis. Future work is aimed at evaluating the developed device performance under varying environmental conditions and cultivars to define the best indicator of water stress under variable conditions.

The envisaged manufacture costs enable a large margin with the establishment of a very competitive sale price compared with other devices used for water status monitoring. The pieces of equipment used in this research study (pressure chamber and leaf porometer) have final costs of around 1500 euros each. Regarding the cost of the developed device (145 euros) (see Table 1), it is more than an order of magnitude less. On the other hand, if compared with other commercially available devices with similar features, it is still cheaper. For example, the FLIR^{TM} thermal camera TG165 has a final cost of around 350 euros, which is more than double the expense of the developed device. Furthermore, automated industrial manufacturing would significantly reduce costs. It is true that this device has better features than the proposed device (it has a resolution of 80 × 60 pixels). However, this could be considered as a strength of the proposed device, since even assuming the worst features enables detection of water stress with similar efficacy.

In summary, the new low-cost device based on the thermal infrared sensor presented in this paper would improve the current state-of-the-art in olive tree canopy temperature measurement and water status monitoring from different points of view. On the one hand, it has an excellent accuracy–cost ratio. Additionally, it is easier and quicker to use than the traditional methodology. In addition, it runs in a non-destructive way and can be operated by non-expert personnel. The reduced cost also enables its integration into a sensor network for permanent monitoring, where the price per device is a key factor to determine the number of nodes, and in turn, the precision of the collected data. Moreover, this approach would further reduce costs, since some components (screen, trigger button) would be expendable. On the other hand, its installation on vehicles or even in autonomous robots would enable the monitoring and mapping of large crop areas with minimal effort.

6. Conclusions

In this work, a new low-cost device based on thermal infrared sensors was presented to measure, in a non-destructive way, the olive tree canopy temperature and to monitor its water status. Sensor

performance was evaluated against a commercially available thermal camera with a cost of around 20 times higher, showing comparable accuracy. The device was also tested in-field, measuring the canopy temperature and crop water stress index (CWSI) (calculated from the IR measurements), which showed high correlation indices when compared to two standardized water stress assessment methods: predawn leaf water potential (Ψ_{PD}) and stomatal conductance (g_s). Although the results were promising, further work is needed to expand the experimental setup to different environmental conditions and plant water statuses. Nevertheless, the aim of this research was to develop a low-cost alternative for plant water status estimation based on thermal IR measurements. Water stress estimation by canopy temperature has been widely studied and accepted [11–14,17,19,20], although it still has some limitations.

The low-cost of the developed device, along with its ease of use (it does not need to be operated by expert personnel), labour cost savings, and high precision, paves the way for the implementation of an olive orchard water status appraisal system as an alternative to more costly current technologies, and consequently, to increased efficiency and production. These numerous advantages could create new paths in sustainable oliviculture, enabling the deployment of solutions for automatic and continuous evaluation of water needs for more precise and efficient irrigation. Future works will include the evaluation of the suitability of the developed device for the monitoring of different vegetal species in addition to the olive tree, as well as its accuracy under different environmental conditions, in the context of precision agriculture. Moreover, the reduced cost of the sensor itself enables its integration into wireless sensor networks or robotic devices. Continuous monitoring of plant water status will lead to water use optimization during the growing season, reducing environmental impacts in the current context of climate change and water scarcity.

Author Contributions: J.M.A., M.N., and B.M. conceived, designed, and directed the experiments. M.N., A.A., J.M.P., and J.J.P.-P. performed the data acquisition. The software operation and physical fabrication of the device were performed by J.J.P.-P. and B.M.; M.N. and B.M. designed and developed the methodology. M.N. and B.M. drafted the manuscript, which was revised and edited by J.M.A. All authors read and approved the final manuscript.

Funding: The research and APC were funded by the Interreg Cooperation Program V-A SPAIN-PORTUGAL (POCTEP) 2014–2020 and co-financed with ERDF (European Regional Development Fund), grant number 0155_TECNOLIVO_6_E, within the scope of the TecnOlivo Project. Dr. Borja Millán is funded by the Spanish Ministry of Science, Innovation, and Universities through a Juan de la Cierva-Formación Grant (FJCI-2017-31824).

Acknowledgments: The authors acknowledge Diego Tejada for his support in the device design. Special thanks to Antonio Cordeiro and José Silvestre for his assistance in the experimental layout and plant-based variables acquisition, and Elaia™ (Sovena™ Group) for providing the olive orchard on which conduct the study.

Conflicts of Interest: The authors declare no conflict of interest. The founding sponsors had no role in the design of the study; in the collection, analyses, or interpretation of data; in the writing of the manuscript, and in the decision to publish the results.

Abbreviations

ADC	Analog-to-digital converter
AM	Ante meridian
ANOVA	Analysis of variance
ATV	All-terrain vehicle
CEa	Electrical conductivity
CWSI	Crop water stress index
RDC	Regulated deficit irrigated
ETc	Crop evapotranspiration
EEPROM	Electrically erasable programmable read-only memory
EP	Error probability
ERDF	European Regional Development Fund
FI	Fully irrigated
FOV	Field of view

I^2C	Inter-integrated circuit protocol
IC	Integrated circuit
IR	Infrared
ISO	International Standarization Organization
LiPo	Lithium-ion Polymer
NETD	Noise equivalent temperature difference
PLA	Polylactic acid
Ψ_{PD}	Predawn leaf water potential
Ψ	Leaf water potential
PCB	Printed Circuit Board
PM	Post meridian
PTAT	Proportional to absolute temperature
RAM	Random access memory
RPAS	Remotely piloted aircraft systems
g_s	Stomatal conductance
SD	Secure digital
SHD	Super-high density
SPI	Serial peripheral interface
T_{canopy}	Canopy temperature from the thermal images
T_{dry}	Temperature of a non-transpiring leaf
T_{wet}	Temperature of a fully transpiring leaf
TFT-LCD	Thin film transistor- liquid crystal display
σ	Data standard deviation

References

1. Iglesias, A.; Garrote, L. Local and collective actions for adaptation to use less water for agriculture in the mediterranean region. In *Water Scarcity and Sustainable Agriculture in Semiarid Environment*; Elsevier: Amsterdam, The Netherlands, 2018; pp. 73–84.
2. Anuario de Estadística. Available online: https://www.mapa.gob.es/en/estadistica/temas/publicaciones/anuario-de-estadistica/default.aspx (accessed on 16 January 2020).
3. Connor, D.J.; Gómez-del-Campo, M.; Rousseaux, M.C.; Searles, P.S. Structure, management and productivity of hedgerow olive orchards: A review. *Sci. Hortic.* **2014**, *169*, 71–93. [CrossRef]
4. Fernández, J.E.; Perez-Martin, A.; Torres-Ruiz, J.M.; Cuevas, M.V.; Rodriguez-Dominguez, C.M.; Elsayed-Farag, S.; Morales-Sillero, A.; García, J.M.; Hernandez-Santana, V.; Diaz-Espejo, A. A regulated deficit irrigation strategy for hedgerow olive orchards with high plant density. *Plant Soil* **2013**, *372*, 279–295. [CrossRef]
5. Sepúlveda-Reyes, D.; Ingram, B.; Bardeen, M.; Zúñiga, M.; Ortega-Farías, S.; Poblete-Echeverría, C. Selecting canopy zones and thresholding approaches to assess grapevine water status by using aerial and ground-based thermal imaging. *Remote Sens.* **2016**, *8*, 822. [CrossRef]
6. Fernández, J.-E. Understanding olive adaptation to abiotic stresses as a tool to increase crop performance. *Environ. Exp. Bot.* **2014**, *103*, 158–179. [CrossRef]
7. Poblete-Echeverría, C.; Sepulveda-Reyes, D.; Ortega-Farias, S.; Zuñiga, M.; Fuentes, S. Plant water stress detection based on aerial and terrestrial infrared thermography: A study case from vineyard and olive orchard. *Acta Hortic.* **2016**, *1112*, 141–146. [CrossRef]
8. Scholander, P.F.; Bradstreet, E.D.; Hemmingsen, E.A.; Hammel, H.T. Sap pressure in vascular plants: Negative hydrostatic pressure can be measured in plants. *Science* **1965**, *148*, 339–346. [CrossRef]
9. Gutiérrez, S.; Diago, M.P.; Fernández-Novales, J.; Tardaguila, J. Vineyard water status assessment using on-the-go thermal imaging and machine learning. *PLoS ONE* **2018**, *13*, e0192037. [CrossRef]
10. Brown, H.T.; Escombe, F. Researches on some of the physiological processes of green leaves, with special reference to the interchange of energy between the leaf and its surroundings. *Proc. R. Soc. B Biol. Sci.* **1905**, *76*, 29–111.

11. Jones, H.G.; Stoll, M.; Santos, T.; de Sousa, C.; Chaves, M.M.; Grant, O.M. Use of infrared thermography for monitoring stomatal closure in the field: Application to grapevine. *J. Exp. Bot.* **2002**, *53*, 2249–2260. [CrossRef]
12. Fuchs, M.; Tanner, C.B. Infrared thermometry of vegetation. *Agron. J.* **1966**, *58*, 597. [CrossRef]
13. Idso, S.B.; Jackson, R.D.; Reginato, R.J. Extending the "degree day" concept of plant phenological development to include water stress effects. *Ecology* **1978**, *59*, 431–433. [CrossRef]
14. Jones, H.G. Use of infrared thermometry for estimation of stomatal conductance as a possible aid to irrigation scheduling. *Agric. For. Meteorol.* **1999**, *95*, 139–149. [CrossRef]
15. Idso, S.B.; Jackson, R.D.; Pinter, P.J.; Reginato, R.J.; Hatfield, J.L. Normalizing the stress-degree-day parameter for environmental variability. *Agric. Meteorol.* **1981**, *24*, 45–55. [CrossRef]
16. Diaz-Espejo, A.; Nicolás, E.; Fernández, J.E. Seasonal evolution of diffusional limitations and photosynthetic capacity in olive under drought. *Plant Cell Environ.* **2007**, *30*, 922–933. [CrossRef]
17. Maes, W.H.; Steppe, K. Estimating evapotranspiration and drought stress with ground-based thermal remote sensing in agriculture: A review. *J. Exp. Bot.* **2012**, *63*, 4671–4712. [CrossRef] [PubMed]
18. Bian, J.; Zhang, Z.; Chen, J.; Chen, H.; Cui, C.; Li, X.; Chen, S.; Fu, Q. Simplified evaluation of cotton water stress using high resolution unmanned aerial vehicle thermal imagery. *Remote Sens.* **2019**, *11*, 267. [CrossRef]
19. Pou, A.; Diago, M.P.; Medrano, H.; Baluja, J.; Tardaguila, J. Validation of thermal indices for water status identification in grapevine. *Agric. Water Manag.* **2014**, *134*, 60–72. [CrossRef]
20. Poblete-Echeverría, C.; Espinace, D.; Sepúlveda-Reyes, D.; Zúñiga, M.; Sanchez, M. Analysis of crop water stress index (CWSI) for estimating stem water potential in grapevines: Comparison between natural reference and baseline approaches. *Acta Hortic.* **2017**, *1150*, 189–194. [CrossRef]
21. Usamentiaga, R.; Venegas, P.; Guerediaga, J.; Vega, L.; Molleda, J.; Bulnes, F. Infrared thermography for temperature measurement and non-destructive testing. *Sensors* **2014**, *14*, 12305–12348. [CrossRef]
22. Jones, H.G. Application of thermal imaging and infrared sensing in plant physiology and ecophysiology. In *Advances in Botanical Research*; Academic Press: Cambridge, MA, USA, 2004; Volume 41, pp. 107–163, ISBN 9780120059416.
23. Rashid, A.; Stark, J.C.; Tanveer, A.; Mustafa, T. Use of canopy temperature measurements as a screening tool for drought tolerance in spring wheat. *J. Agron. Crop Sci.* **1999**, *182*, 231–238. [CrossRef]
24. Fuentes, S.; de Bei, R.; Pech, J.; Tyerman, S. Computational water stress indices obtained from thermal image analysis of grapevine canopies. *Irrig. Sci.* **2012**, *30*, 523–536. [CrossRef]
25. Petrie, P.R.; Wang, Y.; Liu, S.; Lam, S.; Whitty, M.A.; Skewes, M.A. The accuracy and utility of a low cost thermal camera and smartphone-based system to assess grapevine water status. *Biosyst. Eng.* **2019**, *179*, 126–139. [CrossRef]
26. Bellvert, J.; Zarco-Tejada, P.J.; Marsal, J.; Girona, J.; González-Dugo, V.; Fereres, E. Vineyard irrigation scheduling based on airborne thermal imagery and water potential thresholds. *Aust. J. Grape Wine Res.* **2016**, *22*, 307–315. [CrossRef]
27. Anderson, M.C.; Allen, R.G.; Morse, A.; Kustas, W.P. Use of landsat thermal imagery in monitoring evapotranspiration and managing water resources. *Remote Sens. Environ.* **2012**, *122*, 50–65. [CrossRef]
28. Egea, G.; Padilla-Díaz, C.M.; Martinez-Guanter, J.; Fernández, J.E.; Pérez-Ruiz, M. Assessing a crop water stress index derived from aerial thermal imaging and infrared thermometry in super-high density olive orchards. *Agric. Water Manag.* **2017**, *187*, 210–221. [CrossRef]
29. Crawford, K.E. *Remote Sensing of Almond and Walnut Tree Canopy Temperatures Using An Inexpensive Infrared Sensor on A Small Unmanned Aerial Vehicle*; University of California Davis: Davis, CA, USA, 2012.
30. Gago, J.; Douthe, C.; Coopman, R.E.; Gallego, P.P.; Ribas-Carbo, M.; Flexas, J.; Escalona, J.; Medrano, H. UAVs challenge to assess water stress for sustainable agriculture. *Agric. Water Manag.* **2015**, *153*, 9–19. [CrossRef]
31. Sepulcre-Cantó, G.; Zarco-Tejada, P.J.; Jiménez-Muñoz, J.C.; Sobrino, J.A.; de Miguel, E.; Villalobos, F.J. Detection of water stress in an olive orchard with thermal remote sensing imagery. *Agric. For. Meteorol.* **2006**, *136*, 31–44. [CrossRef]
32. Martínez, J.; Egea, G.; Agüera, J.; Pérez-Ruiz, M. A cost-effective canopy temperature measurement system for precision agriculture: A case study on sugar beet. *Precis. Agric.* **2017**, *18*, 95–110. [CrossRef]
33. Parker, J.S.; DeNiro, J.; Ivey, M.L.; Doohan, D. Are small and medium scale produce farms inherent food safety risks? *J. Rural Stud.* **2016**, *44*, 250–260. [CrossRef]

34. Marinetti, S.; Cesaratto, P.G. Emissivity estimation for accurate quantitative thermography. *NDT E Int.* **2012**, *51*, 127–134. [CrossRef]
35. Köppen, W.; Geiger, R. *Handbuch der Klimatologie: Das Geographische System der Klimate*, 1st ed.; Borntraeger: Berlin, Germany, 1936; ISBN 0936-577X.
36. Gucci, R.; Lombardini, L.; Tattini, M. Analysis of leaf water relations in leaves of two olive (Olea europaea) cultivars differing in tolerance to salinity. *Tree Physiol.* **1997**, *17*, 13–21. [CrossRef] [PubMed]
37. Jones, H.G. *Plants and Microclimate: A Quantitative Approach to Environmental Plant Physiology*, 3rd ed.; Cambridge University Press: New York, NY, USA, 2013.
38. Park, S.; Ryu, D.; Fuentes, S.; Chung, H.; Hernández-Montes, E.; O'Connell, M. Adaptive estimation of crop water stress in nectarine and peach orchards using high-resolution imagery from an unmanned aerial vehicle (UAV). *Remote Sens.* **2017**, *9*, 828. [CrossRef]
39. García-Tejero, I.F.; Hernández, A.; Padilla-Díaz, C.M.; Diaz-Espejo, A.; Fernández, J.E. Assessing plant water status in a hedgerow olive orchard from thermography at plant level. *Agric. Water Manag.* **2017**, *188*, 50–60. [CrossRef]
40. López, A.; Molina-Aiz, F.D.; Valera, D.L.; Peña, A. Determining the emissivity of the leaves of nine horticultural crops by means of infrared thermography. *Sci. Hortic.* **2012**, *137*, 49–58. [CrossRef]
41. Moriana, A.; Villalobos, F.J.; Fereres, E. Stomatal and photosynthetic responses of olive (Olea europaea L.) leaves to water deficits. *Plant Cell Environ.* **2002**, *25*, 395–405. [CrossRef]
42. Torres-Ruiz, J.M.; Diaz-Espejo, A.; Morales-Sillero, A.; Martín-Palomo, M.J.; Mayr, S.; Beikircher, B.; Fernández, J.E. Shoot hydraulic characteristics, plant water status and stomatal response in olive trees under different soil water conditions. *Plant Soil* **2013**, *373*, 77–87. [CrossRef]
43. Gonzalez-Dugo, V.; Zarco-Tejada, P.J.; Fereres, E. Applicability and limitations of using the crop water stress index as an indicator of water deficits in citrus orchards. *Agric. For. Meteorol.* **2014**, *198–199*, 94–104. [CrossRef]
44. Blonquist, J.M.; Norman, J.M.; Bugbee, B. Automated measurement of canopy stomatal conductance based on infrared temperature. *Agric. For. Meteorol.* **2009**, *149*, 2183–2197. [CrossRef]
45. Ben-Gal, A.; Agam, N.; Alchanatis, V.; Cohen, Y.; Yermiyahu, U.; Zipori, I.; Presnov, E.; Sprintsin, M.; Dag, A. Evaluating water stress in irrigated olives: Correlation of soil water status, tree water status, and thermal imagery. *Irrig. Sci.* **2009**, *27*, 367–376. [CrossRef]

4.2. Nutritional status assessment

4.2.1. Article 2

Nutritional status assessment of olive crops by means of the analysis and modelling of multispectral images taken with UAVs

Miguel Noguera, Arturo Aquino, Juan Manuel Ponce, António Cordeiro, José Silvestre, Rocío Calderón, Maria da Encarnação Marcelo, Pedro Jordão, and José Manuel Andújar.

Journal: Biosystems Engineering (ISSN: 15375110).

Editorial: Elsevier.

Reference: Biosystems Engineering. 2021, 211, 1-18.

DOI: 10.1016/j.biosystemseng.2021.08.035

Year: 2021

Quality index (Journal Citation Reports®, 2021): 8/59 (Q1) in the category "Agriculture, Multidisciplinary", and 4/14 (Q2) in the category "Agricultural Engineering". Impact Factor of 5.002.

RESULTS

Debido a restricciones relativas a derechos de autor, el artículo “Nutritional status assessment of olive crops by means of the analysis and modelling of multispectral images taken with UAVs” ha sido retirado de la tesis. En sustitución del mismo ofrecemos la siguiente información: referencia bibliográfica, enlace a la revista y resumen.

-Noguera, M., Aquino, A., Ponce, J. M., Cordeiro, A., Silvestre, J., Arias-Calderón, R., Marcelo, M. da E., Jordão, P., & Andújar, J. M. (2021). Nutritional status assessment of olive crops by means of the analysis and modelling of multispectral images taken with UAVs. In Biosystems Engineering (Vol. 211, pp. 1–18). Elsevier BV. https://doi.org/10.1016/j.biosystemseng.2021.08.035

Enlace al texto completo: https://doi.org/10.1016/j.biosystemseng.2021.08.035

RESUMEN:

This research was aimed at developing an efficient method for Nitrogen, Phosphorus, and Potassium (NPK) foliar content retrieval in olive trees by means of the analysis and modelling multispectral images taken by an unmanned aerial vehicle (UAV) under field conditions. To this end, an experiment was carried out in a super hight density olive orchard. The fertirrigation system of the experimental area was sectorized to obtain plots with different status of NPK. The orchard was overflown with a UAV equipped with a multispectral camera that photographed the entire experimental surface. A new image analysis approach was developed for integrating all the spectral images gathered during the flight in orthomosaics from which to automatically extract information from discrete points. Finally, several retrieval techniques (partial least squares regression, artificial neural network (ANN), support vector regression and Gaussian process regression) were evaluated for NPK leaf content retrieval by using the spectral data as input variables, and the results of chemical analyses as reference. Among all, the best results were obtained by ANN approach (N ($R2 = 0.63$), P ($R2 = 0.89$), K ($R2 = 0.93$)). These results showed the suitability of the proposed image processing approach and indicate ANN as the best recovery technique for the experimental conditions evaluated. However, the approach must be validated under other environmental conditions, olive varieties and plant vegetative stages before making fertilization recommendations.

4.3. Quality status assessment of fruits

4.3.1. Article 3

Methodology for Olive Fruit Quality Assessment by Means of a Low-Cost Multispectral Device

Miguel Noguera, Borja Millán, Arturo Aquino, and José Manuel Andújar.

Journal: Agronomy (ISSN: 2073-4395).

Editorial: MDPI.

Reference: Agronomy. 2022, 12(5), 979.

DOI: 10.3390/agronomy12050979

Year: 2022

Quality index (Journal Citation Reports®, 2022): 16/88 (Q1) in the category "Agronomy", and 60/239 (Q2) in the category "Plant Science". Impact Factor of 3.700.

agronomy

MDPI

Article

Methodology for Olive Fruit Quality Assessment by Means of a Low-Cost Multispectral Device

Miguel Noguera, Borja Millan, Arturo Aquino and José Manuel Andújar *

Centro de Investigación en Tecnología, Energía y Sostenibilidad (CITES), Universidad de Huelva, La Rábida, Palos de la Frontera, 21819 Huelva, Spain; miguel.noguera@diesia.uhu.es (M.N.); borja.millan@diesia.uhu.es (B.M.); arturo.aquino@diesia.uhu.es (A.A.)
* Correspondence: andujar@diesia.uhu.es; Tel.: +34-959-21-77-20

Abstract: The standard methods for determining the quality of olives involve chemical methods that are time-consuming and expensive. These limitations lead growers to homogeneous harvesting based on subjective criteria such as intuition and visual decisions. In recent times, precision agriculture techniques for fruit quality assessment, such as spectroscopy, have been introduced. However, they require expensive equipment, which limit their use to olive mills. This work presents a complete methodology based on a new low-cost multispectral sensor for assessing quality parameters of intact olive fruits. A set of 507 olive samples were analyzed with the proposed device. After data pre-processing, artificial neural network (ANN) models were trained using the 18 reflectance signals acquired by the sensor as input and three olive quality indicators (moisture, acidity, and fat content) as targets. The responses of the ANN models were promising, reaching coefficient-of-determination values of 0.78, 0.86, and 0.62 for fruit moisture, acidity, and fat content, respectively. These results show the suitability of the proposed device for assessing the quality status of intact olive fruits. Its performance, along with its low cost and ease of use, paves the way for the implementation of an olive fruit quality appraisal system that is more affordable for olive growers.

Keywords: AS7265x; multispectral; remote sensing; precision agriculture

Citation: Noguera, M.; Millan, B.; Aquino, A.; Andújar, J.M. Methodology for Olive Fruit Quality Assessment by Means of a Low-Cost Multispectral Device. *Agronomy* **2022**, *12*, 979. https://doi.org/10.3390/agronomy12050979

Academic Editors: Gerardo Fernández Barbero and Ana V. González-de-Peredo

Received: 16 March 2022
Accepted: 15 April 2022
Published: 19 April 2022

1. Introduction

Olea europaea L. is one of the most important fruit trees cultivated in the Mediterranean basin, where it has been a socio-economic engine. Nowadays, it continues to constitute an economic support for rural areas. In fact, in 2018, European olive groves extended for more than 5 Mha, yielding a production of 13.7 Mt of olives, which represented approximately 65% of the worldwide production that year [1].

Traditionally, olive cultivation has been characterized by limited technological support. Nevertheless, in the last decades, the sector has experienced a modernization aimed at increasing orchard profitability. A key milestone of this evolution has been the conversion of non-irrigated orchards into intensive and super-high-density (SHD) hedgerow systems. In this context, precision agriculture techniques have been introduced in the sector, resulting in modern olive orchards. These new crops are usually drip-irrigated, kept under no-tillage techniques, and planted with quick-growing young olive plantings in rows, allowing for mechanized harvesting [2]. Thus, due to an increase in mechanization and automation, olive orchards with higher yields per ha and reduced managing costs have emerged. However, some production stages still need optimization; a good example of this is the decision of the optimum harvest time.

Water and oil are the major components of olives fruits [3]. The ripening process begins after a period of 25 weeks of fruit growth. After this time, the fruit develops to its final size, keeping the original green skin color. Following that, chlorophyll pigments in the olive skin are progressively replaced by anthocyanins, acquiring the characteristic purple coloration.

This change in appearance is also reflected in the chemical composition of the fruits. Indeed, an accumulation of fatty acids occurs, mainly oleic acid, which is responsible for the acidity of the oil. At a certain moment lipogenesis stops, which is a milestone that represents a peak in the quality status of olive fruits, thus being an objectively optimum harvest time [4]. Hence, there are objective parameters such as fat content, moisture, and free acidity that determine quality of olive fruits [5]. As long as the ripening process takes place, these variables can evolve at a diverse pace in the different areas of a field, resulting in a quality indicator heterogeneity that can be managed using precision agriculture techniques.

The determination of the quality parameters in the laboratory is carried out by standard analytical methods [5]. A usual methodology for acidity determination in olive fruits is titration of olive oil. The fat content could be determined by Soxhlet or other techniques such as nuclear magnetic resonance (NMR) [6]. The moisture is normally determined by using a drying oven and Karl Fischer titration [7]. These techniques are expensive, destructive, and provide incomplete information since sampling is based on a limited number of sample points. Furthermore, the results usually take several days, so the decision of the harvest time may therefore be delayed. All the mentioned limitations of traditional olive quality determination techniques lead to a homogeneous harvesting based on subjective criteria such as intuition and visual decisions. We argue that this approach can be improved by objective monitoring of fruit ripening. In order to achieve olives with optimal fruit quality, harvest time should be adapted to the actual conditions of each plot in the field. This reveals the necessity to develop new methods for monitoring the ripening process of olive fruits. These instruments would allow collection of all fruit in an optimum state, assuring a high-quality olive oil and the best economic return for growers.

This research presents a complete methodology based on a new low-cost multispectral sensor for assessing quality parameters of intact olive fruits. In the last decades, numerous studies have focused on the determination of biophysical parameters of vegetation by means of spectroscopy [8–10]. Concretely, the use of spectroscopy to estimate the quality status of olive fruits has also been widely studied, with works based on a great variety of spectral sensors and retrieval methods [11–16]. Some of these works have reported good results even with spectral data obtained in field conditions [17–20]. The mentioned studies have demonstrated the suitability of spectroscopy for olive quality assessment under both laboratory and field conditions. However, all these publications have been accomplished using hyperspectral devices. In fact, nowadays there are NIR scanners commercially available for the determination of basic chemical parameters in olives under laboratory conditions [21]. Nevertheless, these instruments are expensive, and because of their operability, they are not an option to be used under field conditions. However, low-cost spectral sensors have recently emerged that are attracting interest for agricultural applications. Trang et al. [22] tested a 7-band VIS sensor to evaluate leaf chlorophyll content. Moreover, Moinard et al. [23] performed a preliminary evaluation of the same three cheap-based sensors (18 bands VIS-NIR) used in this study to estimate vine vigor and NDVI index. These sensors have the potential to provide objective information to growers, so the goal of this research is to continue exploring its potential by assessing the suitability of low-cost devices based on multispectral data to assess quality parameters of intact olive fruits. In spectroscopy studios, the retrieval method used is an important step. Quantification of biophysical parameters of vegetation from spectral data relies on a model, enabling the interpretation of spectral observations and their translation into a biophysical variable. Since the advent of optical remote sensing science, numerous retrieval methods for vegetation attribute extraction emerged [24]. In this work, an artificial neural network (ANN) approach was used. This is a nonlinear non-parametric method (machine learning method). The main strength of this method is its extraordinary ability to link complex spectral information with key parameters without any constraints on the sample distribution. This makes ANN approaches suitable for defining the intricate nonlinear relationships that normally exist between the spectral signatures of vegetation and biophysical parameters [8]. Several authors have reported on the good performance of

ANN methods in spectroscopy studios as applied to precision agriculture [10,25–30]. The reduced cost of the proposed methodology (including the sensor and the ANN approach) compared to commercially available alternatives would make it more accessible to growers. Thereby, they could assess the quality of their harvest by themselves. This could allow them to decide the harvest time according to the optimum quality state of the olive fruit, so that they could get the best economic return. Furthermore, the limited cost of this device allows for in-field evaluation by either installing the sensors in mobile platforms like agricultural vehicles and autonomous robots, or in the form of a static sensor network.

2. Materials and Methods

2.1. Samples

Olive samples (n = 507) of four varieties (*Olea europaea* L., cv. Picual (54.2%), cv. Arbequina (28.6%), cv. Arbosana (7.7%), and cv. Verdial (9.5%)) were collected in the olive mill *Nuestra Señora de la Oliva* located in the village of Gibraleón (Huelva, Andalusia, Spain). During the harvest season 2020–2021, numerous olive growers provided olive samples to the mill for their appraisal. These fruit samples were analyzed with the mill's resources and subsequently with the proposed device.

2.2. Reference Analyses

The reference data of the target parameters (moisture, acidity, and fat content) were determined by an industrial-standard near-infrared analyzer (OliveScan^{TM} 2, Foss, Hilleroed, Denmark) [31]. The used NIR scanner was subjected to periodic calibrations. This methodology has been widely tested and it has been used as a reference method in numerous research studies [32–36].

2.3. Spectral System

The proposed spectral system is composed of three main components:

- Spectral sensor: the AS7265x development board (Figure 1), based on the AS7265x smart spectral sensor family (AMS, AG, Premstätten, Austria), was used. The sensor is composed of three chips, and each of them have six independent on-device optical filters whose spectral response is defined at a range between 410 nm and 940 nm, with full width at half maximum (FWHM) of 20 nm. The combination of the three sensors results in an 18-channel multispectral sensor.
- Light source: a 35 W dichroic halogen bulb, which offers a broadband spectrum allowing for accurate reflectance measurements, was employed. Halogen lamps have a wider spectral range of emission than that of LEDs, which enabled taking advantage of the sensor capabilities in the NIR domain. Moreover, using a relatively high power reduced the influence of ambient light interference, as the magnitude of the reflectance signal from the olive samples is considerably higher when compared to background and ambient light. Notwithstanding, an acquisition chamber was used to isolate the spectral measurement procedure to minimize signal noise.
- Controller board: the communication between the spectral sensor and a computer was implemented using an Arduino MKR board (Arduino LLC, Monza, Italy). A custom software was developed for the configuration of the capturing parameters (exposure time and gain). The software awaits user input to capture a sample spectrum. When capturing is triggered, the Arduino board sends the command to the sensor and gathers data. Then, the acquired data are sent to a computer and stored in an SD card for further analysis.

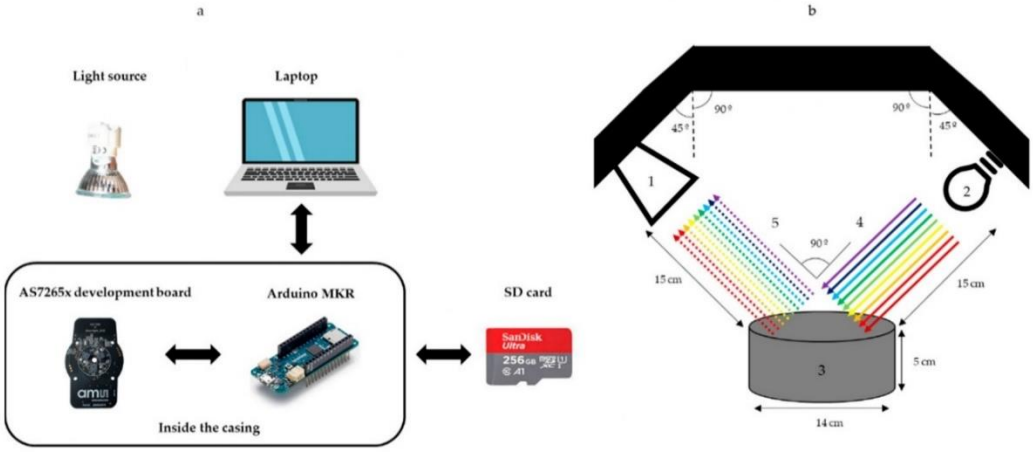

Figure 1. (**a**) Schematic of the components of the developed low-cost device based on a multispectral sensor. (**b**) Basic diagram of the developed device: (1) spectral detector, (2) light source, (3) sample, (4) incident light, and (5) reflected light.

Figure 1 shows the schematic of the components of the developed spectral system. Apart from the previously described elements, a bracket based on a photographic tripod allowed for the setup of the sensor and the light source with a 90° angle of incidence between them and a fixed distance to the olive fruits. This scheme aimed to ensure the capture of the spectral signal by the sensor after being reflected by the samples. In addition, a custom-developed enclosure was designed and 3D-printed to install and protect the electronics. A round thin layer of PTFE was placed in front of the sensor to act as a diffuser and to standardize the spectral signal. The operation of the spectral system was carried out inside an opaque chamber to isolate the measurement from outdoor lighting.

System Components and Cost

The labor required to manufacture, assemble, and test every element of the developed device was about 3 h for circuit board manufacturing and interconnection, 10 h for printing the custom 3D enclosure, and 1 h for final assembling and testing. The cost of the circuit and sensor components are shown in Table 1. Note that the total cost for all the materials needed for the system's implementation remained below 200€ (this does not include the computer and sensor mount, as they are not exclusive to the system and are usually available for laboratory use).

Table 1. List of the developed device components and associated cost.

Description	Approx. Cost (€)
AS7265x development board	150
Arduino MKR	24
Light source	3
Other components (PTFE disc, PLA for device enclosure, etc.)	10
Total	187

2.4. Methodology

2.4.1. Multispectral Signal Capture

All the olive samples were stabilized during 24 h at laboratory temperature (25 °C) using air conditioner equipment, as temperature can strongly affect background levels during spectrum acquisition [37].

Once the standard analysis of the olive samples was carried out by the mill's specialized personnel, the results related to fat content, moisture, and acidity were recorded in writing. Immediately after that, the olive samples were placed in a circular container with 14 cm of diameter, 5 cm of depth, and 500 g of capacity. Then, the olive samples were placed inside the acquisition chamber of the spectral system and positioned under the light source and the multispectral sensor at the same distance from both (15 cm) (Figure 2).

Figure 2. Example of an olive sample measurement taken during the spectral data acquisition.

Four spectral captures were taken for each olive sample. Between captures, the olive samples were rotated 90°, being the average reflectance of the four spectra considered as representative data of each sample.

2.4.2. Data Pre-Processing

The reflectance of each olive sample was calibrated to prevent eventual errors due to variations of the light source. For this purpose, a capture of a known reflectance surface (53%) (Labsphere, Inc, North Sutton, NH, USA) was taken every five samples. This level of reflectance allowed obtainment of a better resolution as the reflectance of the samples was less than 50% for all the considered bands. The 18 reflectance signals of the known reflectance surface were used as reference for calibrating the spectral response of the subsequent twenty captures according to the next equation:

$$Rcal_{wl} = \frac{R_{wl} * 0.53}{Rref_{wl}}, \quad (1)$$

where R_{wl} is the reflectance value measured for a given spectral band in a capture of a sample, $Rref_{wl}$ is the reflectance value measured for that spectral band in the previous capture of the known reflectance surface, and $Rcal_{wl}$ is the corrected value of reflectance in the sample for the given band. A representation of the spectrum measured from a sample, the calibration pattern for all the bands, and the resulting corrected signal are shown in Figure 3.

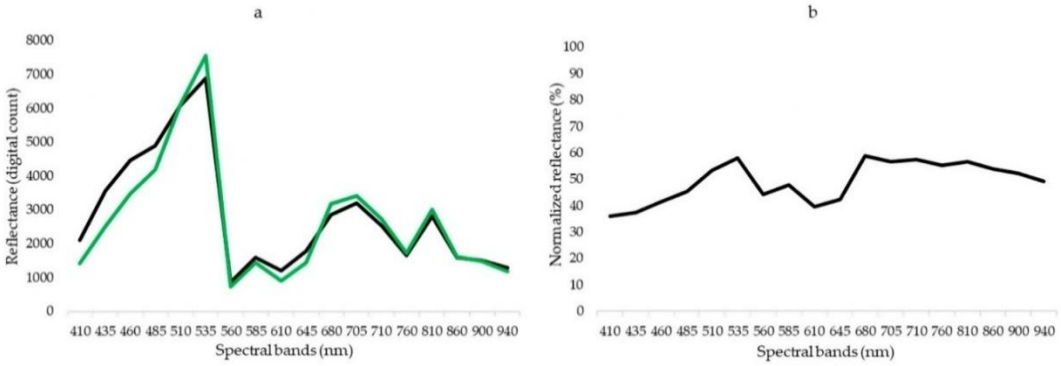

Figure 3. Pre- and post-processed spectrum (410–940 nm) of a given sample. (**a**) Raw spectrum of the known reflectance surface (black), and raw spectrum of the given sample (green). (**b**) Calibrated spectrum of the given sample based on the reflectance of the known reference surface.

Once corrected, the mean reflectance value of the four captures of a given sample for each spectral band (18) were stored.

2.4.3. Reference Parameter Modeling by Means of Multispectral Data

The corrected reflectance of the 18 spectral bands captured by the sensor were used as input variables to train three artificial neural networks (ANN) to estimate the following olive fruit quality parameters: fat content, moisture, and acidity. MATLAB R2020a (The MathWorks Inc.) was used for data processing and ANN training. The complete dataset (n = 507) was randomly divided into three subsets: train (80%), internal validation (10%), and external validation (test) (10%). The ANN architecture was composed of a hidden layer with ten neurons, eighteen inputs, and one output. Thus, each ANN model was trained to estimate a unique olive quality parameter. The Levenberg–Marquardt algorithm was selected as the training algorithm because of the volume and the range of the used dataset. The training process was automatically finished when generalization stopped improving, as indicated by an increase in the mean square error (RMSE) when estimating the fruit quality parameter using the internal validation set.

2.5. Criteria for Model Performance Evaluation

The performance of the quality estimation models was measured by the coefficient of determination (R^2) and the root mean square error of prediction (RMSEP). These parameters were calculated using the reference values of fat content, moisture, and acidity obtained by the automatic analyzer and the responses of each model for the estimation of the different parameters in the external validation groups. In order to make the RMSEP value comparable between variables, it was expressed as the percentage of RMSEP with respect to the mean of the observed values. Thus, higher R^2 and smaller RMSEP values indicated better model performance. RMSEP can be mathematically formulated as:

$$\text{RMSEP} = \sqrt{\sum_{i=1}^{n} \frac{(Ypred - Yref)^2}{n}}, \quad (2)$$

where $Ypred$ is the response of the model, $Yref$ is the reference data acquired by means of the automatic analyzer, and n is the number of measurements in the respective external validation dataset.

3. Results

3.1. Quality Condition of Samples

A total of 507 olive samples from four olive varieties were considered in this research, including 275 of cv. Picual (54.2%), 145 of cv. Arbequina (28.6%), 39 of cv. Arbosana (7.7%)

and 48 of cv. Verdial (9.5%). This experiment was carried out under real conditions in a commercial olive mill. Thus, the olive varieties used in this research represent the most commonly cultivated in western Andalusia. The set of samples was considered as a unique dataset (not dissociating between olive varieties), aiming to increase the volume and the range of the different target quality parameters to consequently improve the predictive models' generalization.

Table 2 summarizes the statistical details of the full dataset in relation to the target quality parameters. In the case of moisture (expressed as % of water in fresh weight), the olive samples varied between 44.58% and 68.29%, with an average value of 60.40% ± 3.26%. On the other hand, the acidity (expressed as % of oleic acid) of the olive samples ranged between 0.25% and 0.52% with an average value of 0.38% ± 0.06%. Finally, regarding fat content (expressed as % of fat in fresh weight), a variation between 8.92% and 24.43% was observed, with an average value of 16.32% ± 2.45%. The ranges of the different parameters were wide enough, considering that all the olive samples were at an optimum quality state according to the growers' criteria.

Table 2. Statistics for the olive fruit dataset in relation to moisture, acidity, and fat content.

	Range	Mean	SD
Moisture (%)	44.58–68.29	60.40	3.26
Acidity (%)	0.25–0.52	0.38	0.06
Fat content (%)	8.92–24.43	16.32	2.45

3.2. Spectral Signature of Samples

Figure 4 represents the reflectance responses corresponding to approximately the 5th and above the 95th percentile of the histogram of the studied parameters. Overall responses were similar throughout the measured spectrum, although in the case of acidity (4c), differences between acidity levels can be observed. These reflectance peaks were especially noticeable between 410–535 nm, which includes the first half of the visible domain, until the green region. On the other hand, the differences of the spectral signature of olive fruits relative to its moisture and fat content were more uniform.

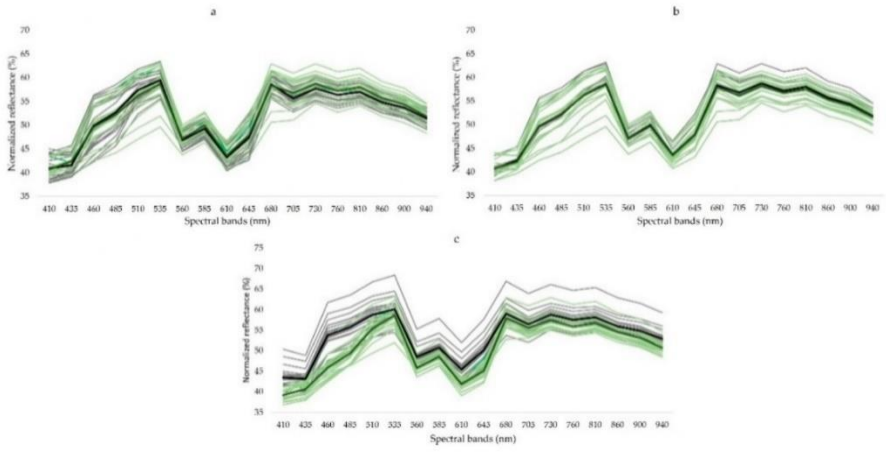

Figure 4. Reflectance responses of olive fruits in the upper limit (grey) and the lower limit (green) of moisture (**a**), fat content (**b**), and acidity (**c**). Each graph includes 40 samples (corresponding to approximately the 5th and above the 95th percentile respectively for each parameter). Furthermore, the mean reflectance curve of the 20 samples in the upper limit (black) and the 20 samples in the lower limit (dark green) are represented.

3.3. Performance of Estimation Models

Table 3 shows the accuracy achieved by the proposed ANN models in the estimation of the considered target quality parameters. As it can be observed, the performance of the ANN approaches was suitable in the estimation of the three target parameters. The best result was obtained when estimating olive fruit acidity, with an R^2 value of 0.86 and a RMSEP of 5.83% measured on the external validation dataset. On the other hand, the model aimed at estimating olive fruit moisture also reached satisfactory results, giving an R^2 value of 0.78 and a RMSEP value of 3.31%. Finally, the performance of the ANN approach for fat content estimation was lower, although considerably valid, yielding an R^2 value of 0.62 and a RMSEP of 10.44%.

Table 3. R^2 and RMSEP between reference values of olive fruit moisture, acidity, and fat content and those estimated values based on ANN approaches.

	Moisture (%)	Acidity (%)	Fat Content (%)
R^2	0.78	0.86	0.62
RMSEP	3.31	5.83	10.44

The linear relationship between fruit moisture (estimated VS reference) for the different datasets (train, internal validation, external validation, and all combined) is shown in Figure 5. The analysis for fruit acidity and fat content for the different datasets is also drawn in Figure 6; Figure 7, respectively.

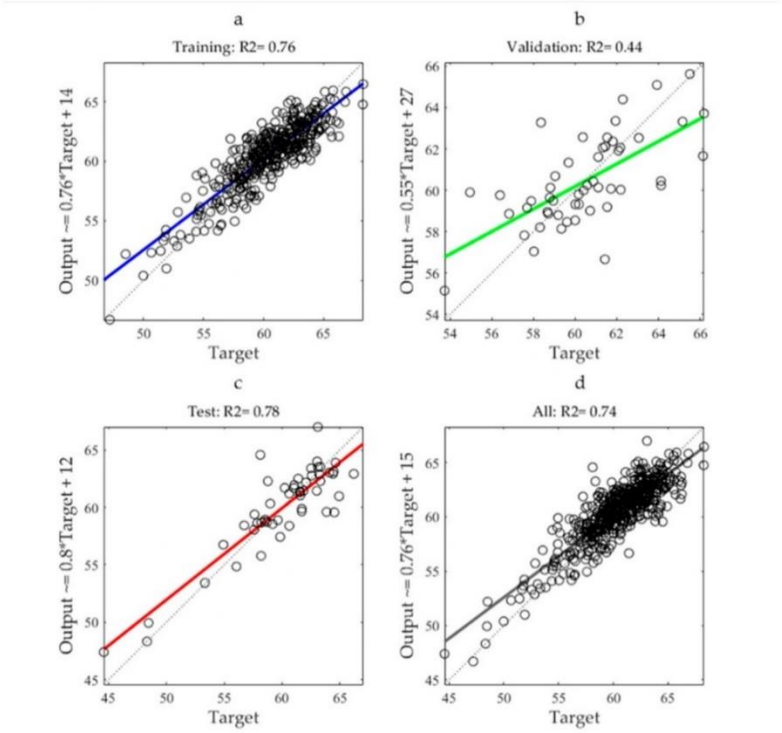

Figure 5. Linear regression between fruit moisture target values and those estimated through ANN model. Each subfigure represents the dataset of training (**a**), validation (**b**), test (**c**), and the whole dataset (**d**).

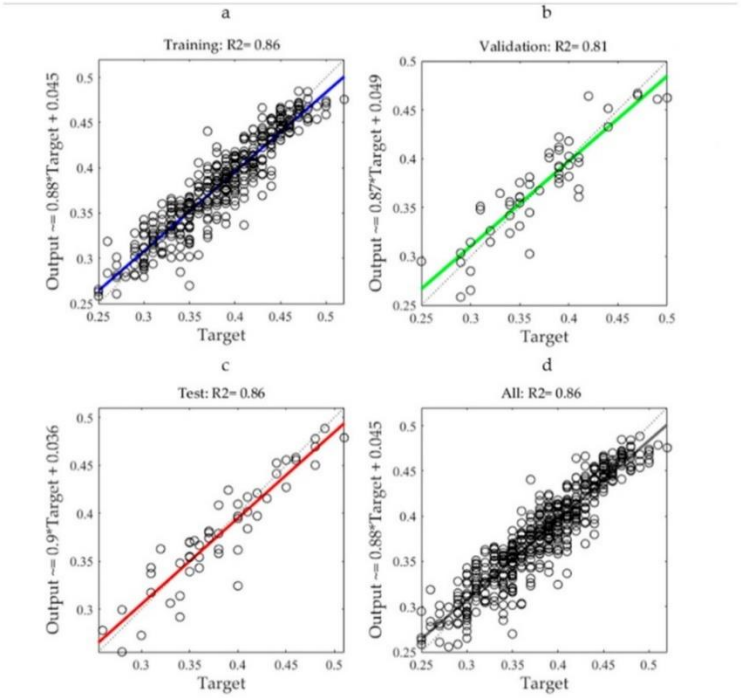

Figure 6. Linear regression between fruit acidity target values and those estimated through ANN model. Each subfigure represents the dataset of training (**a**), validation (**b**), test (**c**), and the whole dataset (**d**).

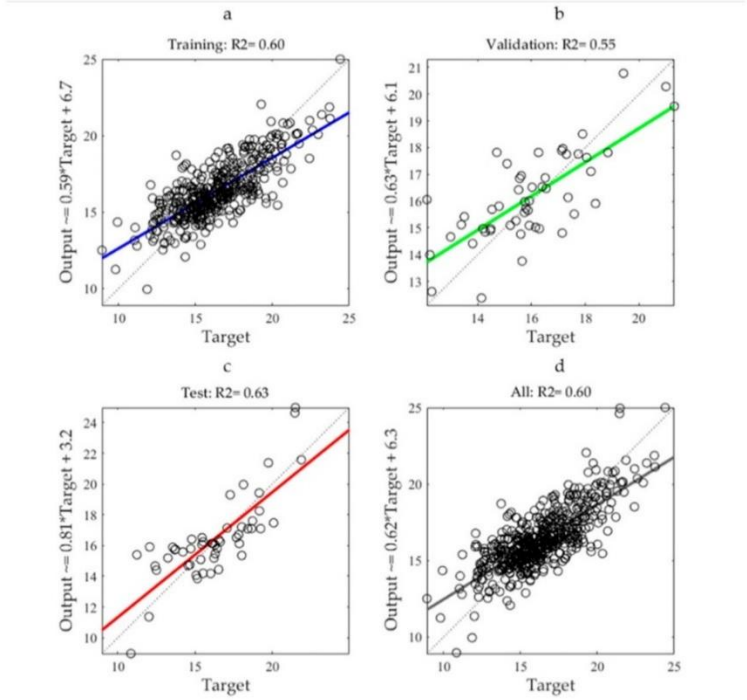

Figure 7. Linear regression between fruit fat content target values and those estimated through ANN model. Each subfigure represents the dataset of training (**a**), validation (**b**), test (**c**), and the whole dataset (**d**).

4. Discussion

The aim of this research is to validate a complete methodology based on a custom-built low-cost multispectral device for monitoring the quality status of intact olive fruits. For this purpose, ANN models were trained to estimate parameters indicative of the quality status of olive fruit (moisture, acidity, and fat content) by using the spectral information acquired by the sensor as input. This work was carried out under laboratory conditions as a first step towards the validation of the use of the proposed device in the field.

Numerous studies have demonstrated the suitability of spectral sensing for the characterization of agronomic parameters of interest for crop management [9,38]. Concretely, the assessment of fruit ripeness by means of remote sensing has received increasing interest, with numerous research studies focused on several crops [39]. Concerning olive fruit, spectroscopy was applied to the olive oil production process to determine the properties of the different products that appear in the process, such as olive fruit, paste, and oil [40,41]. The present work focused on olive fruits, since directly analyzing the fruit implies monitoring olive oil constituents at the beginning of the production process, before the milling phase, and even in the field. To this end, several authors have explored the potential of spectroscopy for olive fruit quality assessment. Table 4 summarizes the results obtained by other research aimed at modeling the same target parameters considered in the present work. Cayuela et al. [13] evaluated the suitability of a portable visible/NIR spectrometer for moisture, free acidity, and fat content prediction of olive fruits by using PLSR for modelling. They reported R^2 values for determining the moisture, acidity, and oil content of 0.88, 0.79, and 0.72 and RMSEP of 1.52%, 0.05%, and 7.98%, respectively. Salguero-Chaparro et al. [15] evaluated an NIR diode array installed on a conveyor belt and combined with PLSR to determine moisture, acidity, and oil content in intact olive fruits. They reached coefficient-of-determination (R^2) values of 0.88, 0.72, and 0.79, and RMSEP values of 3.3%, 2.7%, and 2.36% between the measured values and the response of the PLSR model in the estimation of moisture, acidity, and oil content, respectively [15]. More recently, Fernández-Espinosa et al. [20] investigated the prediction of moisture, fat content, and free acidity in olive fruits with different ripening states along two consecutive campaigns. They used online NIR spectroscopy combined with chemometric techniques. Concretely, the predictive models were developed by PLSR previous principal component and linear discriminant analyses (PCA and LDA). They obtained coefficient-of-determination (R^2) values of 0.88, 0.83, and 0.76 and RMSEP values of 4.98%, 38.8%, and 20%, between the measured and the estimated values of moisture, acidity, and fat content, respectively [20]. In the present work, comparable results to those reviewed were obtained (Table 4). In relation to acidity, the R^2 value between the measured data and the response of the ANN model for the external validation group was 0.86, which was better than those obtained by the mentioned works (0.83, 0.72, and 0.79). Regarding RMSEP, it was 5.83%, which is lower than 10%, which could be considered as an acceptable predictive potential [14]. These results were significantly positive considering that acidity is a particularly challenging feature, as it is inherent to olive oil characterization, but not considered for intact olive fruit characterization. On the other hand, according to fruit moisture, the obtained R^2 value calculated on the external validation set was 0.78, which was slightly lower than those published in the mentioned works (0.88, 0.88, and 0.88). However, upon considering this value along with that obtained for RMSEP (3.3%), there is an argument for considering the performance of the proposed ANN model satisfactory in this case as well, when estimating fruit moisture from the multispectral data acquired with the developed low-cost device. Finally, regarding fat content, the R^2 value yielded when analyzing the external validation set was 0.62, with an RMSEP of 10.44%. In this case, the R^2 value obtained when facing the reference measures and the responses of the ANN model was also lower than those noticed by the reviewed works (0.76, 0.79, and 0.72). Furthermore, the obtained RMSEP (10.44%) was higher than those published by Cayuela et al. [13] and Salguero-Chaparro et al. [15] (7.98 and 2.36). However, it was very close to 10%, thus indicating an acceptable assessment potential [14].

Table 4. Summary of articles addressing the estimation of olive fruit moisture, acidity, and fat content by means of spectral data.

	This Work		**Fernández-Espinosa (2016) [20]**		**Salguero-Chaparro et al., (2013) [15]**		**Cayuela et al., (2009) [13]**	
Chemometric	ANN		PCA-PLS		PCA-PLS		PCA-PLS	
Range	410–940		1000–2300		380–1690		1100–2300	
Statistics	R^2	RMSEP	R^2	RMSEP	R^2	RMSEP	R^2	RMSEP
Moisture	0.78	3.31	0.88	4.98	0.88	3.3	0.88	1.52
Acidity	0.86	5.83	0.83	38.8	0.72	2.7	0.79	0.05
Fat content	0.62	10.44	0.76	20	0.79	2.36	0.72	7.98

In the last decades, the use of low-cost spectral sensors for agricultural applications has been a topic of increasing interest [42]. This is due to a technical boom in the microelectronic industry, which has resulted in a lowering of the cost and an improvement of the features of commercially available components. There are numerous publications centered on Arduino-based devices with applications in the agri-food industry [43–45]. However, to our knowledge, no work focused on the quality assessment of intact olive fruit has been reported. In fact, most of the publications aimed at modeling agronomic parameters of interest for crop management by means of spectral data have focused on hyperspectral imaging systems. The works reviewed above are illustrative of this fact. The main advantage of these kinds of devices is their spatial resolution, as they generate images which allow contrasting of different parts of the sample. Furthermore, they offer a very high spectral resolution, as they catch multiple narrow spectral bands. Another characteristic of these devices is their spectral range, as they cover the near infra-red (NIR) band through frequencies distant from those of the red edge. All these features lead to high costs. Unlike these, a new custom-built multispectral device was used in this work, covering the spectral range 410–940 nm, which comprises the visible spectrum (VIS) and a close and narrow band of the near infra-red (NIR); it has a spectral resolution of eighteen bands with full width at half maximum (FWHM) of 20 nm. Compared to NIR spectrophotometers, the proposed multispectral sensor has a considerably lower spectral range and resolution. These more modest features may explain the slightly lower coefficients of determination reached in this work when estimating fruit moisture and fat content compared to the mentioned previous research, as there exist overtones out of the range covered by the proposed device related to the presence of water (1460 and 1920 nm (hydroxyl groups)) and fat content (1145 nm and 1160 nm (aliphatic esters), and 1175 nm, 1185 nm, 1210 nm, 1245 nm, 1260 nm, and 1275 nm (alkyl groups and alkenes)) [46]. Notwithstanding, even assuming this limitation, the results obtained in the present research indicate that the overtones considered are descriptive enough, denotating the suitability of the proposed multispectral device. The good performance displayed by the proposed device takes on a greater importance considering the price gap between it and the NIR spectrometers used in the mentioned research.

These satisfactory results may be due to the high flexibility of the ANN approach, which adjusts more effectively to the feature space, as it enables the non-linearity of data to be modeled using local or specific equations. These features result in an extraordinary ability to link complex spectral information with key parameters without any constraints on the sample distribution. This makes ANN approaches suitable for defining the intricate non-linear relationships that exist between olive fruit spectral signature and the studied quality indicators. This fact is evidenced by the good performance reported by the ANN model in the estimation of olive fruit moisture despite the reduced impact of the variation of this parameter on the spectral signature (Figure 4). Furthermore, the mentioned features of the ANN model allowed us to omit post-processing spectral techniques beyond the normalization based on known reflectance surfaces.

On the other hand, the good performance of ANN models in this work may also be due to the greater simplicity of the input data offered by the proposed multispectral device compared to those coming from hyperspectral systems. This kind of mathemat-

ical approach could encounter difficulties in data processing with the large information offered by hyperspectral devices. This is the reason why most of the publications based on hyperspectral systems have used PLSR as their mathematical model (Table 4), since it reduces the large amount of measured collinear spectral variables to non-correlated principal components by using data compression [47].

One widespread problem of ANN approaches is that they are susceptible to overfitting, which results in lower performance and generalization capabilities of the estimation models. In the present study, the annotated values for the coefficient of determination (R^2) when confronting reference and estimated values were slightly greater in the case of the external validation group than those resulting from the internal validation during training (Figures 5–7), which increases confidence in the adequate training of the net.

5. Conclusions

This work presents a complete methodology based on a low-cost and custom-built multispectral device for assessing quality parameters of intact olive fruits in a non-destructive way under laboratory conditions. ANN models were trained using the fruit moisture, acidity, and fat content as targets. Better results were obtained for the cases of the estimation of fruit moisture and acidity. However, the resulting performance regarding fat content estimation was also promising. The accuracy shown by the ANN models for estimating the mentioned quality parameters by means of the spectral data acquired with the proposed device, along with its low cost and ease of use, paves the way for the implementation of an olive fruit quality appraisal system that is more affordable for olive growers. Continuous monitoring of fruit quality conditions would allow adjustment of the moment of harvest according to objective standards instead of subjective criteria such as a visual judgment. This would improve the oleic sector as olive growers would reach the optimum economic return and olive mills would access better raw material.

Although the results were promising, further work is needed to expand the experimental setup to operate the system under field conditions, where the influence of natural light is a decisive factor.

Author Contributions: J.M.A., M.N., B.M. and A.A. conceived and directed the experimental layout. B.M. manufactured, assembled, and tested the proposed device. M.N. and B.M. carried out the data curation. M.N. developed the methodology for olive fruit quality status estimation from multispectral data. M.N. and B.M. drafted the manuscript, which was revised and edited by J.M.A. and A.A. The project administration and the funding acquisition were accomplished by J.M.A. All authors have read and agreed to the published version of the manuscript.

Funding: This work was supported by grant PID2020-119217RA-I00 funded by MCIN/AEI/ 10.13039/501100011033, and grant IJC2019-040114-I funded by MCIN/AEI/ 10.13039/501100011033, and also by project TIColiVA with grant P18-RTJ-4539 funded by the Regional Government of Andalusia through the "PAIDI, Plan Andaluz de Investigación, Desarrollo e Innovación".

Data Availability Statement: The data presented in this study are available upon request from the corresponding author.

Acknowledgments: The authors acknowledge Francisco Dominguez Calvo, the Nuestra señora de la oliva manager, for providing the olive samples and reference data on which the study was conducted, as well as Diego Tejada, for his support in the device design.

Conflicts of Interest: The authors declare no conflict of interest. The funders had no role in the design of the study; in the collection, analyses, or interpretation of data; in the writing of the manuscript, or in the decision to publish the results.

References

1. FAOSTAT. Available online: https://www.fao.org/faostat/en/#data/QV (accessed on 12 January 2022).
2. López-Granados, F.; Jurado-Expósito, M.; Álamo, S.; García-Torres, L. Leaf nutrient spatial variability and site-specific fertilization maps within olive (Olea europaea L.) orchards. *Eur. J. Agron.* **2004**, *21*, 209–222. [CrossRef]

3. Gunstone, F. *Vegetable Oils in Food Technology: Composition, Properties and Uses*, 2nd ed.; Gunstone, F., Ed.; Wiley-Blackwell: Oxford, UK, 2011; ISBN 9781444339918.
4. Barranco Navero, D.; Fernandez Escobar, R.; Rallo Romero, L. *El Cultivo del Olivo*, 7th ed.; Mundi-Prensa Libros: Madrid, Spain, 2017.
5. IOC (International Olive Council). Trade Standard Applying to Olive Oils and Olive Pomace Oils. 2019. Available online: https://www.internationaloliveoil.org/wp-content/uploads/2019/12/trade-standard-REV-14-Eng.pdf (accessed on 12 January 2022).
6. Sánchez, A.G.; Martos, N.R.; Ballesteros, E. Estudio comparative de distintas técnicas analíticas (espectroscopía de NIR y RMN y extracción mediante Soxhlet) para la determinación del contenido graso y de humedad en aceitunas y orujo de Jaén. *Grasas y Aceites* **2005**, *56*, 220–227.
7. Ragni, L.; Berardinelli, A.; Cevoli, C.; Valli, E. Assessment of the water content in extra virgin olive oils by Time Domain Reflectometry (TDR) and Partial Least Squares (PLS) regression methods. *J. Food Eng.* **2012**, *111*, 66–72. [CrossRef]
8. Verrelst, J.; Malenovský, Z.; Van der Tol, C.; Camps-Valls, G.; Gastellu-Etchegorry, J.P.; Lewis, P.; North, P.; Moreno, J. Quantifying Vegetation Biophysical Variables from Imaging Spectroscopy Data: A Review on Retrieval Methods. *Surv. Geophys.* **2019**, *40*, 589–629. [CrossRef]
9. Noguera, M.; Aquino, A.; Ponce, J.M.; Cordeiro, A.; Silvestre, J.; Calderón, R.; Marcelo, M. da E.; Pedro Jordão; Andújar, J.M. Nutritional status assessment of olive crops by means of the analysis and modelling of multispectral images taken with UAVs. *Biosyst. Eng.* **2021**, *211*, 1–18. [CrossRef]
10. Fazari, A.; Pellicer-Valero, O.J.; Gómez-Sanchıs, J.; Bernardi, B.; Cubero, S.; Benalia, S.; Zimbalatti, G.; Blasco, J. Application of deep convolutional neural networks for the detection of anthracnose in olives using VIS/NIR hyperspectral images. *Comput. Electron. Agric.* **2021**, *187*, 106252. [CrossRef]
11. León, L.; Rallo, L.; Garrido, A. Análisis de aceituna intacta mediante espectroscopia en el Infrarrojo Cercano (NIRS): Una herramienta de utilidad en programas de mejora de olivo. *Grasas y Aceites* **2003**, *54*, 41–47. [CrossRef]
12. Kavdir, I.; Buyukcan, M.B.; Lu, R.; Kocabiyik, H.; Seker, M. Prediction of olive quality using FT-NIR spectroscopy in reflectance and transmittance modes. *Biosyst. Eng.* **2009**, *103*, 304–312. [CrossRef]
13. Cayuela, J.A.; García, J.M.; Caliani, N. NIR prediction of fruit moisture, free acidity and oil content in intact olives. *Grasas y Aceites* **2009**, *60*, 194–202. [CrossRef]
14. Cayuela, J.A.; Camino, M. del C.P. Prediction of quality of intact olives by near infrared spectroscopy. *Eur. J. Lipid Sci. Technol.* **2010**, *112*, 1209–1217. [CrossRef]
15. Salguero-Chaparro, L.; Baeten, V.; Fernández-Pierna, J.A.; Peña-Rodríguez, F. Near infrared spectroscopy (NIRS) for on-line determination of quality parameters in intact olives. *Food Chem.* **2013**, *139*, 1121–1126. [CrossRef] [PubMed]
16. Salguero-Chaparro, L.; Peña-Rodríguez, F. On-line versus off-line NIRS analysis of intact olives. *LWT Food Sci. Technol.* **2014**, *56*, 363–369. [CrossRef]
17. Gracia, A.; León, L. Non-destructive assessment of olive fruit ripening by portable near infrared spectroscopy. *Grasas y Aceites* **2011**, *62*, 268–274.
18. Bellincontro, A.; Taticchi, A.; Servili, M.; Esposto, S.; Farinelli, D.; Mencarelli, F. Feasible application of a portable NIR-AOTF tool for on-field prediction of phenolic compounds during the ripening of olives for oil production. *J. Agric. Food Chem.* **2012**, *60*, 2665–2673. [CrossRef]
19. Bellincontro, A.; Caruso, G.; Mencarelli, F.; Gucci, R. Oil accumulation in intact olive fruits measured by near infrared spectroscopy-acousto-optically tunable filter. *J. Sci. Food Agric.* **2013**, *93*, 1259–1265. [CrossRef]
20. Fernández-Espinosa, A.J. Combining PLS regression with portable NIR spectroscopy to on-line monitor quality parameters in intact olives for determining optimal harvesting time. *Talanta* **2016**, *148*, 216–228. [CrossRef]
21. FOSS. Analytical Solutions for Food Quality Improvement and Control. Available online: https://www.fossanalytics.com/en (accessed on 21 April 2021).
22. Trang, N.M.; Duy, T.K.; Huyen, T.T.N.; Danh, L.V.Q.; Dinh, A. An investigation into the use of a low-Cost NIR integrated circuit spectrometer to measure chlorophyll content index. *Int. J. Innov. Technol. Explor. Eng.* **2019**, *8*, 35–38.
23. Moinard, S.; Brunel, G.; Ducanchez, A.; Crestey, T.; Rousseau, J.; Tisseyre, B. Testing the potential of a new low-cost multispectral sensor for decision support in agriculture. In *Precision Agriculture ´21*; Wageningen Academic Publishers: Wageningen, The Netherlands, 2021; pp. 411–418.
24. Verrelst, J.; Muñoz, J.; Alonso, L.; Delegido, J.; Rivera, J.P.; Camps-Valls, G.; Moreno, J. Machine learning regression algorithms for biophysical parameter retrieval: Opportunities for Sentinel-2 and -3. *Remote Sens. Environ.* **2012**, *118*, 127–139. [CrossRef]
25. Kalacska, M.; Lalonde, M.; Moore, T.R. Estimation of foliar chlorophyll and nitrogen content in an ombrotrophic bog from hyperspectral data: Scaling from leaf to image. *Remote Sens. Environ.* **2015**, *169*, 270–279. [CrossRef]
26. Wang, F.; Huang, J.; Wang, Y.; Liu, Z.; Peng, D.; Cao, F. Monitoring nitrogen concentration of oilseed rape from hyperspectral data using radial basis function. *Int. J. Digit. Earth* **2013**, *6*, 550–562. [CrossRef]
27. Huang, Z.; Turner, B.J.; Dury, S.J.; Wallis, I.R.; Foley, W.J. Estimating foliage nitrogen concentration from HYMAP data using continuum removal analysis. *Remote Sens. Environ.* **2004**, *93*, 18–29. [CrossRef]
28. Jensen, R.R.; Hardin, P.J.; Hardin, A.J. Estimating urban leaf area index (LAI) of individual trees with hyperspectral data. *Photogramm. Eng. Remote Sensing* **2012**, *78*, 495–504. [CrossRef]

29. García-Martínez, H.; Flores-Magdaleno, H.; Ascencio-Hernández, R.; Khalil-Gardezi, A.; Tijerina-Chávez, L.; Mancilla-Villa, O.R.; Vázquez-Peña, M.A. Corn Grain Yield Estimation from Vegetation Indices, Canopy Cover, Plant Density, and a Neural Network Using Multispectral and RGB Images Acquired with Unmanned Aerial Vehicles. *Agriculture* **2020**, *10*, 277. [CrossRef]
30. Liu, W.Y.; Pan, J. A hyperspectral assessment model for leaf chlorophyll content of Pinus massoniana based on neural network. *Chinese J. Appl. Ecol.* **2017**, *28*, 1128–1136.
31. Zipori, I.; Bustan, A.; Kerem, Z.; Dag, A. Olive paste oil content on a dry weight basis (OPDW): an indicator for optimal harvesting time in modern olive orchards. *Grasas y Aceites* **2016**, *67*, e137.
32. Gracia, P.; Sánchez-Gimeno, A.C.; Benito, M.; Oria, R.; Lasa, J.M. Short communication. Harvest time in hedgerow 'Arbequina' olive orchards in areas with early frosts. *Span. J. Agric. Res.* **2012**, *10*, 179–182. [CrossRef]
33. Abenoza, M.; Lasa, J.M.; Benito, M.; Oria, R.; Sánchez Gimeno, A.C. The evolution of Arbequina olive oil quality during ripening in a commercial super-high density orchard in north-east Spain. *Riv. Ital. Delle Sostanze Grasse* **2015**, *93*, 83–92.
34. Haberman, A.; Dag, A.; Shtern, N.; Zipori, I.; Erel, R.; Ben-Gal, A.; Yermiyahu, U. Significance of proper nitrogen fertilization for olive productivity in intensive cultivation. *Sci. Hortic.* **2019**, *246*, 710–717. [CrossRef]
35. Haberman, A.; Dag, A.; Shtern, N.; Zipori, I.; Erel, R.; Ben-Gal, A.; Yermiyahu, U. Long-Term Impact of Potassium Fertilization on Soil and Productivity in Intensive Olive Cultivation. *Agronomy* **2019**, *9*, 525. [CrossRef]
36. Ben-Gal, A.; Ron, Y.; Yermiyahu, U.; Zipori, I.; Naoum, S.; Dag, A. Evaluation of regulated deficit irrigation strategies for oil olives: A case study for two modern Israeli cultivars. *Agric. Water Manag.* **2021**, *245*, 106577. [CrossRef]
37. Williams, P.C. *Handbook of Near Infrared Analysis*, 2nd ed.; Burns, D.A., Ciurczak, E.W., Eds.; Marcel Dekker: New York, NY, USA, 2001.
38. Maes, W.H.; Steppe, K. Perspectives for Remote Sensing with Unmanned Aerial Vehicles in Precision Agriculture. *Trends Plant Sci.* **2019**, *24*, 152–164. [CrossRef] [PubMed]
39. Li, B.; Lecourt, J.; Bishop, G. Advances in Non-Destructive Early Assessment of Fruit Ripeness towards Defining Optimal Time of Harvest and Yield Prediction—A Review. *Plants* **2018**, *7*, 3. [CrossRef] [PubMed]
40. Casale, M.; Simonetti, R. Review: Near infrared spectroscopy for analysingolive oils. *J. Near Infrared Spectrosc.* **2014**, *22*, 59–80. [CrossRef]
41. Guzmán, E.; Baeten, V.; Pierna, J.A.F.; García-Mesa, J.A. A portable Raman sensor for the rapid discrimination of olives according to fruit quality. *Talanta* **2012**, *93*, 94–98. [CrossRef] [PubMed]
42. Walsh, K.B.; Blasco, J.; Zude-Sasse, M.; Sun, X. Visible-NIR 'point' spectroscopy in postharvest fruit and vegetable assessment: The science behind three decades of commercial use. *Postharvest Biol. Technol.* **2020**, *168*, 111246. [CrossRef]
43. Di Nonno, S.; Ulber, R. Portuino—A Novel Portable Low-Cost Arduino-Based Photo- and Fluorimeter. *SSRN Electron. J.* **2022**, 12. [CrossRef]
44. Poh, J.J.; Wu, W.L.; Goh, N.W.J.; Tan, S.M.X.; Gan, S.K.E. Spectrophotometer on-the-go: The development of a 2-in-1 UV–Vis portable Arduino-based spectrophotometer. *Sensors Actuators A Phys.* **2021**, *325*, 112698. [CrossRef]
45. Noguera, M.; Millán, B.; Pérez-Paredes, J.J.; Ponce, J.M.; Aquino, A.; Andújar, J.M. A New Low-Cost Device Based on Thermal Infrared Sensors for Olive Tree Canopy Temperature Measurement and Water Status Monitoring. *Remote Sens.* **2020**, *12*, 723. [CrossRef]
46. Westad, F.; Schmidt, A.; Kermit, M. Incorporating chemical band-assignment in near infrared spectroscopy regression models. *J. Near Infrared Spectrosc.* **2008**, *16*, 265–273. [CrossRef]
47. Wold, S.; Sjöström, M.; Eriksson, L. PLS-regression: A basic tool of chemometrics. *Chemom. Intell. Lab. Syst.* **2001**, *58*, 109–130. [CrossRef]

4.3.2. Article 4

Olive fruit ripening assessment under field conditions based on a low-cost multispectral device and ANN models

Miguel Noguera, Borja Millán, Arturo Aquino, and José Manuel Andújar.

(As of June 2024, in peer review process)

Below, the respective work in its current form is presented. Although it is susceptible to minor changes as a result of the peer review process, the main results and findings of the work are depicted in it.

Olive fruit ripening assessment under field conditions based on a low-cost multispectral device and ANN models

Miguel Noguera [1*], Borja Millan [2], Arturo Aquino [1], and José Manuel Andujar [1]

[1] Centro de Investigación en Tecnología, Energía y Sostenibilidad (CITES), Universidad de Huelva, La Rábida, Palos de la Frontera, 21819 Huelva, Spain; miguel.noguera@diesia.uhu.es (M.N.); arturo.aquino@diesia.uhu.es (A.A.); andujar@diesia.uhu.es (J.M.A.).

[2] Departamento de Ingeniería Eléctrica, Electrónica, Informática y de Sistemas, Universidad de Oviedo, C/ Pedro Puig Adam, 33203 Gijón, Spain; millanborja@uniovi.es (B.M.).

* Correspondence: miguel.noguera@diesia.uhu.es

Abstract: Olive fruit ripening characterization is a critical factor for olive growers. The traditional chemical methods imply numerous limitations (requirement for expert personnel, tedious procedures, high cost, etc.), which lead to a poor spatial-temporal resolution in the monitoring. These facts lead growers to base the decision of the moment of harvest on subjective criteria such as visual assessment. In the last decades, spectroscopy-based approaches have been proposed as an alternative to chemical methods. However, these approaches rely on the use of hyperspectral devices, whose complexity and high cost limits their applicability for smallholder farming settings. Under this context, the present work proposes a methodology based on a low-cost multispectral device (18 bands between 410-940 nm), and artificial neural network (ANN) models to estimate ripening parameters of intact olive fruits under field conditions. To evaluate the potential of the device, a two-seasons field experiment was conducted. During two consecutive campaigns, the ripening process of an olive experimental field was monitored in parallel with the proposed device and with traditional methods. Thus, a dataset of ground truth values of various ripening indicators (oil content per dry matter (OCDM), oil content per fresh weight (OCFW), moisture (M), and titratable acidity (TA)), and the spectral signature of the samples was acquired.

Afterwards, these parameters were used as target to develop ANN models fed with the spectral signature of the samples. The ANN models showed promising results with a high accuracy in the estimation of OCFW ($R^2 = 0.86$), OCDM ($R^2 = 0.86$), and M ($R^2 = 0.89$) in external tests.

Keywords: sensor; multispectral; precision farming; machine learning; artificial neural network; AS7265x

1. Introduction

Olive crops extension exceeds 12 million hectares around the world. Olive growing is linked to the Mediterranean climate conditions, as most of cultivars require a specific temperature regime during the winter rest for a suitable flowering. This limits the optimal area for olive growing approximately between the latitudes of 30° and 45° [1]. Thus, the primary producers of olives are Spain, Italy, Greece, and Portugal, followed by other Mediterranean countries such as Tunisia, Morocco, Algeria, Egypt, and Turkey. However, over the last few decades, there have emerged producing countries from lower latitudes such as Argentina, Peru, Chile, and Australia. This competitive scenario has led to a transformation from the traditional olive orchards to hedgerow systems characterized by high (>1500 trees ha^{-1}), or super high plant densities (2116 trees ha^{-1})[2]. These new crop settings involve modern resources like drip irrigation systems, no-tillage techniques, and quick-growing young olive plantings in rows, which enable management labors mechanization (harvest, prune, fertilize, phytosanitary application, etc.). This new paradigm results in an increase in yield per hectare, while reducing management costs, thus making the crop more profitable. This modernization of olive growing has incentivized investigations aimed to explore the applicability of precision agriculture techniques, such as the use of remote sensing. In this sense, there have been numerous researches focused on different applications of remote sensing in olive growing, namely: identification of olive-cultivated areas and tree counting [3], evaluation of the effects of pruning strategies [4], plant phenotyping [5], fertigation management [6], irrigation management and water stress assessment [7,8], yield

estimation [9], detection of pathogen infections [10,11], and quality assessment of fruits [12–14]. Among all those mentioned, fruit quality assessment is the main objective of this research.

Olive fruit ripening assessment is a critical choice for olive producers. The criteria for deciding the moment of harvest must be based on the best combination of oil quantity and quality. After reaching the pit hardening stage, the fruit starts a curve of oil accumulation whose course depends on several factors, such as the cultivar, the soil properties, the environmental conditions, and pathologies. These factors vary throughout the crop area, so maturation can occur at a diverse pace along the different areas of a field, generating a heterogeneous ripening status. This heterogeneity can be compensated by means of agronomic practices. For these reasons, an efficient method for ripening status assessment is essential for a proper olive crop management.

Fat content, moisture, and titratable acidity of olive fruits are key parameters widely accepted for classifying them into different commercial qualities. Traditionally, the determination of these parameters in the laboratory is conducted by standard analytical methods. A usual methodology for acidity determination in olive fruits relies on titration of olive oil. Fat content can be determined by Soxhlet or other techniques such as nuclear magnetic resonance (NMR). Moisture is normally determined by using a drying oven and Karl Fischer titration. These classical chemical methods cause a negative impact on the environment owing to the excessive solvent consumption. In addition, they require expert personnel and specific laboratory equipment, which encompasses a high cost. Furthermore, they are destructive, labor-demanding due to sample collection, and time-consuming as results availability usually takes several days, which may delay the decision of harvest. These facts limit the number of sample points that growers can consider, thus resulting in a poor spatial resolution in the monitorization. On the other hand, the mentioned constraints also limit the number of sampling campaigns that growers can accomplish during the season, which leads to a poor temporal resolution. All these limitations result in a homogeneous harvesting supported by subjective criteria such as intuition and visual interpretation. A precise control of the quality state of olive fruits would enable to manage the

crop surface in an optimum way. Firstly, it would allow to conduct site-specific treatments to compensate the heterogeneity during growth and early ripening phases. Besides that, growers could define harvest strategies intended to diversify the production, which would improve the economic return of growers, as well as the capacity of the agri-food sector to develop products with greater added value.

The discussed context reveals the necessity to develop new methods for monitoring the ripening process of olive fruits. In this regard, the present work proposes a non-destructive methodology implementing a handheld multispectral device for estimating quality indicators of olive fruits under field conditions. Spectroscopy-based techniques have been widely investigated in the precision farming sector [15]. Briefly, the agronomical applications of spectroscopy rely on the interaction between electromagnetic radiation and vegetal tissues. Each vegetal tissue (leaves, fruits, stems, etc.) has a different chemical composition which also varies along the vegetative cycle. When an electromagnetic beam interacts with a vegetal tissue, it is modified in a specific way which is determined by its chemical composition. This modification can be assessed by analyzing the three processes of absorption, reflection, and transmission. So, as no two organic compounds have the same characteristics, a compound can be identified by characterizing its absorption spectrum and matching it with a database. The extent of the electromagnetic spectrum, and the complexity of the interaction between light and objects have led to a large array of spectral-based sensors and techniques. In the precision farming sector, numerous applications of these kind of technologies have been explored in order to asses several biophysical parameters of vegetation (fluorescence spectroscopy [16], Raman spectroscopy [17], multispectral imaging [6], hyperspectral imaging [18], and visible, near-infrared (VIS-NIR) 'point' spectroscopy [19]). However, the research focused on olive crop and concretely in ripening status assessment is scarce.

The first approaches exploiting spectroscopy for olive quality estimation were centered in olive by-products such as olive paste and pomace [20,21]. These techniques showed accuracy

comparable to those provided by standard chemical methods with the advantages of involving less intensive sample handling, less reagents and solvents usage, and being faster than the official procedures. However, they still implied the sample destruction. Afterwards, numerous works centered on olive quality assessment from intact olive fruits have been published. Related to this concern, the works using spectral data acquired in laboratory [13,22–25], should be differentiated from those analyzing data acquired under field conditions [12,26–28]. Indeed, getting spectral measurements in the field implies additional challenges, such as variable lighting and climate conditions. Among the works investigated on the basis of field measurements, the works aimed to classify olive fruits into several ripening categories [29] can be separated from those based on quantitative estimation models [12]. This work belongs to this last category, as it describes a methodology which proposes the use of a low-cost multispectral device for quantitatively estimating ripening indicators of intact olive fruits under field conditions. The related previous research relied on the use of hyperspectral devices for data acquisition. Hyperspectral sensors have a larger spectral resolution than multispectral sensors, as they can identify multiple narrow spectral bands in a wider range. However, these features make them unaffordable for most producers, preventing the practical application of the methodologies and their popularization.

In recent times, the microelectronic industry has made significant advancements, offering components with enhanced features at reduced costs. These upgrades have aroused an increasing interest in the use of low-cost spectral sensors for precision farming applications. This trend has been materialized in diverse research. For example, Trang *et* al. [30] proposed a method to measure chlorophyll content of leaves by using a six-channel NIR sensor (AS7263, AMS AG). Li *et* al. [31] evaluated a commercially available spectral sensor (SCIO) to predict the quality of kiwifruit, apples, feijoas, and avocados. Kitić *et* al. [32] proposed an affordable, portable, and active multispectral optical device for accurate plant stress detection and field mapping, based on NDVI assessment.

The present research continues with this trend as the proposed device integrates a low-cost development board (AS7265x, AMS AG). This component has been previously evaluated for several agronomic applications. Moinard *et* al. [33] demonstrated its suitability to assess the percentage of grass cover and vine vigour. Leon-salas *et* al. [34] used it to develop a photosynthetically active radiation (PAR) sensor. They evaluated it indoors and outdoors, obtaining results that outperformed lab-grade commercially available PAR sensors. Stevens *et* al. [35] used it to develop an loT spectroscopic system aimed to monitor the nutrient status in micro indoor smart hydroponics. Tran *et* al. [36] evaluated its potential in this case to estimate the soluble solid content of apples with promising results. Zhang *et* al. [37] proposed a methodology for classifying apples in three ripening categories using a device based on that sensor. In a previous work, the same authors demonstrated the suitability of this sensor for quality assessment of olive fruits in laboratory conditions [14]. Afterwards, a prototype was developed intended to operate under field conditions, which was evaluated for grape ripening evaluation with promising results [38]. Given these backgrounds, the goal of this research was to transfer the results obtained previously in laboratory conditions to the olive grove. To this end, the prototype was upgraded with an original hardware specially adapted for measuring olives fruits. Furthermore, a two seasons field experiment was conducted to demonstrate the suitability of the proposed device to quantitatively assess the quality status of intact olive fruits in the orchard. This work compilate the results obtained in that experiment.

2. Materials and Methods.

2.1. Device Description

The aim of this research was to develop a dependable, low-cost and easy to use tool, suitable to quantitatively assess the ripening status of olive fruits under field conditions. The developed device (Figure 1) includes several commercially available components, connected with a specially designed PCBs (printed circuit boards), enclosed in a custom 3D-printed container.

The use of commercial components lowers costs and makes maintenance easier. The principal component of the proposed device is an AS7265x development board, based on the AS7265x smart spectral sensor family (AMS, AG, Austria). This board includes three main chips: AS72651, AS72652, and AS72653. Each of them includes six optical filters, which make them sensible to six spectral bands. This results in an 18-channel multispectral sensor with a spectral response defined in a range from 410 nm to 940 nm, with full width at half maximum (FWHM) of 20 nm. On the other hand, the device equips an array of three IR broadband emitter (OSLON P1616 SFH 4737, OSRAM, Germany) as light source. This component was developed especially for spectroscopy applications, providing a wide and stable emission spectrum, with a low power, and heat dissipation requirements. The fact that the device has its own light source allows to characterize the incident radiation on the sample in the moment of the measurement, and thus to obtain comparable spectral signatures. Furthermore, the device includes a 1.3-inch display OLED panel with a resolution of 128 by 64 pixels, which guides the user during the measurement, offering important information such as configuration parameters, the file name, the number of measurements performed, and the actual status of the device. These three components communicate with an Arduino MKRZero Board (Arduino LLC, Monza, Italy). This controller board was selected because of its small form factor, low power consumption, low cost, and the availability of an SD card slot.

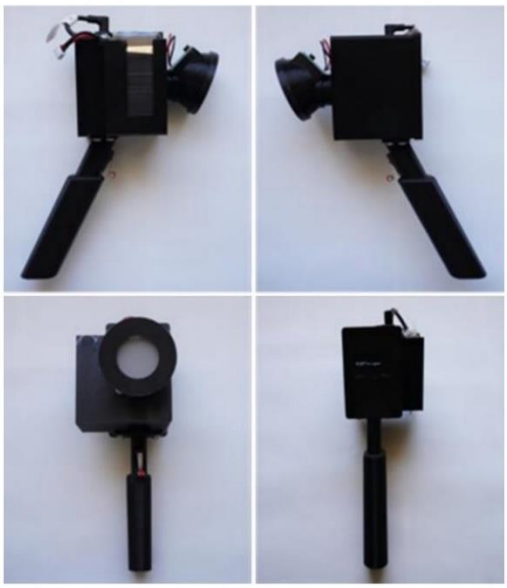

Figure 1. Developed prototype from four different views. The three parts of the framework (handle, dome, and box-type enclosure), the trigger button, the OLED screen, and the external battery are showed.

The software of the system was programmed using Arduino IDE, and designed to be user-friendly. Once the device is turned on, a new data file is generated to store the measurements. Then, the device enters on idle state, waiting for a user input (pressing of the trigger button) to capture a sample spectrum. When the trigger is activated, the Arduino board sends the command to the sensor, and turns on the LEDs (with software configurable intensity levels) and gathers data. Then, the acquired data and interesting information, such as file names, are stored in an SD-card for further analysis (Figure 2). Then, the device returns to idle state. The controller board can be connected to a PC for configuring internal parameters of the device (exposure time, gain, lighting time, and led current).

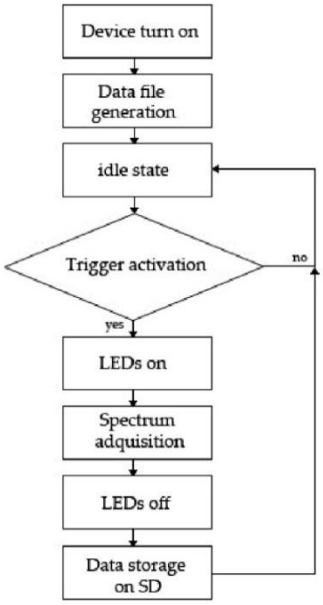

Figure 2. Flow-chart diagram of the device operation.

The power supply of the device is done by a 2s LiPo (Lithium-ion Polymer) battery connected to the controller board. All these components are hosted in a framework designed using Freecad 0.16 and manufactured with a 3D printer using biodegradable polylactic acid (PLA) filament. The designed framework is composed of three different parts: a handle that holds the trigger button, a dome that holds the light source, and an integrated a light diffusion film (OptSaver L-9960, Kimoto LDT, Switzerland) placed in front of the sensor to homogenize the radiation reflected by the sample. This dome was developed to position the sample at a 45◦ angle with respect to the light source and the sensor. Finally, the framework encompasses a box-type enclosure that host the AMS AS7265x development board, Arduino MKR Zero, interconnection board, and a lid that seals the sensor to allow in-field operation. The OLED screen is fixed to the lid of the main enclosure, and its position allows for easy visualization of the data when taking a measurement. All the device's elements are housed inside the developed case, excepting the battery, which was installed outside to avoid temperature interferences with the sensor that could affect the precision of the measurement, as well as to simplify its in-field replacement.

A more exhaustive description of the hardware and software of the device can be found in Noguera *et* al, 2022 [38]. Which respect the device presented in that work, some modifications were made to adapt the system to measure olive fruits. In this sense, a container was designed to fit with the device's dome. Thus, this container allows to hold the olive samples during the measurement, thus avoiding environmental radiation interferences. The volume of the container enables to measure approximately 50 g of olive samples. An image of the developed device and the specific sample container is depicted below (Figure 3).

Figure 3. Images of the measuring container alone (left), and fitted with the device's dome during measurement (right)

2.1.2 Evaluation of environmental radiation interference

In order to evaluate the capabilities of the proposed device to avoid the interference of environmental radiation, an specific experiment was carried out. This experiment consisted in facing the device to different levels of environmental radiation. Thus, three reference scenarios were defined. Firstly, the device was used in a dark room, completely isolated from environmental radiation. Complementary, the device was used in two differentiated in-field environmental illumination conditions; sheltered by the shade of an olive tree, and completely exposed to the sun radiation. To isolate the environmental radiation as the unique variable to be considered in the comparison, the measuring container was remained empty in this experiment.

Ten measurements were acquired in each scenerio, wich were calibrated using the reflectance of a calibrated surface, as it is described in section 2.3.1.

To determine the statistical significance of the levels of environmental radiation on the performance of the proposed device, an analysis of variance (ANOVA) of a single factor with a significance level $\alpha = 0.05$ was made. The ANOVA analysis has the ability of estimating the effect of any treatment by taking the difference between the mean of the observations that receive the treatment and the general mean.

2.2. Validation Experiment

A field experiment was carried out to evaluate the capability of the proposed device for quantitatively assessing quality indicators of intact olive fruits.

2.2.1. Study site description

The study site was a commercial olive orchard (*Olea europaea* L., cv. Picual), provided by *Nuestra Señora de la Oliva, S.C.A.*, and placed in the province of Huelva, Andalusia, Spain (37°20'28.96" N and 7°01'54.98" O). It has a plant spacing pattern of 7x7 m, which corresponds to a traditional olive orchard. This farm has an extension of more than 200 hectares, however, for this experiment, a plot of one hectare was delimited (highlighted in red in Figure 4). This delimitation was intended to obtain a homogeneous pace of ripening in the experimental plot. The climate of the experimental location is Csa (hot-summer Mediterranean climate), according to the Köppen-Geiger classification. It has an average annual rainfall of approximately 600 mm, distributed from October to May. Thus, there is a marked drought period during spring and summer. This hydrological stress period coincides with demanding phenological processes for the plants (inflorescences/flowering/fruit set, fruit growth and fat accumulation). So, the experimental field has a drip irrigation system for supplying water during that period.

Figure 4. Bird eye image (Google-maps satellite view) of the cultivar used for experimentation; the red square represents the delimited area.

2.2.2. Experimental field protocol design

The development of mathematical estimation models from sensing data requires a dataset composed of the data acquired by the sensors and reference values acquired by standard methods. To obtain that dataset, periodical sample collections were carried out, covering the whole ripening process of olives fruits. Thus, the first sample collection was conducted after the post-summer fruit growth (October), and was repeated weekly until harvest (December). Each sample consisted in approximately 200 g of olives collected from the same branch of a randomly selected tree. The spectral signature of the samples was acquired immediately after being picked, being then packaged, labelled, and refrigerated for their transport to the laboratory. The field experiments began in the 2021 campaign. However, due to a maturation peak occurred between the second and third sampling session, a gap in the ripening status distribution was found (Section 3.2). Consequently, the field experiment was repeated to cover that gap in the 2022 season. Thus, the final dataset was composed of 86 samples collected in 2021 and 60 collected in 2022 (n=146).

2.2.3. Spectral data collection

The spectral signature of the samples was acquired under field conditions, immediately after being picked. As soon as the olive fruits were collected, they were put in the specific container, the container was fitted with the device dome, and three consecutive spectral captures were taken; the three spectral readings were subsequently averaged. The fruits were then packaged, labelled, and chemically analyzed as described in section 2.2.4. to generate the reference information. The chemical methods required a minimum amount of 200 g of olive fruits, so four containers of fruit (~50 g each) were required to configure a sample unit (~200g). Thus, 12 spectral acquisitions were performed per sample unit (3 captures/container x 4 containers), thus allowing to register all the existing variability. Once every five samples, three captures of a characterized reflectance surface were taken (Labsphere, Inc, North Sutton, NH, USA) (53% calibrated reflectance). The average signal of the three captures was used as a reference to normalize the spectral signatures of the following five samples registered.

2.2.4. Reference analysis

In this research, the oil content (OC), moisture (M), and titratable acidity (TA) were used as target parameters, as they are widely used for classifying olive fruits into different commercial qualities. The reference analysis of these parameters was made in the laboratory, in accordance with official methodologies. The determination of moisture was carried out through the drying method in an oven at 105 °C (ISO662:2016)[39]. According to this method, a 25 g portion of the sample is placed in a porcelain capsule and dried in the oven at 105 °C for 6 h. Then, the sample is cooled in a desiccator, weighed, and returned to the oven, repeating these operations until, between two consecutive weightings, the variation in weight loss of moisture is less than 0,02 g. At this point, the difference between the initial and final weight is considered as the moisture content of the sample. Oil content was determined in its two variants: oil content per dry matter (OCDM) and oil content per fresh weight (OCFW). Reference analysis of OCFW was undergone by using the Soxhlet methodology (UNE 55030:1961)[40]. This method involves introducing the dried sample, used for moisture determination, into a Soxhlet extractor, where the fat is extracted

by exposing the sample to n-hexane for 4 h. Then, the sample is placed into the oven again at 105 °C to remove the traces of solvents. The amount of oil recovered is used to determine the OCFW and, from this measure, the OCDM is calculated according to the following equation:

$$\text{OCDM} = \frac{\text{OCFW}}{100 - \text{M}}$$

The TA of the olive samples was determined by means of titration, according to the international standard methodology (UNE-EN ISO 660:2020)[41]. This method consists in a titration of 1-3 g of oil with ethanolic potash in a 5 mL-microburette.

2.3. Methodology for Olive Quality Indicators Estimation from Multispectral Data

2.3.1. Data Pre-processing

During the field experimentation, 12 spectral readings were registered per olive sample (3 captures/container x 4 containers). Thus, the first step of the data pre-processing was to average those 12 spectral signatures from each olive sample. As a result, each sample was summarized to 18 reflectance data. Then, these data were normalized using as reference the spectral signature of a calibrated reflectance surface (53%) (Labsphere, Inc, North Sutton, NH, USA), which was captured once every five samples. The 18 reflectance signals of the calibration surface were used as references for the spectral signature of the subsequent five samples according to the following equation:

$$Rcal_{wl} = \frac{R_{wl}}{Rref_{wl}/53}$$

where R_{wl} is the reflectance value measured for a given spectral band in a capture of a sample, $Rref_{wl}$ is the reflectance value measured for that spectral band in the previous capture of the calibrated reflectance surface, and $Rcal_{wl}$ is the corrected value of reflectance in the sample of the given band. After this normalization, the data were transformed to fall in the interval [0, 100], thus making the reflectance values of the 18 spectral bands mathematically comparable. Additionally, the pre-processed spectra were smoothed for noise removal by applying the Savitzky–Golay method [42]. After considering different parameter settings, the width of the

selection window was adjusted to five points and a second order polynomial was used to fit the data. No derivatives of the data were made, as just a simple smoothing was intended.

2.3.2. Estimation model development

The pre-processed reflectance values of the 18 spectral bands acquired by the sensor were used as input variables to train 4 artificial neural networks (ANN) using OCFW, OCDM, M, and TA, respectively, as target. The software used for data processing and ANN training was MATLAB R2022b (The MathWorks Inc.). The ANN was a two-layer perceptron algorithm with back propagation. The architecture of the neural networks employed were composed of a hidden layer with ten neurons, eighteen inputs (the corrected reflectance values of the 18 spectral bands acquired by the sensor), and one output (the respective target parameter). The activation function for the hidden layer was sigmoid while the output layer function was linear. The Levenberg-Marquardt backpropagation method was used as training algorithm.

The validation of the models was made through a random sampling (RS) test. For that purpose, the complete data set was randomly divided into three subsets: 70% for model training (n = 102), 15% for internal validation (n = 22), and 15% for external validation or testing (n = 22). The training set is presented to the network during training, and the network is adjusted according to its error. The internal validation set is used to measure network generalization, and to halt training when generalization stops improving. The external validation set has no effect on training, so it provides an independent measure of network performance after training.

2.3.3. Criteria for model performance evaluation

The performance of the estimation models was evaluated, during training and using the external validation dataset, through the coefficient of determination (R^2), the root–mean–square error of prediction (RMSE), and the ratio of performance to deviation (RPD) between the reference values of ripening indicators determined by standard methods and those estimated by ANN models. The coefficient of determination (R^2) was used to assess the relationship between the actual and predicted target parameters. Concretely, R^2 indicates the percentage of the variance

in the target variable that is accounted for the response of the model. A value of R^2 between 0.50-0.65 indicates that more than 50% of the variance in the target variable is accounted by the variance in the response of the model, so that discrimination between high and low levels can be made. A value of R^2 between 0.66-0.81 indicates approximate quantitative predictions, whereas values of R^2 higher than 0.82 reveals good predictions, been better as R^2 approaches to 1 [43]. On the other hand, the RMSE is the standard deviation of the residuals (prediction errors). Residuals are a measure of the distance of data points to the regression line; RMSE is a measure of how spread out these residuals are. Thus, low values of RMSE indicate a better model performance. RMSE was calculated as follow:

$$RMSE = \sqrt{\sum_{i=1}^{n} \frac{(Ypred_i - Yref_i)^2}{n}}$$

where $Ypred_i$ is the response of the model, $Yref_i$ is the reference data, and n is the number of measurements in the respective external validation dataset. Furthermore, it also was considered the coefficient of variation of the RMSE (CVRMSE), which is the result of normalizing the RMSE by the mean value of the measurement. This allows for the avoidance of ambiguity, facilitating the comparison between datasets or models with different scales. In this sense, RPD is the ratio between the standard deviation of the validation set and the RMSE of the response of the model, so it standardizes the corresponding RMSE with respect to the population spread. Thus, RPD is dimensionless, because it is a ratio of two quantities with the units of the reference measurement. It can therefore, to some extent, be also interpreted independently of the considered variable.

Additionally, paired *t*-tests for dependent samples were also conducted to verify the results from the R^2, RMSE, CVRMSE, and RPD analyses. For this purpose, the reference values, and the models' predictions on the external validation set were compared. The paired t-test is a parametric method, useful for testing whether the means of two groups are different when the samples are drawn in pairs. The t-test was conducted using Microsoft® Excel® for Microsoft 365 MSO (version 2211) software. The compliance with the null Hypothesis ($p > 0.05$) indicates that

there were no significative differences between the mean of the measures based on the proposed device and those obtained with the reference methods.

3. Results.

3.1. Effect of environmental radiation on device performance

As a first step to evaluate the capacity of the proposed device to avoid environmental radiation, an experiment consisted on exposing it to different measuring scenarios was carried out. In this sense, 10 spectral readings, being the device's container empty, were acquired in a dark room, under field conditions in a shaded area, and completely exposed to sun radiation. Figure 5 shows the mean reflectance responses obteined captured under the three estudied scenarios for every single band. Here, it can be observed that the mean spectral signatures overlaps, which suggests that there was not effect of environmental radiation on the device performance. This visual asumption was corroborated by the results obtained in the analysis of variance (ANOVA) of a single factor, as no significative differences ($\alpha = 0.05$) were found between the mean of the measurements taken under each single scenario, and the general mean of the three scenarios for all the considered bands.

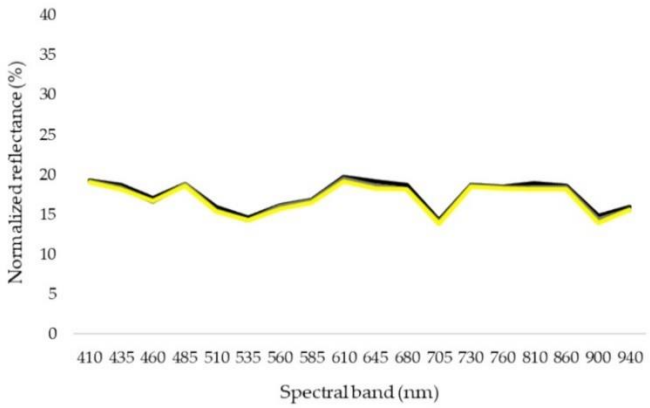

Figure 5. Mean reflectance response of the empty measuring container in a dark room (black), under field conditions under shadow (grey), and exposed to sun radiation (yellow).

3.2. Reference values of target quality parameters

146 olive samples (*Olea europaea* L., cv. Picual) were considered for the development of artificial neural network models (ANN), aimed to estimate quality parameters of olive fruits from the information provided by the proposed sensor. This dataset was composed of data from two consecutive campaigns analyzed as a whole. The explored quality indicators were oil content per fresh weight (OCFW), oil content per dry matter (OCDM), moisture (M), and titratable acidity (TA). Figure 6 represents the values of the four studied parameters for each individual sample, taken weekly, during the two consecutive campaigns. The samples between 0 and 86 corresponds to the first campaign, while the resting are the samples acquired during the next season. In the figures 6a and 6b, it can be observed how OCFW and OCDM values increased drastically between the second and third data sampling carried out during the first season. This resulted in a gap in the data distribution which prevented from an appropriate training of the ANN models. The figures also show how this drawback was corrected with the samples taken during the second campaign, which allowed to cover the 'gap'. Thus, considering the two seasons as a whole, OCFW varied between 13.36% and 23.87%, with an average value of 19.21% ± 2.68%, while OCDM ranged between 32.70% and 51.73%, with an average value of 44.55% ± 5.20% (Table 1). In the case of M (Figure 6c), the values were quite stable during the first season, without remarkable variations throughout the weekly samplings. This fact might be due to a drought stress period, especially noteworthy during that campaign. In contrast, M values had a steady increase throughout the weekly sampling during the second season. Hence, considering the two campaigns together, M values varied between 52.04% and 70.94%, with an average of 56.79% ± 4.17% (Table 1). The replication of the experimental protocol resulted in a wide distribution of OCFW, OCDM, and M, with values above and below the minima recommended for harvesting [44]. Regarding TA, a variation between 0.20% and 0.82% was observed, with an average value of 0.37% ± 0.11% (Table 1). Figure 6d reveals that TA values showed large variations even among the samples collected in the same sampling event, not showing a clear dynamic related to the ripening process. This fact might be due to TA levels are highly influenced by fruit damage caused

by different factors (hail, frost, insect bites, phytopathogens infections, etc.). For this reason, there is no minimum recommended TA value for collection; instead, the lower the TA of olives, the higher the quality of the olive oil produced. Hence, considering that all the samples were picked directly from trees, the range of TA was wide enough.

Table 1. Summary descriptive statistics of the olive fruit dataset related to OCFW, OCDM, M, and TA.

	Min	Max	Mean	SD
OCFW (%)	13.36	23.87	19.21	2.68
OCDM (%)	32.70	51.73	44.55	5.20
M (%)	52.04	70.94	56.79	4.17
TA (%)	0.20	0.82	0.37	0.11

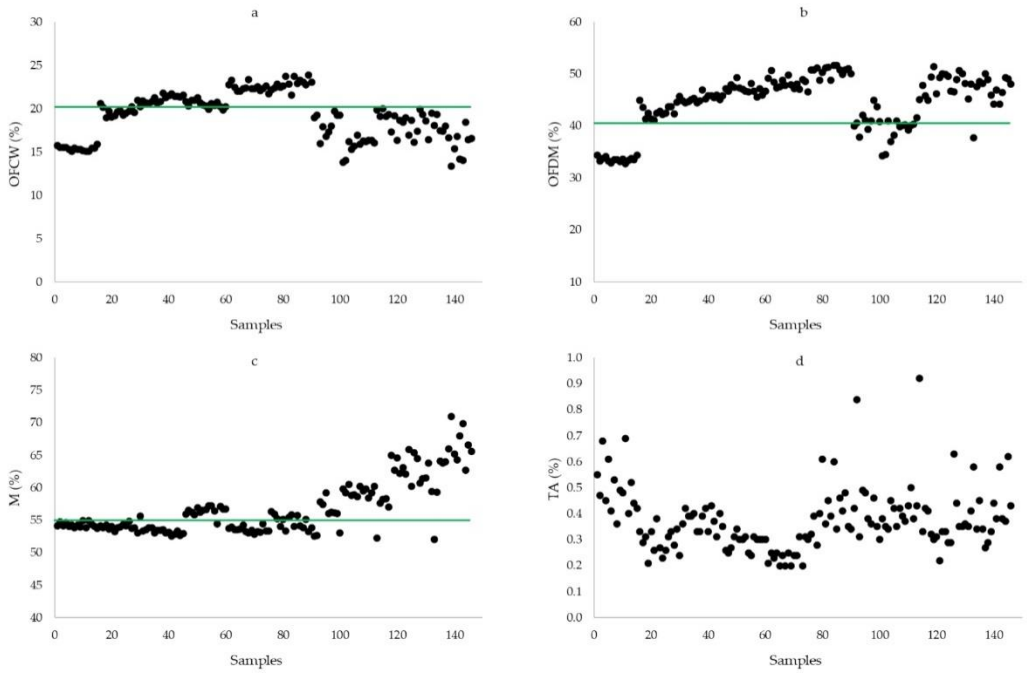

Figure 6. OCFW, OCDM, M, and TA of all the olive samples (n=146). The green line represents the recommended levels of OCFW, OCDM, and M for harvest.

3.3. Spectral signature of olive samples

Prior to the development of the estimation models, a visual inspection of the spectral response of the olive samples was conducted. Visual features and patterns of the spectra conform with those previously reported in the literature for intact olive drupes [45]. Figure 7 represents the mean spectral signature of the samples corresponding to the 10^{th} and above the 90^{th} percentile of the studied parameters. Indee, for the cases of OCFW (Fig6a) and OCDM (Fig6b), overall shapes were rather similar at both ends of the histogram. Generally, reflectance decreasing can be observed in the case of those samples with higher levels of OCFW and OCDM, compared to those samples with lower levels. Notwithstanding, reflectance decreasing was higher for those samples with higher OCDM values. Especially noteworthy were the reflectance peaks between 585-900 nm in the case of samples with lower levels of OCFW and OCDM, regarding those with higher levels. In relation to M, the trend was similar, showing reflectance decreasing linked an increase of M levels. In this case, reflectance decreasing was extended to 435-560nm. However, the reflectance decreases observed in the samples with high levels of M at 610 nm and 645 nm were lesser than the showed by the samples with elevated levels of OCFW, and OCDM. Finally, there were not differences in the spectral signature of the samples related to TA level variations.

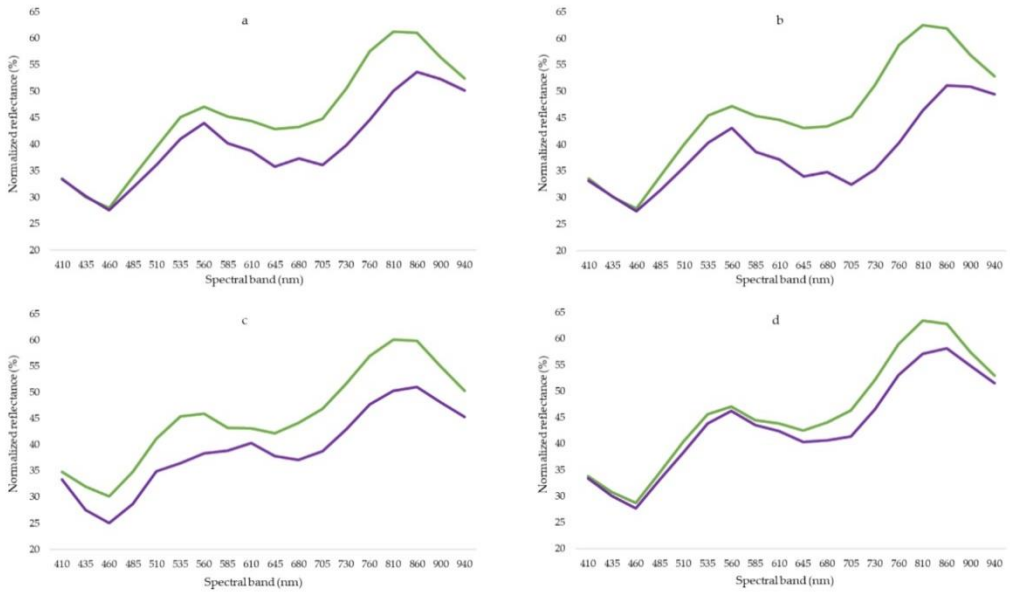

Figure 7. Mean reflectance response of olive samples corresponding to the 10th (green line) and above the 90th (purple line) percentile of OCFW (a), OCDM (b), M (c), and TA (d).

3.4. Performance of estimation models

The performance of the four ANN models was evaluated by means of a random sampling test (RS). Table 2 shows the statistics comparing the ANNs' output and the reference data in the external validation set. Additionally, the statistics measured during models training are also depicted. The output of the ANN models showed good relationships with the values of OCFW, OCDM, and M determined by standard methods, with coefficients of determination (R^2) of 0.86, 0.86, and 0.89 (Figure 8). For the training set, the statistics regarding R^2 were slightly lower (0.83 for OCFW; 0.84 for OCDM; 0.89 for M). In the case of TA, the performance of the ANN model was lower, with an R^2 of 0.21 measured when facing the output of the model and the reference data in the external validation set (Figure 8); R^2 value reached 0.30 during training. RMSE between the estimated and predicted values were 1.29 for OCFW, 2.74 for OCDM, 1.66 for M, and 0.17 for TA in the external validation set, and 1.10 for OCFW, 1.88 for OCDM, 1.45 for M, and 0.09 for TA in the training set. The representativeness of these values depends on the magnitude of the respective parameter. For this reason, to make the performance of the different models

comparable, the coefficient of variation of the RMSE (CVRMSE) and the ratio of performance to deviation (RPD) were also calculated. Thus, CVRMSE revealed a similar performance of the models aimed to estimate OCFW and OCDM, as RMSE in the external validation resulted in 6.48 % and 6.24 % of the mean value of the measurements, respectively. In this concern, the M model obtained the best results, as RMSE supposed 2.88% of the mean value of the measurements in the external validation set. Regarding TA, CVRMSE confirmed the results showed by R^2, as RMSE supposed 42.38 % of the mean value of the measurements in the external validation set. With respect to the training set, CVRMSE values were slightly lower for the four models (5.83% for OCFW, 4.17% for OCDM, 2.55% for M, and 26.27% for TA). The results related to RPD values agreed with those of CVRMSE, as they were 2.71 for OCFW, 2.70 for OCDM, 3.02 for M, and 1.13 for TA in the external validation set, and 2.48 for OCFW, 2.55 for OCDM, 3.07 for M, and 1.20 for TA in the training set.

Table 2. R^2, RMSE, CVRMSE, RPD and *p* (*p*-value from paired samples t-test) between reference values of OCFW, OCDM, M, and TA, measured by chemical methods, and those estimated based on ANN approaches in the training and external validation sets.

	Training				**External validation**				
	R^2	**RMSE**	**CVRMSE**	**RPD**	**R^2**	**RMSE**	**CVRMSE**	**RPD**	***p***
OCFW (%)	0.83	1.10	5.83	2.48	0.86	1.29	6.48	2.71	0.46
OCDM (%)	0.84	1.88	4.17	2.55	0.86	2.74	6.24	2.70	0.48
M (%)	0.89	1.45	2.55	3.07	0.89	1.66	2.88	3.02	0.26
TA (%)	0.30	0.09	26.27	1.20	0.21	0.17	42.38	1.13	0.02

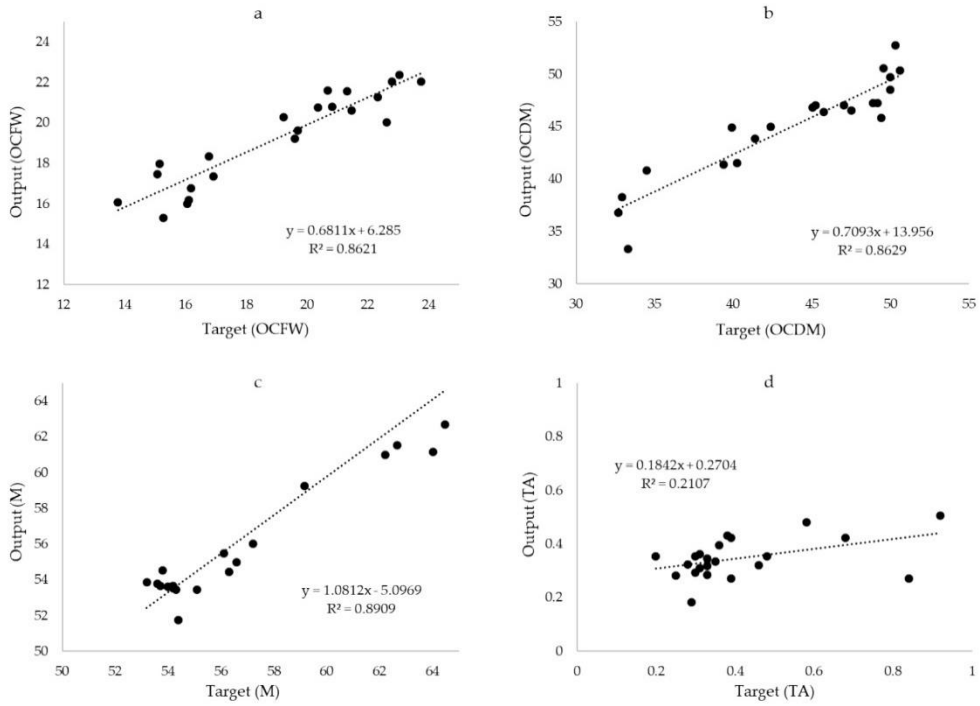

Figure 8. Linear regressions between OCFW (a), OCDM (b), M (c), and TA (d) measured by chemical methods, and those estimated based on ANN approaches in the external validation set.

In accordance with the trends observed, the contrasts of hypothesis based on a t confidence interval for paired samples indicated that there were not significant differences ($p \leq 0.05$) between the reference data and the response of the models for the estimation of OCFW, OCDM, and M. On the contrary, in the case of TA estimation, the contrast of hypothesis revealed significant differences ($p \leq 0.05$) between the reference data and the response of the models.

4. Discussion.

The aim of this research is to evaluate the suitability of a methodology based on a custom-built multispectral device and neural network estimation models, for quantitatively estimating olive fruit ripening status under field conditions. To this end, a two-season field experiment was conducted, consisting in periodical sample collection throughout the olive ripening process. The proposed device was used to acquire the spectral signature of samples under field conditions.

Afterwards, the samples were characterized by means of chemical standard methods to obtain reference values of ripening state: oil content per fresh weight (OCFW), oil content per dry matter (OCDM), moisture (M), and titratable acidity (TA). These parameters were used as target to develop artificial neural network (ANN) models fed with the spectral signature of the samples.

Previously to the in-vivo experiment, a test was done to evaluate the capacity of the proposed device to avoid the effect of the environmental radiation. Thus, the device was used to assess the spectral signature of the same target under three scenarios with increasing levels of environmental radiation. The mean reflectance signal in each individual band acquired by the sensor (18 bands) were compared among the scenarios, by means of an ANOVA of a single factor. The results indicated that the levels of environmental radiation did not cause significative differences ($\alpha = 0.05$) in any band of the spectrum acquired by the sensor. This result suggests that the performance of the proposed device is unaffected by the levels of environmental radiation, indicating its suitability for in-field operation.

The field sampling began in the 2021 season. However, due to a ripening peak between two sampling events, a gap in the ripening status distribution was found. The range and the distribution of the dataset used for training are relevant factors which determine the success of a machine learning estimation model, such as an ANN. For this reason, in order to cover that gap, the field experiments were repeated in the 2022 season. Finally, considering the data collected during both seasons as a whole, the distributions of the target parameters were homogeneous, and wide enough, with values over and under the threshold recommended for harvesting [44]. Furthermore, the fact that the dataset covers two consecutive campaigns improve the confidence in the generalization capacity of the subsequently developed estimation models.

As a first step, the mean spectral signatures of the samples corresponding to the 10^{th} and above the 90^{th} percentile of these parameters were compared. The analysis related to OCFW and OCDM showed comparable results, with spectral profiles with similar overall shapes in both extremes of the histograms. OCDM is calculated based on OCFW and M, so there is a strong

relation between both parameters, which may explain the similarities of their spectra. In both cases, a decrease in the reflectance of the samples associated with elevated levels of OCDM and OCFW, was observed. Especially remarkable were the reflectance peaks between 585-900 nm. In relation to M, a similar effect was observed, this characterized by a decrease of reflectance associated with elevated levels of M. However, the reflectance decreases observed in the samples with high levels of M at 610 nm and 645 nm were lesser than the observed in the samples with high levels of OCFW, and OCDM. Nevertheless, reflectance decreasing associated with M accumulation at 460-560 nm was more evident. Finally, the differences in the spectral response of the samples associated with its TA levels were insignificant. The spectral range acquired by the proposed device (410 - 940 nm) encompasses the visible domain (410 – 760 nm), so reflectance decreasing linked to high levels of OCFW, OCDM, and M may be due to an increase of the absorbance of the samples because of variations in the content of pigments (carotenoids, anthocyanins, chlorophyll a and b). During the ripening process, anthocyanins accumulate in the olive fruit as oil content increases. As ripening progresses, photosynthetic activity decreases and the concentration of both chlorophylls and carotenoids progressively decreases [46]. At the end of the maturation process, the fruit becomes violet or purple due to the accumulation of anthocyanins [47]. Thus, the observed variations of the samples' spectral signature at the extremes of the histograms, may be due to coloration changes accompanying the accumulation dynamics of these parameters. Otherwise, the unequal trend observed in the case of TA may respond to the fact that its accumulation is more influenced by fruit damage rather than by ripening dynamics [44]. So, TA increasing owing to fruit damage in the early stage of ripening may decrease the correlation between colorations changes associated to ripening process and the increase of TA. On the other hand, the proposed device also encompasses a part of the NIR domain (810 – 940 nm), which have been associated with the first and second overtones of O–H stretching [19]. Thus, the variations in these spectral bands associated with the levels of the studied ripening indicators may be due to a water accumulation in the fruits.

One advantage of ANN methods is that the weights of the model's parameters are automatically adjusted during training. So, a precise knowledge about how each single spectral band is related to the target parameters is not needed. For this reason and considering the limited number of spectral bands acquired by the sensor (18), none of them were discarded for feeding the ANN models. To evaluate the proposed methodology, an external validation of the models was carried out, which was based on random sampling tests (RS). RS tests showed promising relationships between the response of the models and the reference values obtained by chemical methods in the external validation set for OCFW ($R^2 = 0.86$), OCDM ($R^2 = 0.86$), and M ($R^2 = 0.89$). The performance of the model aimed to estimate TA was lesser ($R^2 = 0.21$). The elevated coefficients of determination indicate that a high percentage of the variance contained in the target variables were accounted in the response of the models, indicating a good predictive potential [43]. RMSE showed a similar pattern with values of 1.29 for OCFW, 2.74 for OCDM, 1.66 for M, and 0.17 for TA. They accounted for 6.48%, 6.24%, 2.88%, and 42.38% of the average value of the respective parameters. The obtained values of RPD confirmed this trend with values of 2.70 for OCFW, 2.71 for OCDM, 3.02 for M, and 1.13 for TA. This argues in favor models performance aimed to estimate OCFW, OCDM, and M, as values of RPD between 2.5 and 3 or above corresponds to good and excellent prediction accuracy, respectively [48]. These results were confirmed by the contrast of hypothesis based on a *t* confidence interval for paired samples, which indicated that there were not significant differences ($p \leq 0.05$) between the reference data and the response of the models aimed to estimate OCFW, OCDM, and M, in contrast to the TA estimation model (Table 2). The fact that these metrics were similar for the training datasets (Table 2) indicates that the train conditions were suitable, discarding that the satisfactory performance of the models resulted from training overfitting.

The spectral range acquired by the proposed device (410 - 940 nm) encompasses mainly the VIS domain (410 – 760 nm), so a part of the theorical basis of the good performance showed by the ANN is that there is a correlation between the coloration changes undergone by the fruits

and the values of the ripening parameters. This assumption conforms with the fact that fruit color per se serves as a common marker for maturation level, expressed as maturity index [49]. This could explain the deficient performance obtained by the models aimed to estimate TA, as TA is strongly influenced by the damage received by olive fruits. Comparing the spectral signature in the extremes of the TA histograms, the reduced differences of the spectral response of the samples linked to its TA levels was evident. Thus, fruit damage at early ripening stage could increase TA levels, deteriorating the correlation of this variable with fruit color and, consequently, reducing the quality of the input parameters offered to the ANN model. On the other hand, the acquisition of spectral bands situated in the NIR domain (810 – 940 nm), which have been related to water, [19] could explain the better results yielded by the model aimed to estimate M. These results are particularly striking when they are compared to those obtained by Noguera *et* al, 2022 [14]. In this research, a system based in the same spectral sensor (AS7265x) was evaluated to determine the same ripening parameters of olives, but under laboratory conditions. In this job, TA estimation models showed the best results (R^2 = 0.86), followed by M (R^2 = 0.78), and OCFW (R^2 = 0.62). However, there are numerous differences related to the device, and the experimental conditions that may explain these disparities. Firstly, the device has been adapted for being portable, which have supposed major changes in its hardware, including new components (new light source, light diffusion film, etc.) and different geometry of interaction between the light source, the sample, and the sensor. Moreover, the dataset was composed of four olive varieties in its optimum ripening state for harvest according to the grower's criteria, while periodical sample collections were conducted in this research, covering the whole ripening process of just one olive variety. Furthermore, the methods employed to characterize the reference parameters were different. Finally, the fact that the spectral measurement was acquired in the field, instead of under laboratory conditions. All these differences made difficult to do a proper comparison and may explain the disparities in the obtained results.

The use of spectral sensing to characterize intact olive fruits is a relatively mature topic [50]. There has been numerous studies evaluating different spectral sensors and chemometric techniques to assess chemical parameters of olives in a non-destructive way. However, most of them have been accomplished under laboratory conditions [12–14,22–25,45,50–55]. The adaptation of these methodologies to in-field operations would involve several advantages such as, simultaneous multiple measurements, and real-time decision making. However, the effect of environmental variables (temperature, moisture, pressure, ambient light, etc.) on NIR measurements, which are easily controlled under laboratory conditions, makes difficult to apply such a type of methodologies in the field. For this reason, the spectral sensing approaches aimed at assessing the ripening status of olives under field conditions are scarce. Even though, several authors have confronted this challenge [12,26–28]. The results reported in the present study are comparable to those noticed in these investigations. However, it should be considered that the methodologies proposed in these investigations are based on hyperspectral systems. These devices have a higher spectral resolution than the one used in this work, which allows to register multiple narrow-spectral bands further from the VIS domain. Therefore, the acquired spectral signature of the ripening parameters is more descriptive than those obtained with multispectral devices like the one used in this research. The mentioned features of hyperspectral systems generally involve unaffordable costs. Further, the complexity of these devices requires expert personnel for their operation. For these reasons, the methodologies based on hyperspectral devices have limited applications for smallholder farming settings, which represents a significative fraction of the productive sector in many countries. Thus, it is important to develop user-friendly innovative solutions, and also affordable for all kinds of producers. The present job tries to contribute to achieve this goal. In this sense, the present research follows a trend that has occurred in recent decades, which have been motivated by the improvements of the electronics industry [19,56,57]. Enhanced hardware technology has provided sensors bringing higher performance at lower prices. Furthermore, innovative software designs offer algorithms that

enhance the capacity to model biophysical parameters of vegetation by means of the information acquired by sensors. These two concepts are exemplified in the present research. The reliable performance showed by the ANN models, indicates that the spectral bands acquired by the proposed device are highly related to the studied ripening indicators. In this sense, other works have already noticed the suitability of the VIS-NIR range to estimate the quality state of olive fruits, although under laboratory conditions [14,45]. The relationship between the spectral information acquired by the sensor and the considered ripening parameters has been effectively defined by the ANN models, which presents a high flexibility to model the non-linearity of data using local or specific equations. The suitability of ANN models to define the intricate non-linear relationships that normally exist between biophysical parameters of vegetation and spectral data have been previously reported [11,58–63].

5. Conclusions.

This research presents the evaluation of a low-cost multispectral device specially designed to quantitatively assess the ripening status of intact olive fruits under field conditions. The previous test conducted to assess the potential impact of environmental radiation on the device's performance yielded satisfactory results, indicating the suitability of the device for in-field operations. The results obtained in the in-vivo experiments indicate a high potential for estimate OCFW, OCDM, and M even for practical applications. In the case of TA, the results were poor, indicating a lack of correlation between the information acquired by the used sensor and this parameter. The obtained results in the estimation of OCFW, OCDM, and M pave the way for the implementation of an olive ripening appraisal system affordable for all kinds of growers. Moreover, the low cost of the sensor itself allows it to be integrated into wireless sensor networks or robotic devices. The existence of a methodology for olive ripening status assessment affordable for all kinds of olive growers, in terms of price and easy to use, would beneficiate the whole olive sector. The improvement of the spatial-temporal resolution in the monitorization, compared to

the traditional chemical methods, would offer a more accurate and complete view of the ripening process of olive fruits. This would allow growers to apply precision farming techniques to compensate the heterogeneity respect the maturation pace at different plots of a field. On the other hand, it would allow to adapt the time of harvest to this variability, so diversify the production to obtain fruit with specific characteristics. This would give the oleic sector better resources to develop olive oils with a grater added value. Furthermore, expanding the accessibility to this kind of technologies, will improve the understanding of olive maturation and how biotic and abiotic factors can influence it.

Certainly, the addition of the number of samples to the predicting models could improve their robustness; also, the sample collection in additional years of production, or additional olive varieties, could extend their biological variability, so there is room for improving the results obtained in this job in future research.

Author Contributions: Conceptualization, M.N., B.M., A.A., and J.M.A.; data curation, M.N., B.M., and A.A.; formal analysis, M.N.; investigation, M.N.; methodology, M.N., B.M., A.A., and J.M.A.; project administration, B.M.; resources, B.M.; software, B.M.; supervision, B.M., A.A., and J.M.A.; validation, M.N.; visualization, B.M.; writing—original draft, M.N. and B.M.; writing—review & editing, A.A. and J.M.A. All authors have read and agreed to the published version of the manuscript.

Funding: This work was supported by grant PID2020-119217RA-I00, funded by MCIN/AEI/10.13039/ 501100011033; grant IJC2019-040114-I, funded by MCIN/AEI/10.13039/501100011033; grant 0766_OLIVAIS_5_E, funded by the Interreg Cooperation Program V-A SPAIN-PORTUGAL (POCTEP) 2014-2020, and co-financed with ERDF; grant P18-RTJ-4539 funded by the Regional Government of Andalusia through the "PAIDI, Plan Andaluz de Investigación, Desarrollo e Innovación".

Acknowledgments: The authors acknowledge Francisco Dominguez Calvo, the Nuestra señora de la oliva manager, for providing the experimental field in which the study was conducted as

well as the technical support. The authors also acknowledge Kimoto LDT for suppling the material used for making the light-diffuser film.

6. References.

1. Aybar, V.E.; De Melo-Abreu, J.P.; Searles, P.S.; Matias, A.C.; Del Río, C.; Caballero, J.M.; Rousseaux, M.C. Evaluation of olive flowering at low latitude sites in Argentina using a chilling requirement model. *Spanish J. Agric. Res.* **2015**, *13*, e0901–e0901.
2. Rallo, L.; Caruso, T.; Díez, C.M.; Campisi, G. Olive Growing in a Time of Change: From Empiricism to Genomics. In *The Olive Tree Genome*; Rugini, E., Baldoni, L., Muleo, R., Sebastiani, L., Eds.; Springer International Publishing: Cham, 2016; pp. 55–64 ISBN 978-3-319-48887-5.
3. Sarabia, R.; Aquino, A.; Ponce, J.M.; López, G.; Andújar, J.M. Automated identification of crop tree crowns from uav multispectral imagery by means of morphological image analysis. *Remote Sens.* **2020**, *12*, 1–23.
4. Jiménez-Brenes, F.M.; López-Granados, F.; Castro, A.I.; Torres-Sánchez, J.; Serrano, N.; Peña, J.M. Quantifying pruning impacts on olive tree architecture and annual canopy growth by using UAV-based 3D modelling. *Plant Methods* **2017**, *13*, 1–15.
5. Díaz-Varela, R.A.; De La Rosa, R.; León, L.; Zarco-Tejada, P.J.; Lucieer, A.; Rascher, U.; Bareth, G.; Baghdadi, N.; Thenkabail, P.S. High-Resolution Airborne UAV Imagery to Assess Olive Tree Crown Parameters Using 3D Photo Reconstruction: Application in Breeding Trials. *Remote Sens. 2015, Vol. 7, Pages 4213-4232* **2015**, *7*, 4213–4232.
6. Noguera, M.; Aquino, A.; Ponce, J.M.; Cordeiro, A.; Silvestre, J.; Arias-Calderón, R.; Marcelo, M. da E.; Jordão, P.; Andújar, J.M. Nutritional status assessment of olive crops by means of the analysis and modelling of multispectral images taken with UAVs. *Biosyst. Eng.* **2021**, *211*, 1–18.
7. Caruso, G.; Zarco-Tejada, P.J.; González-Dugo, V.; Moriondo, M.; Tozzini, L.; Palai, G.;

Rallo, G.; Hornero, A.; Primicerio, J.; Gucci, R. High-resolution imagery acquired from an unmanned platform to estimate biophysical and geometrical parameters of olive trees under different irrigation regimes. *PLoS One* **2019**, *14*, 1–19.

8. Ben-Gal, A.; Agam, N.; Alchanatis, V.; Cohen, Y.; Yermiyahu, U.; Zipori, I.; Presnov, E.; Sprintsin, M.; Dag, A. Evaluating water stress in irrigated olives: correlation of soil water status, tree water status, and thermal imagery. *Irrig. Sci.* **2009**, *27*, 367–376.
9. Maselli, F.; Chiesi, M.; Brilli, L.; Moriondo, M. Simulation of olive fruit yield in Tuscany through the integration of remote sensing and ground data. *Ecol. Modell.* **2012**, *244*, 1–12.
10. Calderón, R.; Navas-Cortés, J.A.; Lucena, C.; Zarco-Tejada, P.J. High-resolution airborne hyperspectral and thermal imagery for early detection of Verticillium wilt of olive using fluorescence, temperature and narrow-band spectral indices. *Remote Sens. Environ.* **2013**, *139*, 231–245.
11. Fazari, A.; Pellicer-Valero, O.J.; Gómez-Sanchıs, J.; Bernardi, B.; Cubero, S.; Benalia, S.; Zimbalatti, G.; Blasco, J. Application of deep convolutional neural networks for the detection of anthracnose in olives using VIS/NIR hyperspectral images. *Comput. Electron. Agric.* **2021**, *187*, 106252.
12. Fernández-Espinosa, A.J. Combining PLS regression with portable NIR spectroscopy to on-line monitor quality parameters in intact olives for determining optimal harvesting time. *Talanta* **2016**, *148*, 216–228.
13. Salguero-Chaparro, L.; Baeten, V.; Fernández-Pierna, J.A.; Peña-Rodríguez, F. Near infrared spectroscopy (NIRS) for on-line determination of quality parameters in intact olives. *Food Chem.* **2013**, *139*, 1121–1126.
14. Noguera, M.; Millan, B.; Aquino, A.; Andújar, J.M. Methodology for Olive Fruit Quality Assessment by Means of a Low-Cost Multispectral Device. *Agronomy* **2022**, *12*, 979.
15. Cattaneo, T.M.P.; Stellari, A. Review: NIR Spectroscopy as a Suitable Tool for the Investigation of the Horticultural Field. *Agronomy* **2019**, *9*, 503.

16. Comino, F.; Ayora-Cañada, M.J.; Aranda, V.; Díaz, A.; Domínguez-Vidal, A. Near-infrared spectroscopy and X-ray fluorescence data fusion for olive leaf analysis and crop nutritional status determination. *Talanta* **2018**, *188*, 676–684.

17. Guzmán, E.; Baeten, V.; Pierna, J.A.F.; García-Mesa, J.A. A portable Raman sensor for the rapid discrimination of olives according to fruit quality. *Talanta* **2012**, *93*, 94–98.

18. Wang, Y.J.; Jin, G.; Li, L.Q.; Liu, Y.; Kianpoor Kalkhajeh, Y.; Ning, J.M.; Zhang, Z.Z. NIR hyperspectral imaging coupled with chemometrics for nondestructive assessment of phosphorus and potassium contents in tea leaves. *Infrared Phys. Technol.* **2020**, *108*, 103365.

19. Walsh, K.B.; Blasco, J.; Zude-Sasse, M.; Sun, X. Visible-NIR 'point' spectroscopy in postharvest fruit and vegetable assessment: The science behind three decades of commercial use. *Postharvest Biol. Technol.* **2020**, *168*, 111246.

20. García Sánchez, P.A.; Ramos Martos, N.; Ballesteros, E. Comparative study of various analytical techniques (NIR and NMR spectroscopies, and Soxhlet extraction) for the determination of the fat and moisture content of olives and pomace obtained from Jaén (Spain). *Grasas y Aceites* **2005**, *56*, 220–227.

21. Jiménez, A.; Izquierdo, E.; Rodríguez, F.; Dueñas, J.I.; Tortosa, C. Determination of fat and moisture in olives by nearinfrarred reflectance spectroscopy. *Grasas y Aceites* **2000**, *51*, 311–315.

22. Cayuela, J.A.; Camino, M. del C.P. Prediction of quality of intact olives by near infrared spectroscopy. *Eur. J. Lipid Sci. Technol.* **2010**, *112*, 1209–1217.

23. Kavdir, I.; Buyukcan, M.B.; Lu, R.; Kocabiyik, H.; Seker, M. Prediction of olive quality using FT-NIR spectroscopy in reflectance and transmittance modes. *Biosyst. Eng.* **2009**, *103*, 304–312.

24. Beghi, R.; Giovenzana, V.; Civelli, R.; Cini, E.; Guidetti, R. Characterisation of olive fruit for the milling process by using visible/near infrared spectroscopy. *J. Agric. Eng.* **2013**, *44*,

8.

25. Giovenzana, V.; Beghi, R.; Romaniello, R.; Tamborrino, A.; Guidetti, R.; Leone, A. Use of visible and near infrared spectroscopy with a view to on-line evaluation of oil content during olive processing. *Biosyst. Eng.* **2018**, *172*, 102–109.
26. Gracia, A.; León, L. Non-destructive assessment of olive fruit ripening by portable near infrared spectroscopy. *Grasas y Aceites* **2011**, *62*, 268–274.
27. Bellincontro, A.; Taticchi, A.; Servili, M.; Esposto, S.; Farinelli, D.; Mencarelli, F. Feasible application of a portable NIR-AOTF tool for on-field prediction of phenolic compounds during the ripening of olives for oil production. *J. Agric. Food Chem.* **2012**, *60*, 2665–2673.
28. Bellincontro, A.; Caruso, G.; Mencarelli, F.; Gucci, R. Oil accumulation in intact olive fruits measured by near infrared spectroscopy-acousto-optically tunable filter. *J. Sci. Food Agric.* **2013**, *93*, 1259–1265.
29. Khosravi, H.; Saedi, S.I.; Rezaei, M. Real-time recognition of on-branch olive ripening stages by a deep convolutional neural network. *Sci. Hortic. (Amsterdam).* **2021**, *287*.
30. Trang, N.M.; Duy, T.K.; Huyen, T.T.N.; Danh, L.V.Q.; Dinh, A. An investigation into the use of a low-Cost NIR integrated circuit spectrometer to measure chlorophyll content index. *Int. J. Innov. Technol. Explor. Eng.* **2019**, *8*, 35–38.
31. Li, M.; Qian, Z.; Shi, B.; Medlicott, J.; East, A. Evaluating the performance of a consumer scale SCiO™ molecular sensor to predict quality of horticultural products. *Postharvest Biol. Technol.* **2018**, *145*, 183–192.
32. Kitić, G.; Tagarakis, A.; Cselyuszka, N.; Panić, M.; Birgermajer, S.; Sakulski, D.; Matović, J. A new low-cost portable multispectral optical device for precise plant status assessment. *Comput. Electron. Agric.* **2019**, *162*, 300–308.
33. Moinard, S.; Brunel, G.; Ducanchez, A.; Crestey, T.; Rousseau, J.; Tisseyre, B. Testing the potential of a new low-cost multispectral sensor for decision support in agriculture. *Precis. Agric.* **2021**, *21*, 411–418.

34. Leon-salas, W.D.; Rajendran, J.; Vizcardo, M.A.; Postigo-malaga, M. Measuring Photosynthetically Active Radiation with a Multi-Channel Integrated Spectral Sensor. In Proceedings of the 2021 IEEE International Symposium on Circuits and Systems (ISCAS); IEEE Xplore, 2021; pp. 1–5.

35. Stevens, J.D.; Murray, D.; Sozzi, M.; Cogato, A.; Laroche-Pinel, E.; Stevens, J.D.; Murray, D.; Diepeveen, D.; Toohey, D. Development and Testing of an IoT Spectroscopic Nutrient Monitoring System for Use in Micro Indoor Smart Hydroponics. *Hortic. 2023, Vol. 9, Page 185* **2023**, *9*, 185.

36. Tran, N.T.; Fukuzawa, M. A portable spectrometric system for quantitative prediction of the soluble solids content of apples with a pre-calibrated multispectral sensor chipset. *Sensors (Switzerland)* **2020**, *20*, 1–11.

37. Zhang, M.; Shen, M.; Pu, Y.; Li, H.; Zhang, B.; Zhang, Z.; Ren, X.; Zhao, J. Rapid Identification of Apple Maturity Based on Multispectral Sensor Combined with Spectral Shape Features. *Horticulturae* **2022**, *8*, 361.

38. Noguera, M.; Millan, B.; Andújar, J.M. New, Low-Cost, Hand-Held Multispectral Device for In-Field Fruit-Ripening Assessment. *Agriculture* **2022**, *13*, 4.

39. UNE-EN ISO 662:2016 *Animal and vegetable fats and oils - Determination of moisture and volatile matter content*;

40. UNE 55030:1961 *Determination of the content in total fat of olives*;

41. ISO 660:2020 *Animal and vegetable fats and oils — Determination of acid value and acidity*;

42. Savitzky, A.; Golay, M.J.E. Smoothing and Differentiation of Data by Simplified Least Squares Procedures. *Anal. Chem.* **1964**, *36*, 1627–1639.

43. Williams, P.; Manley, M.; Antoniszyn, J. *Near infrared technology: getting the best out of light*; AFRICAN SUN MeDIA, 2019, Ed.; African Sun Media, 2019; ISBN 1928480306.

44. Barranco Navero, Diego, Fernandez Escobar, Ricardo, Rallo Romero, L. *El cultivo del olivo*; Ricardo Fernandez Escobar, L.R.R.D.B.N., Ed.; 7ª ed.; Mundi-Prensa Libros:

Madrid, 2017;

45. Grassi, S.; Jolayemi, O.S.; Giovenzana, V.; Tugnolo, A.; Squeo, G.; Conte, P.; De Bruno, A.; Flamminii, F.; Casiraghi, E.; Alamprese, C. Near infrared spectroscopy as a green technology for the quality prediction of intact olives. *Foods* **2021**, *10*, 1–12.

46. Salvador, M.D.; Aranda, F.; Fregapane, G. Influence of fruit ripening on 'Cornicabra' virgin olive oil quality A study of four successive crop seasons. *Food Chem.* **2001**, *73*, 45–53.

47. Roca, M.; Mínguez-Mosquera, M.I. Change in the natural ratio between chlorophylls and carotenoids in olive fruit during processing for virgin olive oil. *JAOCS, J. Am. Oil Chem. Soc.* **2001**, *78*, 133–138.

48. Nicolaï, B.M.; Beullens, K.; Bobelyn, E.; Peirs, A.; Saeys, W.; Theron, K.I.; Lammertyn, J. Nondestructive measurement of fruit and vegetable quality by means of NIR spectroscopy: A review. *Postharvest Biol. Technol.* **2007**, *46*, 99–118.

49. Dag, A.; Kerem, Z.; Yogev, N.; Zipori, I.; Lavee, S.; Ben-David, E. Influence of time of harvest and maturity index on olive oil yield and quality. *Sci. Hortic. (Amsterdam).* **2011**, *127*, 358–366.

50. León, L.; Rallo, L.; Garrido, A. Análisis de aceituna intacta mediante espectroscopia en el Infrarrojo Cercano (NIRS): Una herramienta de utilidad en programas de mejora de olivo. *Grasas y Aceites* 2003, *54*, 41–47.

51. Cayuela, J.A.; García, J.M.; Caliani, N. NIR prediction of fruit moisture, free acidity and oil content in intact olives. *Grasas y Aceites* **2009**, *60*, 194–202.

52. Saha, U.; Jackson, D. Analysis of moisture, oil, and fatty acid composition of olives by near-infrared spectroscopy: development and validation calibration models.

53. Cirilli, M.; Bellincontro, A.; Urbani, S.; Servili, M.; Esposto, S.; Mencarelli, F.; Muleo, R. On-field monitoring of fruit ripening evolution and quality parameters in olive mutants using a portable NIR-AOTF device. *Food Chem.* **2016**, *199*, 96–104.

54. Giovenzana, V.; Beghi, R.; Civelli, R.; Trapani, S.; Migliorini, M.; Cini, E.; Zanoni, B.; Guidetti, R. Rapid determination of crucial parameters for the optimization of milling process by using visible/near infrared spectroscopy on intact olives and olive paste. *Ital. J. Food Sci.* **2017**, *29*, 357–369.

55. Salguero-Chaparro, L.; Peña-Rodríguez, F. On-line versus off-line NIRS analysis of intact olives. *LWT - Food Sci. Technol.* **2014**, *56*, 363–369.

56. Bec, K.B.; Grabska, J.; Huck, C.W. Miniaturized NIR Spectroscopy in Food Analysis and Quality Control: Promises, Challenges, and Perspectives. *Foods 2022, Vol. 11, Page 1465* **2022**, *11*, 1465.

57. Krause, J.; Grüger, H.; Gebauer, L.; Zheng, X.; Knobbe, J.; Pügner, T.; Kicherer, A.; Gruna, R.; Längle, T.; Beyerer, J. SmartSpectrometer—Embedded Optical Spectroscopy for Applications in Agriculture and Industry. *Sensors* **2021**, *21*, 4476.

58. Allouche, Y.; López, E.F.; Maza, G.B.; Márquez, A.J. Near infrared spectroscopy and artificial neural network to characterise olive fruit and oil online for process optimisation. *J. Near Infrared Spectrosc.* **2015**, *23*, 111–121.

59. Kalacska, M.; Lalonde, M.; Moore, T.R. Estimation of foliar chlorophyll and nitrogen content in an ombrotrophic bog from hyperspectral data: Scaling from leaf to image. *Remote Sens. Environ.* **2015**, *169*, 270–279.

60. Wang, F.; Huang, J.; Wang, Y.; Liu, Z.; Peng, D.; Cao, F. Monitoring nitrogen concentration of oilseed rape from hyperspectral data using radial basis function. *Int. J. Digit. Earth* **2013**, *6*, 550–562.

61. Huang, Z.; Turner, B.J.; Dury, S.J.; Wallis, I.R.; Foley, W.J. Estimating foliage nitrogen concentration from HYMAP data using continuum removal analysis. *Remote Sens. Environ.* **2004**, *93*, 18–29.

62. Pôças, I.; Gonçalves, J.; Costa, P.M.; Gonçalves, I.; Pereira, L.S.; Cunha, M. Hyperspectral-based predictive modelling of grapevine water status in the Portuguese

Douro wine region. *Int. J. Appl. Earth Obs. Geoinf.* **2017**, *58*, 177–190.

63. Mayr, S.; Beć, K.B.; Grabska, J.; Wiedemair, V.; Pürgy, V.; Popp, M.A.; Bonn, G.K.; Huck, C.W. Challenging handheld NIR spectrometers with moisture analysis in plant matrices: Performance of PLSR vs. GPR vs. ANN modelling. *Spectrochim. Acta - Part A Mol. Biomol. Spectrosc.* **2021**, *249*.

4.3.3. Article 5

New, Low-Cost, Hand-Held Multispectral Device for In-Field Fruit-Ripening Assessment

Miguel Noguera, Borja Millán and José Manuel Andújar.

Journal: Agriculture (ISSN: 2077-0472).

Editorial: MDPI.

Reference: Agriculture. 2023, 13 (1), 4.

DOI: 10.3390/agriculture13010004.

Year: 2023.

Quality index (Journal Citation Reports®, 2022): 17/88 (Q1) in the category "Agronomy". Impact Factor of 3.600.

agriculture

MDPI

Article

New, Low-Cost, Hand-Held Multispectral Device for In-Field Fruit-Ripening Assessment

Miguel Noguera [1,*], Borja Millan [2] and José Manuel Andújar [1]

[1] Centro de Investigación en Tecnología, Energía y Sostenibilidad (CITES), Universidad de Huelva, La Rábida, Palos de la Frontera, 21819 Huelva, Spain
[2] Departamento de Ingeniería Eléctrica, Electrónica, Informática y de Sistemas, Universidad de Oviedo, C/ Pedro Puig Adam, 33203 Gijón, Spain
* Correspondence: miguel.noguera@diesia.uhu.es

Abstract: The state of ripeness at harvest is a key piece of information for growers as it determines the market price of the yield. This has been traditionally assessed by destructive chemical methods, which lead to low-spatiotemporal resolution in the monitorization of crop development and poor responsiveness for growers. These limitations have shifted the focus to remote-sensing, spectroscopy-based approaches. However, most of the research focusing on these approaches has been accomplished with expensive equipment, which is exorbitant for most users. To combat this issue, this work presents a low-cost, hand-held, multispectral device with original hardware specially designed to face the complexity related to in-field use. The proposed device is based on a development board (AS7265x, AMS AG) that has three sensor chips with a spectral response of eighteen channels in a range from 410 to 940 nm. The proposed device was evaluated in a red-grape field experiment. Briefly, it was used to acquire the spectral signature of eighty red-grape samples in the vineyard. Subsequently, the grape samples were analysed using standard chemical methods to generate ground-truth values of ripening status indicators (soluble solid content (SSC) and titratable acidity (TA)). The eighteen pre-process reflectance measurements were used as input for training artificial neural network models to estimate the two target parameters (SSC and TA). The developed estimation models were evaluated through a leave-one-out cross-validation approach obtaining promising results (R^2 = 0.70, RMSE = 1.21 for SSC; and R^2 = 0.67, RMSE = 0.91 for TA).

Keywords: sensor; multispectral; precision farming; machine learning; artificial neural network; AS7265x

Citation: Noguera, M.; Millan, B.; Andújar, J.M. New, Low-Cost, Hand-Held Multispectral Device for In-Field Fruit-Ripening Assessment. *Agriculture* **2023**, *13*, 4. https://doi.org/10.3390/agriculture13010004

Academic Editors: Ahmed Mustafa Rady and Ewa Ropelewska

Received: 15 November 2022
Revised: 16 December 2022
Accepted: 18 December 2022
Published: 20 December 2022

1. Introduction

Fruit ripening involves a set of morphological, physiological, and biochemical changes that make fruit suitable for consumption. During maturation, a green, firm, immature fruit usually becomes more colourful, softer, sweeter, and aromatic. Furthermore, biotic and abiotic stresses trigger metabolic processes that reduce fruit quality not only during growth but also during harvest and storage [1]. These modifications can be characterized through physical and chemical attributes such as size, shape, texture, firmness, soluble-solids content (SSC), starch, sugars, acids, oils, internal ethylene concentration, external and internal colour, and concentration of chlorophyll, etc. [2]. Thus, there are objective parameters which allow for the monitoring of the quality state of fruit and the carrying out of actions to improve it. Traditionally, the assessment of these fruit-quality indicators has been based on chemical and physical methods, such as high-performance liquid chromatography (HPLC), refractometry, and colorimetry, among others. These kinds of methods require extensive sample preparation, expert workers, and advanced laboratory facilities. All these factors lead to a high cost. Therefore, there are two main concerns accompanying these methods. These include the representativeness of a sample from a field on a given date and the number of sample dates that can be performed during the campaign. These

concerns lead to poor temporal and spatial resolution in the monitorization, which limits the growers' reaction capacities. These facts make the implementation of rapid, economical, and non-destructive alternatives necessary, as they would benefit growers, processors, and consumers alike. The in-field, non-destructive assessment of fruit ripeness would provide numerous benefits compared to traditional destructive techniques such as high-throughput assessment, simultaneous multiple measurements, and real-time decision making.

In recent decades, spectral-based approaches have been proposed as an alternative to fruit-quality assessment because of their speed and non-invasive character [3]. The theorical foundation of this kind of method relies on the interaction between light and objects. Briefly, every molecule consists of several atoms. The bonds between the atoms can be excited by light with a characteristic wavelength (i.e., colour) [4,5]. This leads to short time vibrations within the molecule. This specific wavelength depends on the strength of the bonds and the mass of the atoms and is unique for each molecule. This interaction between light and objects can be assessed by analysing the three processes of absorption, reflection, and transmission. As no two organic compounds have the same characteristics, a compound can be identified accurately by analysing its absorption spectrum and matching it with a database [4].

The complexity of the interaction between light and objects has led to several lines of research, such as fluorescence spectroscopy [6], Raman spectroscopy [7], multispectral imaging [8], hyperspectral imaging [9], and visible, near-infrared (VIS-NIR) 'point' spectroscopy [10]. All the referenced works have demonstrated the suitability of light-based approaches for agricultural applications and specifically fruit-quality assessment. The present work is centred on VIS-NIR 'point' spectroscopy. The particularity of point spectroscopy in terms of spectral imaging is the resolution. While spectral cameras offer images composed of numerous pixels containing information, which allow for contrast in different parts of the sample, the 'point' sensors give just one measure for the focused area.

The use of VIS-NIR spectroscopy for the characterization of agri-food products is a relatively mature topic, even more so regarding precision farming. The combination of chemometrics techniques with spectral data has been widely studied. Fifteen years have passed since the comprehensive review on the use of NIR spectroscopy for non-destructive quality assessment of fruits and vegetables by Nicolaï et al. (2007). The state of the art has been expanded following this review, with works focused on the monitorization of different biophysical parameters beyond the quality status of fruits [3,11–14]. In fact, there are various commercially available instruments dedicated to the post-harvest sector. In this sense, VIS-NIR spectrophotometers have been integrated into commercial packing lines. Additionally, there is also commercially available hand-held equipment for fruit analyses. However, this equipment is very expensive—even exorbitant—for most users. In recent decades, the improvement in the microelectronic industry has resulted in lower costs and improved component features. This development is arousing an increasing interest in the use of low-cost spectral sensors for agricultural applications [15–17], as this would allow for the implementation of these non-destructive methodologies throughout the post-harvest value chain, both upstream (to the field) and downstream (to distribution centres and to consumer use). Thus, there is room to confirm past work and to further improve these processes to underpin adoption.

In this context, this work presents a custom-built, low-cost multispectral device designed especially for in-field applications. The proposed device is based on the "AS7265x" development board (AMS AG). This sensor has been previously tested for agricultural applications. Moinard et al. [18] proved its potential for estimating the percentage of grass cover and estimating vine vigour. Noguera et al. [17] used it to assess the quality status of intact olive fruits under laboratory conditions with promising results. Zhang et al. [19] evaluated it for classifying apples in three ripening categories based on classical maturity indicators. Leon-salas et al. [20] used it to determine photosynthetically active radiation indoors and outdoors. Furthermore, there are other works centred in sensors with similar features. For example, Trang et al. [21] developed and tested a device based on six-channel

NIR sensors (AS7263, AMS AG) for measuring chlorophyll content in a leaf. Li et al. [22] evaluated a commercially available spectral sensor (SCIO) to predict the quality of kiwifruit, apples, feijoas, and avocados. These sensors have the potential to provide objective information to growers. However, most of the previously mentioned works that focused on the use of spectroscopy for fruit quality assessment were conducted under laboratory conditions. This approach allows for the control of external parameters and reduces both the complexity of the problem and the applicability of the solution. Further, the limited works focused on in-field solutions used equipment with very high acquisition costs. Therefore, the goal of this research is to develop a hand-held spectral device, affordable for all kinds of users (growers, processors, and consumers), and to continue exploring its potential for in-field applications. Thus, a prototype was developed with hardware (described in Section 2.2) that was specially designed to acquire data under field conditions. In order to evaluate its suitability, an experiment was designed with the goal of estimating the quality parameters of grapes by means of spectral data acquired with the proposed device under field conditions.

2. Materials and Methods

2.1. Device Description

The multispectral sensor device is composed of different elements that are assembled inside a 3D-printed enclosure. The objective was to develop a tool that is reliable and easy to operate under field conditions by non-specialized personnel. To reduce cost and simplify maintenance, commercial components were selected where available. However, some PCBs (printed circuit boards) were developed to simplify the assembly. A description of the different components is presented in the following sections, introducing the hardware and the software that controls the operation of the sensor.

2.1.1. Hardware: Electronic components

- AMS AS7265x development board (AMS AG, Premstätten, Austria): This board is composed of three main chips: AS72651, AS72652, and AS72653. These chips are sensible to six different bands (by including six optical filters each) in the range between 410 nm and 940 nm, with a full width at half maximum (FWHM) of 20 nm. The AS72651 acts as a master for the chip arrangement and the communication with the rest of the components is performed with this chip. This development board results in a low-cost, 18-channel multispectral sensor.
- Arduino MKRZero Board (Arduino LLC, Monza, Italy): The Arduino MKR Zero board was selected because of its small form factor, low power consumption, low cost, and the availability of an SD card slot. A custom software was developed using the Arduino IDE (described in the software section). This board communicates with the AS7265x development board, OLED screen, and LED PCB to perform data acquisition.
- Interconnection board: There is a high number of interconnected components on the system. An interconnection board was designed and manufactured to generate a reliable connection between them. This board serves as the core of the system, adapting the voltage from the battery, regulating LEDs' signal intensity, and interfacing the different components of the sensor with connectors to different subsystems. A constant-current LED driver (RCD-24, RECOM, Germany) installed on the PCB allows us to modulate capturing parameters (light intensity and power on time), controlled by the Arduino MKR. A schema of the different connections between device components is depicted below (Figure 1).

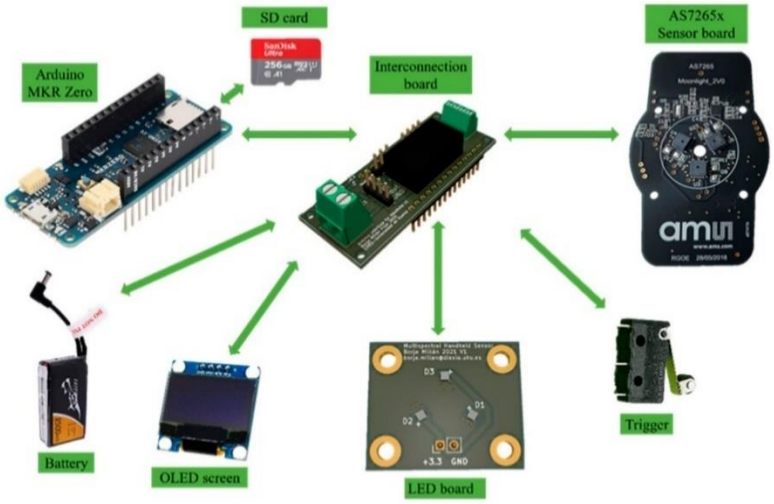

Figure 1. Schema of the different components of the low-cost multispectral device, including the interconnections between them.

- LED PCB: The samples to be measured must be illuminated to obtain the reflectance measurement. An array of three IR-broadband LED emitters (OSLON P1616 SFH 4737, OSRAM, Germany), was used to achieve this goal. This component was developed specifically for spectroscopy applications, providing a wide emission spectrum in the VNIR with the advantage of less power and heat dissipation requirements than a halogen lamp. The PCB allows us to install three LEDs and easily attaches to the 3D-printed reflective dome of the instrument. Although the LEDs are only powered when a measurement is taken, the PCB also acts as a heat dissipator to reduce the damage to this component due to heat build-up.
- OLED Screen: The screen serves as a guide for the user during measurement. The developed device included an OLED display, specifically a 1.3-inch panel with a resolution of 128 by 64 pixels. The availability of an integrated display avoids the necessity of a computer or some other external device to verify the status of the device and its proper operation in the field. The screen shows real-time data, the file name, the number of measurements taken, and the configuration parameters (Figure 2).

Figure 2. Image of the device's integrated OLED screen showing initialization data (**left**) and ready to perform data capture (**right**).

- Battery: The system can be powered from any DC source up to 35 V through a barrel connector (2.1 × 5.5 mm). During the experiments, the prototype was powered by a 2s LiPo (Lithium-ion Polymer) battery connected to the device controller board. The low-power consumption of the sensor allows for extended operation time lasting beyond a workday. In any case, the battery is placed outside the device, so it is easy to replace the depleted battery and continue capturing data in the field.

2.1.2. Hardware: 3D-Printed Enclosure

In order to provide a compact, ergonomic, and low-cost enclosure, a device case was designed using FreeCAD 0.19 (Figure 3) and manufactured with a 3D printer using a biodegradable polylactic acid (PLA) filament. Four different components were designed:

- Main enclosure: A box-type enclosure was designed as the main body of the device. The AMS AS7265x development board, Arduino MKR Zero, and interconnection board are stacked inside and held in place with help from two 3D-printed separators.
- Lid with screen: This lid seals the sensor to allow in-field operation. The OLED screen is fixed to the lid of the main enclosure, and its position allows for easy visualization of the data when taking a measurement.
- Reflective dome and diffuser bracket: A dome that holds the light source (LED PCB) and integrates a light-diffusion film (OptSaver L-9960, Kimoto LDT, Switzerland). The diffuser is placed in front of the sensor to homogenize the illumination and the signal measured an obtain a representative measurement. Data acquisition is performed by making contact between the sample and the diffusive film. The dome is developed to guarantee that the sample is placed at a 45° angle with the light source and the sensor.
- Handle with trigger: This part allows for the simultaneous support and operation of the device with one hand (enabling the use of the other hand for sample manipulation). An end stop switch is used as a trigger. The switch is installed inside the handle and the wires to connect to the interconnection board are conducted inside the handle to the main enclosure.

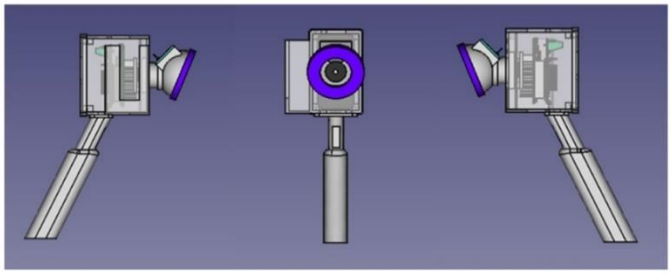

Figure 3. Three-dimensional rendering of different views of the device case designed with FreeCAD 0.19.

2.1.3. Software

The Arduino MKR board was programmed using Arduino IDE. A diagram of software functionality is depicted in Figure 4. At boot, the system will check for a file "UPDATE.bin" in the SD. In the case this file is available, the firmware is updated and the board is rebooted. This allows for a reconfiguration of different parameters of the system without the need for a connection with a PC.

The software operation can be summarized in the following steps:

- The first step is the initialization of all the components of the system, including the input/output configuration and the serial comm parameters definition. Two main serial connections are defined: a connection with the AMS AS7265x development board and with a computer to allow for device control and data monitorization over a computer. Moreover, the OLED screen is connected by a SPI (Serial Peripheral Interface).
- The sensor board (AMS AS7265x) is configured using AT commands over a serial port. Primarily, sensor gain and integration time must be established. Other parameters for calibration can also be configured. All the initialization steps are displayed on the OLED Screen and optionally on the serial connection using a virtual comm over USB. This allows the user to quickly debug any failures during the configuration (i.e., a lost connection with the sensor).

- The next step is to initiate the SD card. A scan of the contents of the card is performed, and a new file is created with the format "dataXXX.csv" where XXX is the last file number stored plus one. Every time the device is powered-up a new file is created, preserving the previously acquired data. The file has a header with a description of the configuration used (mainly integration time, gain, and LED current). The captured spectrum is stored as one measurement per row with reflectance separated by a comma, allowing the file to be processed by standard software compatible with CSV file format.
- After the initialization is completed, the system waits for user input in which the trigger is pressed or a command is sent via serial connection. This dual implementation allows for the control of the system autonomously in the field (via the trigger) or through a connection to a computer, which can be more interesting for in-laboratory operation as it allows for real-time supervision of the measurements.
- When an input is detected, the device begins the capturing process:
  - LEDs are turned on with the configured current at 0–1000 mA.
  - A command is sent to the AMS AS7265X sensor board to perform the acquisition, and the system waits for correct data reception.
  - The LEDs are turned off as soon as all the data are received.
  - Finally, the data are stored in the SD card. Following this, the system is ready for another measurement.

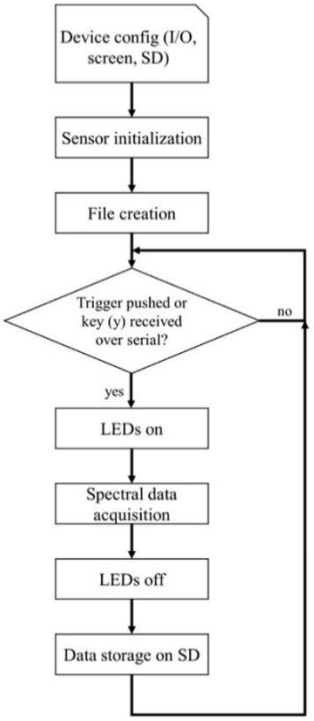

Figure 4. Flow chart of the process for multispectral data capture.

All the data are stored as soon as they are received, reducing the time spent waiting until data has been written to the SD card. This process minimizes information loss in case the power is removed after an acquisition is performed. Additionally, the device can be turned off by removing the power without any special procedure. The only precaution needed to turn off the device (and avoid data corruption) is to allow the system to store the last measurement.

2.2. Validation Experiment

In order to evaluate the suitability of the developed device, an experiment was carried out that was intended to assess ripening indicators of grape berries (*Vitis vinifera* L.) by means of the spectral data acquired with the device under field conditions.

2.2.1. Study Site Description

The study site was situated in the *Condado de Huelva* appellation (Bodegas Contreras Ruiz, S.L, Rociana del Condado, Huelva). It is a commercial vineyard of *Syrah* variety, which is a red-grape variety widely used in the wine industry. The experimental field had an extension of approximately 1000 m^2. The soil in the study area is characterized by a heterogeneous structure and composition. Thus, it presents sandy loam areas alternating with clay-loam zones. This irregular pattern relating to the structure and composition of the soil is reflected in the physiology of the plants. There were plants with different paces of ripening, which resulted in high variability according to the quality parameters considered in this research. This was a key factor for the validation experiment, as variability regarding the target parameters is essential to assure the generalization capacity of the developed estimation models.

2.2.2. Spectral Collection

The field experiment was performed on 22 July 2021. This date was selected for its proximity to the optimum harvest time according to the winery's manager. The first part of the experiment was performed in the vineyard and consisted of a sample collection. To obtain the most variability in terms of the ripening stage of the grapes, the entire vineyard was covered by randomly collecting a total of 80 samples. A grape cluster was considered as a sample unit. Each of the grape clusters was harvested using pruning shears. The spectral signature of the cluster was acquired immediately after harvest. The measuring methodology involved facing the dome of the device against the upper part of the grape cluster and making a capture. The measurements were made in the centre of the row to avoid plant shadows on the sample (Figure 5). Two captures were acquired per sample, taking the average reflectance of the two spectra as representative data for each sample. After being processed, each sample was packaged, labelled, and refrigerated at 3–4 °C in a portable cooler during its transport to laboratory. At the laboratory, the samples were analysed on the same day as the sample collection. Once every fifteen samples, three captures of a surface of known reflectance (Labsphere, Inc, North Sutton, NH, USA) (53% calibrated reflectance) were taken. The average signal of the three captures would be used later as a reference to normalise the following fifteen samples. This enabled the prevention of subsequent errors due to variations in ambient light.

2.2.3. Reference Analysis

The development of estimation models by means of sensor-acquired spectral data requires a reference dataset that indicates the actual state of the samples regarding the target parameters. With this purpose, the samples were subjected to destructive chemical methods to obtain objective indicators of their actual ripening status. In this work, solid soluble content (SSC) and titratable acidity (TA) were used as target parameters, given that they are routinely considered by the wine industry to determine the ripening status of grapes [23]. The SSC is defined as the total content of solids dissolved in a given volume of juice. This includes carbohydrates, organic acids, proteins, fats, and minerals. However, in a grape at a certain grade of maturity, sugars represent around 90–95% of the total solid, so SSC is also considered a good approximation of sugar content (sweetness). Furthermore, the SSC of the grapes in the harvest is directly related to the alcoholic grade of the wine to be produced [24]. TA is defined as the degree of acidity of a substance and is measured by volumetric methods. In the case of grapes, this parameter is correlated to the SSC; as the fruit ripens, the SSC content increases while the TA decreases. The balance between these

two grape parameters at the moment of harvest is decisive of the features of the wine to be produced, which means that controlling these parameters is paramount [23].

Figure 5. Methodology for spectral data acquisition.

The methodologies employed to assess both ripening indicators are standardised by the International Organization of Vine and Wine (OIV) [25]. The first step of the procedure to determine SSC and TA values was the shelling of the grape clusters. Following shelling, fifty grapes per cluster were randomly selected and were then squeezed to obtain the wort. Just a few drops of wort were used to determine the SSC (Brix°) by means of a temperature-compensating digital refractometer (HI96801, Hanna instruments, Spain). On the other hand, an initial volume of 50 mL of wort per sample was used to assess grape TA by titration with 0.1 NaOH to an end point of pH 7.0 using an automatic titralyser (LDS1155500, Dujardin-Salleron, France). The results were expressed as g/L of Chlorohydric acid. The statistics (the range, mean, and standard deviation (SD)) of both parameters were analysed using the Orange 3 software [26].

2.3. Methodology for Ripening Status Estimation from Multispectral Information

2.3.1. Data Pre-Processing

The mean reflectance signature of each grape sample was calibrated to avoid eventual errors due to variations in the ambient light. The calibration consisted of a normalisation, using as reference the spectral signature of the known reflectance surface (53%) (Labsphere, Inc, North Sutton, NH, USA), which was captured once every fifteen samples. The level of reflectance of the known reflectance surface (53%) allowed the attainment of a better resolution as the reflectance of the samples was less than 50% for all the considered bands. The eighteen reflectance signals of the known reflectance surface were used as reference for calibrating the spectral response of the subsequent fifteen samples according to the next equation:

$$\mathrm{Rcal}_{\mathrm{wl}} = \frac{\mathrm{R}_{\mathrm{wl}}}{\mathrm{Rref}_{\mathrm{wl}}/0.53} \quad (1)$$

where R_{wl} is the reflectance value measured for a given spectral band in a capture of a sample, $\mathrm{Rref}_{\mathrm{wl}}$ is the reflectance value measured for that spectral band in the previous capture of the known reflectance surface, and $\mathrm{Rcal}_{\mathrm{wl}}$ is the corrected value of reflectance in the sample for the given band.

2.3.2. Estimation Model Development

The corrected reflectance of the eighteen spectral bands captured by the sensor were used as input variables to train two artificial neural networks (ANN) to estimate the SSC

and TA. An ANN is a non-linear, non-parametric method (machine learning method). This approach consists of a structure of neurons linked together and arranged in layers. The neurons of different layers are interconnected, and each connection has a specific weight. Each neuron essentially realises a linear regression followed by a non-linear function. Briefly, the ANN architecture works to minimize the mean–square deviation trough the error-correction learning rule. Thus, the error will be minimized by adjusting the weight of each layer of neurons. These characteristics allow for an extraordinary connection between complex spectral information and key parameters without any constraint on the sample distribution. This makes ANN approaches appropriate to define complex non-linear relationships that normally exist between spectral signatures of fruits and ripening indicators.

In this work, the software used for data processing and ANN training was Orange 3 [26]. This is an open-source tool for data visualization, pre-processing, and modelling. The ANN used was a multi-layer perceptron (MLP) algorithm with back propagation. The architecture of the neural network employed was composed of a hidden layer with six neurons, eighteen inputs, and one output (one model per target parameter). Identity was used as an activation function for the hidden layer, and an L-BFGS-B (an optimizer in the family of quasi-Newton methods) was used as a Solver for weight optimization. Before the feeding of the ANN model, the dataset was processed with a local outlier factor algorithm. This algorithm computes a score reflecting the degree of abnormality of the observations. It measures the local density deviation of a given data point with respect to its neighbours. The contamination (proportion of outlier in the dataset) was set at 2%, so this previous analysis discarded two samples. Figure 6 shows the workflow of the models. Leave-one-out cross-validation (LOOCV) was used as a validation method, due to it being considered the most suitable due to the volume of the dataset (n = 80). This method holds out one instance at a time, inducing the model from all others and then estimating the held-out instances. This method is obviously very stable and suitable for limited volume datasets as it avoids over-fitting. Alternatively, a random sampling (RS) test was made. For that purpose, the complete data set was randomly divided into two subsets: 75% training and 25% external validation (test). The training was repeated two consecutive times, obtaining a test set of 40 samples.

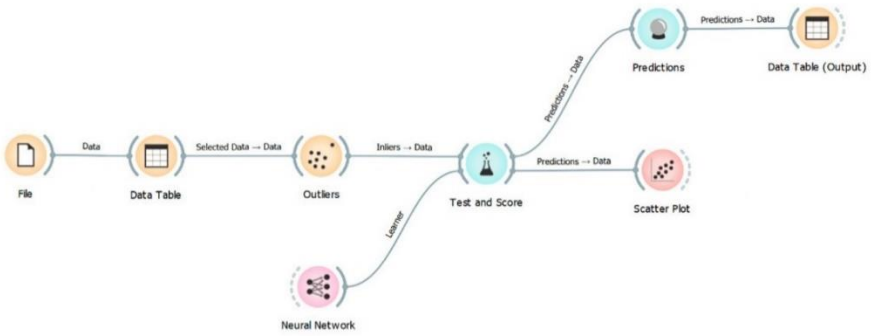

Figure 6. Simulated workflow of the model in Orange 3 data-mining software.

2.4. Criteria for Model Performance Evaluation

The performance of the estimation models was measured by the coefficient of determination (R^2), and the root–mean–square error of prediction (RMSE) between the actual values of the ripening indicators determined by chemical methods and those estimated by ANN models. In the case of LOOCV, the output of the ANN applied to the validation set excluded during training at every iteration was used to determine the mentioned statistical parameters. Thus, a test set of 80 predictions was configured. The coefficient of determination (R^2) was used to assess the relationship between the actual and predicted target parameters. On the other hand, the RMSE is the standard deviation of the residuals (prediction errors). Residuals are a measure of the distance of data points to the regression

line; RMSE is a measure of how spread out these residuals are. In summary, higher R^2 and smaller RMSE values indicated better model performance.

RMSE can be mathematically formulated as:

$$\mathrm{RMSE} = \sqrt{\sum_{i=1}^{n} \frac{(\mathrm{Ypred_i} - \mathrm{Yref_i})^2}{n}} \quad (2)$$

where Y_{predi} is the response of the model, Y_{refi} is the reference data, and n is the number of measurements in the respective external-validation dataset. Furthermore, it also was considered the coefficient of variation of the RMSE (CVRMSE), which is the result of normalizing the RMSE by the mean value of the measurement. This allows for the avoidance of ambiguity, facilitating the comparison between datasets or models with different scales.

Additionally, paired samples (*t*-tests) for dependent samples were also conducted to confirm the results from the R^2, RMSE, and CVRMSE analyses. For this purpose, the data pairs of the output of the ANN and the validation data excluded during training at every iteration of the LOOCV, the reference value, and the resulting prediction corresponding to the external validation sets in the case of the RS were compared. The paired t-test is a parametric method, useful for testing whether the means of two groups are different when the samples are drawn in pairs. The *t*-test was carried out using Microsoft® Excel® for Microsoft 365 MSO (version 2211) software. The compliance with the null Hypothesis in this test ($p > 0.05$) indicates that there were no significative differences between the mean of the measures based on the proposed device and the obtained through the reference methods.

3. Results

3.1. Actual Quality Status of Grape Samples

A total of 80 grape samples of the Syrah variety were considered in this research. Table 1 summarizes the statistical details of the whole dataset related to the explored ripening indicators. In the case of soluble solid content (SSC) (expressed as °Brix), the grape samples varied between 10.4° and 19°, with an average value of 16 ± 1.9°. On the other hand, the titratable acidity (TA) (expressed as g/L of Chlorohydric acid), of the grape samples ranged between 2.7 g/L and 10.9 g/L with an average value of 5.1 ± 1.5 g/L. The ranges of both parameters were quite wide, with grape clusters close to the optimum state for harvest and grape clusters with a further-delayed ripening state. On the other hand, a regression between both ripening indicators showed a coefficient of determination (R^2) of 0.67 between both, indicating a correlation between both parameters.

Table 1. Statistics (range, mean, and standard deviation (SD)) of the grape dataset related to SSC and TA.

	Range	Mean	SD
SSC (°Brix)	10.4–19	16.1	1.87
TA (g/L Chlorohydric acid)	2.7–10.9	5.1	1.50

3.2. Spectral Signature of Samples

In order to detect clear differences in the spectral response of the grapes related to the target parameters, a visual inspection of the spectral responses of the samples situated in the limits of the histograms was undertaken. Figure 7 represents the reflectance response corresponding to approximately the 10th and above the 90th percentile of the histogram of the SSC (a) and TA (b). Similarity between the spectral responses related to both ripening indicators was most remarkable. However, this fact may be due to the correlation between both parameters during the ripening process ($R^2 = 0.67$). If we attend to the differences in the spectral response related to the levels of both parameters, an increment of reflectance can be observed in the samples with high levels of SSC and low levels of TA. These reflectance

peaks were especially noticeable between 410–680 nm and 860–940 nm, which includes the visible domain, and the further away bands of the red edge.

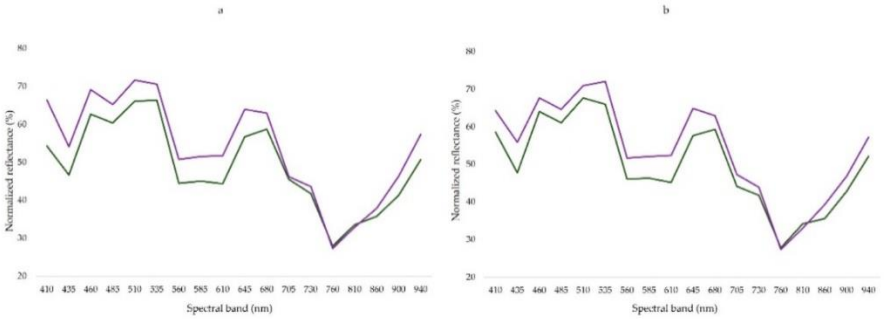

Figure 7. Mean reflectance responses of grape clusters with an advanced ripening state (purple) and an initial state (green) relating their levels of SSC (**a**) and TA (**b**). Each line includes the mean reflectance of eight samples (corresponding to approximately the 10th and above the 90th percentile, respectively, for each parameter).

3.3. Evaluation of the Performance of the Estimation Models

The performance of the ANN models was evaluated based on an LOOCV and a random-sampling (RS) test. Table 2 shows the statistics between the output of the ANN and the validation data excluded during training at every iteration in the case of LOOCV and the external validation set in the case of RS. The goodness-of-fit of the estimation models was similar for the two target parameters. This fact may be due to an inter-correlation between the two target parameters (R^2 = 0.67). In the LOOCV, the output of the ANN model showed a good relationship between the values of the target parameters determined by standard methods (SSC and TA), with coefficients of determination of 0.70 for SSC and 0.67 for TA (Figure 8). In this instance, the RMSE was 1.00 (Brix°) for the estimation of SSC, and 0.83 (g/L Chlorohydric acid) for TA. When normalising the RMSE value by the mean of the measurement (CVRMSE), it was found that the RMSE supposed a 6% respect to the mean for the estimation of the SSC and a 16% for the estimation of the TA. The above-mentioned metrics were supported by the *p*-value obtained in the paired samples *t*-test (p = 0.15 for SSC and p = 0.66 for TA).

Table 2. R^2, RMSE, CVRMSE, and p (p-value from paired samples *t*-test) between reference values of SSC and TA, measured by chemical methods, and those estimated based on ANN approaches during the LOOCV and random sampling.

	LOOCV				Random Sampling			
	R^2	**RMSE**	**CVRMSE**	***p***	**R^2**	**RMSE**	**CVRMSE**	***p***
SSC (°Brix)	0.70	1.00	0.06	0.15	0.72	1.1	0.07	0.20
TA (g/L Chlorohydric acid)	0.67	0.83	0.16	0.66	0.74	0.84	0.17	0.53

On the other hand, the RS displayed better performance in terms of coefficients of determination (R^2 = 0.72 for SSC and R^2 = 0.74 for TA). However, the RMSE slightly increased (RMSE = 1.1 for SSC and RMSE = 0.84), being 7% with respect to the mean in the case of SSC and 17% in the case of TA. Again, the *p*-values obtained in the paired samples *t*-test (p = 0.20 for SSC, and p = 0.53 for TA) were over the significance limit (p = 0.05) in both cases.

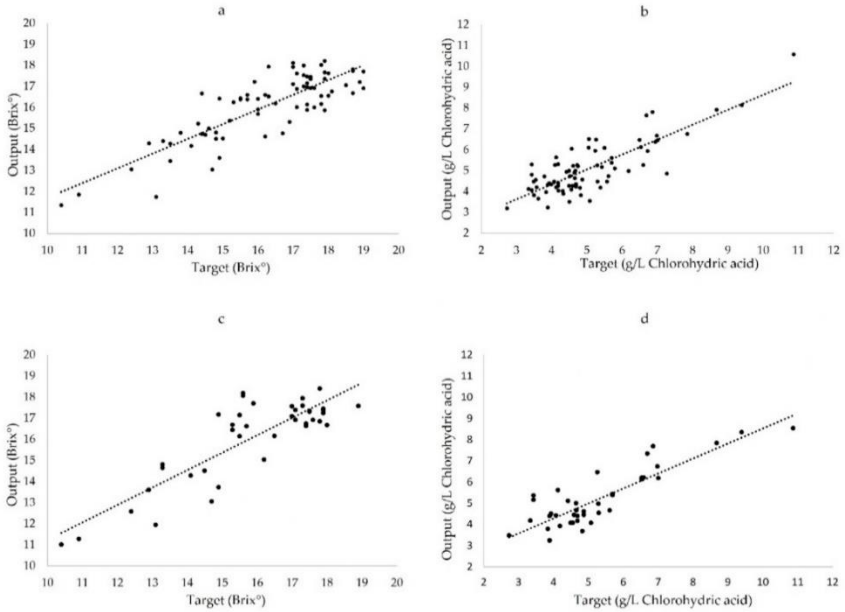

Figure 8. Output of the ANN models versus the validation data excluded during training at every iteration of the LOOCV (SSC (**a**) and TA (**b**)) and random sampling (SSC (**c**) and TA (**d**)).

4. Discussion

This work presents a custom-built, low-cost multispectral device specially designed for fruit-quality assessment under field conditions. In order to evaluate the suitability of the proposed device, an experiment aimed to estimate quality indicators of red grapes was performed. The selected target-quality indicators were the solid soluble content (SSC) and the titratable acidity (TA). The experiment consisted of a sample collection in a red-grape vineyard. The proposed multispectral sensor was used to collect the spectral signature of the samples under field conditions. Subsequently, the samples were packed in zip bags, tagged, and carried to the laboratory, where they were processed through destructive chemical methods to obtain ground-truth values of the target quality indicators. Finally, these quality indicators were used as a target to train artificial neural network (ANN) models using the corrected reflectance of the eighteen spectral bands captured by the sensor as inputs.

Prior to the model generation, a visual inspection of the spectral fingerprint of the samples was carried out to detect evidence of the correlation between the target parameters and the spectral signatures of the samples (Section 3.2). This previous analysis was based on the samples at the 10th and the 90th percentiles of the SSC and TA histograms. At first sight, the similarity of the spectral signature related to both ripening indicators stood out. This fact may be due to the correlation between both parameters (R^2 = 0.67). This correlation is due to the fact that grape maturation leads to an increase in SSC levels as the TA level decreases [23]. On the other hand, the analysis related to the influence of the levels of both parameters on the spectral signature of the samples showed overtones between 410–680 nm and 860–940 nm in the samples with high levels of SSC and low TA with respect to the samples with low SSC and high TA. The spectral range between 410–680 nm encompasses the visible domain (VIS), so the overtones in these wavelengths may be due to a correlation between the colouration changes of the grapes during ripening (the accumulation of red pigments—carotenoids and anthocyanins,—and chlorophyll a and b) and the levels of both parameters [2]. Furthermore, the spectral range between 860–940 nm covers a part of the NIR domain, which is associated with the first and second overtones of O–H stretching [10]. Therefore, the overtones observed in that spectral region may be due to variations in the

water content of the samples, which is related to the values of the target parameter. In addition, it is expected that sugars absorb at the spectral range between 740–984 nm [24]. These facts may explain the effect of the SSC and TA on the spectral signal of the samples identified in the previous visual inspection (Section 3.2). Machine learning methods—and concretely, ANN—have the capability to capture non-linear relationships between related parameters without explicitly knowing the underlying data distribution. The use of an ANNs makes having a precise knowledge about how spectral information and the target parameters are related unnecessary. So, although the reflectance signal of the samples in the spectral bands between 705 - 810 nm seemed to be less affected by the target parameters, they were finally considered in the estimation models as their exclusion did not improve the model's performance. Therefore, the corrected reflectance in the eighteen bands acquired by the sensors were used to train two ANN models aimed at estimating the SSC and the TA of the grapes. A leave-one-out cross-validation (LOOCV) algorithm was used as a validation method. This method uses a single observation from the original sample as the validation data and uses the remaining observations as training data. This is repeated for the entire dataset. After applying an LOOCV, the whole dataset participates in both training and validation. Thus, LOOCV avoids the uncertainty arising from the random division of the dataset into training and external validation (test) subgroups. As there is no random disaggregation of the data, the LOOCV results are fully reproducible. For this reason, LOOCV was considered the most suitable validation method for this research, especially considering that the limited volume of the dataset (n = 80) allowed for the use of a processing-intensive methodology such as LOOCV. As an alternative to the LOOCV, a random-sampling test was applied in order to confirm the performance observed in the LOOCV.

The obtained results were promising. In the case of the SSC, the LOOCV showed a good performance of the ANN model with a coefficient of determination (R^2) between the estimated and the actual values of the SSC of 0.70, and a root–mean–square error (RMSE) of 1.00, which supposed the 6% of the mean value of the measurement (CVRMSE = 0.06). These metrics indicated a good predictive potential and were supported by the *p*-value obtained in the paired samples t-test ($p = 0.15$), which was higher than the significance limit ($p = 0.05$). This argues for the similarity between the means of the measures obtained by the proposed device and those achieved with the digital refractometer. On the other hand, the ANN model aimed at estimating the grapes' TA displayed a similar performance, yielding an R^2 value of 0.67, and an RMSE of 0.83, which supposed the 16% of the mean value of the measurement (CVRMSE = 0.16). In this case, the CVRMSE value indicated a lower predictive potential than what was obtained for the SSC. However, the results were also supported by the *p*-value obtained in the paired samples t-test ($p = 0.66$), which was also above than the significance limit. This indicated that there were no significant differences between the measures determined with the proposed device and those obtained through titration. The trends observed in the LOOCV were confirmed by the results obtained in the external validation of the random-sampling test for the SSC ($R^2 = 0.72$; RMSE = 1.10; CVRMSE = 0.07; $p = 0.20$) and TA estimation ($R^2 = 0.74$; RMSE = 0.84; CVRMSE = 0.17; $p = 0.53$). The few differences observed between the two validation methods are owed to the random division of the data set during the RS test.

In recent decades, there have been numerous studies concerning the characterization of horticultural products through machine-vision methods [3]. Concretely, the ripeness estimation in the viticulture sector has been widely studied, with works centred in different machine-vision techniques and ripening indicators [27,28]. In this sense, there have been numerous publications focused on the use of RGB images for estimating the ripening status of grapes, even under field conditions [29,30]. RGB colour imaging is a cost-effective way to determine colour channel values. In RGB colour imaging, however, only three visible bands are available, resulting in limited chemical composition identification capability. For this reason, most publications on the topic of RGB colour imaging for ripening-status assessment have been centred in classification models using subjective ripening indicators

as reference, such as visual assessment [31,32]. Because these works used classification models with different performance criteria than were used in this research, it makes no sense to do an actual comparison. On the other hand, spectral sensors can record numerous bands across a wide spectral band. Further, spectroscopic features may better correlate with maturity since they are extracted from the absorption bands that are related to chemical attributes. Therefore, spectroscopy-based works rely on estimation models aimed at determining objective ripening indicators. In this sense, there are numerous works concerning the monitorization of grape-ripening using different spectroscopy-based techniques (VIS-NIR spectroscopy, hyperspectral imaging, multispectral imaging, etc.), and target parameters (SSC, TA, pH, flavonoids, anthocyanins, etc.). However, most of these works have been accomplished under laboratory conditions [24,33–37], where ambient light can be reasonably controlled by using a housing over the spectral system. This fact assumes an ease of use in contrast to spectrometers intended for in-vineyard use, such as the device proposed in this work. The shift of grape-composition measurements from the laboratory to the vineyard has become possible due to the advent of portable sensors and the rapid development of machine learning algorithms. An example of such an application is the work by Fernández-Novales et al. [38], who used a VIS–NIR hyperspectral camera (Resonon, Bozeman, MA, USA) (300 bans from 400 to 1000 nm) mounted on an all-terrain vehicle to acquire hyperspectral images from which to estimate the SSC and TA of grapes (along with other ripening parameters) using partial least squares regression (PLSR) models. They reported good correlations between the estimated and the measured values for the prediction of an external test set (SSC (R^2 = 0.82, RMSE = 1.21), TA (R^2 = 0.81, RMSE = 1.08)). Similarly, Guidetti et al. [39] used an experimental Vis/NIR spectrophotometer (AvaSpec-2048, Avantes, Eerbeek, The Netherlands) (450–980 nm) for estimating the SSC and TA of red grapes. They also used PLRS models for training and for external validation, obtaining an R^2 value of 0.67 and an RMSE of 1.48 for SSC, and an R^2 value of 0.66 and an RMSE of 1.48 for TA. On the other hand, Urraca et al. [40] used a portable NIR spectrophotometer (microPHAZIR™; Thermo Fisher Scientific, Waltham, MA, USA) (100 bands from 1595.7 to 2396.3 nm) for estimating the SSC of grapes under field conditions. They used a PLSR model as the retrieval method, which reported a 10-fold cross-validation R^2 up to 0.90 (with an RMSE of 1.47 Brix). The results obtained in the present work are comparable to those reported in the mentioned research. However, it is important to take into account that these works were performed using hyperspectral systems that offer a very high spectral resolution, which are capable of catching multiple narrow-spectral bands. This enables the acquisition of a more detailed spectral signature. Therefore, the acquired spectral footprint of the target chemical parameter is more descriptive than what is obtained with multispectral devices using more expensive equipment. Furthermore, the NIR spectrophotometer used by Urraca et al. [40] covers the NIR domain with frequencies away from the red edge. In this region, several frequencies related to the SSC have been reported (1450, 1690, 1750, 1950, and 2260 nm (glucose)) [27]. However, the good correlation between the estimated and reference values of the SSC and TA founded in this work indicate that the spectral range considered is descriptive enough. This good performance may be due to the high flexibility of the ANN models, which adjust effectively in the feature space, as they enable the non-linearity of data to be modelled using local or specific equations. The aforementioned works used PLSR models to reduce the large amount of collinear spectral variables (offered by hyperspectral sensors) to non-correlated principal components by using data compression. On the other hand, it is important to take into account that the chemical analysis of grapes requires several berries per single sample (fifty berries per sample in this research). This implies that the sample unit must be comprised of the whole cluster. Thus, the variability concerning the ripening state in the berries of a cluster can constitute a source of error against studies focused on larger-size fruits. It is therefore possible to expect a better performance of the proposed device by evaluating such a type of fruit.

The results obtained in the present research take on a greater importance considering the price gap between the devices used in the previously mentioned research and the equipment proposed in this work. The performance showed by the proposed device, in addition to its price and the possibility to acquire measurement under field conditions, evince it as a promising and affordable solution to monitor grape-ripening status. The cost reduction achieved in the proposed design was possible due to the modernization of the electronics industry in recent decades. Improved hardware technology has provided sensors that deliver high performance at a reasonable price. Furthermore, innovative software designs offer algorithms that enhance the capacity to correlate the intricate relations that exist between spectral signatures and fruit biophysical parameters. This work, therefore, contributes to the trend toward the development of cheaper technologies with applications in precision agriculture [10,15,16].

5. Conclusions

This work presents the evaluation of a low-cost, multispectral sensor for grape-ripening-status assessment under field conditions. The performance achieved by the ANN models, fed with the spectral data acquired with the proposed device, shows a promising potential for the monitoring of grape ripening under field conditions. In-field monitoring, in addition to its price and ease of use, paves the way for the implementation of a fruit-ripening appraisal system that is affordable for all kinds of growers. The implementation of this technology in the vineyard would reduce laborious sampling and extensive chemical analysis for many workers. Furthermore, it would improve the spatiotemporal resolution in the monitorization, as it would increase both the number of sample points considered in each trial and the number of samples taken during the campaign. Moreover, the low cost of the sensor itself allows it to be integrated into wireless sensor networks or robotic devices. Regarding grapes, this device would enable the mapping of quality variability across the vineyard. It would therefore create opportunities to either exploit those variations to craft different wine styles or to apply precision viticultural techniques to optimize inputs and minimise variability. All of these factors would result in an increase in the expected market price of the wine produced. On the other hand, improving the accessibility of non-destructive and rapid technologies would improve the understanding of fruit maturation and how agronomic factors influence it.

The results obtained in the present work will encourage further work to expand this experimental setup to other grape varieties and other kinds of fruits.

Author Contributions: Conceptualization, M.N., B.M., and J.M.A.; data curation, M.N. and B.M.; formal analysis, M.N.; investigation, M.N.; methodology, M.N., B.M., and J.M.A.; project administration, B.M.; resources, B.M.; software, B.M.; supervision, B.M. and J.M.A.; validation, M.N.; visualization, B.M.; writing—original draft, M.N. and B.M.; writing—review & editing, J.M.A. All authors have read and agreed to the published version of the manuscript.

Funding: This work was supported by grant PID2020-119217RA-I00, funded by MCIN/AEI/10.13039/501100011033; grant IJC2019-040114-I, funded by MCIN/AEI/10.13039/501100011033; and grant 0766_OLIVAIS_5_E, funded by the Interreg Cooperation Program V-A SPAIN-PORTUGAL (POCTEP) 2014-2020, and co-financed with ERDF.

Institutional Review Board Statement: Not applicable.

Informed Consent Statement: Not applicable.

Data Availability Statement: The data presented in this study are available upon request from the corresponding author.

Acknowledgments: The authors acknowledge Bodegas Contreras Ruiz, S.L, for providing the experimental vineyard in which the study was conducted as well as the technical support. The authors also acknowledge Kimoto LDT for suppling the material used for making the light-diffuser film and the "Cátedra del Vino" from the University of Huelva for their support regarding chemical analysis.

Conflicts of Interest: The authors declare no conflict of interest. The funders had no role in the design of the study; in the collection, analyses, or interpretation of data; in the writing of the manuscript, or in the decision to publish the results.

References

1. López, M.I.; Sánchez, M.T.; Díaz, A.; Ramírez, P.; Morales, J. Influence of a deficit irrigation regime during ripening on berry composition in grapevines (*Vitis vinifera* L.) grown in semi-arid areas. *Int. J. Food Sci. Nutr.* **2007**, *58*, 491–507. [CrossRef] [PubMed]
2. Vanoli, M.; Buccheri, M. Overview of the methods for assessing harvest maturity. *Stewart Postharvest Rev.* **2012**, *8*, 1–11. [CrossRef]
3. Cattaneo, T.M.P.; Stellari, A. Review: NIR Spectroscopy as a Suitable Tool for the Investigation of the Horticultural Field. *Agronomy* **2019**, *9*, 503. [CrossRef]
4. Lu, R.; Van Beers, R.; Saeys, W.; Li, C.; Cen, H. Measurement of optical properties of fruits and vegetables: A review. *Postharvest Biol. Technol.* **2020**, *159*, 111003. [CrossRef]
5. Nicolaï, B.M.; Beullens, K.; Bobelyn, E.; Peirs, A.; Saeys, W.; Theron, K.I.; Lammertyn, J. Nondestructive measurement of fruit and vegetable quality by means of NIR spectroscopy: A review. *Postharvest Biol. Technol.* **2007**, *46*, 99–118. [CrossRef]
6. Comino, F.; Ayora-Cañada, M.J.; Aranda, V.; Díaz, A.; Domínguez-Vidal, A. Near-infrared spectroscopy and X-ray fluorescence data fusion for olive leaf analysis and crop nutritional status determination. *Talanta* **2018**, *188*, 676–684. [CrossRef] [PubMed]
7. Guzmán, E.; Baeten, V.; Pierna, J.A.F.; García-Mesa, J.A. A portable Raman sensor for the rapid discrimination of olives according to fruit quality. *Talanta* **2012**, *93*, 94–98. [CrossRef]
8. Noguera, M.; Aquino, A.; Ponce, J.M.; Cordeiro, A.; Silvestre, J.; Arias-Calderón, R.; da Marcelo, M.E.; Jordão, P.; Andújar, J.M. Nutritional status assessment of olive crops by means of the analysis and modelling of multispectral images taken with UAVs. *Biosyst. Eng.* **2021**, *211*, 1–18. [CrossRef]
9. Wang, Y.J.; Jin, G.; Li, L.Q.; Liu, Y.; Kianpoor Kalkhajeh, Y.; Ning, J.M.; Zhang, Z.Z. NIR hyperspectral imaging coupled with chemometrics for nondestructive assessment of phosphorus and potassium contents in tea leaves. *Infrared Phys. Technol.* **2020**, *108*, 103365. [CrossRef]
10. Walsh, K.B.; Blasco, J.; Zude-Sasse, M.; Sun, X. Visible-NIR 'point' spectroscopy in postharvest fruit and vegetable assessment: The science behind three decades of commercial use. *Postharvest Biol. Technol.* **2020**, *168*, 111246. [CrossRef]
11. Li, B.; Lecourt, J.; Bishop, G. Advances in Non-Destructive Early Assessment of Fruit Ripeness towards Defining Optimal Time of Harvest and Yield Prediction—A Review. *Plants* **2018**, *7*, 3. [CrossRef] [PubMed]
12. Walsh, K.B.; McGlone, V.A.; Han, D.H. The uses of near infra-red spectroscopy in postharvest decision support: A review. *Postharvest Biol. Technol.* **2020**, *163*, 111139. [CrossRef]
13. Millan, B.; Velasco-Forero, S.; Aquino, A.; Tardaguila, J. On-the-go grapevine yield estimation using image analysis and boolean model. *J. Sensors* **2018**, *2018*, 14. [CrossRef]
14. Diago, M.P.; Aquino, A.; Millan, B.; Palacios, F.; Tardaguila, J. On-the-go assessment of vineyard canopy porosity, bunch and leaf exposure by image analysis. *Aust. J. Grape Wine Res.* **2019**, *25*, 363–374. [CrossRef]
15. Bec, K.B.; Grabska, J.; Huck, C.W. Miniaturized NIR Spectroscopy in Food Analysis and Quality Control: Promises, Challenges, and Perspectives. *Foods* **2022**, *11*, 1465. [CrossRef]
16. Krause, J.; Grüger, H.; Gebauer, L.; Zheng, X.; Knobbe, J.; Pügner, T.; Kicherer, A.; Gruna, R.; Längle, T.; Beyerer, J. SmartSpectrometer—Embedded Optical Spectroscopy for Applications in Agriculture and Industry. *Sensors* **2021**, *21*, 4476. [CrossRef]
17. Noguera, M.; Millan, B.; Aquino, A.; Andujar, J.M. Methodology for Olive Fruit Quality Assessment by Means of a Low-Cost Multispectral Device. *Agronomy* **2022**, *12*, 979. [CrossRef]
18. Moinard, S.; Brunel, G.; Ducanchez, A.; Crestey, T.; Rousseau, J.; Tisseyre, B. Testing the potential of a new low-cost multispectral sensor for decision support in agriculture. *Precis. Agric.* **2021**, *21*, 411–418. [CrossRef]
19. Zhang, M.; Shen, M.; Pu, Y.; Li, H.; Zhang, B.; Zhang, Z.; Ren, X.; Zhao, J. Rapid Identification of Apple Maturity Based on Multispectral Sensor Combined with Spectral Shape Features. *Horticulturae* **2022**, *8*, 361. [CrossRef]
20. Leon-salas, W.D.; Rajendran, J.; Vizcardo, M.A.; Postigo-malaga, M. Measuring Photosynthetically Active Radiation with a Multi-Channel Integrated Spectral Sensor. In Proceedings of the 2021 IEEE International Symposium on Circuits and Systems (ISCAS), Daegu, Republic of Korea, 23–26 May 2021; IEEE Xplore: Piscataway, NJ, USA, 2021; pp. 1–5.
21. Trang, N.M.; Duy, T.K.; Huyen, T.T.N.; Danh, L.V.Q.; Dinh, A. An investigation into the use of a low-Cost NIR integrated circuit spectrometer to measure chlorophyll content index. *Int. J. Innov. Technol. Explor. Eng.* **2019**, *8*, 35–38.
22. Li, M.; Qian, Z.; Shi, B.; Medlicott, J.; East, A. Evaluating the performance of a consumer scale SCiO^{TM} molecular sensor to predict quality of horticultural products. *Postharvest Biol. Technol.* **2018**, *145*, 183–192. [CrossRef]
23. de Toda Fernández, M. *Claves de la Viticultura de Calidad: Nuevas Técnicas de Estimación y Control de la Calidad de la Uva en el Viñedo*, 2nd ed.; Ediciones Mundi-Prensa: Madrid, Spain, 2011; ISBN 9788484764229.
24. Gomes, V.M.; Fernandes, A.M.; Faia, A.; Melo-Pinto, P. Comparison of different approaches for the prediction of sugar content in new vintages of whole Port wine grape berries using hyperspectral imaging. *Comput. Electron. Agric.* **2017**, *140*, 244–254. [CrossRef]
25. International Organisation of Vine and Wine. *Compendium of International Methods of Wine and Must Analysis*, 2020th ed.; International Organisation of Vine and Wine: Paris, France, 2020; ISBN 9782850380167.

26. Demšar, J.; Erjavec, A.; Hočevar, T.; Milutinovič, M.; Možina, M.; Toplak, M.; Umek, L.; Zbontar, J.; Zupan, B. Orange: Data Mining Toolbox in Python. *J. Mach. Learn. Res.* **2013**, *14*, 2349–2353.
27. Vrochidou, E.; Bazinas, C.; Manios, M.; Papakostas, G.A.; Pachidis, T.P.; Kaburlasos, V.G. Machine Vision for Ripeness Estimation in Viticulture Automation. *Horticulturae* **2021**, *7*, 282. [CrossRef]
28. Dambergs, R.; Gishen, M.; Cozzolino, D. A Review of the State of the Art, Limitations, and Perspectives of Infrared Spectroscopy for the Analysis of Wine Grapes, Must, and Grapevine Tissue. *Appl. Spectrosc. Rev.* **2014**, *50*, 261–278. [CrossRef]
29. Nuske, S.; Nuske, S. Automated Assessment and Mapping of Grape Quality through Image-cased Color Analysis. *IFAC-PapersOnLine* **2016**, *49*, 72–78. [CrossRef]
30. Rahman, A.; Hellicar, A. Identification of Mature Grape Bunches using Image Processing and Computational Intelligence Methods. In Proceedings of the 2014 IEEE Symposium on Computational Intelligence for Multimedia, Signal and Vision Processing (CIMSIVP), Orlando, FL, USA, 9–12 December 2014; IEEE Xplore: Piscataway, NJ, USA, 2014; pp. 1–6.
31. Cavallo, D.P.; Cefola, M.; Pace, B.; Logrieco, A.F.; Attolico, G. Non-destructive and contactless quality evaluation of table grapes by a computer vision system. *Comput. Electron. Agric.* **2019**, *156*, 558–564. [CrossRef]
32. Kangune, K.; Kulkarni, V.; Kosamkar, P. Grapes Ripeness Estimation using Convolutional Neural network and Support Vector Machine. In Proceedings of the 2019 Global Conference for Advancement in Technology (GCAT), Bangalroe, India, 18–20 October 2019; IEEE Xplore: Piscataway, NJ, USA, 2019; pp. 1–5.
33. Baiano, A.; Terracone, C.; Peri, G.; Romaniello, R. Application of hyperspectral imaging for prediction of physico-chemical and sensory characteristics of table grapes. *Comput. Electron. Agric.* **2012**, *87*, 142–151. [CrossRef]
34. Fernandes, A.M.; Franco, C.; Mendes-Ferreira, A.; Mendes-Faia, A.; da Costa, P.L.; Melo-Pinto, P. Brix, pH and anthocyanin content determination in whole Port wine grape berries by hyperspectral imaging and neural networks. *Comput. Electron. Agric.* **2015**, *115*, 88–96. [CrossRef]
35. Gabrielli, M.; Lançon-Verdier, V.; Picouet, P.; Maury, C. Hyperspectral Imaging to Characterize Table Grapes. *Chemosensors* **2021**, *9*, 71. [CrossRef]
36. Piazzolla, F.; Amodio, M.L.; Colelli, G. Spectra evolution over on-vine holding of Italia table grapes: Prediction of maturity and discrimination for harvest times using a Vis-NIR hyperspectral device. *J. Agric. Eng.* **2017**, *48*, 109–116. [CrossRef]
37. Fernández-Novales, J.; López, M.-I.; Sánchez, M.-T.; García-Mesa, J.-A.; González-Caballero, V. Assessment of quality parameters in grapes during ripening using a miniature fiber-optic near-infrared spectrometer. *Int. J. Food Sci. Nutr.* **2009**, *60*, 265–277. [CrossRef] [PubMed]
38. Fernández-Novales, J.; Barrio, I.; Diago, M.P. Non-invasive monitoring of berry ripening using on-the-go hyperspectral imaging in the vineyard. *Agronomy* **2021**, *11*, 2534. [CrossRef]
39. Guidetti, R.; Beghi, R.; Bodria, L. Evaluation of Grape Quality Parameters by a Simple Vis/NIR System. *Am. Soc. Agric. Biol. Eng.* **2010**, *53*, 477–484. [CrossRef]
40. Urraca, R.; Sanz-Garcia, A.; Tardaguila, J.; Diago, M.P. Estimation of total soluble solids in grape berries using a hand-held NIR spectrometer under field conditions. *J. Sci. Food Agric.* **2016**, *96*, 3007–3016. [CrossRef]

5. Discussion

The most relevant findings derived from the investigation conducted on the diverse topics addressed in this Thesis are summarized below. For a more extended discussion of the results obtained in the different parts of the research, the reader is encouraged to consult the respective documents, compiled in section 4.

The evaluation of the developed device, based on a thermal IR sensor, to assess the water status of olive trees yielded promising results. The comparison of the device's performance against a commercially available thermal camera showed similar accuracy, despite the considerable price gap between the two devices. Once validated for accuracy, the developed device was tested in a field experiment aimed at assessing the water status of olive trees in a Super High-Density (SHD) olive orchard. The high correlation between the information inferred from the sensor (canopy temperature and the calculated crop water stress index (CWSI)) and two standardized water stress indicators (predawn leaf water potential (Ψ_{PD}) and stomatal conductance (g_s)) indicates the suitability of the proposed system for accomplishing this characterization. It is pertinent to highlight that the proposed methodology for determining the temperature thresholds needed to calculate the CWSI avoids the need for using reference surfaces or acquiring meteorological data. Instead, these thresholds are estimated from the temperature distribution histogram of the complete set of thermal images, which offers an operational advantage. Similar approaches had previously been tested in other crops [86,87]. However, to the best of our knowledge, this research represents the first attempt to apply this approach with olive crops. Although future research is required to expand this experimental setup to additional environmental conditions, the low-cost of the developed device, coupled with its ease of use (it does not need to be operated by expert personnel), labour cost savings, and high precision, paves the way for implementing an olive orchard water status appraisal system. The possibility of monitoring the water status of olive trees with high spatial and temporal resolution increases the potential to develop more efficient irrigation programs. This is particularly significant for olive crops, since olive quality/yield can benefit from exposure to water stress at specific stages of their vegetative cycle [30].

The research conducted to develop a methodology for assessing the nutritional status of olive trees using multispectral images captured by a UAV also produced promising results. One of the main drawbacks of acquiring reflectance data from an aerial perspective is the contamination of information related to the crop canopy with noise from the background (soil, ground vegetation, etc.). To address this issue, a new image processing approach was developed, enabling the integration of all spectral images acquired during the flights into single orthomosaics. This approach eliminates background information, allowing the extraction of reflectance data from discrete points. By optimizing and simplifying the phase of the process related to the acquisition of reflectance data, this approach enhances the quality of the input data provided to the estimation models and consequently improves their performance. In relation to the

phase of the research aimed at developing estimation models, several retrieval techniques (PLSR, ANN, SVR, and GPR) were evaluated. The results obtained demonstrate the effectiveness of the proposed image processing approach and indicate that the Artificial Neural Network (ANN) was the most suitable retrieval technique among those evaluated under these experimental conditions. Although the results were promising, further work is needed to expand the experimental setup to different environmental conditions, olive varieties, and plant vegetative stages. Nevertheless, the higher spatial and temporal resolution compared to current methods paves the way for implementing an olive orchard nutrient status appraisal system. These technical improvements could open new avenues in sustainable oliviculture, facilitating the deployment of solutions for the automatic and continuous evaluation of fertilizer needs. This, in turn, would enable the design of more precise and efficient fertigation programs.

The third objective of this Thesis was focused on developing an affordable device for assessing the quality parameters of olive fruits. For this purpose, preliminary research was conducted to evaluate the potential of a commercial multispectral development board integrated into an initial prototype under controlled laboratory conditions. The 18 reflectance measurements acquired by the developed device were used as inputs to train ANN models, using reference values of moisture, acidity, and fat content of olive fruits as outputs. The best results were obtained for the estimation of moisture and acidity; however, the performance of the estimation of fat content was also promising. These results encouraged a second phase of the research aimed at developing a handheld device adapted for use in field conditions. This second prototype was evaluated in a field experiment. ANN models were trained using the spectral data acquired on the field as inputs and the results of chemical analysis as target. In this case, the results related to the estimation of fat content, in its both variants (oil content per dry matter (OCDM) and oil content per fresh weight (OCFW)), and moisture (M) were even better than the ones obtained in the previous research, showing a high potential even for practical applications. However, the results related to the estimation of acidity (TA) did not improve upon the previously obtained ones. The disparities between the results obtained in both investigations may be due to the variations related to the devices and the experimental conditions. Regardless, the results in the estimation of OCFW, OCDM, and M showed the suitability of the developed device for the quality assessment of olive fruits, even in field conditions. Furthermore, the fact that this experiment covered two consecutive campaigns enhance the reliability of the obtained results. These results pave the way for the implementation of an olive ripening appraisal system that is affordable for all types of growers. The higher spatial-temporal resolution in the monitoring, compared to the traditional chemical methods, would offer more accurate and complete view of the ripening process of olive fruits to the crop manager. This would enable growers to employ precision farming techniques to address anomalous situations affecting ripening at discrete locations within the crops. Additionally, it would facilitate the adjustment of harvest timing to the variability regarding maturation pace in the field, enabling diversification of production to obtain fruit with specific characteristics. Such

an approach would provide the olive sector with enhanced resources to develop olive oils with greater added value.

On the other hand, the promising results obtained in the complementary research aimed at using the developed device to assess quality indicators of grape berries indicates the potential of this system in other crops besides olives.

One of the main milestones of this Thesis was to ensure the accessibility of the developed solutions to the growers. The low-cost and compact size of the sensors used in this Thesis enable their integration into wireless sensor networks or robotic devices, presenting high potential for data acquisition logistics. Furthermore, ensuring the accessibility of precision farming technologies in terms of ease of use and price is crucial to ensure their standardization. The standardized use of such monitoring technologies, with enhanced spatial-temporal resolution compared to traditional resources, will facilitate the expansion of knowledge on how biotic and abiotic factors affect crop development. This, in turn, will enable the improvement of traditional management strategies, resulting in more productive and sustainable crops.

6. Conclusions

The present Thesis has demonstrated the utility of low-cost spectral sensors in assessing olive crop parameters crucial for supporting management decisions in the scope of precision oliviculture. Broadly, the objectives set in this thesis can be categorized into technologies for supporting irrigation, fertilization, and fruit quality assessment in the context of olive cultivation. The main conclusions derived from the investigation conducted to achieve each of these objectives are summarized below.

6.1. Objective 1. Development and evaluation of a low-cost device based on a thermal infrared sensor to assess water status of olive trees.

- The accuracy of the developed thermal IR device is comparable to that of a commercially available thermal camera.
- The developed thermal IR device has demonstrated its ability to provide a useful estimation of the water status of olive trees.
- Canopy temperature measured at 10 AM on the sunlit side showed a higher correlation with water stress variables.
- The proposed methodology for calculating the crop water stress index has proven to be suitable and offers operational advantages compared to existing methods in the literature.

6.2. Objective 2. Development of a methodology to assess the nutritional status of olive trees based on the analysis and modelling of multispectral images taken with an UAV.

- The spectral data acquired from an aerial perspective has demonstrated providing useful information regarding the nutritional status of olive trees.
- The proposed image processing method enhances the quality of the acquired spectral data, which is crucial to ensure the accuracy of the method.
- The artificial neural network has proven to be the most suitable method among the different retrieval methods evaluated for modelling nutritional status parameters using spectral data.

6.3. Objective 3.1. Evaluation of the capabilities of a low-cost multispectral sensor for assessing quality parameters of intact olive fruits under laboratory conditions.

- The developed multispectral system has demonstrated its ability to provide useful information on the quality parameters of intact olive fruits under laboratory conditions.
- The estimation of olive fruit quality parameters using spectral data has been successfully applied to different olive varieties.

6.4. Objective 3.2. Development and evaluation of a low-cost multispectral device for assessing quality parameters of intact olive fruits under field conditions.

- The performance of the developed handheld multispectral device is unaffected by the levels of environmental radiation, indicating its suitability for in-field operation.

- The developed handheld multispectral device has demonstrated its ability to provide useful information on the quality parameters of olive fruits under field conditions.
- The results obtained in the complementary research focused on the assessment of quality parameters of grape berries suggest the applicability of the device in crops beyond olives.

6.5. Global conclusion.

The research conducted to achieve the objectives set in this Thesis has demonstrated the suitability of low-cost solutions for precision oliviculture. The constrained costs and user-friendly nature of the solutions proposed in this Thesis make them affordable for olive farms of all scales. This is a key factor for standardizing management strategies based on the precision oliviculture paradigm. The widespread adoption of such management strategies would reduce the costs and environmental impact of olive crops while enhancing fruit quality. All these factors would contribute to increased profitability and sustainability in the olive sector.

7. Conclusiones

La presente Tesis ha demostrado la utilidad de los sensores espectrales de bajo costo para evaluar parámetros del cultivo del olivo cruciales para respaldar la toma de decisiones en el contexto de la olivicultura de precisión. En términos generales, los objetivos establecidos en esta Tesis se pueden categorizar en tecnologías para apoyar el riego, la fertilización y la evaluación de la calidad del fruto en el contexto del cultivo del olivo. A continuación, se resumen las principales conclusiones derivadas de la investigación realizada para lograr cada uno de estos objetivos.

7.1. Objetivo 1. Desarrollo y evaluación de un dispositivo de bajo costo basado en un sensor infrarrojo térmico para evaluar el estado hídrico de los olivos

- La precisión del dispositivo IR térmico desarrollado es comparable a la de una cámara térmica disponible comercialmente.
- El dispositivo IR térmico desarrollado ha demostrado su habilidad para proveer una estimación útil del estado hídrico de olivos.
- La temperatura del dosel medida a las 10 AM en la cara soleada demostró una mayor correlación con las variables de estrés hídrico.
- La metodología propuesta para calcular el índice de estrés hídrico de los cultivos ha demostrado ser adecuada y ofrece ventajas operativas en comparación con los métodos existentes en la bibliografía.

7.2. Objetivo 2. Desarrollo de una metodología para evaluar el estado nutricional de los olivos basada en el análisis y modelización de imágenes multiespectrales tomadas con un UAV.

- Los datos espectrales adquiridos desde una perspectiva aérea han demostrado proporcionar información útil sobre el estado nutricional de los olivos.
- El método de tratamiento de imágenes propuesto mejora la calidad de los datos espectrales adquiridos, lo que es crucial para garantizar la precisión del método.
- La red neuronal artificial ha demostrado ser el método más adecuado para modelizar los parámetros del estado nutricional a partir de datos espectrales, entre los diferentes métodos de recuperación evaluados.

7.3. Objetivo 3.1. Evaluación de las capacidades de un sensor multiespectral de bajo coste para evaluar parámetros de calidad de aceitunas intactas en condiciones de laboratorio.

- El sistema multiespectral desarrollado ha demostrado su capacidad para proporcionar información útil sobre parámetros de calidad de aceitunas intactas en condiciones de laboratorio.
- La estimación de parámetros de calidad aceitunas intactas mediante datos espectrales se ha aplicado con éxito a distintas variedades de olivo.

7.4. Objetivo 3.2. Desarrollo y evaluación de un dispositivo multiespectral de bajo coste para evaluar parámetros de calidad de aceitunas intactas en condiciones de campo.

- El rendimiento del dispositivo multiespectral portátil desarrollado no se ve afectado por los niveles de radiación ambiental, lo que indica su idoneidad para el funcionamiento sobre el terreno.
- El dispositivo multiespectral portátil desarrollado ha demostrado su capacidad para proporcionar información útil sobre parámetros de calidad de aceitunas en condiciones de campo.
- Los resultados obtenidos en la investigación complementaria centrada en la evaluación de parámetros de calidad de uvas sugieren la aplicabilidad del dispositivo en cultivos más allá del olivo.

7.5. Conclusión global.

La investigación realizada para alcanzar los objetivos fijados en esta Tesis ha demostrado la idoneidad de las soluciones de bajo coste para la olivicultura de precisión. Los costes limitados y la facilidad de uso de las soluciones propuestas en esta Tesis las hacen asequibles para explotaciones olivareras de todas las escalas. Este es un factor clave para la estandarización de las estrategias de gestión basadas en el paradigma de la olivicultura de precisión. La adopción generalizada de estas estrategias de gestión reduciría los costes y el impacto medioambiental de los cultivos de olivo, al tiempo que mejoraría la calidad del fruto. Todos estos factores contribuirían a aumentar la rentabilidad y la sostenibilidad del sector olivarero.

8. References

1. Zohary, D.; Hopf, M. *Domestication of plants in the Old World: the origin and spread of cultivated plants in West Asia, Europe and the Nile Valley.*; Zohary, D.; Hopf, M., Ed.; Ed. 3.; Oxford University Press: Oxford, 2000; ISBN 0198503.

2. Besnard, G.; Baradat, P.; Bervillé, A. Genetic relationships in the olive (Olea europaea L.) reflect multilocal selection of cultivars. *Theor. Appl. Genet.* **2001**, *102*, 251–258.

3. Amouretti, M.-C. La fabricación de aceite de oliva: una historia técnica original. *VVAA, Encicl. Mund. del Olivo, Barcelona, Plaza y Janés* **1996**, 26–29.

4. Infante-Amate, J. The Ecology and History of the Mediterranean Olive Grove: The Spanish Great Expansion, 1750 - 2000. *Rural Hist.* **2012**, *23*, 161–184.

5. Ghanbari, R.; Anwar, F.; Alkharfy, K.M.; Gilani, A.H.; Saari, N. Valuable Nutrients and Functional Bioactives in Different Parts of Olive (Olea europaea L.)—A Review. *Int. J. Mol. Sci. 2012, Vol. 13, Pages 3291-3340* **2012**, *13*, 3291–3340.

6. International Olive Council (IOC) Word Olive Oil Figures. Available online: https://www.internationaloliveoil.org/wp-content/uploads/2021/12/IOC-Olive-Oil-Dashboard-1.html#production-2 (accessed on Nov 17, 2023).

7. Struik, P.C.; Kuyper, T.W. Sustainable intensification in agriculture: the richer shade of green. A review. *Agron. Sustain. Dev.* **2017**, *37*, 1–15.

8. Lo Bianco, R.; Proietti, P.; Regni, L.; Caruso, T. Planting Systems for Modern Olive Growing: Strengths and Weaknesses. *Agric. 2021, Vol. 11, Page 494* **2021**, *11*, 494.

9. Fernández, J.-E.E. Understanding olive adaptation to abiotic stresses as a tool to increase crop performance. *Environ. Exp. Bot.* **2014**, *103*, 158–179.

10. Godini, A.; Bellomo, F. Olivicoltura superintensiva in Puglia per la raccolta meccanica con vendemmiatrice. In Proceedings of the International Congress of Oliveculture. Spoleto (Italy), April; 2002; pp. 22–23.

11. Lodolini, E.M.; Polverigiani, S.; Grossetti, D.; Neri, D. Pruning management in a high-density olive orchard. *Acta Hortic.* **2018**, *1199*, 385–390.

12. Connor, D.J.; Gómez-del-Campo, M.; Rousseaux, M.C.; Searles, P.S. Structure, management and productivity of hedgerow olive orchards: A review. *Sci. Hortic. (Amsterdam).* **2014**, *169*, 71–93.

13. Barranco Navero, Diego, Fernandez Escobar, Ricardo, Rallo Romero, L. *El cultivo del olivo*; Ricardo Fernandez Escobar, L.R.R.D.B.N., Ed.; 7ª ed.; Mundi-Prensa Libros: Madrid, 2017;

14. Bouhafa, K. Nitrogen Fertilization of Olive Orchards under Rainfed Mediterranean Conditions. *Am. J. Exp. Agric.* **2014**, *4*, 890–901.

15. Rosati, A.; Caporali, S.; Paoletti, A. Fertilization with N and K increases oil and water content in olive (Olea europaea L.) fruit via increased proportion of pulp. *Sci. Hortic. (Amsterdam).* **2015**, *192*, 381–386.

16. Fernández-Escobar, R. Use and abuse of nitrogen in olive fertilization. *Acta Hortic.* **2011**, *888*, 249–258.

17. Fernández-Escobar, R.; Beltrán, G.; Sánchez-Zamora, M.A.; García-Novelo, J.; Aguilera, M.P.; Uceda, M. Olive oil quality decreases with nitrogen over-fertilization. *HortScience* **2006**, *41*, 215–219.

18. Dag, A.; Ben-David, E.; Kerem, Z.; Ben-Gal, A.; Erel, R.; Basheer, L.; Yermiyahu, U. Olive oil composition as a function of nitrogen, phosphorus and potassium plant nutrition. *J. Sci. Food Agric.* **2009**, *89*, 1871–1878.

19. Savci, S. An Agricultural Pollutant: Chemical Fertilizer. *Int. J. Environ. Sci. Dev.* **2012**, *3*, 73–80.

20. Fernández, J.E.; Diaz-Espejo, A.; Romero, R.; Hernandez-Santana, V.; García, J.M.; Padilla-Díaz, C.M.; Cuevas, M. V. Precision Irrigation in Olive (Olea europaea L.) Tree Orchards. In *Water Scarcity and Sustainable Agriculture in Semiarid Environment*; Iván Francisco García Tejero, V.H.D.Z., Ed.; Elsevier Inc., 2018; pp. 179–217 ISBN 9780128131640.

21. Fernández, J.E.; Alvino, A.; Freire, M.I.; Ferreira, R. Plant-Based Methods for Irrigation Scheduling of Woody Crops. *Hortic. 2017, Vol. 3, Page 35* **2017**, *3*, 35.

22. Fernández, J.E. Plant-based sensing to monitor water stress: Applicability to commercial orchards. *Agric. Water Manag.* **2014**, *142*, 99–109.

23. Rallo, L.; Díez, C.M.; Morales-Sillero, A.; Miho, H.; Priego-Capote, F.; Rallo, P. Quality of olives: A focus on agricultural preharvest factors. *Sci. Hortic. (Amsterdam).* **2018**, *233*, 491–509.

24. International Organization of Standardization. ISO 660:2020. *Animal and vegetable fats and oils — Determination of acid value and acidity*; Switzerland, 2020;

25. Asociación Española de Normalización y Certificación. UNE 55030:1961. *Determination of the content in total fat of olives*; España., 1961;

26. Nordon, A.; McGill, C.A.; Littlejohn, D. Process NMR spectrometry. *Analyst* **2001**, *126*, 260–272.

27. International Organization of Standardization. ISO 662:2016. *Animal and vegetable fats and oils - Determination of moisture and volatile matter content*; España, 2016;

28. Haberman, A.; Dag, A.; Shtern, N.; Zipori, I.; Erel, R.; Ben-Gal, A.; Yermiyahu, U. Significance of proper nitrogen fertilization for olive productivity in intensive cultivation. *Sci. Hortic. (Amsterdam).* **2019**, *246*, 710–717.

29. Haberman, A.; Dag, A.; Shtern, N.; Zipori, I.; Erel, R.; Ben-Gal, A.; Yermiyahu, U. Long-Term Impact of Potassium Fertilization on Soil and Productivity in Intensive Olive Cultivation. *Agron. 2019, Vol. 9, Page 525* **2019**, *9*, 525.

30. Fernández, J.E.; Perez-Martin, A.; Torres-Ruiz, J.M.; Cuevas, M. V.; Rodriguez-Dominguez, C.M.; Elsayed-Farag, S.; Morales-Sillero, A.; García, J.M.; Hernandez-Santana, V.; Diaz-Espejo, A. A regulated deficit irrigation strategy for hedgerow olive orchards with high plant density. *Plant Soil* **2013**, *372*, 279–295.

31. Ben-Gal, A.; Ron, Y.; Yermiyahu, U.; Zipori, I.; Naoum, S.; Dag, A. Evaluation of regulated deficit irrigation strategies for oil olives: A case study for two modern Israeli cultivars. *Agric. Water Manag.* **2021**, *245*, 106577.

32. Ben-Gal, A.; Agam, N.; Alchanatis, V.; Cohen, Y.; Yermiyahu, U.; Zipori, I.; Presnov, E.; Sprintsin, M.; Dag, A. Evaluating water stress in irrigated olives: correlation of soil water status, tree water status, and thermal imagery. *Irrig. Sci.* **2009**, *27*, 367–376.

33. Nissim, Y.; Shloberg, M.; Biton, I.; Many, Y.; Doron-Faigenboim, A.; Zemach, H.; Hovav, R.; Kerem, Z.; Avidan, B.; Ben-Ari, G. High temperature environment reduces olive oil yield and quality. *PLoS One* **2020**, *15*, e0231956.

34. Navajas-Porras, B.; Pérez-Burillo, S.; Morales-Pérez, J.; Rufián-Henares, J.A.; Pastoriza, S. Relationship of quality parameters, antioxidant capacity and total phenolic content of EVOO with ripening state and olive variety. *Food Chem.* **2020**, *325*, 126926.

35. Fountas, S.; Aggelopoulou, K.; Gemtos, T.A. Precision agriculture: Crop management for improved productivity and reduced environmental impact or improved sustainability. In *Supply Chain Management for Sustainable Food Networks*; Eleftherios Iakovou, Dionysis Bochtis, Dimitrios Vlachos, D.A., Ed.; John Wiley & Sons, Ltd, 2015; pp. 41–65 ISBN 9781118937495.

36. Roma, E.; Catania, P. Precision Oliviculture: Research Topics, Challenges, and Opportunities—A Review. *Remote Sens.* **2022**, *14*, 1668.

37. Robinson, D.A.; Jones, S.B.; Wraith, J.M.; Or, D.; Friedman, S.P. A Review of Advances in Dielectric and Electrical Conductivity Measurement in Soils Using Time Domain Reflectometry. *Vadose Zo. J.* **2003**, *2*, 444–475.

38. Blonquist, J.M.; Jones, S.B.; Robinson, D.A. Standardizing Characterization of Electromagnetic Water Content Sensors: Part 2. Evaluation of Seven Sensing Systems. *Vadose Zo. J.* **2005**, *4*, 1059–1069.

39. Kojima, Y.; Shigeta, R.; Miyamoto, N.; Shirahama, Y.; Nishioka, K.; Mizoguchi, M.; Kawahara, Y. Low-Cost Soil Moisture Profile Probe Using Thin-Film Capacitors and a Capacitive Touch Sensor. *Sensors* **2016**, *16*, 1292.

40. Gaskin, G.J.; Miller, J.D. Measurement of Soil Water Content Using a Simplified Impedance Measuring Technique. *J. Agric. Eng. Res.* **1996**, *63*, 153–159.

41. Steeneken, P.G.; Kaiser, E.; Verbiest, G.J.; ten Veldhuis, M.C. Sensors in agriculture: towards an Internet of Plants. *Nat. Rev. Methods Prim. 2023 31* **2023**, *3*, 1–2.

42. Anastasiou, E.; Castrignanò, A.; Arvanitis, K.; Fountas, S. A multi-source data fusion approach to assess spatial-temporal variability and delineate homogeneous zones: A use case in a table grape vineyard in Greece. *Sci. Total Environ.* **2019**, *684*, 155–163.

43. Sehrawat, D.; Gill, N.S. Smart sensors: Analysis of different types of IoT sensors. *Proc. Int. Conf. Trends Electron. Informatics, ICOEI 2019* **2019**, 523–528.

44. Anastasiou, E.; Balafoutis, A.T.; Fountas, S. Trends in Remote Sensing Technologies in Olive Cultivation. *Smart Agric. Technol.* **2023**, *3*, 100103.

45. Lu, R.; Van Beers, R.; Saeys, W.; Li, C.; Cen, H. Measurement of optical properties of fruits and vegetables: A review. *Postharvest Biol. Technol.* **2020**, *159*, 111003.

46. Travlos, I.; Mikroulis, A.; Anastasiou, E.; Fountas, S.; Bilalis, D.; Tsiropoulos, Z.; Balafoutis, A. The use of RGB cameras in defining crop development in legumes. *Adv. Anim. Biosci.* **2017**, *8*, 224–228.

47. Barzin, R.; Pathak, R.; Lotfi, H.; Varco, J.; Bora, G.C. Use of UAS multispectral imagery at different physiological stages for yield prediction and input resource optimization in corn. *Remote Sens.* **2020**, *12*, 2392.

48. Mahajan, G.R.; Pandey, R.N.; Sahoo, R.N.; Gupta, V.K.; Datta, S.C.; Kumar, D. Monitoring nitrogen, phosphorus and sulphur in hybrid rice (Oryza sativa L.) using hyperspectral remote sensing. *Precis. Agric.* **2017**, *18*, 736–761.

49. Guzmán, E.; Baeten, V.; Pierna, J.A.F.; García-Mesa, J.A. A portable Raman sensor for the rapid discrimination of olives according to fruit quality. *Talanta* **2012**, *93*, 94–98.

50. Walsh, K.B.; Blasco, J.; Zude-Sasse, M.; Sun, X. Visible-NIR 'point' spectroscopy in postharvest fruit and vegetable assessment: The science behind three decades of commercial use. *Postharvest Biol. Technol.* **2020**, *168*, 111246.

51. Comino, F.; Ayora-Cañada, M.J.; Aranda, V.; Díaz, A.; Domínguez-Vidal, A. Near-infrared spectroscopy and X-ray fluorescence data fusion for olive leaf analysis and crop nutritional status determination. *Talanta* **2018**, *188*, 676–684.

52. Moorthy, I.; Miller, J.R.; Berni, J.A.J.; Zarco-Tejada, P.; Hu, B.; Chen, J. Field characterization of olive (Olea europaea L.) tree crown architecture using terrestrial laser scanning data. *Agric. For. Meteorol.* **2011**, *151*, 204–214.

53. Quebrajo, L.; Perez-Ruiz, M.; Pérez-Urrestarazu, L.; Martínez, G.; Egea, G. Linking thermal imaging and soil remote sensing to enhance irrigation management of sugar beet. *Biosyst. Eng.* **2018**, *165*, 77–87.

54. Colaço, A.F.; Molin, J.P.; Rosell-Polo, J.R.; Escolà, A. Application of light detection and ranging and ultrasonic sensors to high-throughput phenotyping and precision horticulture: Current status and challenges. *Hortic. Res.* **2018**, *5*.

55. Lee, W.S.; Alchanatis, V.; Yang, C.; Hirafuji, M.; Moshou, D.; Li, C. Sensing technologies for precision specialty crop production. *Comput. Electron. Agric.* **2010**, *74*, 2–33.

56. Sishodia, R.P.; Ray, R.L.; Singh, S.K. Applications of Remote Sensing in Precision Agriculture: A Review. *Remote Sens. 2020, Vol. 12, Page 3136* **2020**, *12*, 3136.

57. Rouse, J.W.; Haas, R.H.; Schell, J.A.; Deering, D.W. Monitoring vegetation systems in the Great Plains with ERTS. *NASA Spec. Publ* **1974**, *351*, 309.

58. Huete, A.R. A soil-adjusted vegetation index (SAVI). *Remote Sens. Environ.* **1988**, *25*, 295–309.

59. Xue, J.; Su, B. Significant remote sensing vegetation indices: A review of developments and applications. *J. Sensors* **2017**, *2017*.

60. Bian, J.; Zhang, Z.; Chen, J.; Chen, H.; Cui, C.; Li, X.; Chen, S.; Fu, Q. Simplified Evaluation of Cotton Water Stress Using High Resolution Unmanned Aerial Vehicle Thermal Imagery. *Remote Sens.* **2019**, *11*, 267.

61. Rubio-Delgado, J.; Carlos, ·; Pérez, J.; Vega-Rodríguez, M.A.; Es, J. Predicting leaf nitrogen content in olive trees using hyperspectral data for precision agriculture. **2020**, *22*, 1–21.

62. Verrelst, J.; Malenovský, Z.; Van der Tol, C.; Camps-Valls, G.; Gastellu-Etchegorry, J.-P.; Lewis, P.; North, P.; Moreno, J. Quantifying Vegetation Biophysical Variables from Imaging Spectroscopy Data: A Review on Retrieval Methods. *Surv. Geophys.* **2019**, *40*, 589–629.

63. Rotbart, N.; Schmilovitch, Z.; Cohen, Y.; Alchanatis, V.; Erel, R.; Ignat, T.; Shenderey, C.; Dag, A.; Yermiyahu, U. Estimating olive leaf nitrogen concentration using visible and near-infrared spectral reflectance. *Biosyst. Eng.* **2013**, *114*, 426–434.

64. Liakos, K.G.; Busato, P.; Moshou, D.; Pearson, S.; Bochtis, D. Machine Learning in Agriculture: A Review. *Sensors 2018, Vol. 18, Page 2674* **2018**, *18*, 2674.

65. Liu, H.; Zhu, H.; Wang, P. Quantitative modelling for leaf nitrogen content of winter wheat using UAV-based hyperspectral data. *Int. J. Remote Sens.* **2017**, *38*, 2117–2134.

66. Lee, H.; Wang, J.; Leblon, B. Using Linear Regression, Random Forests, and Support Vector Machine with Unmanned Aerial Vehicle Multispectral Images to Predict Canopy Nitrogen Weight in Corn. *Remote Sens.* **2020**, *12*, 2071.

67. Zhang, X.; Liu, F.; He, Y.; Gong, X. Detecting macronutrients content and distribution in oilseed rape leaves based on hyperspectral imaging. *Biosyst. Eng.* **2013**, *115*, 56–65.

68. Berger, K.; Verrelst, J.; Féret, J.B.; Wang, Z.; Wocher, M.; Strathmann, M.; Danner, M.; Mauser, W.; Hank, T. Crop nitrogen monitoring: Recent progress and principal developments in the context of imaging spectroscopy missions. *Remote Sens. Environ.* **2020**, *242*, 111758.

69. Sebastiani, L.; Gucci, R.; Kerem, Z.; Fernández, J.E. Physiological Responses to Abiotic Stresses. **2016**, 99–122.

70. Jones, H.G. Monitoring plant and soil water status: established and novel methods revisited and their relevance to studies of drought tolerance. *J. Exp. Bot.* **2007**, *58*, 119–130.

71. Allen, R.G.; Pereira, L.S.; Raes, D.; Smith, M. Crop evapotranspiration-Guidelines for computing crop water requirements-FAO Irrigation and drainage paper 56. *Fao, Rome* **1998**, *300*, D05109.

72. Testi, L.; Villalobos, F.J.; Orgaz, F.; Fereres, E. Water requirements of olive orchards: I simulation of daily evapotranspiration for scenario analysis. *Irrig. Sci.* **2006**, *24*, 69–76.

73. Orgaz, F.; Testi, L.; Villalobos, F.J.; Fereres, E. Water requirements of olive orchards-II: Determination of crop coefficients for irrigation scheduling. *Irrig. Sci.* **2006**, *24*, 77–84.

74. Gerhards, M.; Schlerf, M.; Mallick, K.; Udelhoven, T. Challenges and future perspectives of multi-/Hyperspectral thermal infrared remote sensing for crop water-stress detection: A review. *Remote Sens.* **2019**, *11*.

75. Gao, Y.; Walker, J.P.; Allahmoradi, M.; Monerris, A.; Ryu, D.; Jackson, T.J. Optical Sensing of Vegetation Water Content: A Synthesis Study. *IEEE J. Sel. Top. Appl. Earth Obs. Remote Sens.* **2015**, *8*, 1456–1464.

76. Rallo, G.; Minacapilli, M.; Ciraolo, G.; Provenzano, G. Detecting crop water status in mature olive groves using vegetation spectral measurements. *Biosyst. Eng.* **2014**, *128*, 52–68.

77. Brown, H.T.; Escombe, F. Researches on some of the Physiological Processes of Green Leaves, with Special Reference to the Interchange of Energy between the Leaf and Its Surroundings. *Proc. R. Soc. B Biol. Sci.* **1905**, *76*, 29–111.

78. Jones, H.G.; Stoll, M.; Santos, T.; Sousa, C. de; Chaves, M.M.; Grant, O.M. Use of infrared thermography for monitoring stomatal closure in the field: application to grapevine. *J. Exp. Bot.* **2002**, *53*, 2249–2260.

79. Jones, H.G. Use of infrared thermometry for estimation of stomatal conductance as a possible aid to irrigation scheduling. *Agric. For. Meteorol.* **1999**, *95*, 139–149.

80. Pou, A.; Diago, M.P.; Medrano, H.; Baluja, J.; Tardaguila, J. Validation of thermal indices for water status identification in grapevine. *Agric. Water Manag.* **2014**, *134*, 60–72.

81. Jackson, R.D.; Idso, S.B.; Reginato, R.J.; Pinter, P.J. Canopy temperature as a crop water stress indicator. *Water Resour. Res.* **1981**, *17*, 1133–1138.

82. Idso, S.B.; Jackson, R.D.; Pinter, P.J.; Reginato, R.J.; Hatfield, J.L. Normalizing the stress-degree-day parameter for environmental variability. *Agric. Meteorol.* **1981**, *24*, 45–55.

83. Cohen, Y.; Alchanatis, V.; Meron, M.; Saranga, Y.; Tsipris, J. Estimation of leaf water potential by thermal imagery and spatial analysis. *J. Exp. Bot.* **2005**, *56*, 1843–1852.

84. Egea, G.; Padilla-Díaz, C.M.; Martinez-Guanter, J.; Fernández, J.E.; Pérez-Ruiz, M. Assessing a crop water stress index derived from aerial thermal imaging and infrared thermometry in super-high density olive orchards. *Agric. Water Manag.* **2017**, *187*, 210–221.

85. Meron, M.; Sprintsin, M.; Tsipris, J.; Alchanatis, V.; Cohen, Y. Foliage temperature extraction from thermal imagery for crop water stress determination. *Precis. Agric.* **2013**, *14*, 467–477.

86. Rud, R.; Cohen, Y.; Alchanatis, V.; Levi, A.; Brikman, R.; Shenderey, C.; Heuer, B.; Markovitch, T.; Dar, Z.; Rosen, C.; et al. Crop water stress index derived from multi-year ground and aerial thermal images as an indicator of potato water status. *Precis. Agric.* **2014**, *15*, 273–289.

87. Park, S.; Ryu, D.; Fuentes, S.; Chung, H.; Hernández-Montes, E.; O'Connell, M. Adaptive Estimation of Crop Water Stress in Nectarine and Peach Orchards Using High-Resolution Imagery from an Unmanned Aerial Vehicle (UAV). *Remote Sens.* **2017**, *9*, 828.

88. Möller, M.; Alchanatis, V.; Cohen, Y.; Meron, M.; Tsipris, J.; Naor, A.; Ostrovsky, V.; Sprintsin, M.; Cohen, S. Use of thermal and visible imagery for estimating crop water status of irrigated grapevine. *J. Exp. Bot.* **2007**, *58*, 827–838.

89. Abasi, S.; Minaei, S.; Jamshidi, B.; Fathi, D. Dedicated non-destructive devices for food quality measurement: A review. *Trends Food Sci. Technol.* **2018**, *78*, 197–205.

90. Nicolaï, B.M.; Beullens, K.; Bobelyn, E.; Peirs, A.; Saeys, W.; Theron, K.I.; Lammertyn, J. Nondestructive measurement of fruit and vegetable quality by means of NIR spectroscopy: A review. *Postharvest Biol. Technol.* **2007**, *46*, 99–118.

91. Arendse, E.; Fawole, O.A.; Magwaza, L.S.; Opara, U.L. Non-destructive prediction of internal and external quality attributes of fruit with thick rind: A review. *J. Food Eng.* **2018**, *217*, 11–23.

92. Li, B.; Lecourt, J.; Bishop, G. Advances in Non-Destructive Early Assessment of Fruit Ripeness towards Defining Optimal Time of Harvest and Yield Prediction—A Review. *Plants* **2018**, *7*, 3.

93. Beltrán Ortega, J.; Martínez Gila, D.M.; Aguilera Puerto, D.; Gámez García, J.; Gómez Ortega, J. Novel technologies for monitoring the in-line quality of virgin olive oil during manufacturing and storage. *J. Sci. Food Agric.* **2016**, *96*, 4644–4662.

94. Muik, B.; Lendl, B.; Molina-Díaz, A.; Pérez-Villarejo Luis; Ayora-Cañada, M.J. Determination of oil and water content in olive pomace using near infrared and Raman spectrometry. A comparative study. *Anal Bioanal Chem* **2004**, *379*, 35–41.

95. Barros, A.S.; Nunes, A.; Martins, J.; Delgadillo, I. Determination of oil and water in olive and olive pomace by NIR and multivariate analysis. *Sens. Instrum. Food Qual. Saf.* **2009**, *3*, 180–186.

96. Bendini, A.; Cerretani, L.; Di Virgilio, F.; Belloni, P.; Lercker, G.; Toschi, T.G. In-process monitoring in industrial olive mill by means of FT-NIR. *Eur. J. Lipid Sci. Technol.* **2007**, *109*, 498–504.

97. Casale, M.; Simonetti, R. Review: Near infrared spectroscopy for analysing olive oils. *J. Near Infrared Spectrosc.* **2014**, *22*, 59–80.

98. Mailer, R.J. Rapid evaluation of olive oil quality by NIR reflectance spectroscopy. *J. Am. Oil Chem. Soc.* **2004**, *81*, 823–827.

99. Armenta, S.; Moros, J.; Garrigues, S.; de la Guardia, M. The Use of Near-Infrared Spectrometry in the Olive Oil Industry. *Crit. Rev. Food Sci. Nutr.* **2010**, *50*, 567–582.

100. Öztürk, B.; Özdemir, D.; Yalçin, A. Determination of Olive Oil Adulteration with Vegetable Oils by near Infrared Spectroscopy Coupled with Multivariate Calibration. *J. Near Infrared Spectrosc. Vol. 18, Issue 3, pp. 191-201* **2010**, *18*, 191–201.

101. Jiménez, A.; Beltrán, G.; Aguilera, M.P.; Uceda, M. A sensor-software based on artificial neural network for the optimization of olive oil elaboration process. *Sensors Actuators, B Chem.* **2008**, *129*, 985–990.

102. Allouche, Y.; López, E.F.; Maza, G.B.; Márquez, A.J. Near infrared spectroscopy and artificial neural network to characterise olive fruit and oil online for process optimisation. *J. Near Infrared Spectrosc.* **2015**, *23*, 111–121.

103. León, L.; Rallo, L.; Garrido, A. Análisis de aceituna intacta mediante espectroscopia en el Infrarrojo Cercano (NIRS): Una herramienta de utilidad en programas de mejora de olivo. *Grasas y Aceites* **2003**, *54*, 41–47.

104. León-Moreno, L. Usefulness of portable near infra- red spectroscopy in olive breeding programs. *Spanish J. Agric. Res.* **2012**, *10*, 141–148.

105. Bellincontro, A.; Caruso, G.; Mencarelli, F.; Gucci, R. Oil accumulation in intact olive fruits measured by near infrared spectroscopy-acousto-optically tunable filter. *J. Sci. Food Agric.* **2013**, *93*, 1259–1265.

106. Bellincontro, A.; Taticchi, A.; Servili, M.; Esposto, S.; Farinelli, D.; Mencarelli, F. Feasible application of a portable NIR-AOTF tool for on-field prediction of phenolic compounds during the ripening of olives for oil production. *J. Agric. Food Chem.* **2012**, *60*, 2665–2673.

107. Salguero-Chaparro, L.; Baeten, V.; Fernández-Pierna, J.A.; Peña-Rodríguez, F. Near infrared spectroscopy (NIRS) for on-line determination of quality parameters in intact olives. *Food Chem.* **2013**, *139*, 1121–1126.

108. Salguero-Chaparro, L.; Peña-Rodríguez, F. On-line versus off-line NIRS analysis of intact olives. *LWT - Food Sci. Technol.* **2014**, *56*, 363–369.

109. Kavdir, I.; Buyukcan, M.B.; Lu, R.; Kocabiyik, H.; Seker, M. Prediction of olive quality using FT-NIR spectroscopy in reflectance and transmittance modes. *Biosyst. Eng.* **2009**, *103*, 304–312.

110. FOSS analytical solutions for food quality improvement and control Available online: https://www.fossanalytics.com/en (accessed on Apr 21, 2021).

111. Dupuy, N.; Galtier, O.; Le Dréau, Y.; Pinatel, C.; Kister, J.; Artaud, J. Chemometric analysis of combined NIR and MIR spectra to characterize French olives. *Eur. J. Lipid Sci. Technol.* **2010**, *112*, 463–475.

112. Cayuela, J.A.; Camino, M. del C.P. Prediction of quality of intact olives by near infrared spectroscopy. *Eur. J. Lipid Sci. Technol.* **2010**, *112*, 1209–1217.

113. Cayuela, J.A.; García, J.M.; Caliani, N. NIR prediction of fruit moisture, free acidity and oil content in intact olives. *Grasas y Aceites* **2009**, *60*, 194–202.

114. Giovenzana, V.; Beghi, R.; Romaniello, R.; Tamborrino, A.; Guidetti, R.; Leone, A. Use of visible and near infrared spectroscopy with a view to on-line evaluation of oil content during olive processing. *Biosyst. Eng.* **2018**, *172*, 102–109.

115. Escolar, D.; Haro, M.R.; Ayuso, J. The color space of foods: Virgin olive oil. *J. Agric. Food Chem.* **2007**, *55*, 2085–2093.

116. Gracia, A.; León, L. Non-destructive assessment of olive fruit ripening by portable near infrared spectroscopy. *Grasas y Aceites* **2011**, *62*, 268–274.

117. Fernández-Espinosa, A.J. Combining PLS regression with portable NIR spectroscopy to on-line monitor quality parameters in intact olives for determining optimal harvesting time. *Talanta* **2016**, *148*, 216–228.

118. Zhang, C.; Valente, J.; Kooistra, L.; Guo, L.; Wang, W. Opportunities of uavs in orchard management. In Proceedings of the International Archives of the Photogrammetry, Remote Sensing and Spatial Information Sciences - ISPRS Archives; International Society for Photogrammetry and Remote Sensing, 2019; Vol. 42, pp. 673–680.

119. Bec, K.B.; Grabska, J.; Huck, C.W. Miniaturized NIR Spectroscopy in Food Analysis and Quality Control: Promises, Challenges, and Perspectives. *Foods 2022, Vol. 11, Page 1465* **2022**, *11*, 1465.

120. Krause, J.; Grüger, H.; Gebauer, L.; Zheng, X.; Knobbe, J.; Pügner, T.; Kicherer, A.; Gruna, R.; Längle, T.; Beyerer, J. SmartSpectrometer—Embedded Optical Spectroscopy for Applications in Agriculture and Industry. *Sensors* **2021**, *21*, 4476.

121. Trang, N.M.; Duy, T.K.; Huyen, T.T.N.; Danh, L.V.Q.; Dinh, A. An investigation into the use of a low-Cost NIR integrated circuit spectrometer to measure chlorophyll content index. *Int. J. Innov. Technol. Explor. Eng.* **2019**, *8*, 35–38.

122. Li, M.; Qian, Z.; Shi, B.; Medlicott, J.; East, A. Evaluating the performance of a consumer scale SCiO™ molecular sensor to predict quality of horticultural products. *Postharvest Biol. Technol.* **2018**, *145*, 183–192.

123. Kitić, G.; Tagarakis, A.; Cselyuszka, N.; Panić, M.; Birgermajer, S.; Sakulski, D.; Matović, J. A new low-cost portable multispectral optical device for precise plant status assessment. *Comput. Electron. Agric.* **2019**, *162*, 300–308.

124. Moinard, S.; Brunel, G.; Ducanchez, A.; Crestey, T.; Rousseau, J.; Tisseyre, B. Testing the potential of a new low-cost multispectral sensor for decision support in agriculture. *Precis. Agric.* **2021**, *21*, 411–418.

125. Leon-salas, W.D.; Rajendran, J.; Vizcardo, M.A.; Postigo-malaga, M. Measuring Photosynthetically Active Radiation with a Multi-Channel Integrated Spectral Sensor. In Proceedings of the 2021 IEEE International Symposium on Circuits and Systems (ISCAS); IEEE Xplore, 2021; pp. 1–5.

126. Stevens, J.D.; Murray, D.; Sozzi, M.; Cogato, A.; Laroche-Pinel, E.; Stevens, J.D.; Murray, D.; Diepeveen, D.; Toohey, D. Development and Testing of an IoT Spectroscopic Nutrient Monitoring System for Use in Micro Indoor Smart Hydroponics. *Hortic. 2023, Vol. 9, Page 185* **2023**, *9*, 185.

127. Malmir, M.; Tahmasbian, I.; Xu, Z.; Farrar, M.B.; Bai, S.H. Prediction of macronutrients in plant leaves using chemometric analysis and wavelength selection. *J. Soils Sediments* **2020**, *20*, 249–259.

128. Pandey, P.; Ge, Y.; Stoerger, V.; Schnable, J.C. High throughput in vivo analysis of plant leaf chemical properties using hyperspectral imaging. *Front. Plant Sci.* **2017**, *8*, 1–12.

129. Wang, Y.J.; Jin, G.; Li, L.Q.; Liu, Y.; Kianpoor Kalkhajeh, Y.; Ning, J.M.; Zhang, Z.Z. NIR hyperspectral imaging coupled with chemometrics for nondestructive assessment of phosphorus and potassium contents in tea leaves. *Infrared Phys. Technol.* **2020**, *108*, 103365.

130. Savitzky, A.; Golay, M.J.E. Smoothing and Differentiation of Data by Simplified Least Squares Procedures. *Anal. Chem.* **1964**, *36*, 1627–1639.

131. Martinez de Toda, F. *Claves de la viticultura de calidad: Nuevas técnicas de estimación y control de la calidad de la uva en el viñedo*; 2nd ed.; Ediciones Mundi-Prensa: Madrid, 2011; ISBN 9788484764229.

132. Vogel, A.I. *Vogel's Textbook of quantitative inorganic analysis*; Longman, Ed.; 4th Ed.; Londres, 1978;

133. Michael Thompson, J.N.W. *Handbook of Inductively Coupled Plasma Spectrometry*; Media, S.S.& B., Ed.; 2nd ed.; Springer New York, NY: New York, NY, 2012; ISBN 978-1-4613-0697-9.

134. Kalacska, M.; Lalonde, M.; Moore, T.R. Estimation of foliar chlorophyll and nitrogen content in an ombrotrophic bog from hyperspectral data: Scaling from leaf to image. *Remote Sens. Environ.* **2015**, *169*, 270–279.

135. Malenovský, Z.; Homolová, L.; Zurita-Milla, R.; Lukeš, P.; Kaplan, V.; Hanuš, J.; Gastellu-Etchegorry, J.P.; Schaepman, M.E. Retrieval of spruce leaf chlorophyll content from airborne image data using continuum removal and radiative transfer. *Remote Sens. Environ.* **2013**, *131*, 85–102.

136. Uno, Y.; Prasher, S.O.; Lacroix, R.; Goel, P.K.; Karimi, Y.; Viau, A.; Patel, R.M. Artificial neural networks to predict corn yield from Compact Airborne Spectrographic Imager data. *Comput. Electron. Agric.* **2005**, *47*, 149–161.

137. Wang, F.; Huang, J.; Wang, Y.; Liu, Z.; Peng, D.; Cao, F. Monitoring nitrogen concentration of oilseed rape from hyperspectral data using radial basis function. *Int. J. Digit. Earth* **2013**, *6*, 550–562.

138. Jensen, R.R.; Hardin, P.J.; Hardin, A.J. Estimating urban leaf area index (LAI) of individual trees with hyperspectral data. *Photogramm. Eng. Remote Sensing* **2012**, *78*, 495–504.

139. Chen, B.; Wu, Z.; Wang, J.; Dong, J.; Guan, L.; Chen, J.; Yang, K.; Xie, G. Spatio-temporal prediction of leaf area index of rubber plantation using HJ-1A/1B CCD images and recurrent neural network. *ISPRS J. Photogramm. Remote Sens.* **2015**, *102*, 148–160.

140. Feng, H.; Yang, F.; Li, Z.; Yang, G.; Guo, J.; He, P.; Wang, Y. Hyperspectral estimation of leaf total phosphorus content in apple tree based on optimal weights combination model. *Trans Chin Soc Agric Eng* **2016**, *32*, 173–180.

141. Pôças, I.; Gonçalves, J.; Costa, P.M.; Gonçalves, I.; Pereira, L.S.; Cunha, M. Hyperspectral-based predictive modelling of grapevine water status in the Portuguese Douro wine region. *Int. J. Appl. Earth Obs. Geoinf.* **2017**, *58*, 177–190.

142. Demšar, J.; Erjavec, A.; Hočevar, T.; Milutinovič, M.; Možina, M.; Toplak, M.; Umek, L.; Zbontar, J.; Zupan, B. Orange: Data Mining Toolbox in Python. *J. Mach. Learn. Res.* **2013**, *14*, 2349–2353.

List of Tables

Section 4. Results

List of Figures

Section 1. Introduction

Section 3. Materials

Section 4. Results